Ammonium Signalling in Dimorphic Fungi

Siobhan Hope Lister

Thesis submitted for the degree of Doctor of Philosophy

Newcastle University Biosciences Institute

September 2019

Abstract

Ammonium is a preferred source of nitrogen utilised by fungi. In some fungi ammonium availability is sensed by ammonium transporters belonging to the Amt/Mep/Rh superfamily. During ammonium limiting conditions these transporters trigger a signalling cascade to induce a morphological change. The molecular basis for signalling and the extent to which these transporters are conserved are important questions within the field. We have investigated morphological change in response to ammonium availability in two divergent fungi. The wheat pathogen *Zymoseptoria tritici* and the human pathogen *Cryptococcus neoformans* serotype D JEC20 (MATa) and JEC21 (MATα). We show that low ammonium dependent filamentation is ZtMep2 independent and that mutants lacking ZtMep3 acquire a severe growth defect during ammonium sufficient conditions. Moreover, *Ztmep3Δ* mutants display a different type of filamentation which may be as a result of ammonium starvation as opposed to ammonium signalling. ZtMep3 does however act as an ammonium sensor when expressed in yeast, to regulate pseudohyphal growth, despite lacking the conserved twin-histidine motif previously believed to be essential for signalling. Furthermore, the dual loss of ZtMep2 and ZtMep3 renders *Z. tritici* hypervirulent in the wheat infection assay suggesting that a lack of internal ammonium is the trigger for virulence. In *C. neoformans*, we show that hyphal growth, induced during ammonium limiting conditions, is CnAmt2 dependent and that the expression of the CnAmt2^{N241A} mutant in yeast uncouples transport from signalling. Therefore, signalling by CnAmt2 is not the consequence of internal ammonium metabolism and is due to the physical act of transport. Fundamental questions now exist as to why these two diverse fungi have adopted different modes of ammonium signalling and about how prevalent these starvation responses are throughout fungi.

Declaration

I certify that this thesis contains my own work, except where acknowledged, and that no part of this material has previously been submitted for a qualification at this or any other university.

Dedication

I would like to dedicate this thesis to my mum and fiancé for their continued love and support and to my grandfather who I know would be proud.

Acknowledgements

Firstly, I would like to thank my primary supervisor Julian Rutherford for the opportunity to undertake this project and for his constant guidance and support. I also thank Julian for generating the MATa *amt2Δ* mutant and Amt2 R–pPZP-Hyg plasmid. I express gratitude to my secondary supervisor Bert van den Berg for his advice and assistance and I thank my progress panel, Simon Whitehall and Janet Quinn, for their critical appraisals and suggestions during my annual progression meetings. I acknowledge Jason Rudd, from Rothamsted Research, for performing the wheat infection assays and express thanks to Anu Chembath for her coaching and support. I thank Raphaela Konrath for generating the ZtMep3-pCGEN vector and Callum Fraser for coaching me in qPCR. Sincere thanks to all members of the Rutherford lab, van den Berg lab, Yeast lab and Khan lab for their friendship and lending of equipment and reagents. Furthermore, I greatly appreciate the funding I have received from the BBSRC DTP and the support received from my institute (NUBI, formally ICAMB) over this four-year studentship.

Next I would like to thank all my family and friends who have helped me get to where I am today. I am very grateful to Uncle Brian who provided me with additional science tutoring throughout my GCSEs and A levels. Without his help I would not have achieved what I did. Finally, thank you to my mum and Andrew for their unconditional emotional support and for always believing in me.

Table of Contents

2. Materials and Methods

3. Ammonium Signaling in *Zymoseptoria tritici*

List of Tables

List of Figures

List of Abbreviations

1A5 – ST99CH_1A5

1E4 – ST99CH_1E4

3D7 – ST99CH_3D7

AA – Amino acids

ACT1 – Actin

AI – Autoinhibitory

AIDS – Acquired Immune Deficiency Syndrome

AMT – Ammonium Transporter

Amu1 – Ammonium Uptake 1

AS – Ammonium Sulphate

CCCP – Carbonyl Cyanide M-Chlorophenyl Hydrazone

cDNA – Complimentary DNA

CF – 5-Carboxy Fluorescein

CS – Chinese Spring

Ct – Cycle Threshold

CTR – C-Terminal Region

CWDE - Cell wall degrading enzyme

DC – Dendritic Cell

DMI – Demethylation Inhibitor

DNA – Deoxyribose Nucleic Acid

dNTP – Deoxyribonucleotide Triphosphate

DPI – Days Post Infection

ECL – Enhanced Chemiluminescence (Methods section)

ECL – Extracellular Loop

EDTA – Ethylenediaminetetraacetic acid

FCCP – Carbonyl Cyanide-P-Trifluoromethoxyphenylhydrazone

FEB – Free Energy Perturbation

GAP – GTPase-Activating Protein

Gap1 – General Amino Acid Permease

GDH – Glutamate Dehydrogenase

GEF – Guanine Exchange Factor

GEN – Geneticin (G418)

Glu – Glutamate

GPCR – G-Protein Coupled Receptor

GS – Glutamine Synthetase

GST – Glutathione S-Transferase

HIV – Human Immunodeficiency Virus

HYG – Hygromycin

ICL – Intracellular Loop

IFN – Interferon

IL – Interleukin

IM – Induction Medium

LB – Luria Bertani

LTR – Long Terminal Repeat

MAPK – Mitogen Activated Protein Kinase

MeA – Methylammonium

Mep – Methylammonium Permease

MFS – Major Facility Subfamily

MM – Minimal Medium (Methods section)

MM – Molecular Mechanics

MSF – Multi-Site Fungicide

MSX – L-Methionine Sulfoximine

NCR – Nitrogen Catabolite Repression

NEP – Necrosis And Ethylene-Inducing Peptide

NLP – NEP-like protein

Npr1 – Nitrogen Permease Reactivator 1

OD – Optical Density

ORF – Open Reading Frame

PAMP – Pathogen Associated Molecular Pattern

Par32 – Phosphorylated After Rapamycin 32

PBS – Phosphate Buffered Saline

PCR – Polymerase Chain Reactivation

PG – Pseudohyphal Growth

PKA – Protein Kinase A

PMF – Penitential Mean Force

PTI – PAMP-Triggered Immunity

QM – Quantum Mechanics

QoI – Quinone Outside Inhibitor

qPCR – Quantitative PCR

RNA – Ribonucleic Acid

ROS – Reactive Oxygen Species

RPM – Revolutions Per Minute

RRes – Rothamsted Research

SCAM – Substituted Cysteine Accessibility Method

SD – Synthetic Dextrose

SDI – Succinate Dehydrogenase Inhibitor

SDS – Sodium Dodecyl Sulphate

SEACAT – Seh1-Associated Subcomplex Activating TORC1

SEACIT – Seh1-Associated Subcomplex Inhibiting TORC1

SHAD – Synthetic High Ammonium Dextrose

SLAD – Synthetic Low Ammonium Dextrose

SNP – Single Nucleotide Polymorphism

SSM – Solid-Supported Membrane

STB – Septoria Tritici Leaf Blotch

STET – Sucrose-Tris-EDTA-Triton-X

TBE – Tris-Borate-EDTA

TBS – Tris Buffered Saline

TCA – Trichloroacetic Acid

TE – Transposable Element

TE – Tris-EDTA (Methods section)

TIR – Terminal Inverted Repeat

TMD – Transmembrane Domain

TOR – Target Of Rapamycin

UAS – Upstream Activation Sequence

URA – Uracil

UTR – Untranslated Region

1. Introduction

1.1 Ammonium as a nutrient

In everchanging environments, fungal pathogens must sense and adapt to their respective niches to aid survival. Despite some pathogens being evolutionarily very distinct the elements which require careful monitoring are conserved and include pheromones, stress and nutrients. Nitrogen is a vital nutrient for many organisms as it serves as a building block for the biosynthesis of amino acids and, therefore, acts as a limiting factor for growth.

Along with glutamine and glutamate, the precursors for all nitrogenous compounds, ammonia, ammonium, and asparagine are the preferred sources of nitrogen utilised by plants, fungi and bacteria. These sources yield relatively high growth rates (Boer *et al.*, 2007). In mammals, ammonium serves as the regulator of blood pH and is toxic to cells (Ludewig *et al.*, 2001). When the preferred nitrogenous compounds are not readily available, fungi will utilise poorer sources of nitrogen which include leucine, phenylalanine, proline, urea and methionine, which yield lower growth rates (Boer *et al.*, 2007). With regards to the preferred sources of nitrogen, ammonia exists as an uncharged gas molecule (NH_3), when at high concentration, which can readily permeate the membrane. However, in aqueous solutions ammonia becomes protonated resulting in the formation of ammonium (NH_4^+) which requires transmembrane transporters to facilitate its passage through the membrane. At 25 °C ammonium has a pKa ≈ 9.25, therefore, at pH ≤ 7, > 99 % of the ammonium available is in the protonated form (NH_4^+) (Antonenko *et al.*, 1997) (Cueto-Rojas *et al.*, 2017) (**Figure 1**). On the other hand, too much ammonium can be cytotoxic, therefore, ammonium levels are tightly regulated (Hess *et al.*, 2006). In the model yeast *Saccharomyces cerevisiae,* ammonia is incorporated into the amide groups of glutamate and glutamine which are the source of 80 % and 20 % of cellular nitrogen respectively (Magasanik, 2003).

Conversion of ammonia and 2-ketoglutarate (source of carbon) to glutamate is catalysed by glutamate dehydrogenase (GDH) which is dependent on NADPH (Nagasu and Hall, 1985) (Huergo and Dixon, 2015).

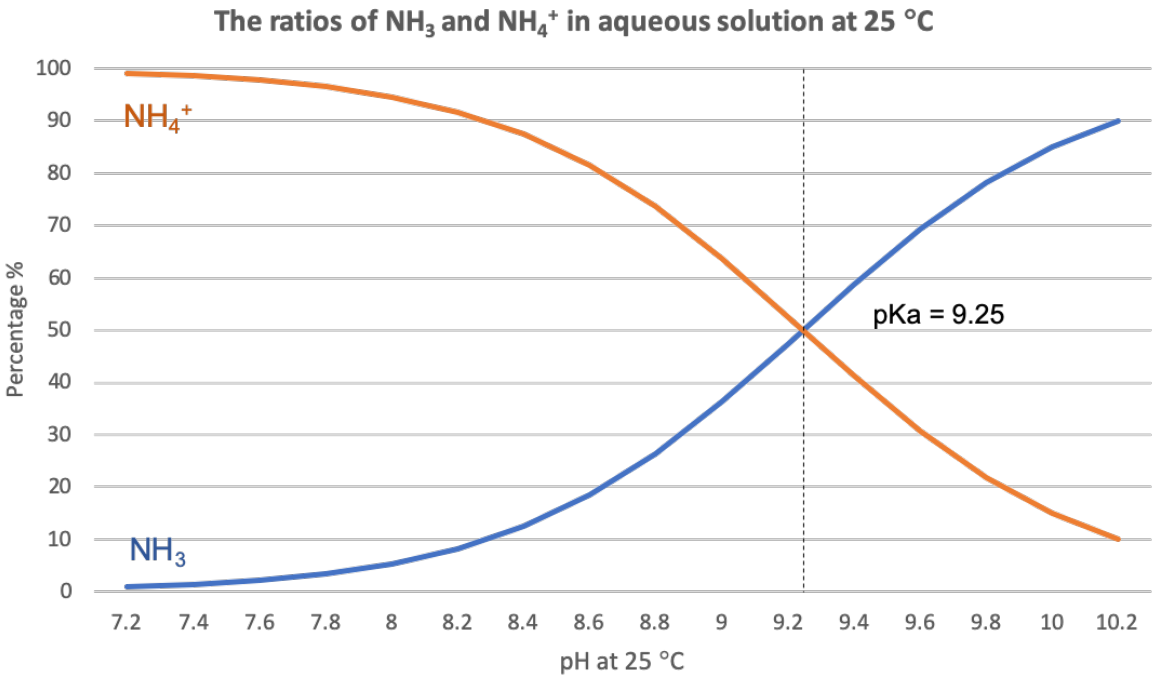

Figure 1: The ratios of NH_3 and NH_4^+ in aqueous solution at 25 ℃. *The percentages of charged and uncharged ammonia from pH 7.2 – 10.2 are depicted. The orange line represents charged ammonia (NH_4^+), while the blue line represents uncharged ammonia (NH_3). The dashed line indicates the pH at which both species are in equilibrium. Values for the graph were taken from (Emerson et al., 1975).*

$$2-Ketoglutarate + NH_3 + NADPH \xrightarrow{GDH} Glutamate + NADP^+$$

Biosynthesis of glutamine is catalysed by glutamine synthetase (GS); glutamate is also required for this reaction (Mitchell and Magasanik, 1984).

$$Glutamate + NH_3 + ATP \xrightarrow{GS} Glutamine + ADP + Pi$$

1.2 Ammonium transporters

Methylammonium permeases belong to the evolutionarily conserved Amt/Mep/Rh protein superfamily, which have been identified in plants, bacteria, fungi and humans (Andrade and Einsle, 2007). These proteins facilitate the transport of ammonium across the membrane by utilising the negative membrane potential (Ullmann *et al.*, 2012). All fungi contain at least two of these transporters in their proteome. *S. cerevisiae* possesses three ammonium transporters (Mep1, Mep2, and Mep3). A strain lacking all three ammonium transporters is unable to grow on media where the sole nitrogen source is <5 mM NH_4^+. On the contrary, at concentrations >20 mM, ammonium transporters are dispensable for transport. Mep2 is the high affinity, low capacity transporter (K_m, 1 to 2 μM) with an additional role in ammonium signalling, while Mep1 (K_m, 5 to 10 μM) and Mep3 (K_m, ~1.4 to 2.1 mM) are high capacity transporters which possess lower affinities for ammonium (Marini *et al.*, 1997). Moreover, Mep1 and Mep3 possess the highest sequence identity to each other (79 %). On non-preferred nitrogenous compounds, such as proline, Mep1 and Mep2 are additionally required to re-import ammonium which has leaked from the cell to maintain ammonium homeostasis (Boeckstaens *et al.*, 2007).

1.2.1 *Ammonium transporter structure*

Expansion in the library of solved Amt/Mep/Rh structures has broadened our knowledge in how these proteins transport their substrate. Despite differences in function, all ammonium transporters have a similar architecture. They are trimeric complexes with each monomer composed of 11 or 12 (in human Rhesus proteins) transmembrane domains (TMDs). The N-terminus dwells on the extracellular, or periplasmic, side and the C-terminus resides on the intracellular side. Furthermore,

each monomer possess an extracellular ammonium binding site, two conserved phenylalanine residues, and a narrow hydrophobic pore which is lined by two conserved histidine residues. The latter is referred to as the twin-histidine motif; in some homologues the first histidine is replaced by glutamate. The phenylalanine pair are located at the entrance to the hydrophobic pore and are, hence, designated as the Phe gate (Andrade *et al.*, 2005) (Zheng *et al.*, 2004) (van den Berg *et al.*, 2016) (Gruswitz *et al.*, 2010).

Monomer pseudo-symmetry

In *Escherichia coli* EcAmtB the first five alpha helical TMDs, of each monomer, show structural duplication to TMDs six to ten and have opposite polarity with respect to the membrane (Khademi *et al.*, 2004). *Archaeoglobus fulgidus* AfAmt-1, *Candida albicans* CaMep2, *S. cerevisiae* ScMep2 and human RhCG similarly exhibit this quasi-twofold symmetry, however, there are differences in how these structures are maintained (Andrade *et al.*, 2005) (van den Berg *et al.*, 2016) (Gruswitz *et al.*, 2010). Antiparallel halves are 'clamped' together in AfAmt-1 and RhCG by TMD 11, with the latter additionally requiring TMD 0 (Andrade *et al.*, 2005) (Gruswitz *et al.*, 2010). In ScMep2 and CaMep2, the pseudo-symmetrical halves are connected by intracellular loop (ICL) 3 (van den Berg *et al.*, 2016). The region between the two halves in each protein forms the substrate conducting pore (Andrade *et al.*, 2005) (Zheng *et al.*, 2004) (van den Berg *et al.*, 2016) (Gruswitz *et al.*, 2010), therefore pseudo-symmetry serves functional importance (**Figure 2a**).

Trimeric stability

Maintenance of the trimeric architecture varies between different members of the Mep/Amt/Rh family. In *Arabidopsis thaliana* AtAmt1;1, the C-terminus of one monomer interacts with the ICLs of another (**Figure 2b**). In addition to stabilising the trimer, these interactions also regulate allosteric activation of the protein (Loque *et al.*, 2007). The tomato plant, *Lycopersicon esculentum*, encodes three ammonium transporters, LeAMT1;1, LeAmt1;2 and LeAmt1;3. The N-terminus of LeAmt1;3 is relatively shorter than its two other homologues and is separated by SDS-PAGE in dimeric and monomeric forms under both reducing and non-reducing conditions. LeAmt1;1 and LeAmt1;2 are detected in the trimeric form under non-reducing conditions. Substitution of the N-terminus of LeAmt1;1 with the N-terminus of LeAmt1;3 resulted in a loss of

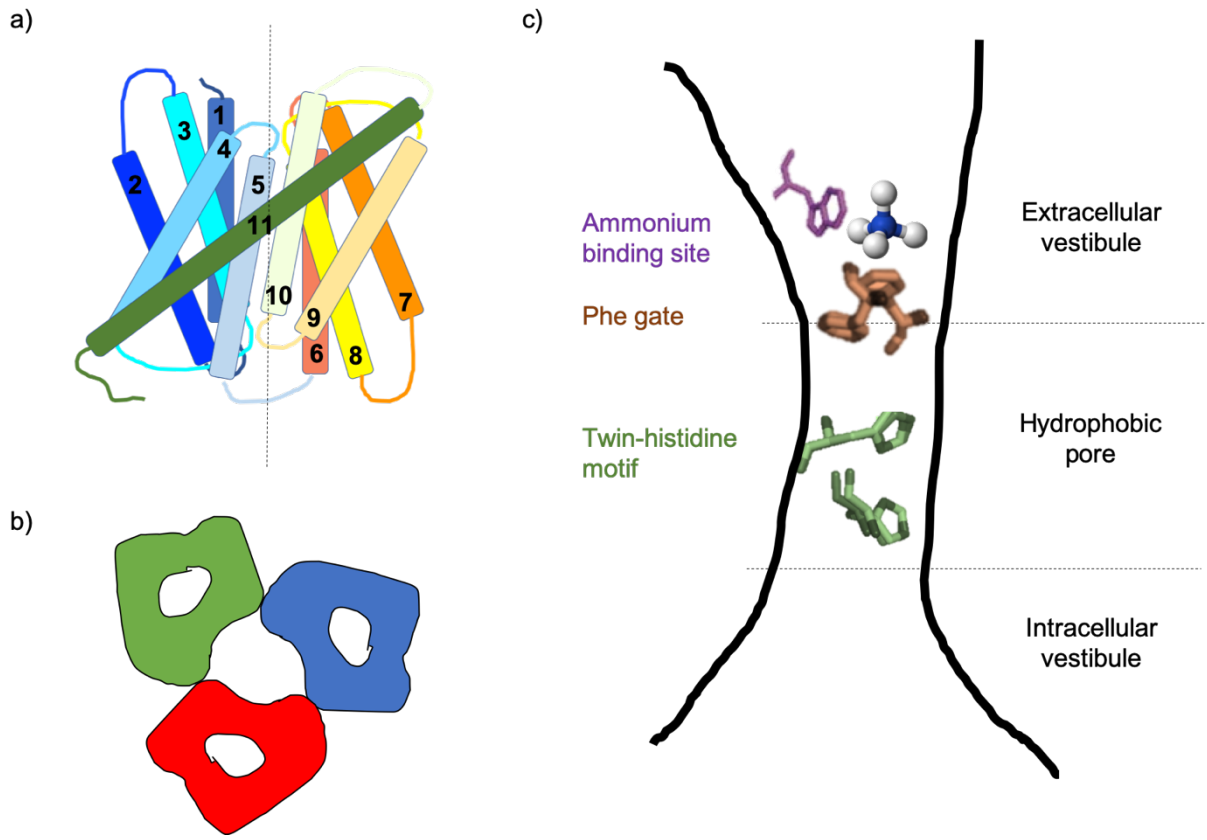

Figure 2: Summary of ammonium transporter features. *a) Cartoon image representative of monomer pseudo-symmetry. TMDs one to five (blue and cyan) show structural duplication to TMDs six to ten (red, orange and yellow). TMD 11 (green) clamps the symmetrical halves together in AfAmt-1. The black dashed line indicates the interface between the two symmetrical halves and identifies the conducting pore. b) Cartoon image of the trimeric complex. Each monomer (green, blue, or red) contains a conducting pore (white). c) Cartoon image of the conducting pore. A tryptophan residue (purple), conserved within the ammonium binding site is depicted. The Phe gate (orange), at the foot of the extracellular vestibule, blocks the entrance to the hydrophobic pore. Movement of the conserved phenylalanine residues permit ammonium conductance through the pore. Hydrophobic residues line the hydrophobic pore, as do two conserved histidine residues (green). The orientation of the residues depicted may vary between different ammonium transporter orthologues.*

the trimeric form. Equally, the opposite experiment resulted in detection of an LeAmt1;3 trimer suggesting that the N-terminus is important for trimer stability. Site-directed mutagenesis identified two cysteine residues within the N-terminus of LeAmt1;1 which form disulphide bridges between the monomers to stabilise the trimeric complex (Graff *et al.*, 2010). The N-termini of CaMep2 and ScMep2 are also believed to be important in trimer stabilisation. As their N-termini are comparatively longer, than their bacterial orthologues, their extracellular domains are larger. Extracellular loop (ECL) 5 of one monomer interacts with the N-terminus of another monomer. Counterintuitively, the growth of an N-terminal ScMep2 deletion mutant is alike to WT (van den Berg *et al.*, 2016), but the equivalent LeAmt1;1 mutant is non-functional. Therefore, the significance of the N-terminus is unclear (Graff *et al.*, 2010).

N-glycosylation

In RhCG, a hydrophobic region which dwells within ICL1 (loop between TMD0 and TMD1) is concealed by polysaccharide. In non-glycosylated Rh proteins this region is shorter. It is hypothesised that glycosylation may be necessary to defend the longer ICL1 from proteolytic degradation (Gruswitz *et al.*, 2010). ScMep2, but not ScMep1 or ScMep3, is also a glycosylated ammonium transporter. However, mutation to the N4 glycosylation site, to prevent glycosylation, does not impact on any known Mep2 functions (Marini and André, 2000). Hence, the importance of N-glycosylation is ambiguous.

Ammonium binding site

Electron density peaks observed at the foot of the periplasmic vestibule of EcAmtB suggested that this site was occupied by ammonium and/or water and could, thus, be a putative substrate binding site. Aromatic side chains of two phenylalanine residues (F103 and F107), where F107 is a member of the Phe gate, and a tryptophan residue (W148), which is conserved between the fungal Meps and Amts, surround this site. Furthermore, the hydroxyl group of serine 219 was found to be in close enough proximity to form a hydrogen bond with the recruited NH_4^+ (Zheng *et al.*, 2004). Similar structural studies and molecular simulation studies are consistent with this being the NH_4^+ binding site. π-cation interactions are proposed between the charged ion and the aromatic side chains of F107 and W148 and less frequently with F103 (Khademi *et al.*, 2004) (Wang *et al.*, 2012). Structural studies into the fungal Meps are also consistent with the ammonium binding site being located at the equivalent position.

However, minimal differences between the bacterial Amt ECLs and the ECLs in ScMep2 and CaMep2 cause the ammonium binding site to be more prominent in the fungal Meps (van den Berg *et al.*, 2016). Dissimilar to the Meps and Amts, RhCG lacks this conserved tryptophan in the equivalent location but instead possesses an acidic glutamate (E166) residue that is alternatively postulated to bind NH_4^+. In addition to a putative NH_4^+ recruitment site on the extracellular side of the transporter, other acidic residues, D218, D27 and E329, on the intracellular side are hypothesised to serve the same purpose to provide a different path for NH_4^+ entry. Specifically, these acidic residues are located on the shunt. This is a region which is conserved throughout human Rh glycoproteins but not with other Mep/Amt proteins. The shunt leads from the cytosolic vestibule, which is polar and hydrated, to the horizontal peripheral surface. This region of the shunt, which makes contact with lipid hydrocarbons, is highly hydrophobic and lacking water. In Amt proteins the equivalent space is a closed cavity. It has been hypothesised that the shunt may provide a different pathway for NH_4^+ to enter or for the transported substrate to be delivered (Gruswitz *et al.*, 2010). Nonetheless, ammonium binding sites located on the extracellular side are common to all members of the Mep/Amt/Rh family and this is consistent with NH_4^+, as opposed to NH_3, being the recruited molecule (**Figure 2c**).

The Phe gate

The Phe gate is composed of two conserved phenylalanine residues at the interface of the extracellular vestibule and the hydrophobic pore. In EcAmtB, the phenyl ring of F107 is stacked above F215 which occludes the pore blocking subsequent substrate transport (Zheng *et al.*, 2004). As this region is 1.2 Å in diameter it is postulated that the side chains of the Phe gate move dynamically to allow ammonium conductance through the pore (Khademi *et al.*, 2004). The same mechanism is projected for the side chains of F96 and F204 in AfAmt-1 which are similarly stacked. Elevated B factors, the extent to which electron density is dispersed, at this location is indicative of possible movement by the Phe gate alike with EcAmtB (Andrade *et al.*, 2005). In RhCG, the upper F130 does not block the pore and is positioned perpendicular to F235. This F130 conformation is likely favoured because a neighbouring submerged aspartate residue (D129) is hydrogen bonded to adjacent residues in the adjoining monomer. The restricted movement in D129 is hypothesised to hamper F130 mobility preventing obstruction of the pore at this location. However, F235 does block the pore. Small gaps on either side of the F235 side chain could provide the freedom for F235

motion which is required for ammonium to transverse the pore (Gruswitz *et al.*, 2010). Translocation through the pore has been found to be relatively slow, therefore, transient alterations in the Phe gate may be important in limiting the entry rate into the pore (Zheng *et al.*, 2004) (**Figure 2c**).

The hydrophobic pore

The pore of AfAmt-1 is highly hydrophobic as identified by pressurising crystals with the noble gas xenon. Xenon binding sites, within the channel, are located at the Phe gate, near the twin histidine motif and at the interface between two monomers of the trimer (**Figure 2c**). Furthermore, xenon was found to bind to a large hydrophobic pocket residing on the cytoplasmic side of a membrane spanning zone of the protein (Andrade *et al.*, 2005). Similar regions are documented in EcAmtB (Khademi *et al.*, 2004) (Zheng *et al.*, 2004). Large internal hydrophobic regions are typically associated with active transporters, to allow for conformational change, rather than passive transporters or channels. Therefore, this region may be required for AfAmt-1 to undergo conformational change. In support of this notion, the amino acid sequence is 12.9 % glycine. Glycine residues increase flexibility within a protein and, thus, favour a motile structure (Andrade *et al.*, 2005). An important question within the field is whether these proteins are more like channels rather than transporters.

The twin-histidine motif

Within the hydrophobic pore is the twin-histidine motif (**Figure 2c**). In EcAmtB, the imidazole rings of the adjacent H168 and H315 are orientated towards the interior of the pore. Their alignment suggests that their δ nitrogen atoms form a bond with one another. Their ε nitrogen atoms have additionally been proposed to be important for their transport function. Moreover, mutation of the first conserved histidine in ScMep2 to alanine abolishes transport function (Rutherford *et al.*, 2008a) (Javelle *et al.*, 2006). In human RhD and RhCE, both histidines are substituted and do not transport (Westhoff and Wylie, 2006). A distinguishing feature between ScMep2 and its two other homologues is the twin-histidine motif. The first conserved histidine is replaced with glutamate in ScMep1 and ScMep3, however, unlike in RhD and RhCE, this does not abolish transport. These homologues instead possess a higher capacity for transport but lower affinity for ammonium than ScMep2 (Marini *et al.*, 1997). Thus, the presence of the twin-histidine motif, as opposed to the glutamate-histidine motif, may be crucial in determining the affinity and capacity of the transporter.

Interestingly, dissimilar to bacterial AmtB, which was crystallised in an open conformation, eukaryotic Mep2 was crystallised in a closed conformation. The closed conformation is the result of a two-tier channel block (**Figure 3**). Firstly, the hydroxyl group of a conserved tyrosine residue (Y53) is hydrogen bonded to the latter histidine of the twin-histidine motif as a result of the ICL1 being moved inwards. In addition to this inward position of ICL1 this loop is longer than the bacterial versions due to the unwinding of TMD2 at the cytoplasmic end. This is not the consequence of amino acid insertions within ICL1 (van den Berg *et al.*, 2016). The equivalent tyrosine residue in the bacterial orthologues is rotated approximately 4 Å away resulting in the open conformation of the transporters (Wang *et al.*, 2012). Secondly, the position of the region responsible for linking the pseudo-symmetrical halves of Mep2, ICL3, is altered by approximately 10 Å, with respect to the bacterial orthologues, resulting in the closure of the channel on the cytoplasmic side. In support of the closed structure, no density corresponding to ammonium, or water, was identified near to the twin-histidine motif within the hydrophobic conducting pore. Additionally, the C-terminal region (CTR) in ScMep2 and CaMep2 is distanced with respect to the bacterial Amts. This incurs fewer connections between the CTR with the rest of the transporter (van den Berg *et al.*, 2016). In the bacterial transporters the CTR is tightly docked onto TMDs one to five (Severi *et al.*, 2007). Specifically in AfAmt-1, D381 interacts with the oppositely charged N-terminal end of TMD2. D381 is the terminal residue of the ExxGxD motif which is located within the CTR (van den Berg *et al.*, 2016). Mutations to residues within the ExxGxD motif, which is conserved, have been found to generate inactive transporters (Severi *et al.*, 2007) (Loque *et al.*, 2007). Being in the centre of the transporter this interaction is proposed to maintain the open conformation of the trimer. Furthermore, tyrosine 390 in AfAmt-1, located after the conserved ExxGxD motif, is hydrogen bonded to the first conserved histidine of the twin-histidine motif which dwells at the latter end of ICL3. Arginine 370, residing at the start of the CTR is hydrogen bonded to other residues at the opposite end of the ICL3 in AfAmt-1. AtAmt-1;1 modelling studies have also identified similar interactions, thus, interactions between the CTR and ICL3 appear to be conserved throughout Amt proteins, which are open (Loque *et al.*, 2007), but not in the purified Meps, which are closed. Thus, ICL3-CTR interactions could be the distinguishing feature between open and closed transporters.

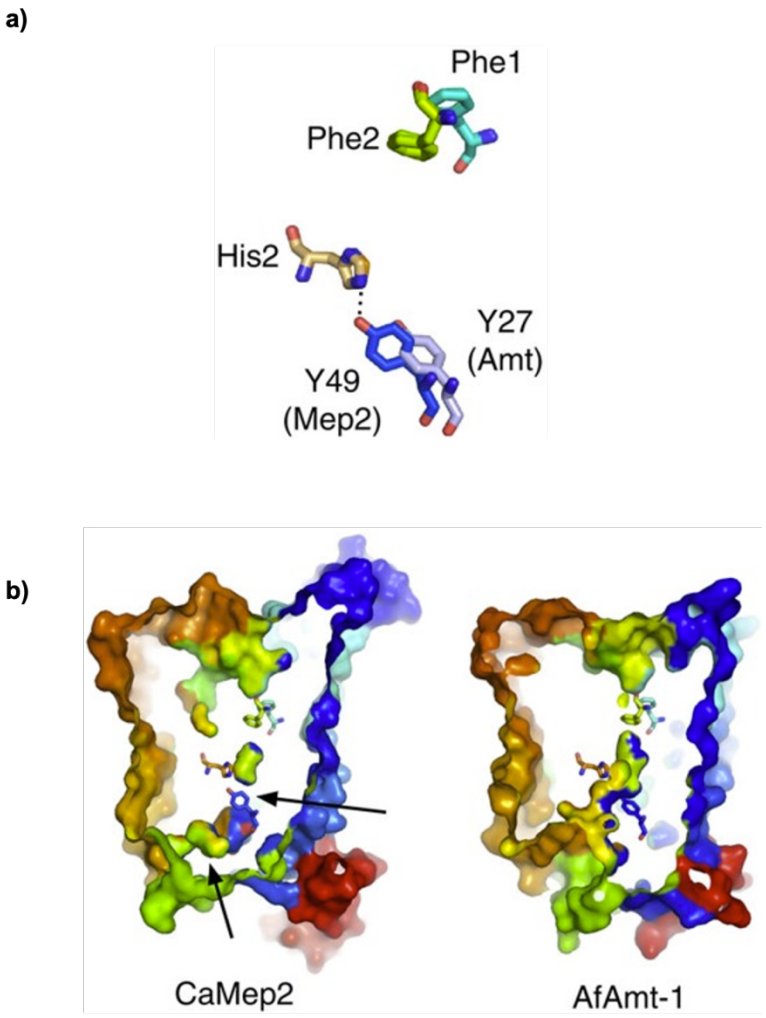

Figure 3: Two tier channel block in Mep2. *a) Archaeoglobus fulgidus Amt-1 and Candida albicans Mep2 are superimposed. The Phe gate is depicted above the conserved twin-histidine motif and conserved tyrosine residue. The latter residue forms a hydrogen bond with the ε_2 nitrogen atom on the second histidine in Mep2. b) The two tier channel block in CaMep2 is indicated by the arrows. Surface views of the channel are shown for both CaMep2 (left) and AfAmt1-1 (right). Figure adapted from (van den Berg et al., 2016).*

In most prokaryotic organisms AmtB is found in an operon with GlnK which is a cellular nitrogen sensor belonging to the P_{II} protein family (Thomas *et al.*, 2000). GlnK is a trimeric complex which possesses a disordered loop (T-loop) projecting from the upper surface (Xu *et al.*, 1998). During nitrogen starvation, a tyrosine residue (Y51), located at the summit of the T-loop, is uridylated (Atkinson and Ninfa, 1998) (Atkinson and Ninfa, 1999). A mutation to this residue, which inhibits uridylation, results in AmtB and GlnK being permanently bound together. This mutation mimics the situation during ammonium sufficient conditions when the intracellular glutamine pool increases leading to GlnK becoming deuridylated (Javelle *et al.*, 2004). Glutamine is an inhibitor of uridyltransferase activity (Jiang *et al.*, 1998). Binding of GlnK to AmtB prevents the transport activity of AmtB. Therefore, Glnk, in its deuridylated state, is a negative regulator of AmtB transport activity (Javelle *et al.*, 2004). Using a homology model of GlnB-1 (GlnK homologue in *A. fulgidus*), based on the EcGlnK crystal structure, GlnB-1 is predicted to insert its T loops into the cytoplasmic side of AfAmt-1 to form a tight complex. Both interacting surfaces are complimentary to one another; as is the positive charge on the cytoplasmic side of AfAmt-1 and the negative electrostatic surface potential of GlnB-1. Notably, the main region of AfAmt-1 which is docked to GlnB-1 is disordered in EcAmtB but not in AfAmt-1 (Andrade *et al.*, 2005). Although Amts have been crystallised in an open conformation they do not freely allow ammonium conductance.

Eukaryotes do not possess an orthologue to GlnK and hence recruit different mechanisms to regulate activity. In *A. thaliana*, phosphorylation of threonine 460, in the CTR of one AtAmt1;1 monomer, is proposed to induce a conformational change which evokes a simultaneous closure of the trimer. This closure reduces ammonium uptake by the roots of the plant (Lanquar and Frommer, 2010). On the contrary, phosphorylation of serine 457 in the CTR of ScMep2, by Npr1 (Nitrogen Permease Reactivator) kinase, is critical for ScMep2 transport activity. Interestingly, this residue is located far from the channel exit and is the last residue which possesses electron density; the rest of the CTR is disordered. The hydroxyl group of serine 453 is 3-4 Å away from the carbonyl atoms of three other negatively charged residues in CaMep2, hence, forming an electronegative pocket within the structure. Mutation of this crucial serine to glutamate, to mimic the phosphorylation event, and mutation of the preceding arginine residue to glutamate, to increase the negative charge, resulted in a large conformational change in the CTR, supposedly as a consequence of electrostatic

repulsion. Moreover, glutamic acid residues 420 and 421, which were in close proximity to the serine, became disordered. During molecular dynamic simulations these residues persistently interacted with serine 453 in the WT protein, however, in the phospho-mimicking (DD) mutant the sides chains of R452D and S453D become distanced throughout the simulation abolishing the interaction observed in the WT version. Glu421 is within the conserved ExxGxD motif (van den Berg *et al.*, 2016). Mutation of the glycine residue within the ExxGxD motif in either EcAmtB or AtAmt-1;1 generates an inactive transporter. This may be because the CTR in these transporters is tightly docked onto their N-terminal half (Severi *et al.*, 2007) (Loque *et al.*, 2007). Mutation of the glycine residue in EcAmtB and AfAmt1-;1 may prevent the tight interactions between the CTR and the N-terminal side of the transporter and, hence, lock the trimers in a closed conformation. As the CTR has moved away in the WT Mep2 transporters, in comparison to the bacterial orthologues, the CTR makes fewer connections with the rest of the transporter, therefore, potentially resulting in their closed conformation (van den Berg *et al.*, 2016).

Comparison of the positions of the CTR and ICL1/ICL3 between the open and closed structures and consideration of the conformational changes observed within the DD mutant directed van den Berg *et al.*, (2016) to propose the phosphorylation based model of Mep2 opening. In its inactive, non-phosphorylated and closed state, the CTR and ICL3 are distant from one another. Upon phosphorylation, the region around the ExxGxD motif undergoes a conformational change to overcome the electrostatic repulsion. However, the conserved tyrosine and latter histidine, of the twin-histidine motif are still hydrogen bonded together. Thus, the transporter is still in a closed conformation. It is proposed that the CTR undergoes a subsequent conformational change, which is predicted to allow the CTR to interact with the ICL3, resulting in Mep2 being in an open state (**Figure 4**) (van den Berg *et al.*, 2016) similar to the open bacterial Amts. This may disrupt the hydrogen bond between the second conserved histidine and conserved tyrosine. As conformational change would not be required by the bacterial Amts, it may be that these transporters are more like channels, whereas the fungal Meps are more characteristic of active transporters. However, it is equally possible that all members of the Mep/Amt/Rh family are indeed open or closed, but the crystallisation procedure may favour one conformation more than the other.

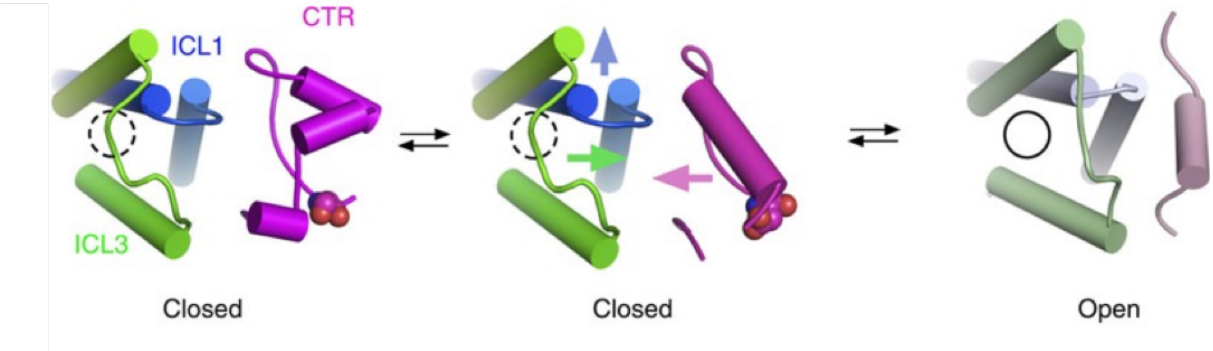

Figure 4: Model for phosphorylation based regulation of Mep2. *Mep2 is not phosphorylated (first panel). ICL3 (green) is blocking the channel exit (dashed circle). Mep2 phosphorylation in the CTR (magenta) (second panel) causes a conformational change around the ExxGxD motif. This is hypothesised to cause the CTR to interact with the inward-moving ICL3 opening the channel (sold circle) (third panel). Figure adapted from (van den Berg et al., 2016).*

Transport activity by ScMep1 and ScMep3 is regulated by Npr1 kinase. This may mirror the regulation provided by the P_{II} protein family in prokaryotes. Additional deletion of Amu1 (Ammonium Uptake), also known as Par32 (Phosphorylated After Rapamycin), to a strain lacking Npr1 kinase, complements the growth defect, of the strain, on low ammonium but makes the strains susceptible to toxic concentrations of methylammonium. Moreover, when *npr1Δ* cells are only expressing *MEP1* or *MEP3*, but not *MEP2*, the additional loss of *AMU1* restores the ability of the proteins to transport while reconstitution of Amu1 does not. Amu1 is phosphorylated by Npr1 kinase during poor nitrogen supply, such as proline, or during limiting ammonium conditions and is primarily cytosolic. When Npr1 kinase is lacking, Amu1 is primarily localised to the plasma membrane which is characteristic of its location during ammonium sufficient conditions or after glutamine supplementation. $Amu1^{phos}$, a mutant in which its nine putative phosphorylation sites have been substituted with alanine, was partially directed to the plasma membrane despite the mutant being less phosphorylated that WT Amu1 in the presence of Npr1 kinase. This suggested that the phosphorylation state of Amu1 could be linked to its cellular location. In co-immunoprecipitation experiments, Mep1 and Mep3 were co-immunoprecipitated with Amu1 suggesting that Amu1 forms a complex with Mep1 and Mep3 to inhibit ammonium flux. Thus, Amu1 was hypothesised to act as a plug, much alike with GlnK, or to act as a scaffold to direct another, as yet unidentified, negative regulatory protein of Mep1 and Mep3 (Boeckstaens *et al.*, 2015). If analogous to GlnK, Amu1 could be physically interacting with the C-terminal end of Mep1 and Mep3 to regulate their transport activity. Interactions between the CTR and the rest of the transporter appear to be important for an open structure (Andrade *et al.*, 2005) (Severi *et al.*, 2007) (Loque *et al.*, 2007) (van den Berg *et al.*, 2016). The structure of ScMep1 and ScMep3 has thus far not been solved, but if Amu1 is acting as a plug, perhaps ScMep1 and ScMep3 would be crystallised in the open conformation similar to the Amt proteins.

1.2.2 *The transported substrate*

The identity of the transported molecule is still under debate. The following species have been proposed: NH_3, NH_3/H^+ cotransport, or NH_4^+, where the latter two and former species represent electrogenic and electroneutral transport respectively (Wang *et al.*, 2012). It was originally accepted that EcAmtB transported NH_3 and, hence, transport was regarded as electroneutral. This conclusion was made because the

investigators observed no conformational change in the transporter upon conductance of ammonium, or the non-metabolisable analogue methylammonium, and they identified the conducting pore as being highly narrow, and hydrophobic, consistent with NH_3 being the substrate. Furthermore, in an assay which quantified the influx of ammonia into 5-carboxy fluorescein ((CF), pH-sensitive dye) loaded AmtB proteoliposomes, or protein free liposomes, a rise in internal pH was observed when the AmtB proteoliposomes were mixed with 5 mM ammonium chloride (NH_4Cl). This rise was 10-fold quicker than the liposomes which lacked AmtB. This initial pH rise reflected the influx of NH_3 which acquired a proton from the water in the cytosol to generate NH_4^+ (Khademi *et al.*, 2004). In CF loaded RhCG proteoliposomes a rise in internal pH was also observed indicating that NH_3 and not NH_4^+ was being transported (Gruswitz *et al.*, 2010). When AmtB proteoliposomes were placed in 250 mM sucrose water efflux by the AmtB proteoliposomes and liposomes were equivalent leading to the conclusion that AmtB is not a water conductor. Conductance of NH_3 over NH_4^+ was discussed to be the more favourable substrate as NH_4^+ is similar in size to potassium ions. If AmtB was a conductor of NH_4^+ it would likely additionally leak potassium ions which would impact on the membrane potential. Although Khademi *et al.*, (2004) concluded that NH_3 was the transported substrate, NH_4^+ was accepted as the molecule initially recruited to the transporter (Khademi *et al.*, 2004) as did Zheng *et al*., (2004). At the conserved twin-histidine motif the adiabatic free energy profile identified an electrostatic barrier. Therefore, it was suggested that diffusion of NH_3 would be favoured over the passage of NH_4^+ and, hence, NH_4^+ deprotonation would be required with the proton leaving on the periplasmic side (Zheng *et al.*, 2004).

Several years later, *Wang et al*, contradicted this idea of electroneutral transport and suggested that this was an electrogenic process. Molecular simulation studies confirmed that NH_4^+ was stable in the putative ammonium binding site. The authors designated this site as S1. A site designated as S2 is composed of F215, W212 and H168 (the first histidine of the twin histidine motif) and directly proceeds the S1 site. The side chains of F107 and F215, the Phe gate, were motile during simulations which were postulated to bind NH_4^+ to direct the molecule from S1 to S2. During the molecular simulation studies water molecules were present below S2 and NH_4^+ was stably hydrogen bonded to H163. Quantum mechanics (QM) simulations identified H168 hydrogen bonded to NH_4^+ or NH_3 (as a result of NH_4^+ deprotonation) hydrogen bonded to protonated H168. Furthermore, water molecules were more distanced from

the twin histidine motif compared to in the molecular simulations. Protonated H168 was observed to relay the proton, acquired from NH_4^+ deprotonation at the S2 site, to H318 resulting in a charge-delocalised construct. Adaptive biasing force simulations identified a low energy barrier which would favour NH_3 diffusion, potentially aided by one water molecule through S3, the region between S2 and S4, to the next site S4. Upon NH_3 reaching the S4 site, composed of H318, NH_3 accepted the relayed proton to reconstitute NH_4^+. The protonation states of the conserved histidine motifs are proposed to be reset by a water chain composed of four to five water molecules (Wang *et al.*, 2012) (**Figure 5**). Utilisation of solid-supported membrane (SSM)-based electrophysiology, where proteoliposomes containing AfAmt-1 covered a phosphatidylcholine monolayer coating a gold electrode, confirmed that transport by AfAmt-1 is indeed electrogenic. Perfusion of the sensor with 300 mM ammonium initiated a rapid increase in current to a maximum of 2.2 nA followed by a slower decrease in current to baseline. The initial increase in current is consistent with the membrane potential being more positive inside the vesicles than outside. The subsequent decrease is consistent with a decrease in the initial driving force which incurs a decrease in the transport rate (Wacker *et al.*, 2014). Furthermore, deprotonation was subsequently confirmed by exploiting N isotope discrimination experiments using Mep/Amt/Rh proteins expressed in yeast. Cells expressing these proteins exhibit internal ^{15}N rather than ^{14}N depletion, relative to the external ammonium medium, which is consistent with cells transporting NH_3. NH_4^+ containing ^{14}N is favoured for deprotonation over an NH_4^+ containing ^{15}N (Ariz *et al.*, 2018). Thus, Amt proteins recruit NH_4^+ which is deprotonated to NH_3. NH_3 gas, along with the excess proton, transverse the pore before reconstituting NH_4^+ on the cytoplasmic side.

In a homology model of the tomato ammonium transporter, LeAmt1;1, the equivalent residues which are predicted to recruit incoming NH_4^+ have been predicted to serve the same purpose. *Xenupus oocyctes* expressing LeAmt1;1, which have a resting membrane potential of +4±1 mM, were incubated with 1 mM carbon 14 labelled methylammonium ([^{14}C]-MeA which can exist as $H_3{}^{14}C\text{-}NH_3^+$/$H_3{}^{14}C\text{-}NH_2$). According to Avogadro's constant each $H_3{}^{14}C\text{-}NH_3^+$ molecule transported would generate a current of -14.4±2.4 nA. The recorded inward current recorded by the LeAmt1;1 expressing oocytes was -12.5 nA. This current was LeAmt1;1 dependent, hence, the authors suggested that approximately 100 % of the [^{14}C]-MeA transported was in the

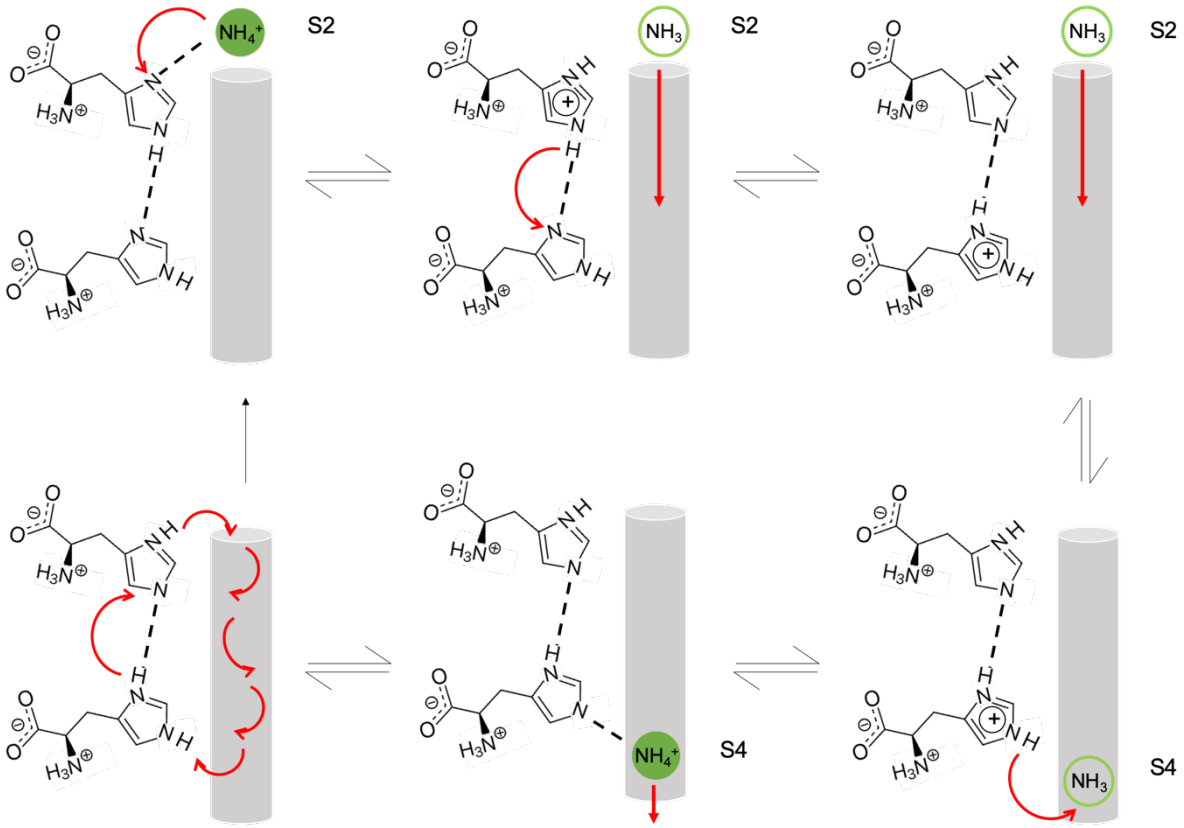

***Figure 5: Diagram of ammonia transport through AmtB**. The twin histidine motif is depicted on the left hand side of the pore (grey tube). NH_4^+ is deprotonated at the S2 site. NH_3 gas diffuses through the pore to the S4 site, while the proton is relayed from the first conserved histidine to the second conserved histidine. NH_3 gas is re-protonated using the relayed proton at the S4 site. Proton transfer through a water chain resets the protonation state of the twin histidine motif. Straight and curved red arrows represent diffusion and proton transfer respectively. Figure adapted from (Wang et al., 2012).*

charged form. However, when considering the errors associated with each value they could not reject the possibility that some $H_3{}^{14}C\text{-}NH_2$ could transverse the pore. In support of NH_4^+ being the transported substrate, inwards currents of -150 nA, and maintained acidification of the cytosol was observed when the BCECF-loaded LeAmt1;1 expressing oocytes (BCECF is a pH sensitive due) were voltage clamped at -80 mV and exposed to 500 μM ammonium (Mayer *et al.*, 2006).

Dissimilar to the Amts, transport through human Rh proteins is deemed electroneutral. Potential mean force (PMF), calculated from QM and molecular mechanics (MM) simulations, show that a NH_4^+ deprotonation event at the first histidine of the twin histidine motif (H185), where the excess proton is transferred to H185, is likely. Classical simulation studies showed that following deprotonation the excess proton is relocated back to the extracellular space. This involves indirect hydrogen bonding between H185 and an above aspartate residue (D177). This hydrogen bond connection is dependent on adjacent water molecules and a separating serine residue (S181) and could plausibly facilitate the transfer of the excess proton to the extracellular side. QM and MM simulations showed that the excess proton is either relayed from H185 to a water molecule to S181 and finally to D177, or the excess proton is relayed from H185 to a water chain and finally to D177. In the latter scenario, S181 is proposed to maintain D177 in the correct position allowing the formation of the bridging water chain. A similar proton route to the one confirmed in AmtB was rejected in RhCG because no water chain was found to form in the pore during simulation studies. If the proton was relayed from H185 to H344, which forms a charge delocalised structure, a water chain would be required in the pore to reset the protonation states of the histidine-dyad. Free energy perturbation (FEB) calculations showed that release of the excess proton from D177 to the extracellular solution was favourable. Moreover, the authors hypothesised that the excess proton may react with NH_3 in the extracellular solution to form NH_4^+. Diffusion of NH_3 gas through the pore is more favourable than back-diffusion to the extracellular space. Thus, transport through RhCG is overall electroneutral (Baday *et al.*, 2015).

As recruitment of NH_4^+ followed by deprotonation appears to be a preserved mechanism the pathway the proton follows may be the distinguishing factor in whether transport by the Mep/Amt/Rh protein family is electrogenic (as discussed for AmtB) or electroneutral (as described for RhCG). Moreover, RhCG does not possess the

conserved tryptophan, associated with NH_4^+ recruitment by Mep/Amt proteins, and the Phe gate is orientated differently creating less obstruction at the entry to the pore (Gruswitz *et al.*, 2010). Perhaps these features are characteristic of electroneutral transport and can distinguish between channels and transporters within the Mep/Amt/Rh protein family. Transport through the fungal Mep2 proteins has not been confirmed as being electrogenic or electroneutral. However, as the position of the residues lining the sites, in Amt proteins, important for NH_4^+ recruitment, deprotonation and re-protonation are similar to the position of the residues in eukaryotic Mep2 proteins, the same electrogenic mechanism, which couples NH_3 and proton symport, may occur in fungal Mep2 (van den Berg *et al.*, 2016) (Wang *et al.*, 2012) (Wacker *et al.*, 2014) (Ariz *et al.*, 2018). Despite similarities between the positions of the functional residues, Mep2 proteins were crystallised in a closed conformation suggesting that conformational changes are required to open the channel (van den Berg *et al.*, 2016) and, thus, are more characteristic of active transporters rather than channels. Amt proteins were originally regarded as gas channels (Zheng *et al.*, 2004) (Khademi *et al.*, 2004). Conversely, the Amt proteins may be more characteristic of active transporters as small conformational changes may be required to allow passage of NH_4^+ through the Phe gate, to the S2 site for deprotonation, and as the excess proton is simultaneously transported through the pore in an electrogenic process (Wacker *et al.*, 2014) (Wang *et al.*, 2012) (Ariz *et al.*, 2018). The discrimination between ammonium transporters as channels or transporters is still a topic of debate.

1.3 Regulation of fungal Meps

In order for nitrogen to be utilised from different sources, but not become cytotoxic, different uptake mechanisms are recruited. This is referred to as nitrogen catabolite repression (NCR). When nitrogen levels are limiting, whether this be due to low levels of ammonium or the presence of non-preferred nitrogen sources, the NCR target genes are upregulated (Magasanik and Kaiser, 2002). These encompass approximately 90 target genes in the budding yeast *Saccharomyces cerevisiae*, including the Meps (Methylammonium Permeases), and Gap1 (General Amino Acid Permease), which facilitate the transport of ammonium and amino acids across the membrane respectively (Broach, 2012). When sufficient levels of the preferred sources of nitrogen become available these target genes are repressed. The master

regulator of cell growth (TORC1) is responsible for relaying this nutrient availability signal (Cardenas *et al.*, 1999).

1.3.1 *Regulation by TOR*

TORC1 is a member of the TOR (Target Of Rapamycin) pathway (Loewith *et al.*, 2002). TOR is a conserved serine/threonine kinase which combines the energy status of the cell with the availability of nutrients to regulate cell growth (Heitman *et al.*, 1991). In mammalian systems, mTOR controls protein synthesis and autophagy (Kim *et al.*, 2011) and is additionally associated with dysregulation, including cancers (Bar-Peled *et al.*, 2013), neurodegeneration and type 2 diabetes (Khamzina *et al.*, 2005). In *S. cerevisiae*, TORC1 is composed of TOR1 or TOR2, Kog1, Lst8 and non-essential Tco89 (Loewith *et al.*, 2002). Supplementation of amino acids activates TORC1 which promotes anabolic processes, such as ribosome biogenesis, but represses catabolic processes, such as autophagy and nitrogen assimilation (Barbet *et al.*, 1996) (Noda and Ohsumi, 1998) (Loewith and Hall, 2011). TORC1 inactivity occurs during nitrogen or amino acid starvation. Moreover, treatment with rapamycin renders TORC1 inactive (Cardenas *et al.*, 1999); rapamycin somewhat mimics nitrogen starvation (Barbet *et al.*, 1996). TORC1 activity is dependent on the GTP/GDP status of the Rag GTPase heterodimer Gtr1/Gtr2 which is regulated by guanine exchange factors (GEFs) and GTPase-activating proteins (GAP). Gtr1/Gtr2 is anchored to the vacuolar membrane by the EGO complex which is composed of Ego1, Ego2 and Ego3 (Zhang *et al.*, 2012). Ego1 and Ego2 form a weak interaction with the C-terminal roadblock domain of Gtr1 but not Gtr2 (Kira *et al.*, 2016). Dissimilar to mTORC1, which is recruited to the lysosome for activation when the RAG heterodimer is in its active state (Sancak *et al.*, 2010), yeast TORC1 is constantly maintained at the membrane of the vacuole independent of the GTP/GDP status of Gtr1/Gtr2 (Kira *et al.*, 2016). In the presence of amino acids, Gtr1 is bound to GTP and Gtr2 is loaded with GDP to form the active heterodimer which binds via Kog1 to activate TORC1 (Sancak *et al.*, 2008). Vam6 has been proposed to be the GEF which exchanges GDP for GTP on Gtr1 (Binda *et al.*, 2009). During amino acid and nitrogen starvation, the SEACIT complex (Seh1-associated sub complex inhibiting TORC1), composed of Npr2, Npr3 and Iml1, binds to Gtr1, via the catalytic Iml1 subunit, to activate its GTPase activity hydrolysing GTP to GDP. The SEACIT complex is, thus, the GAP of Gtr1. When Gtr1 is bound by GDP, and Gtr2 is loaded with GTP, a conformational change occurs in the heterodimer which

weakens its interaction with TORC1 and hence inactivates TORC1. SEACIT is itself negatively regulated by the SEACAT complex (Seh1-associated sub complex activating TORC1), composed of Sec13, Seh1, Sea2, Sea3 and Sea4 (Panchaud *et al.*, 2013) (**Figure 6**).

The type of TORC1 activation is dependent on the distinct amino acids available. In response to poor nitrogen sources, such as leucine, TORC1 activation is transient and Gtr1 dependent; a lack of growth is observed in a *gtr1Δ* mutant on leucine. On the contrary, the *gtr1Δ* mutant, and the *vam6Δ* mutant, grow on preferred nitrogen sources such as glutamine. Furthermore, TORC1 activation is maintained in response to accumulation of internal glutamine (Stracka *et al.*, 2014). Therefore, it was concluded that a Rag GTPase independent mechanism must exist to sustain TORC1 activity. Recently, Pib2 has been found to interact with TORC1 via its E motif. This interaction is mutually exclusive to TORC1's interaction with Gtr1/Gtr2 as identified by pull-down experiments. As radioactively labelled glutamine has been found to bind directly to Pib2, and because the TORC1/Pib2 complex increases with rising glutamine concentration, Pib2 has been proposed to be an internal glutamine sensor (Ukai *et al.*, 2018).

TORC1 exerts its signalling effect by phosphorylating downstream effectors (Gonzalez and Hall, 2017). One target is Sch9 kinase which contains six TORC1 phosphorylation sites in its C terminus. Through Sch9, TORC1 exerts its regulation of several processes including entry into G0 of the cell cycle (Urban *et al.*, 2007). Another target for TORC1 is the Tap42-PP2A phosphatase which promotes stress resistance, autophagy and nitrogen transport and utilisation. Tap42-PP2A is inhibited by active TORC1 (Loewith and Hall, 2011). A downstream target of Tap42-PP2A is the Npr1 kinase. Upon TORC1 inactivity, Npr1 kinase is weakly phosphorylated and in its active state. Npr1 kinase is responsible for the trafficking and stabilisation of certain transporters at the plasma membrane (Schmidt *et al.*, 1998), including Gap1. Npr1 indirectly prevents the recruitment of Rsp5 to the membrane via the phosphorylation of arrestin-like proteins, which are responsible for the endocytic removal of some transporters (De Craene *et al.*, 2001). In the presence of preferred nitrogen sources both Sch9 and Npr1 kinase are hyperphosphorylated, thus, the phosphorylation status of both proteins can been utilised as a readout for TORC1 activity (Urban *et al.*, 2007)

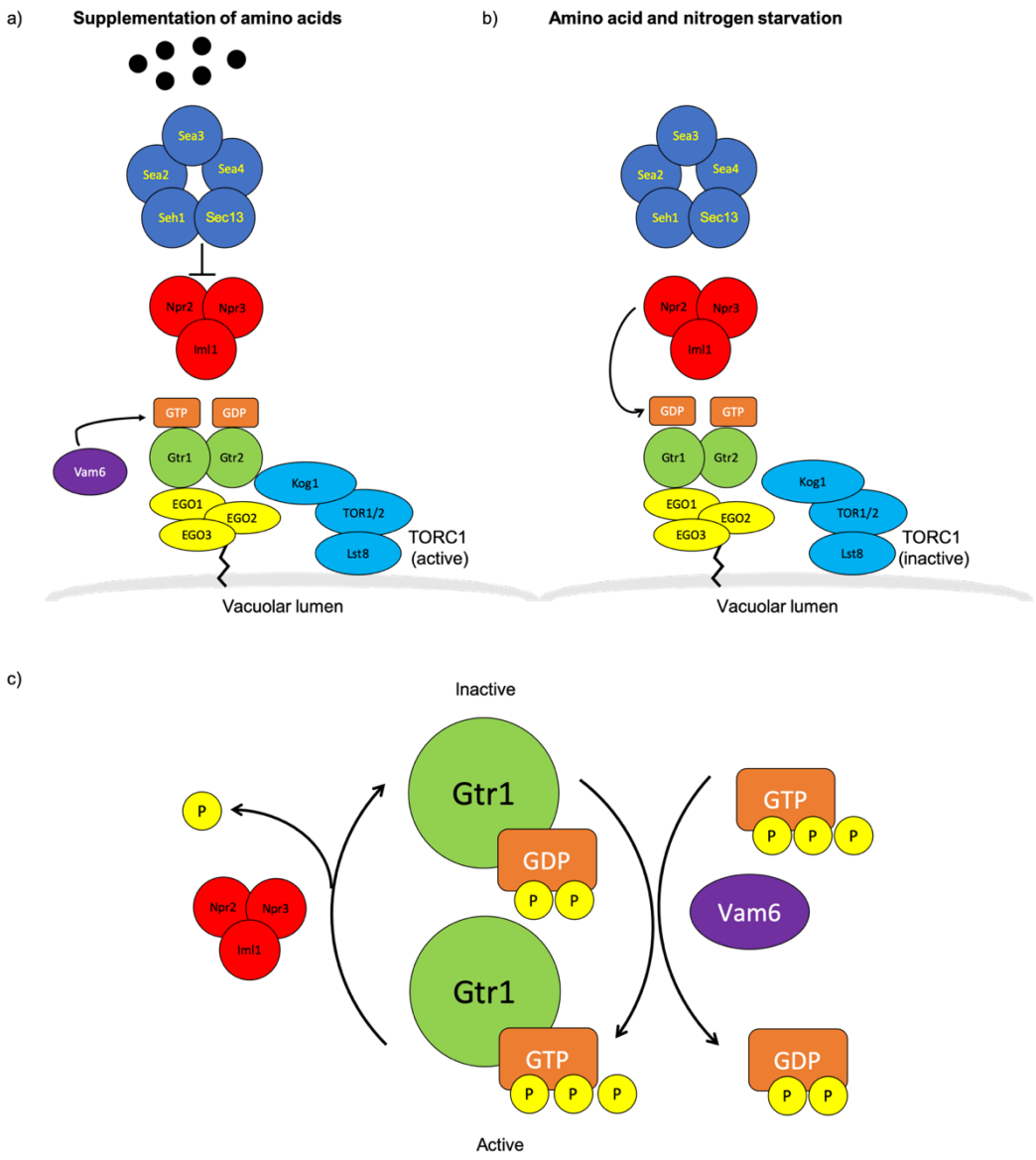

Figure 6: Rag GTPase regulation of TORC1*. a) In the presence of amino acids SEACAT (top blue complex) inhibits the GAP activity of SEACIT (red complex below). The Rag GTPase Gtr1/Gtr2 is in its active state, bound to TORC1 (aqua blue bottom complex) via Kog1. This interaction stimulates TORC1 activity. b) During amino acid or nitrogen starvation SEACIT is not inhibited by SEACAT therefore the Rag GTPase Gtr1/Gtr2 is in its inactive state. This inactive state causes a conformational change which loosens the interaction with TORC1 and therefore inactivates TORC1. In both a) and b) the Roadblock domain of Gtr1 is bound to EGO1 of the EGO complex (yellow complex) which anchors the Rag GTPases to the vacuolar membrane. c). Vam6 acts as the Gtr1 GEF substituting GDP for GTP. SEACIT acts as the Gtr1 GAP. Based on figure by (Panchaud et al., 2013).*

(Schmidt *et al.*, 1998). Specifically for Gap1, when TORC1 activity is sustained, by the uptake of NH_4^+, Gap1 is ubiquitinated before being removed and degraded. However, a Gap1 mutant, which is insensitive to ubiquitination by TORC1, can trigger its own ubiquitination and removal from the membrane following uptake of its substrate. Furthermore, transport of the Gap1 non-metabolisable substrate, β-alanine (β-ala), in proline grown cells triggers ubiquitination of Gap1 and activates TORC1 in a Gtr1/Gtr2 dependent manner as evidenced by phosphorylated Npr1 kinase and Sch9. Hence, TORC1 activation is not dependent on the internal pool of amino acids. Gap1, along with other amino acid permeases, couples amino acid transport with H^+ influx and, thus, relies on the plasma membrane H^+ gradient to function. β-ala uptake by Gap1 is hindered in cells exposed to the protonophore FCCP or when grown in glucose free media, (Saliba *et al.*, 2018), which inhibits the H^+ ATPase Pma1 (Kane, 2016), because both conditions disrupt the plasma membrane H^+ gradient. Fsy1 and Hxt1 are both hexose transporters with only the former coupling hexose transport with H^+ symport. Interestingly, Sch9 phosphorylation is observed with Fsy1 transport but not Hxt transport, suggesting that H^+ influx is the stimulus for TORC1 activation. Equally, H^+ influx elicited solely by the FCCP protonophore is sufficient to activate TORC1 in cells grown in proline medium with limited glucose as evidenced by Npr1 kinase phosphorylation but not Sch9 phosphorylation. A lack of Sch9 phosphorylation was proposed to be attributable to the acidic cytosolic pH, elicited by the protonophore. Although this TORC1 activation was found to be Rag GTPase dependent, sustained FCCP stimulation in *seh1Δ* (SEACAT component) was sufficient to phosphorylate Npr1 kinase, however, this was Pib2 independent. Furthermore, TORC1 activation in response to H^+ influx was found to be Pma1 dependent (Saliba *et al.*, 2018). Under acidic conditions Pma1 is known to be more active (Eraso and Gancedo, 1987) and optimal Pma1 activity requires TORC1 (Mahmoud *et al.*, 2017). Expression of endogenous *PMA1,* but not a truncated orthologue from the tobacco plant (*Nicotiana plumbarginifolia*), $PMA4^{822ochre}$, in a *pma1Δ/pma2Δ* double mutant activated TORC1 despite both transporters coupling H^+ and β-ala uptake and hence having a more acidic cytosol. The authors, therefore, proposed that Pma1 may stimulate a signalling cascade which targets TORC1 upon the cytosol increasing in acidity (Saliba *et al.*, 2018).

TORC1 exerts its regulation on Mep2 via Npr1 kinase. Visualisation of Mep2 by western blot reveals two bands where the slower running, higher molecular weight,

band is sensitive to lambda (λ) phosphatase treatment. In cells lacking Npr1 kinase, or Npr2, only a single faster running, lower molecular weight, band is detected. Hence the higher molecular weight band is the result of phosphorylation by active Npr1 kinase. Activation of Npr1 kinase occurs after inactivation of TORC1 via Npr2, a component of the SEACIT complex, which hydrolyses GTP to GDP on Gtr1. Dissimilar to other permeases, Mep2 localisation, nor its removal from the membrane, are dependent on Npr1. GFP tagged Mep2 correctly localises to the plasma membrane in proline grown cells lacking Nrp1 kinase and remains at this location after glutamine induced Npr1 kinase inactivation in WT cells. Site-directed mutagenesis studies identified serine 457, located within the CTR, to be the Npr1 phosphorylation site. Expression of $Mep2^{S457A}$ in a strain lacking all three ammonium transporters, and Npr1 kinase, fails to restore growth on low ammonium, however, $Mep2^{S457D}$, a phosphomimic mutant, does restore growth (Boeckstaens *et al.*, 2014).

Ethyl methanesulphonate mutagenesis treatment identified mutations which render Mep2 Npr1 kinase independent. Three quarters of the identified suppressor mutations were mapped to ICL3 and the C-terminus tail. A mutant lacking the entire C-terminus ($Mep^{S246stop}$) partially complemented the growth defect of a strain lacking all three ammonium transporters and this was comparable in a strain additionally lacking Npr1 kinase. Thus, the region before the C-terminal tail possesses a basal level of transport which is optimised by the C-terminal tail. The region spanning from the YIPEPIRS motif (residues 450-457 conserved in several Mep2 orthologues), which contains the Npr1 kinase phosphorylation site, to residue T485 forms the autoinhibitory (AI) domain. The $Mep2^{C\Delta 450-485}$ mutant is hyperactive in *mep123Δ/npr1Δ* cells in comparison to *mep123Δ.* Residues 442-449 forms the linker domain. A mutant lacking this linker domain does not fully complement the growth defect of the *mep123Δ* strain but is greater than two fold more active in the *mep123Δ/npr1Δ* strain. The region before the linker domain, designated as the enhancer domain, is required for optimal Mep2 activity in the absence of Npr1. Hence, active Npr1 kinase alleviates Mep2 autoinhibition by phospho-silencing S457 within the AI domain. Npr1 suppressor mutations were highly localised to ICL3 (Boeckstaens *et al.*, 2014) and a single nucleotide polymorphism (SNP) within ICL3 of RhCG has been found to reduce the proteins transport activity. The SNP is postulated to hinder the interaction between ICL3 and the C-terminal tail (Deschuyteneer *et al.*, 2013). Analysis of bacterial Amt protein structures have equally verified that interactions between the C-terminal tail

and the intracellular loops are important for their activation (Neuhauser *et al.*, 2007) (Severi *et al.*, 2007). Thus, the authors proposed that phosphorylation within the AI domain frees the enhancer domain allowing it to interact with ICL3 (Boeckstaens *et al.*, 2014).

Mep2 is highly expressed and active in proline grown cells. However, addition of glutamine to proline grown cells causes Mep2 dephosphorylation and, hence, inactivation. Deletion of *PSR1* or *PSR2,* phosphatase encoding genes, partially protect against Mep2 inactivation while deletion of both provides full protection. Regardless of whether Npr1 kinase is active or not, the Psr1 and Psr2 phosphatases are always effective. The equilibrium between phosphorylation and dephosphorylation is, therefore, imperative for the activity status of Mep2. In times of poor nitrogen supply, the equilibrium is shifted in favour of phosphorylation by the Npr1 kinase. When glutamine is readily available, the equilibrium shifts in favour of dephosphorylation by the Psr1 and Psr2 phosphatases as Npr1 kinase is hyperphosphorylated and in an inactive state (**Figure 7**). How Npr1 switches from its hyperphosphorylated (inactive) state to its weakly phosphorylated (active) state is still unclear (Boeckstaens *et al.*, 2014). Although deletion of the Sit4 phosphatase, a target of Tap42 (Jacinto *et al.*, 2001), is correlated with Npr1 kinase hyperphosphorylation (Di Como and Arndt, 1996) Mep2 is still identified as a doublet by western blot. Furthermore, Mep2 accumulates [^{14}C]-methylammonium similar to WT cells confirming that the transporter is still active suggesting that Sit4 and Npr1 can act in separate pathways (Boeckstaens *et al.*, 2014).

For Mep1 and Mep3, the transport activity is believed to be dependent on the downstream effector Par32 (Phosphorylated After Rapamycin). Originally, Par32 (also known as Amu1) was believed to inhibit the flux of ammonium ions through Mep1 and Mep3 by physically interacting with the proteins to block transport at the plasma membrane (Boeckstaens *et al.*, 2015). This concept has recently been questioned as Par32 function, to reactivate TORC1 after rapamycin treatment, is not impeded when unable to localise to the membrane, suggesting that another mechanism, other than physical interaction with the ammonium permeases, is preventing the conductance of ammonium (Varlakhanova *et al.*, 2018).

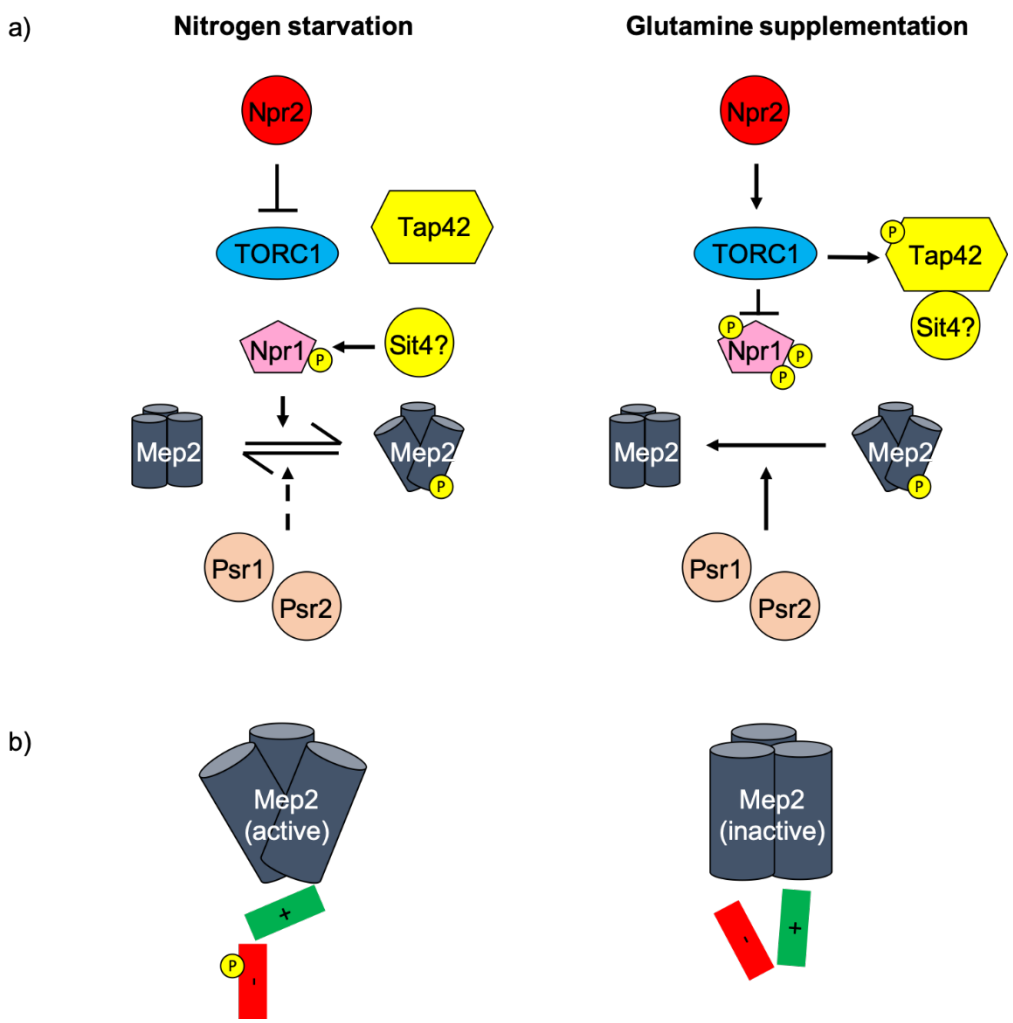

Figure 7: Model of Mep2 activation by Npr1 kinase. *a) During poor nitrogen supply TORC1 is inactivated by Npr2, therefore Npr1 kinase is weakly phosphorylated and free to activate Mep2 via phosphorylation. Upon glutamine supplementation, TORC1 is activated leading to the inactivation of Npr1 kinase. Inactivation of Npr1 kinase may occur via the phosphorylation of Tap42, which inhibits Sit4 dephosphorylation of npr1 kinase, but another additional mechanism likely exists. Mep2 is dephosphorylated by the Psr1 and Psr2 phosphatases. b) Phosphorylation of the Mep2 CTR autoinhibitory domain (red) by Npr1 kinase during poor nitrogen supply allows the enhancer domain (green) to activate the transporter. Upon glutamine supplementation Mep2 is only dephosphorylated by the phosphatases, therefore, the enhancer domain cannot activate the transporter. Based on the figure by (Boeckstaens et al., 2014).*

1.3.2 *Transcriptional regulation of Mep2*

In nitrogen replete conditions transcription of *MEP2* is repressed by NCR. *MEP2* is transcriptionally induced by Gln3 and Gat1 (Scherens *et al.*, 2006) which are TORC1 regulated (Georis *et al.*, 2011) GATA transcription factors specific for NCR genes (Dabas and Morschhauser, 2007). Until most recently the following paradigm for Gln3 regulation was accepted. When nitrogen is readily available Tap42-Sit and Tap42-PP2A are complexed to active TORC1. TORC1, hence, inactivates both phosphatase complexes (Di Como and Arndt, 1996) (Yan *et al.*, 2006). Active TORC1 additionally phosphorylates Gln3 (Bertram *et al.*, 2000), which is bound in a complex to Ure2, to restrict the transcription factor to the cytoplasm (Courchesne and Magasanik, 1988). During nitrogen limiting conditions Tap42-Sit4 and Taqp42-PP2A dissociate from TORC1 (Wang *et al.*, 2003), as TORC1 is inactive, and dephosphorylate Gln3. Gln3 is then freed from the cytoplasmic Gln3-Ure2 complex and re-localises to the nucleus (Beck and Hall, 1999). In the nucleus Gln3 and Gat1 recognise the upstream nitrogen regulated activation sequence (UAS_{NTR}) 5'-GATAAG-3' to activate NCR-sensitive gene expression (Cunningham *et al.*, 1996) (Coffman *et al.*, 1996). Other members of the GATA transcription factor family recognise 5'-WGATAR-3' (W = A/T, R = A/G) (Ko and Engel, 1993). However, in contrast to this model, Sit4 and PP2A have been found to be active in nitrogen replete conditions and Gln3 is more phosphorylated in the nucleus than in the cytoplasm (Tate *et al.*, 2019). Interestingly, <5 % of Sit4 and <2 % of Pph21 (catalytic subunit of PP2A) are documented to be bound to Tap42 respectively (Di Como and Arndt, 1996). Therefore it has been proposed that it is the unbound Sit4 and PP2A that result in Gln3 dephosphorylation under conditions when TORC1 is active (Tate *et al.*, 2019).

1.4 Sensing of ammonium

Unlike Mep1 and Mep3, Mep2 exhibits receptor like properties which allow the transporter to relay the availability of extracellular ammonium into a scavenging, or foraging, response. Hence Mep2 is referred to as a transceptor. In times of limiting ammonium, *S. cerevisiae* cells become elongated and remain physically attached to one another and extend in a polarised fashion. This morphology is designated as pseudohyphal growth and is specifically restricted to ammonium limitation. During

nitrogen starvation, the cells enter the G_0 phase of the cell cycle and arrest growth (Lorenz and Heitman, 1998). Notably, mutations can be made in Mep2 which sustain transport of ammonium but block signalling for the induction of pseudohyphal growth. This uncoupling of functions demonstrates that the physical act of transport by Mep2, rather than internal metabolism of ammonium, is responsible for signalling for pseudohyphal growth. Where Mep2 possesses a conserved twin-histidine motif, proposed to be important for proton relay, a glutamate residue resides at histidine position one in Mep1 and Mep3. In a study where the first histidine in ScMep2 was substituted to glutamate (H191E), to mimic ScMep1, ScMep2 behaved more like ScMep1 as pseudohyphal growth was abolished (Boeckstaens *et al.*, 2008). Interestingly, all the ammonium sensors identified to date possess this conserved twin-histidine motif, suggesting that this is a vital motif for signalling.

1.4.1 *Transceptor regulated morphology*

Dimorphic fungi make the morphological transition from yeast-like growth, where cells divide by budding, to a filamentous growth form (Roberts and Fink, 1994). The filamentous growth form can be split into two modes: the pseudohyphal growth mode and the filamentous growth mode. Pseudohyphal growth, displayed by *S. cerevisiae*, corresponds to cells which do not abscise after cytokinesis and, thus, are non-multinucleate. On the contrary, in the filamentous mode, true-hyphae are multinucleate as they are formed of continuous cells which have extended from the polar tip with each septate containing nuclei. For pathogenic fungi this dimorphic switch can change the growth from saprophytic to pathogenic and, therefore, precedes infection of the target host.

Diploid *S. cerevisiae* cells undergo pseudohyphal growth upon nitrogen limitation, while haploid cells undergo invasive growth under the same conditions (Cullen and Sprague, 2012). Both phenotypes are Mep2 dependent. The MAPK and cAMP-PKA pathways have been implemented in this filamentous mode, where one can compensate for the other, however, the MAPK pathway appears to be most linked to Mep2 (Rutherford *et al.*, 2008a) (Smith *et al.*, 2003). Overexpression of Mep2 in diploid mutants lacking Tpk2, Gpa2, Gpr1 and Ras2, members of the cAMP-PKA pathway, restored pseudohyphal growth. On the contrary, pseudohyphal growth was not restored in the *ste12Δ* mutant. However, expression of $RAS2^{Val19}$ or *STE11-4*, alleles

which constitutively activate the cAMP-PKA and MAPK pathways respectively, or overexpression of *STE12,* restored pseudohyphal growth in a diploid *mep2Δ* mutant. This demonstrated that Mep2 acts above Ste12 in the MAPK pathway or that they operate in analogous mutually dependent pathways (Rutherford *et al.*, 2008a).

The opportunistic fungus, *Candida albicans*, contains two ammonium transporters within its proteome, Mep1 and Mep2 (Biswas and Morschhauser, 2005). In neutral/alkaline pH, *C. albicans* makes the dimorphic switch to form elongated hyphae, an indispensable virulence trait (Biswas *et al.*, 2007). *Ustilago maydis*, the fungal pathogen of maize, also contains two ammonium transporters within its proteome, Ump1 and Ump2 (Smith *et al.*, 2003). Unlike *C. albicans*, *U. maydis* requires acidic pH to transition from budding yeast to a filamentous growth form (Gold *et al.*, 1994), which is formed when yeast-like cells of opposite mating type form a dikaryon (Day and Anagnostakis, 1971). However, despite this discrepancy, both Mep2 and Ump2 complement the growth and pseudohyphal growth defects of *mep123Δ* and *mep2Δ/mep2Δ S. cerevisiae* strains respectively. Mep1 and Ump1 can only complement the growth defect. For both organisms, *mep2Δ* and *ump2Δ* mutants do not undergo filamentation in response to limiting ammonium, indicating that they are sensors of ammonium (Neuhauser *et al.*, 2011) (Smith *et al.*, 2003).

Ammonium transporters have previously been characterised in the *Cryptococcus neoformans* serotype A H99/KN99 strain. The H99 genome encodes two ammonium transporters, *AMT1* and *AMT2*, which are low and high affinity ammonium transporters respectively. *AMT2* is expressed under ammonium limiting conditions whereas *AMT1* is constitutively expressed, to a lower level, under both ammonium limiting and ammonium sufficient concentrations. *AMT2* expression is, therefore, regulated by NCR. Amt2, but not Amt1, is important for haploid cells to undergo invasive growth and mating on low ammonium. Unlike Ump2, in *U. maydis*, Amt2 is not important for virulence (Rutherford *et al.*, 2008b). Similar to *S. cerevisiae*, *C. neoformans* can undergo pseudohyphal growth and this is both Amt1 and Amt2 dependent under ammonium limiting conditions. Mutants lacking only one ammonium transporter produce pseudohyphae on low ammonium but mutants lacking both do not (Lee *et al.*, 2012). Furthermore, ammonium transporters have been identified which complement pseudohyphal growth in *S. cerevisiae*, thereby acting as ammonium sensors, but show no phenotype in their native organism, or have not yet been tested in their native

organism. Examples include MepA from *Fusarium fujikuroi* (Teichert *et al.*, 2008) and Amt1 from *Hebeloma cylindrosporum* (Javelle *et al.*, 2003). Notably, all the ammonium sensors identified to date possess the conserved twin-histidine motif.

1.4.2 *Mechanism of action for ammonium transceptors*

Multiple transceptors which facilitate transport of different nutrients, and regulate other pathways, have been identified. For example, there are an array of nutrient permeases in yeast which regulate the PKA pathway (Steyfkens *et al.*, 2018) and a nitrate transporter in plants which is proposed to be important for nitrate signalling (Krouk *et al.*, 2006). However, ammonium transceptors are the only transceptors to regulate morphology. To date, the signalling mechanism adopted by these transceptors is unknown. With regards to Mep2, two theories have been proposed. The conformational change model and the pH model.

Conformational change model

The conformational change model hypothesises that Mep2 may act like a G-protein coupled receptor (GPRC) which undergoes a conformational change, during transport, allowing Mep2 to interact or cease interacting with a downstream signalling partner (Lorenz and Heitman, 1998) (Rutherford *et al.*, 2008a). It is believed that receptors evolved from transporters which gained a receptor function and subsequently lost their ability to transport, as opposed to the other way round. This is favoured because both transporting transceptors and non-transporting transceptors have been identified. It is also conceivable that before receptors existed nutrients were exploited as signalling ligands (Thevelein and Voordeckers, 2009); neurotransmitters appear to be modestly altered nutrients (Boyd, 1979). Therefore transporting transceptors, such as Mep2, are evolutionary intermediates.

Examples of transporting transceptors are Gap1, Mep2, Pho84 for phosphate and Sul1,2 for sulphate (Donaton *et al.*, 2003) (Van Nuland *et al.*, 2006) (Giots *et al.*, 2003) (Kankipati *et al.*, 2015). In the presence of a fermentable carbon source, such as glucose, the protein kinase A (PKA) pathway is highly active in *S. cerevisiae* cells. This is resultant of cAMP synthesis and its role as a second messenger (Thevelein and de Winde, 1999). Removal of just one essential nutrient from the growth media

downregulates the PKA pathway and causes the cells to arrest growth. Re-addition of the starved nutrient is sensed by the respective transporting transceptor to trigger the PKA pathway (Holsbeeks *et al.*, 2004). The use of cAMP temperature sensitive mutants has confirmed that this reactivation is cAMP independent (Hirimburegama *et al.*, 1992). It is important to note that the role Mep2 plays as a transceptor in regulating the PKA pathway is independent to its role in pseudohyphal growth. The N246A mutation in ScMep2 uncouples signalling from transport but still triggers trehalase activation. Trehalase is a target of the PKA pathway and is, thus, used as a readout for PKA activity (Van Nuland *et al.*, 2006). Mutations to Pho84 and Sul1/2, at putative proton binding sites supports signalling but not transport (Samyn *et al.*, 2012) (Kankipati *et al.*, 2015). Moreover, transport of non-metabolisable analogues can reactivate the PKA pathway. Signalling and transport functions can, therefore, be uncoupled (Van Zeebroeck *et al.*, 2014). With regards to Gap1, substituted cysteine accessibility method (SCAM) analysis confirmed that the same binding site is utilised for both transport and signalling (Van Zeebroeck *et al.*, 2009). However, binding of a competitive inhibitor to Gap1 is not sufficient to induce signalling. The authors propose that binding of the substrate changes the conformation of outwards facing Gap1 to a signalling specific intermediate conformation while the substrate is in transit. A switch to an inward facing conformation, to release the substrate inside the cell, ceases signalling (**Figure 8**). Thus, the physical act of transport, as opposed to internal nutrient metabolism, triggers the signalling cascade (Van Zeebroeck *et al.*, 2014). Support for this model can be provided by considering the non-transporting transceptors that resemble typical transporters.

Three non-transporting transceptors have been discovered in yeast. Ssy1, an amino acid transceptor (Didion *et al.*, 1998), and Snf3 and Rgt2 which are glucose transceptors; the latter exhibits a lower affinity for glucose (Ozcan *et al.*, 1998). All three induce transcription of their respective nutrient transporters but do not exhibit any detectable transport activity themselves (Poulsen *et al.*, 2005) (Ozcan *et al.*, 1996) (Forsberg and Ljungdahl, 2001), thus, suggesting that conformational change is the mechanism of action. Although non-transporting, Ssy1 is assumed to switch between an outward and inward conformation. However, as non-transporting, the inward facing conformation is not possible when loaded with substrate. An increase in intracellular leucine incurred a reduction in signalling by Ssy1. This was postulated to favour the

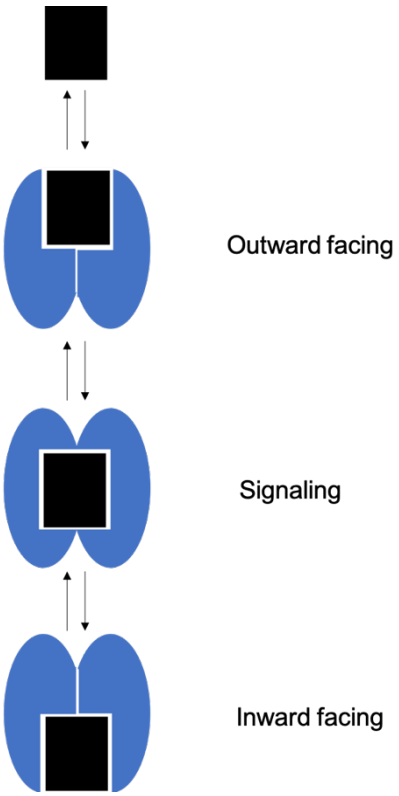

Figure 8: A model for Gap1 transceptor *signalling. A substrate binds to Gap1 which is in the outward facing conformation. This induces the intermediate signalling conformation. The transceptor releases the substrate on the cytoplasmic side of the cell and signalling ceases. Figure based on (Van Zeebroeck et al., 2009).*

inward facing conformation (Wu *et al.*, 2006). Therefore, the outward facing conformation was proposed to be the signalling conformation (Poulsen *et al.*, 2008). However, this model did provide limitations. Ssy1 is a sensor specific for amino acids. If mere binding to the transceptor is enough to trigger signalling then any competitive inhibitor could stabilise the outward facing conformation. Hence the model hypothesised for Gap1, where an intermediate signalling conformation is formed which does not change to inwards facing when loaded with substrate, seems much more plausible (Thevelein and Voordeckers, 2009).

The fact that Mep2 was crystallised in a closed conformation, dissimilar to the bacterial versions, provides support for the conformational change model. Ammonium conductance is blocked by GlnK in bacteria, but no homologue is present in *S. cerevisiae*, suggesting that a different mechanism exists. Interestingly, phospho-mimicking mutations, at the Npr1 kinase phosphorylation site in Mep2, nonetheless resulted in the transporter being in a closed state. However, large conformational changes were observed in the CTR. This finding lead to the phosphorylation based model which results in the opening of Mep2. It is proposed that the CTR interacts with ICL3, by undergoing a further conformational change, resulting in Mep2 acquiring an open state. This subsequent conformational change could allow Mep2 to interact with another protein and thereby induce pseudohyphal differentiation (van den Berg *et al.*, 2016).

Regulation of transport activity by conformational change has also been reported in other Mep2 orthologues. Mutation of a putative threonine phosphorylation site (T472) or a neighbouring glycine residue (G468) in AtAmt1;2, the low affinity Amt in *A. thaliana*, to aspartate results in a non-functional transporter with reduced ^{14}[C]-methylammonium transport rates. On the contrary, T472A only partially reduces transport function. A homology model of AtAmt1;2 shows high structural conservation in the C-terminus. Homology modelling involves aligning the primary sequences of the protein of interest with the primary sequences of one or more known protein structures. In the case of AtAmt1;2 EcAmtB and AfAmt-1 were used. Based on the alignment, and the structures of the known proteins, modelling software is used to generate a putative structure of the protein of interest (AtAmt1;2) (Neuhauser *et al.*, 2007); protein structure has been found to be more conserved than protein sequence (Chothia and Lesk, 1986). The C-terminus of the AtAmt1;2 homology model forms a helix-loop-helix

structure (CH1-CH2) and makes interactions with other monomers of the trimer. The side chain of T472 is firmly packed within the C-terminus but is approachable from the cytoplasmic side, thus, making way for a putative phosphorylation event. The adjacent G468 is located within the loop between CH1 and CH2. From the homology structure, it is apparent that any side chain larger than glycine could not inhabit location 468 without disrupting the CH1-CH2 motif and hence its interactions with neighbouring residues. Co-expression of AtAmt1;2^{G468D} or AtAmt1;2^{T472D} monomers, with WT AtAmt1;2 monomers resulted in reduced NH_4^+ currents in *Xenupus oocytes*. However, co-expression of AtAmt1;2^{T472A} monomers with WT AtAmt1;2 monomers incurred higher transport rates than the other mutants suggesting that the disruption of the C-terminal tail in one monomer by phosphorylation is sufficient to inactivate the residual monomers of the trimer (Neuhauser *et al.*, 2007). Similar findings were documented for LeAmt1;1 (Ludewig *et al.*, 2003). Thus, conformational rearrangements within other Amt proteins appear to be conserved. However, AtAmt1;2 and LeAmt1;1 are not ammonium sensors, so although conformational change may be necessary in Mep2 for its transport function this may not be important for signalling for pseudohyphal growth.

Interaction with a downstream signalling partner has been documented for the Mep2 orthologue in *U. maydis*. Ump2, has been found to physically interact with the GTPase Rho1 (Paul *et al.*, 2014). An interaction between the two proteins was first identified in a split-ubiquitin yeast two-hybrid experiment and confirmed by co-immunoprecipitation (Pham *et al.*, 2009). Genetic interaction was subsequently confirmed. Overexpression of Ump2 or Rac1 (G protein negatively regulated by Rho1 and a controller of polarised growth) increases filamentation of *U. maydis* single colonies on both low and high ammonium. On the contrary, overexpression of Rho1 on low ammonium reduces filamentation. In a mutant lacking Ump2, neither Rac1 nor Rho1 overexpression restores the filamentation defect of the strain. In an *ump2Δ* mutant Rho1 will not be sequestered by Ump2 and is, thus, available to negatively regulate Rac1 and inhibit filamentation (Paul *et al.*, 2014). A split-ubiquitin yeast two-hybrid screen for Mep2 has been conducted which identified an array of putative interacting partners. To verify these interactions GST (Glutathione S-transferase) pull-down assays were performed in *E.coli.* These assays revealed no, or very weak, interactions with the Mep2 C-terminal tail. The authors discussed that the lack of interaction could be due to another region of Mep2 interacting with the protein(s) or

due to the Mep2 C-terminal tail not exhibiting the correct conformation. Lack of post-translational modifications in the C-terminal tail, as a result of being expressed in non-native *E. coli*, or separation of the C-terminal tail from the rest of the transporter, incurred by inclusion of GST, could equally alter the C-terminal tail conformation. However, deletion of one putative interacting partner, Vma4 which did produce a weak band in the pull-down assay, resulted in reduced transport but increased signalling. Reduced transport was likely due to lowered *MEP2* expression and plasma membrane localisation (Van Zeebroeck *et al.*, 2011). As Vma4 is a component of the vacuolar H^+-ATPase (Ho *et al.*, 1993), its deletion would impact on intracellular pH. The vacuolar H^+-ATPase is implicated in activating the PKA pathway which is dependent on cytosolic pH (Dechant *et al.*, 2010). It is important to note that with regards to signalling only trehalase activation and not pseudohyphal growth were investigated (Van Zeebroeck *et al.*, 2011). Both signalling pathways are independent, as evidenced by the ScMep2^{N246A} mutant (Van Nuland *et al.*, 2006), therefore, a protein which signals in one may not in the other.

<u>pH model</u>

The pH model hypothesises that the pathway the proton follows, following deprotonation of NH_4^+, may impact on internal pH which in turn triggers a signalling cascade. If the transport mechanism is electroneutral, following deprotonation the excess proton would leave ScMep2 on the extracellular side leaving only NH_3 to transverse the pore. However, due to the PKA of ammonium, NH_3 would reconstitute NH_4^+ on the cytosolic side by acquiring a proton from the cytosol. This would cause a decrease in the concentration of protons in the cytoplasm and, thus, an increase in cytosolic pH. If the transport mechanism is electrogenic, the excess proton would simultaneously transverse the pore, aided by the twin-histidine motif, before recombining with NH_3 to reconstitute NH_4^+. As no cytosolic protons would be used to reconstitute NH_4^+ no change in pH would occur (***Figure 9***). Whether the proton is released into the extracellular space, or whether the proton enters the cell is unknown (Boeckstaens *et al.*, 2008). However, a diversion in the route the proton follows would impact on internal pH which could subsequently be sensed by a pH responsive pathway. As ScMep1 and ScMep3 are non-signalling homologues perhaps the route the proton follows is different in these transporters as opposed to in ScMep2. As the

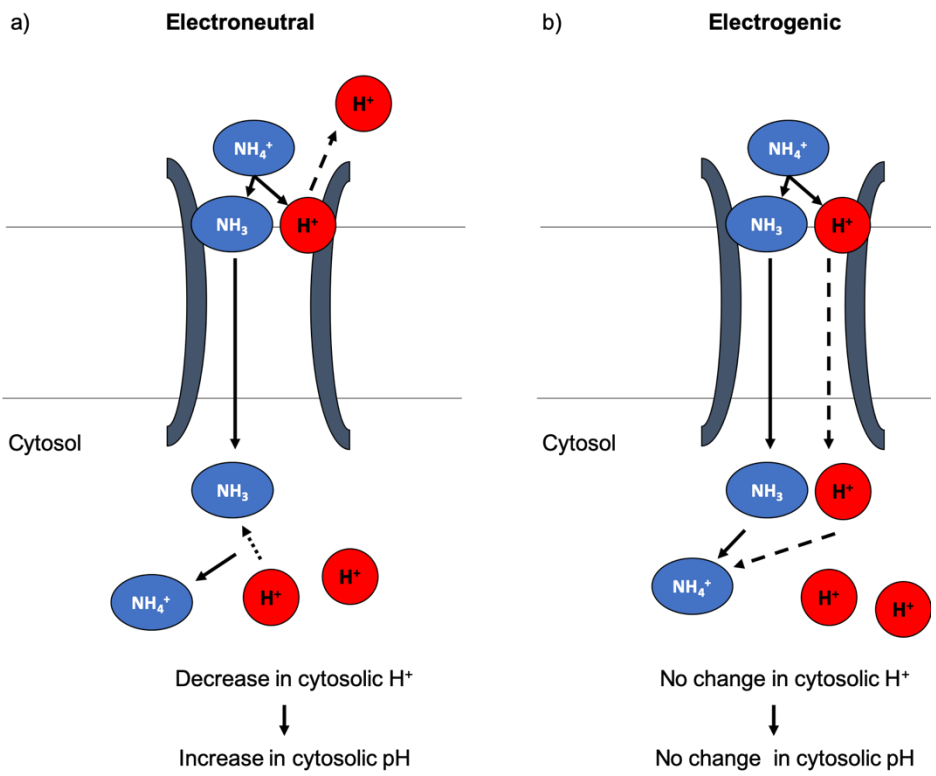

Figure 9: Diagrammatic representation of electroneutral ad electrogenic transport. *NH_4^+ is recruited to the pore of Mep2 and deprotonated. a) In Electroneutral transport NH_3 transverses the pore while the excess proton leaves on the extracellular side. NH_3 acquires a proton from the cytosol incurring an increase in cytosolic pH. b). In Electrogenic transport NH_3 and the excess proton transverse the pore together; proton movement is facilitated by the twin-histidine motif. NH_3 and the excess proton recombine on the extracellular side to reconstitute NH_4^+. As NH_3 does not aquire a proton from the cytosol the cytosolic pH remains unchanged.*

expression of Mep/Amt proteins, from evolutionarily divergent organisms, can complement the pseudohyphal growth defect of a diploid yeast strain lacking Mep2 (Neuhauser *et al.*, 2011) (Smith *et al.*, 2003) (Javelle *et al.*, 2003) (Teichert *et al.*, 2008) it is more plausible that changes in pH, as opposed to interaction with a downstream signalling partner, are triggering pseudohyphal growth. Orthologues of the interacting partners may not be preserved between organisms.

Sensing of pH and induction of filamentation is associated with the Rim101 pathway. Rim101 is a CysHis2 zinc-finger transcription factor which is proteolytically cleaved and activated by the calpain-like protease Rim13 in response to alkaline pH. Rim21 is the pH sensor, located at the plasma membrane, which responds to external alkalisation. External alkalisation results in depolarisation of the plasma membrane, which can additionally be induced by CCCP protonophore treatment in the absence of extracellular alkalisation (Obara *et al.*, 2012). Rim101 is one of an array of transcription factors which regulates the cell surface flocculin, Flo11, which is required for pseudohyphal and invasive growth (Barwell *et al.*, 2005) (Ryan *et al.*, 2012).

Links between the H^+ ATPase Pma1 and polarised growth have also been established. In the fission yeast, *Schizosaccharomyces pombe*, a mutant which exhibits decreased plasma membrane Pma1 activity (Ulaszewski *et al.*, 1986) displays defects in cell polarity and altered morphology. Mutant cells are fatter and rounder than WT cells and possess ectopic protrusions. In WT cells, GFP tagged Pma1 is two-fold more concentrated on the sides of the cells as opposed to within the growing tip. This distribution of Pma1 is proposed to generate a pH gradient which acidifies the growing tip (Minc and Chang, 2010) (**Figure 10**). An analogous pH gradient, as result of asymmetric Pma1 distribution, has similarly been documented in *C. albicans*. In *C. albicans*, increasing Pma1 truncation incurs decreasing hyphal length. Furthermore, cytosolic pH is more acidic in these mutants. For hyphal formation to occur in *C. albicans* cytosolic alkalisation is required. As the function of Pma1 is to remove protons from the cell this would result in the required cytosolic pH (Rane *et al.*, 2019). Thus, pH, regulated by Pma1, is critical in both organisms for cell polarity and hyphal formation. Pseudohyphal growth in *S. cerevisiae* is a polarised growth form (Cullen and Sprague, 2012), therefore, Pma1 could be important in Mep2 signalling. Moreover, Pma1 promotes TORC1 activation in response to proton import by Gap1 (Saliba *et al.*, 2018). When TORC1 is active Npr1 kinase is hyperphosphorylated,

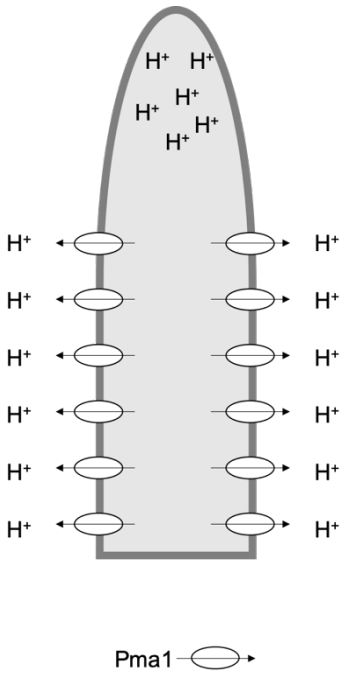

Figure 10: Distribution of Pma1 in S. Pombe. *Pma1 is distributed on the sides of the cell but excluded from the growing tip. This creates a pH gradient which acidifies the tip. Figure based on Minc and Chang, (2010).*

inactive, and unable to activate ScMep2 (Boeckstaens *et al.*, 2014). Perhaps Pma1 responds to changes in internal pH to repress signalling for pseudohyphal growth. In support of this theory, a global screen has identified that *S. cerevisiae* strains lacking Vma4 or Vma6, components of the vacuolar H^+ATPase, exhibit hypoactive pseudohyphal growth (Ryan *et al.*, 2012). Without a functioning H^+ATPase, the cytosol will inevitably be more acidic. If acidity is the repressive signal this would activate TORC1 to repress pseudohyphal growth. This would also favour NH_3 (electroneutral) transport as this would make the cytosol more alkaline. In ScMep2, mutations to the twin histidine motif (H194E and H348A), and asparagine residue adjacent to the putative deprotonation site (N246A), uncouple transport from signalling suggesting that these residues are critical for inducing pseudohyphal growth (Rutherford *et al.*, 2008a) (Van Nuland *et al.*, 2006). The position of these residues is comparable to the position of the equivalent residues in other electrogenic Amts, therefore, the same electrogenic mechanism could be occurring in ScMep2 (van den Berg *et al.*, 2016). In support of electrogenic transport, differences in optimal pH (pH_{opt}) for transport between the non-signalling Meps, ScMep1 and ScMep3, and the signalling Mep, ScMep2, have been identified. Transport by ScMep1 and ScMep3 is favoured at pH_{opt} 6 while transport by ScMep2 is most efficient at the more acidic pH_{opt} 4. Furthermore, substitution of the first conserved histidine in ScMep2 to glutamate (H194E) results in a shift in the pH_{opt} to that of the non-signalling Meps. Additionally, the $ScMep2^{H194E}$ mutant fails to induce pseudohyphal growth (Boeckstaens *et al.*, 2008). At pH ~6.2, or lower, yeast cells produce an inward proton gradient. This proton gradient is reversed at higher pH (Cimprich *et al.*, 1995). As a shift in external pH from 6 to 7 drastically reduces ScMep2 activity, it has been hypothesised that an inward proton gradient is critical for ammonium to transverse the ScMep2 pore (Boeckstaens *et al.*, 2008), and thus favours proton influx coupled to substrate import. Understanding the signalling mechanism and to what extent this is conserved is an important question in the field. Diagrams of each model are depicted in (**Figure 11)**.

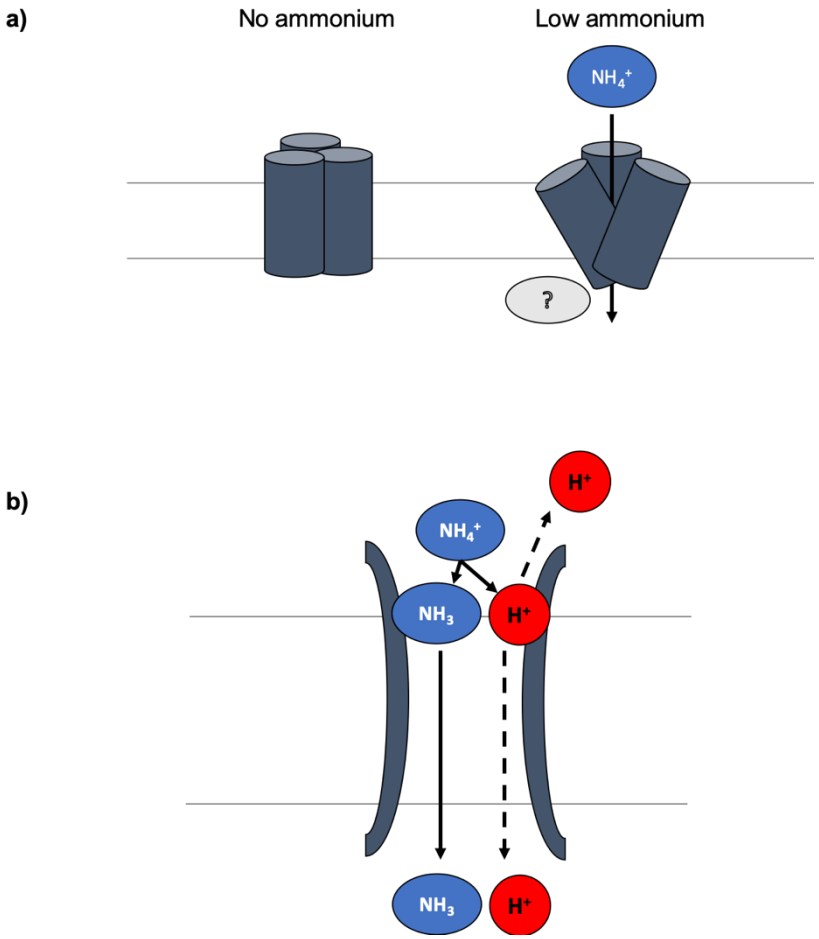

Figure 11: Models of Mep2 signaling. *a) Conformational change model: Under ammonium starvation, Mep2 is present in the membrane in its inactive state. When the environment becomes ammonium limiting Mep2 undergoes a conformational change to interact with a downstream signaling partner which induces pseudohyphal growth. b) The ammonium ion (NH_4^+) is deprotonated to NH_3 and H^+. NH_3 defuses through the pore while the proton exits the pore or enters the cytosol. The change in pH is sensed by a pH sensing pathway to induce pseudohyphal growth. Figure based on (Boeckstaens et al., 2008) and (Rutherford et al., 2008a).*

1.5 *Zymoseptoria tritici*

Zymoseptoria tritici is a filamentous fungus and the causative agent of *Septoria tritici* leaf blotch (STB) on wheat. This disease is responsible for vast wheat crop losses globally (Dean *et al.*, 2012). In some cases this has reduced yields by 50 % (Duba *et al.*, 2018). With resistance to fungicides of this pathogen on the rise, understanding the triggers of virulence is all the more important.

1.5.1 *Cell biology of Z. tritici*

Z. tritici exhibits several morphologies, the most common being 'yeast-like' growth. In this morphology *Z. tritici* forms asexual macropycnidiospores, which dissimilar to yeast cells, are multi-cellular, being composed of four to eight cells. These cells are wide (~1.5 – 3.5 μm) and long (~40 – 100 μm). Budding off the macropycnidiospores are the unicellular micropycnidiospores which are considerably thinner (~1 μm) and shorter (~5 – 10 μm) (Sanderson, 1985). Another morphology is hyphae which are formed when macropycnidiospores germinate into exceedingly narrow and elongated cells (Wiese R.A, 1987). This morphology can be triggered in the laboratory upon nutrient starvation and in response to increased temperature (Mehrabi *et al.*, 2006) (Motteram *et al.*, 2011). Hyphae extend in a polarised fashion (Wiese R.A, 1987) and this is a prerequisite for infection of the host (Yemelin *et al.*, 2017). Asexual micropycnidiospores are also observed budding off these vegetative structures. In addition to the asexual spores, which are formed in asexual fruiting bodies (pycnidia) during infection, *Z. tritici* forms sexual ascospores which are formed in asexual fruiting bodies (perithecia). Ascospores are much wider (~2 – 3 μm) and shorter (~10 – 15 μm) than asexual pycnidiospores (Wiese R.A, 1987) and are produced upon the engagement of cells of the opposite mating type (Kema *et al.*, 1996). Ascospores have an advantage over pycnidiospores in that they can be disseminated by air, as opposed to rain splash, meaning that ascospores can be spread over further distances to cause disease (Sanderson, 1985). Therefore, development of different morphologies throughout the infection cycle is vital.

1.5.2 *Z. tritici infection cycle*

The infection cycle can be split into four distinct phases: entry into the host, colonisation, formation of pycnidia and release of spores (**Figure 12**).

Phase 1

Pycnidiospores and ascospores are dispersed by rain splash and air respectively. Upon contact with the leaf epidermis, the spores germinate into hyphae which enter the wheat leaf through the stomata (Duncan and Howard, 2000). ZtHog1, a MAPK protein, is important for this spore to hyphae transition and, thus, entry into the host (Mehrabi *et al.*, 2006). A debatable subject is whether a stimulus exists to direct the hyphae to the stomata or whether this is a stochastic phenomenon. ZtFus3 mutants do not recognise the stomata and hence do not infect the wheat leaf, suggesting that attraction to the stomata may be targeted (Cousin *et al.*, 2006). ZtFus3 is an orthologue to ScFus3 in *S. cerevisiae,* which is a MAP kinase involved in mating (Elion *et al.*, 1990). Pmk1 is a Fus3-like protein in the rice blast fungus *M. oryzae* which is essential for appressorium formation. Appressoria are hyphal structures required by some phytopathogens to enable them to infect their respective plant through the stomata (Xu and Hamer, 1996) (Deising *et al.*, 2000). Despite other studies reporting on appressorium-like structures, at the tip of invading hyphae (Cohen and Eyal, 1993) (Duncan and Howard, 2000) (Kema *et al.*, 1996), the *Z. tritici* genome lacks many of genes associated with appressoria formation (Goodwin *et al.*, 2011), therefore, it is unclear how ZtFus3 directs *Z. tritici* to the stomata.

Phase 2

12- 24 hr after entry into the host, colonisation by *Z. tritici* hyphae is observed in the substomatal cavity. Hyphae are visible spreading into the substomatal space of the mesophyll layer 3-11 days post infection (DPI) (Cohen and Eyal, 1993) (Duncan and Howard, 2000) (Kema *et al.*, 1996). This stage is dependent on another member of the MAPK pathway, ZtSlt2. Despite colonisation, the biomass of *Z. tritici* does not significantly increase, which suggests that *Z. tritici* utilises internal nutrient stores to survive rather than releasing enzymes to degrade host nutrients, as was previously postulated (Keon *et al.*, 2007). As a result, this stage is asymptomatic, as the wheat leaf shows no visible signs of infection. In a laboratory this stage generally lasts 9-14 days, but lasts 6-36 days in nature (Hilu and Bevee, 1957) (Shearer, 1971). During

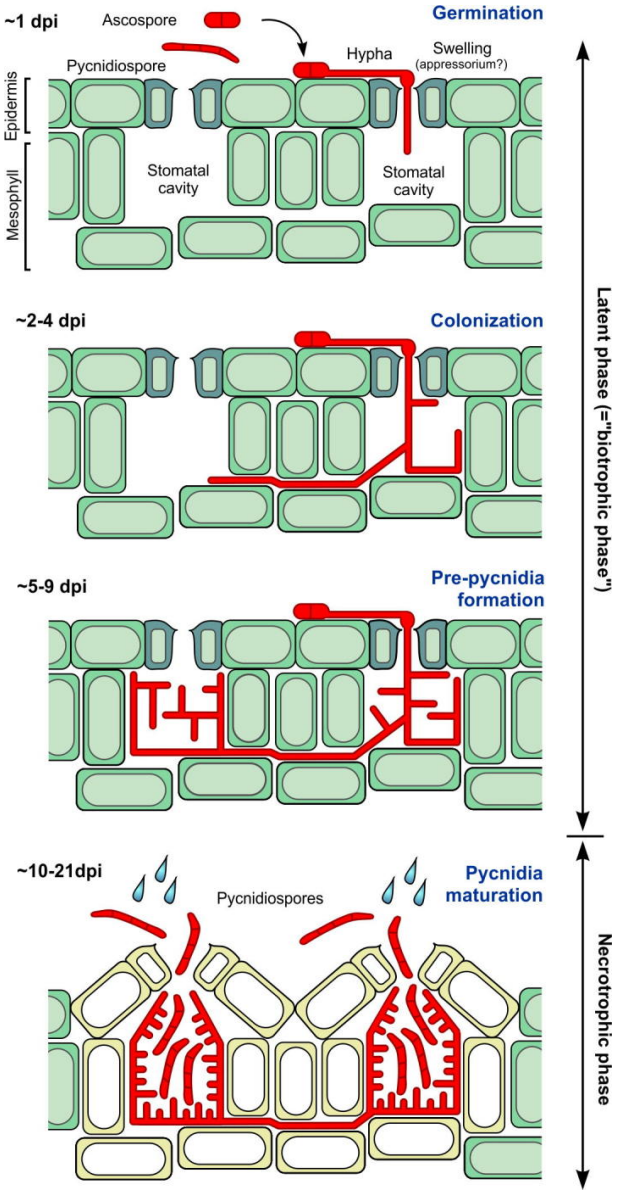

Figure 12: Z. tritici infection cycle. *Top panel: Host entry by hyphae through the stomata. Second panel: colonisation of the substomatal cavity. Third panel: pycnidia begin to develop in the substomatal cavity and the infection switches to being symptomatic. Bottom panel: pycnidia mature and the spores are released. Figure taken form (Steinberg, 2015).*

this latent phase, *Z. tritici* secretes Zt3Lysm to evade host immune defences. Chitin is present in fungal cell walls but absent in plant cell walls (Sanchez-Vallet *et al.*, 2015). Chitin is, therefore, identified as foreign to the plant and acts as a pathogen associated molecular pattern (PAMP) which induces PAMP-triggered immunity (PTI). Zt3Lysm competes with host chitin receptors, which would otherwise interact with chitin fragments, thereby promoting *Z.tritici's* evasion from the host (Mentlak *et al.*, 2012) (Sanchez-Vallet *et al.*, 2015).

Phase 3

5-9 DPI, pycnidia begin to develop into fruiting bodies in the substomatal cavity (Hilu and Bevee, 1957) (Kema *et al.*, 1996). *Z. tritici* begin to proliferate more rapidly and form branching structures (Shetty *et al.*, 2007) (Keon *et al.*, 2007). The significant increase in growth was initially believed to be due to the high expression of cell wall degrading enzymes (CWDEs) which degrade the host cell wall (Kema *et al.*, 2008). Disintegration of the cell wall would release nutrients such as sugars and amino acids which would then be available for utilisation by *Z. tritici* (Shetty *et al.*, 2007) (Keon *et al.*, 2007). However, very few CWDEs have been annotated within the IPO323 genome compared to other phytopathogenic fungi such as *Fusarium graminearum* or *M. oryzae*. Instead, proteases, lipases and amylases have been found to be transcriptionally upregulated and proteins related to protein degradation have been found to be expanded by genetic mapping analysis (Yang *et al.*, 2013) (Morais do Amaral *et al.*, 2012). At the onset of necrotrophy, infection is no longer asymptomatic as identified by necrotic areas (black spots) on the wheat leaf (Duncan and Howard, 2000). In other organisms, the necrosis and ethylene-inducing peptide 1 (Nep1)-like protein (NLP) family induce cell death and hyperactive defence signalling in the host. *ZtNLP* expression is optimal just before the onset of the symptomatic phase yet its deletion does not hinder virulence. This suggests that other effectors exist to elicit the roles usually displayed by the NLP family (Motteram *et al.*, 2009).

Phase 4

The pycnidia mature allowing the release of pycnidiospores to infect new plants (Hilu and Bevee, 1957) (Kema *et al.*, 1996). As well as being important in penetration, ZtFus3 is also proposed to be important for the development of asexual fruiting bodies; ZtFus3 mutants fail to produce pycnidia on plant-derived medium *in vitro*. Moreover, ZtFus3 mutants do not melanise or produce aerial mycelia (Cousin *et al.*, 2006).

Melanin is a trait associated with pycnidia (Duncan and Howard, 2000). Subunits of protein kinase A have also been associated with this stage of the infection cycle. ZtTpk2 and ZtBcy1 mutants are hypo-virulent compared to WT cells. Cytological analysis confirmed this was due to the inability of these mutants to form asexual fruiting bodies and not due to a reduction in penetration or subsequent colonisation (Mehrabi and Kema, 2006).

1.5.3 *Z. tritici genome*

The *Z. tritici* genome comprises 21 chromosomes equating to 39.7 Mb DNA which encodes 10,952 putative genes. While 13 of these are classified as core chromosomes the eight smallest chromosomes (14 -21) are dispensable and are classified as accessory chromosomes. Accessory chromosomes form the dispensome (Goodwin *et al.*, 2011). Their loss during meiosis appears to have no visible effects on the pathogen and, therefore, are not essential for survival (Wittenberg *et al.*, 2009). The dispensome accounts for 12 % of the *Z. tritici* genome yet only encodes 6 % of the genes. However, most dispensome genes are redundant as they are copies of the core chromosome genes. Whether genes were transferred from core to accessory chromosomes or in the opposite direction remains elusive. Furthermore, the dispensome exhibits different codon usage to the rest of the genome and is less G+C rich. The dispensome mainly encodes putative transcription factors, and fewer pathogenicity factors than the core chromosomes. Interestingly, in comparison to other fungal plant pathogens, the *Z. tritici* genome contains far fewer genes involved in cell wall degradation, despite this being observed during phase 3 of the infection cycle (Goodwin *et al.*, 2011). Metabolic profiling studies identified that more than 1000 genes were differentially expressed upon *Z. tritici* spores making contact with the wheat leaf surface suggesting that the pathogen adapts to the changing environment. Sustained from 1 DPI to 4 DPI is the metabolism of lipids and fatty acids, suggesting that *Z. tritici* remains in a starved state; consistent with the limited increase in biomass. At the switch to necrotrophic growth protease secretion is upregulated. This is believed to provide energy to *Z. tritici (Rudd et al., 2015).*

The *Z. tritici* genome is at least 17 % repetitive with transposable elements accounting for the majority of this repetitive fraction (Dhillon *et al.*, 2014). Transposable elements were first discovered in the 1940s (McClintock., 1950) and are now believed to be

important in genome evolution (Kazazian, 2004) as their insertion can promote or restrict transcription, alter chromatin, and affect neighbouring areas (Girard and Freeling, 1999). Their distribution can be both random or clustered (Chen and Manuelidis, 1989) (Acosta *et al.*, 2008). Transposons are classified based on their mode of replication. Class I TEs (transposable elements) are flanked by long terminal repeats (LTRs) and auto-encode a reverse transcriptase. The reverse transcriptase transcribes RNA to cDNA which is subsequently integrated into the genome. Class II TEs are identified by terminal inverted repeats (TIRs) and auto-encode a transposase domain. The transposase excises the DNA at the TIRs and integrates this excised DNA into a new genomic location. Class I TEs therefore follow a copy and paste mechanism of integration while Class II TEs deploy a cut and paste mechanism (Wicker *et al.*, 2007) (**Figure 13**). The insertion of a transposable element upstream of the *ZMR1* promoter in *Z. tritici*, a transcription factor which regulates melanin biosynthesis, has been found to modulate melanin accumulation, to aid its survival upon exposure to stress (Krishnan *et al.*, 2018). Insertion of an LTR into the promoter of MFS1, major facilitator gene, increases fungicide efflux (Omrane *et al.*, 2017). Thus, transposable elements promote genetic variation in the *Z. tritici* population permitting adaptation to varying climates and natural or manmade stresses (Prentis *et al.*, 2008).

1.5.4 *Management of Z. tritici disease*

Z. tritici is a global problem, however this pathogen appears to be most clustered in Western Europe, especially in Germany, France and the United Kingdom. In these countries alone $1.3 bn is spent on wheat fungicides. Intensive farming practices and sufficient rainfall is highly favourable for *Z. tritici* in these regions. In addition to fungicides, several practices are in place to combat the spread of STB.

In Western Europe, before the first recorded outbreak of STB, wheat crops were hypothesised to naturally bear resistance to *Z. tritici* at minimal levels. Selective breeding of wheat has generated greater crop yields, nevertheless, this has come at the expense of greater vulnerability to *Z. tritici* (Torriani *et al.*, 2015). Instead, efforts are now being made to selectively breed for wheat resistance. Resistance genes exploited include *STB6*. This gene is found naturally in several wheat cultivars, including Chinese Spring (CS), where expression is upregulated two-fold during infection with IPO323. Transformation of the *STB6* gene into susceptible wheat

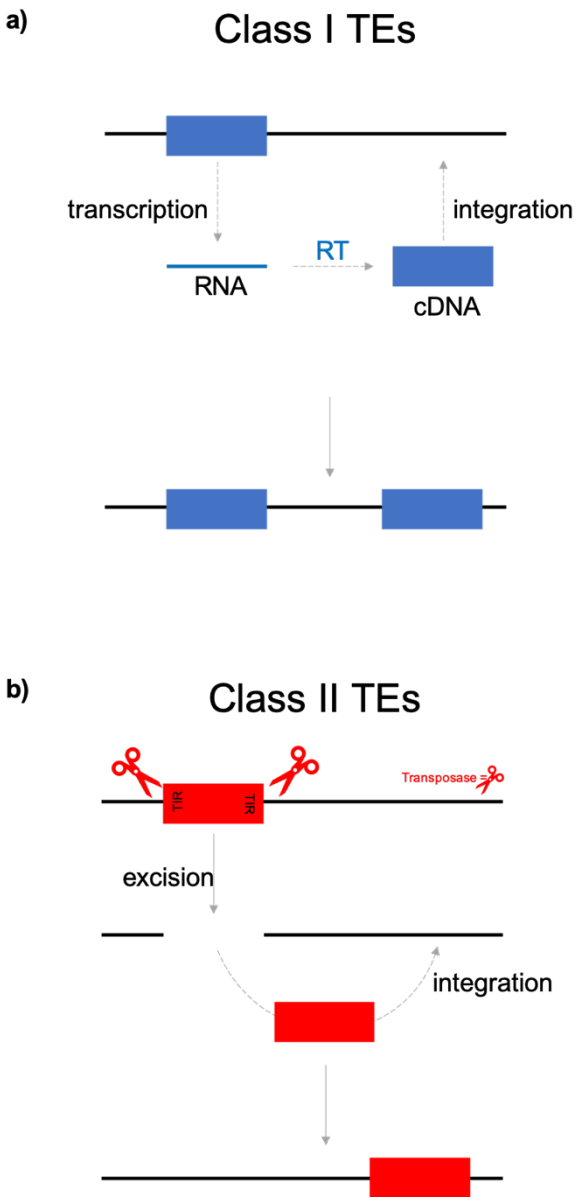

Figure 13: Mechanism of integration by Class I and Class II TEs. *Class I (left panel) depicts the transcription of genomic DNA to RNA, followed by reverse transcription to cDNA, which is integrated into the genome. Class II (right panel) depicts excision of a region of genomic DNA, marked by TIRs, and integration into the genome by the transposase. Integration is not just restricted to the same chromosome.*

varieties, Courtot and Bobwhite, rendered these strains resistant to IPO323, while knockdown of *STB6* in CS abolished resistance (Saintenac *et al.*, 2018). Together with selective breeding is crop rotation which allows the spread of new resistance genes throughout the wheat population (McDonald and Mundt, 2016).

Areas that could be exploited are stubble management. When the wheat is harvested, the wheat stubble is often left to preserve the soil. Nonetheless, reduced tillage results in a nutrient store for *Z. tritici* to aid overwintering. The *Z. tritici* population multiplies, resulting in more variation within the population and the spread of ascospores to neighbouring fields (Schuh, 1990). Increased tillage could reduce the spread, but in order to have any impact this practice would need to be deployed by farmers nationally (McDonald and Mundt, 2016). Another strategy currently being considered is to biologically control *Z. tritici* (Kildea *et al.*, 2008) (Analía Edith Perelló, 2009). *McDonald & Mundt* propose using a cocktail of microbes on wheat stubble to combat *Z. tritici* during its saprophytic stage (McDonald and Mundt, 2016).

In terms of fungicides, quinone outside inhibitors (QoIs) were previously utilised. QoIs elicited their effect by blocking the electron transport chain during respiration (Grasso *et al.*, 2006) (Sierotzki *et al.*, 2007). However, widespread resistance rendered the fungicide inadequate at combating the spread of STB disease. Resistance was linked to a G143A mutation in *CYTB* (Gisi *et al.*, 2002), which had been acquired autonomously at least four times in different areas across Europe (Torriani *et al.*, 2009). As a result, QoIs are no longer exploited. Common fungicides deployed to overcome *Z. tritici* today are succinate dehydrogenase inhibitors (SDIs), demethylation inhibitors (DMIs) and multi-site fungicides (MSFs) e.g. chlorothalonil. The Fungicide Resistance Action Committee have ranked these drug classes, in terms of their risk to developing resistance, from high/medium to low (**Figure 14**) (Torriani *et al.*, 2015). SDIs are more than 40 years old, however they have become increasingly popular since 2003, when broad spectrum versions became available. SDIs block succinate dehydrogenase (SDH), the enzyme important during respiration, by binding to three of its four subunits (Keon *et al.*, 1991). Resistance by *Z. tritici* to SDIs has been evolving, and is characterised by isolates carrying the T79N and W80S mutations in *SDH*. In 2014 a new mutation was identified in France, N225T (Sierotzki and Scalliet, 2013). DMIs have been in use since the 1970s and work by inhibiting 14-α-sterol demethylase (encoded by *CYP51*), a component of sterol biosynthesis (Siegel, 1981), however,

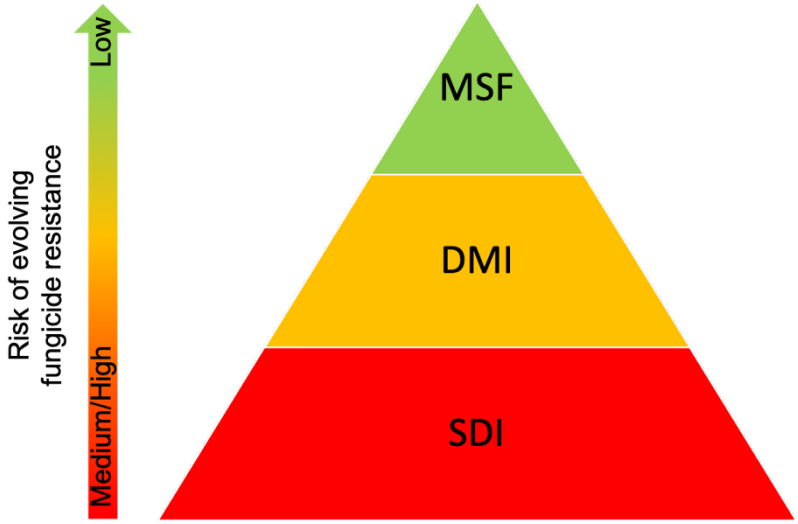

***Figure 14: Diagrammatic representation of the risk of evolving fungicide resistance**. The commonly used fungicides are ranked from medium/high risk to low risk, according to the Fungicide Resistance Action Committee (FRAC). Multi-site fungicide (MSF). Demethylation inhibitor (DMI). Succinate dehydrogenase inhibitor (SDI).*

similar to the SDIs, resistance has prevailed. Resistance is a result of amino acid changes (Leroux *et al.*, 2007), however, overexpression of *CYP51* and use of the ATP-binding cassette and major facility subfamily (MFS) transporters by *Z. tritici*, to pump out the drug, has been hypothesised as a possible mechanism. MSFs, which target multiple biochemical processes, to date, have not developed resistance (Torriani *et al.*, 2015) (Hobbelen *et al.*, 2014). However, renewal of chlorothalonil use, an MFS around since the 1960s, has not been approved by the European Union Standing Committee due to their concern over its effect on fish, amphibians and groundwater (Amara *et al.*, 2018). Deployment of chlorothalonil will, therefore, soon be prohibited. Thus, the urgency to develop new fungicides, which will not promote resistance in the *Z. tritici* population, is greater.

1.6 *Cryptococcus neoformans*

Cryptococcus neoformans is a human fungal pathogen which was first documented in 1894 (Zhao *et al.*, 2019). Belonging to the Basidiomycota division Serotype A (*C. neoformans var. grubii*) and serotype D (*C. neoformans var. neoformans*) are the two presently accepted serotypes with the latter being less virulent. Serotypes B and C are classifications of *Cryptococcus gatti* which are regarded as discrete species (Lin and Heitman, 2006). *C. neoformans* is globally distributed (Khayhan *et al.*, 2013) (Cogliati *et al.*, 2016) (Spina-Tensini *et al.*, 2017) and infects immunocompromised individuals; most commonly HIV/AIDS sufferers (Lui *et al.*, 2006).

1.6.1 *Cell biology of C. neoformans*

C. neoformans is a dimorphic fungus which exists as a budding yeast (typically 5 to 10 μM in diameter) (Okagaki *et al.*, 2010) during vegetative growth and as hyphae during sexual growth (Shadomy and Utz, 1966). Moreover, pseudohyphal growth is possible during asexual growth but has infrequently been identified in clinical samples (Gazzoni *et al.*, 2009). Mating is heterothallic and occurs between haploid cells of the opposite mating type, MATa and MATα, and between cells of the same mating type. Same-sex mating is classified as monokaryotic fruiting, however this has been shown to be a developmental process which can occur in the absence of sexual reproduction (Fu *et al.*, 2013). During opposite-sex mating the fusion of two yeast cells, of opposite mating

type, is induced by the secretion of pheromones by each partner. The fused cells develop into a dikaryon consisting of separate (un-fused) nuclei. Characteristic fused clamp connections develop between each cellular compartment to aid the migration of nuclei, which have simultaneously divided by mitosis, into neighbouring compartments. Nuclei are maintained in their new sections by the formation of septa at the clamp connections. Nuclei in the basidium, a developmental structure in the terminal compartment, fuse and undergo meiosis and mitosis to generate basidiospores which form four chains. Finally, the spores germinate into new yeast cells which are mature enough to enter the sexual cycle (Kwon-Chung, 1975). During same-sex mating cellular and nuclear fusion occurs between cells of the same mating type (most commonly MATα) to produce a monokaryon. Monokaryons are identified by unfused clamp connections. Similar to dikaryons, a basidium forms in the terminal cellular compartment of monokaryons. Meiosis occurs in the basidium which produces four chains of haploid basidiospores (Lin *et al.*, 2006) (**Figure 15**). Monokaryotic hyphae, independent of same-sex mating, are produced by high temperature induced enlarged cells in G2 arrest (Fu *et al.*, 2013). Other growth morphologies associated with dikaryotic and monokaryotic hyphae are blastopores and chlamydospores. Blastopores are yeast cells which bud from the periphery of hyphae or from chlamydospores. Chlamydospores are yeast cells which form within the hyphae and are enriched in glycogen which may act as an energy store (Lin and Heitman, 2005).

1.6.2 *C. neoformans genome*

The *C. neoformans* genome is approximately 20 Mb in length and projected to encompass 6500 genes. Unlike other fungal organisms, the *C. neoformans* genome is highly repetitive leading to genome plasticity. In contrast to the *S. cerevisiae* and *C. albicans* genomes, which contain 24 and 27 amino acid permease encoding genes respectively (Martho *et al.*, 2016), the *C. neoformans* genome only contains 10 suggesting differences in nitrogen assimilation. As the threonine and tryptophan biosynthetic pathways are essential it has been proposed *that C. neoformans* is more dependent on biosynthesis rather than uptake (Fernandes *et al.*, 2015) (Kingsbury and McCusker, 2008). Furthermore, genes are intron-rich and predicted to exhibit enhanced alternative splicing (Loftus *et al.*, 2005) (Goodwin and Poulter, 2001). The *Cryptococcus* genome is also able to undergo microevolution during human infection, as identified by comparing samples isolated from patients at the onset of infection and

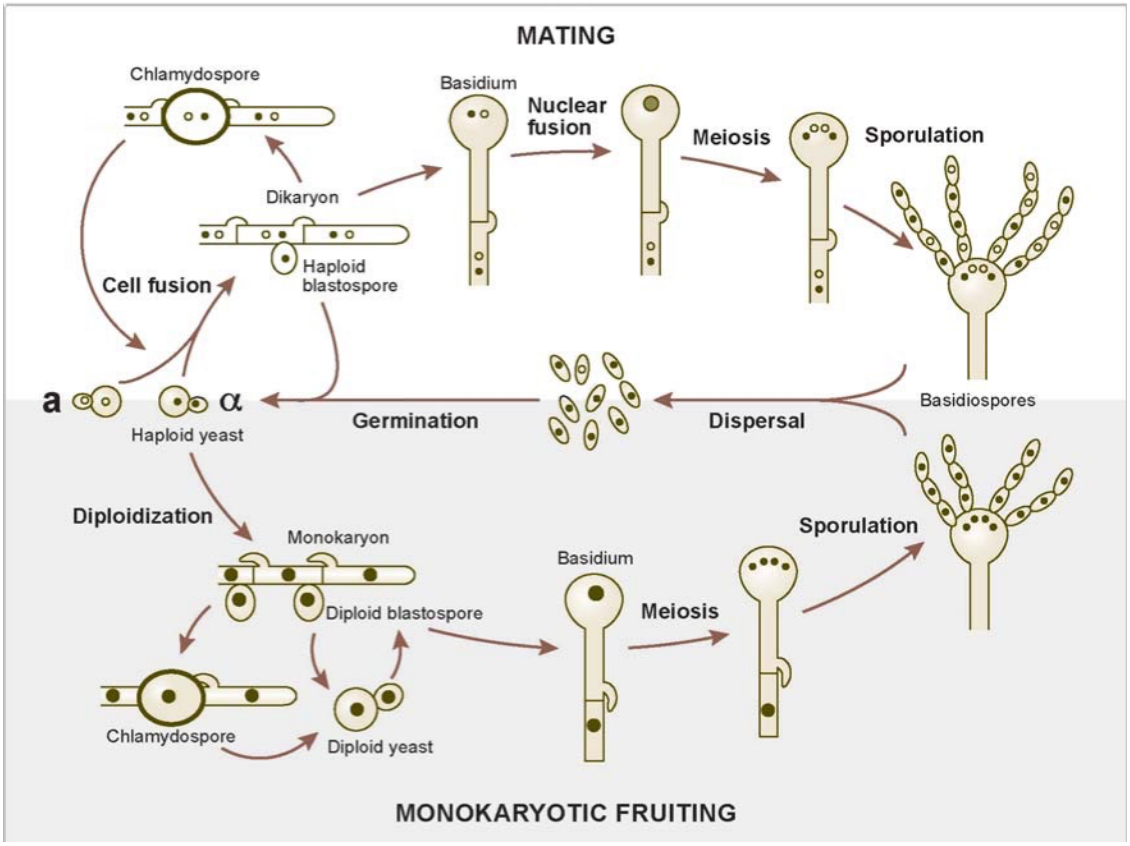

Figure 15: The mating and monokaryotic fruiting lifecycles of C. neoformans. *Top panel: haploid cells of opposite mating type fuse to form a dikaryon. A basidium forms in the terminal cellular compartment and then nuclei fuse. After meiosis and mitosis four chains or basidiospores branch off the apical edge of the basidium. These spores are released to enter the cycle. Bottom panel: haploid cells of the same mating type fuse to form a monokaryon. Meiosis and mitosis occurs in the basidium to form four chains of basidiospores which are released to enter the cycle. Figure taken from from Lin and Heitman, (2006) .*

during relapse, to create an enhanced virulence phenotype (Ormerod *et al.*, 2013). In addition, microevolution has been associated with drug resistance (Chen *et al.*, 2017). A bipolar mating system in *C. neoformans*, governed by the multiallelic mating-type locus, controls sexual development. The mating-type locus is greater than 100 kb which makes it distinctively large in comparison to other fungi with analogous mating systems. For both serotypes A and D, the α alleles are shorter than the a alleles. Despite genetic variation being common in the genome the mating-type locus remains immune to genetic recombination to prevent the production of sterile offspring. The MAT encoded transcriptome includes pheromones and pheromone receptors which are components of the MAP kinase pathway in addition to other genes not associated with mating (Lengeler *et al.*, 2002).

1.6.3 C. neoformans infection cycle

Although *C. neoformans* is a human pathogen this fungus is ubiquitous in the environment. *C. neoformans* is most commonly isolated from pigeon guano contaminated soil (Nosanchuk *et al.*, 1999) but has also been associated with eucalyptus trees (Gugnani *et al.*, 2005), decaying wood (Randhawa *et al.*, 2001) and an array of plant species. Interestingly, specific plant hormones have been documented to enhance mating on plant surfaces in a laboratory setting (Xue *et al.*, 2007). Primary human infection of the host occurs through inhalation of airborne spores or desiccated yeast cells from environmental sources (Velagapudi *et al.*, 2009). These spores colonise the respiratory tract where they are cleared or lie dormant in the resident macrophages yielding an asymptomatic infection. Acute infection in the lungs, resulting in meningococcal pneumonia, is also possible, however, it is unclear whether this could be due to the reactivation of dormant cells (Brizendine *et al.*, 2011). Upon the host immune system becoming compromised the dormant cells are reactivated. This causes systemic infection by hematogenous dissemination (**Figure 16**). *C. neoformans* can transverse the blood brain barrier to cause meningoencephalitis, the most common clinical presentation, which can be fatal if untreated. However, the mechanism by which this pathogen enters this site remains elusive (Liu *et al.*, 2012), but its entrapment within a macrophage is vital, as the depletion of these immune cells prevents dissemination into the mouse brain (Charlier *et al.*, 2009) (Kechichian *et al.*, 2007).

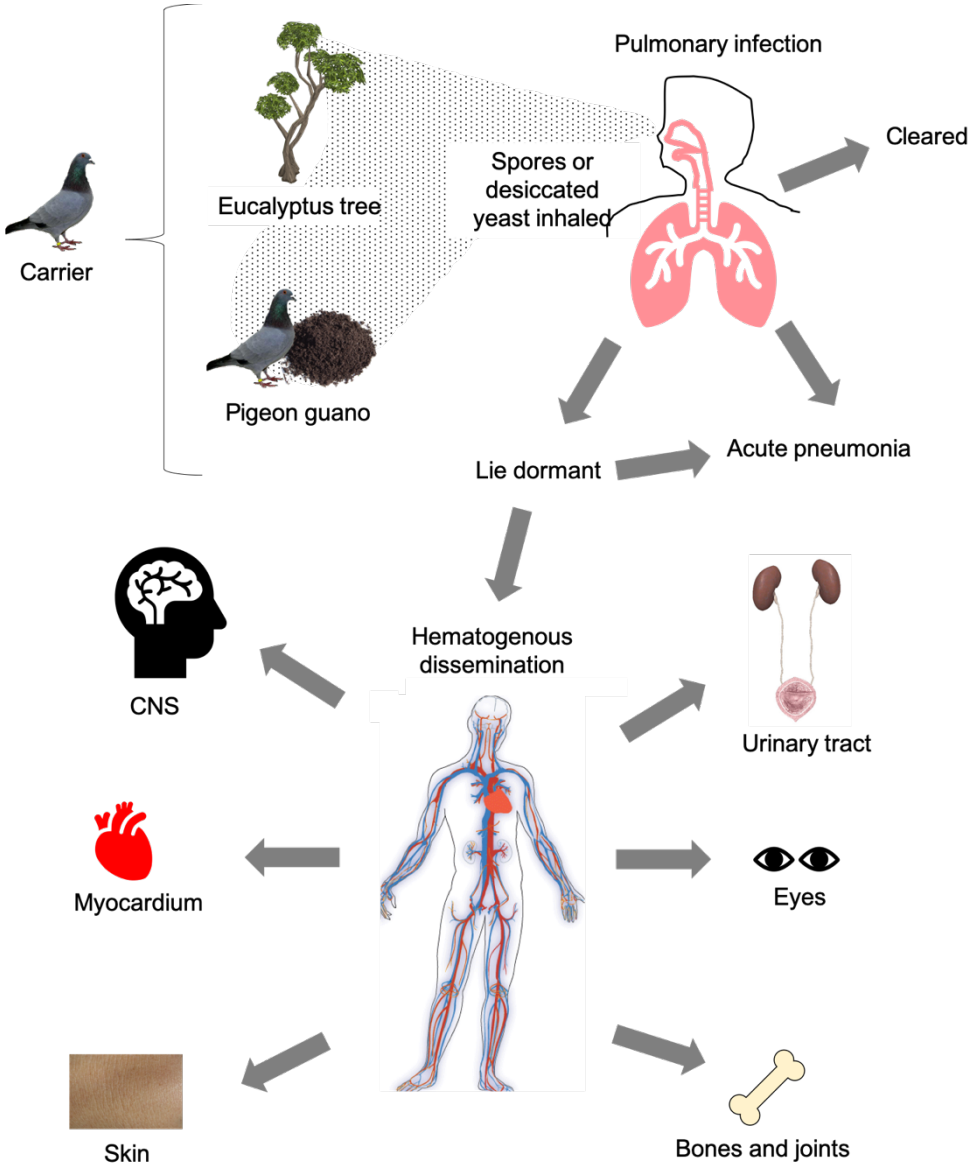

Figure 16: Infection cycle of Cryptococcus. *Pigeons may serve as carriers rather than sufferers of Cryptococcus to distribute the fungus. Cryptococcus has been isolated from eucalyptus trees and pigeon guano and serves as a location for the production of spores. The lungs serve as the port of entry for airborne spores or desiccated yeast cells sourced from the environment. Upon primary infection of the lungs, the infection is typically asymptomatic with the infection being cleared or lying dormant. Acute pneumonia may develop but this could be triggered by reactivated dormant cells. Upon reactivation of dormant cells, Cryptococcus is disseminated by the blood to cause systemic disease.*

1.6.4 The host immune response to C. neoformans

Upon entry into the alveoli of the lungs *C. neoformans* cells are immediately recognised by the innate phagocytic immune cells including the resident macrophages (Lohmann-Matthes *et al.*, 1994). Depending on the activation status of the macrophage, two types of responses can occur: M1 or M2. The cytokine microenvironment is key in orchestrating the macrophage activation status (McQuiston and Williamson, 2012). M1 macrophage activation is stimulated by IFN-γ, which is associated with *C. neoformans* clearance via the production of reactive oxygen species (ROS), while M2 macrophage activation is promoted by IL-4 and/or IL-3, which favours *C. neoformans* survival. IFN-γ is a cytokine produced by Th1-type $CD4^+$ T cells whereas IL-4 and IL-3 are produced by Th2-type $CD4^+$ T cells (Arora *et al.*, 2011). Mice infected with *Cryptococcus*, that cannot produce Th1-type cytokines, are more susceptible to the pathogen than mice that can produce Th1-type cytokines, highlighting the importance of a Th1 response in the clearance of *Cryptococcus* (Decken *et al.*, 1998) (Rayhane *et al.*, 1999) (Kawakami *et al.*, 2000). IFN-γ is also key in the maturation of dendritic cells (DCs). Localised in the airways DCs phagocytose inhaled *Cryptococcus*, degrade and process the fungus. The DCs then mature and present processed *Cryptococcal* antigen to naïve T cells thereby bridging innate and adaptive immune responses (Syme *et al.*, 2000). Mature DCs also have a role in positive feedback to stimulate the Th1-type response (Vieira *et al.*, 2000).

1.6.5 C. neoformans virulence factors

C. neoformans has serval virulence factors to aid its infection of humans and survival in non-human hosts. Upon entry into the host, the production of a polysaccharide capsule is induced. The stimuli for capsule production are iron deprivation (Vartivarian *et al.*, 1993), neutral/basic pH (Meara and Alspaugh, 2012) and increased CO_2 concentration (Granger *et al.*, 1985). It is speculated that the capsule protects the fungus in the environment from predators and dehydration (Chrisman *et al.*, 2011). In the human host, the capsule downregulates both adaptive and innate immune responses (Retini *et al.*, 1998) (Vecchiarelli *et al.*, 1995) (Macher *et al.*, 1978), and guards the cell from ROS after engulfment in a macrophage (Zaragoza *et al.*, 2008). Strains with reduced capsule production exhibit reduced virulence. Mucicarmine staining of the capsule is used by clinicians to diagnose cryptococcal infections (Meara

and Alspaugh, 2012). Moreover, the capsule has been proposed to conceal components of the fungal cell wall from immune PRRs which induce phagocytosis (Giles *et al.*, 2007). Antibodies and complement are instead required to opsonise the pathogen for phagocytosis (Cross and Bancroft, 1995).

Melanin is a pigment which has a protective role against heat and cold shock (Rosas and Casadevall, 1997) and acts as an antioxidant (Wang and Casadevall, 1994). Moreover, melanin can prevent susceptibility to certain antifungal drugs (van Duin *et al.*, 2002). Laccase enzymes oxidise exogenous diphenolic compounds such as L-DOPA to produce melanin (Zhu *et al.*, 2001). A *lac1Δ* mutant *(LAC1* encodes one of two laccase enzymes) displays attenuated virulence (Salas *et al.*, 1996). Hence, melanin is an important virulence factor.

An array of enzymes secreted by the fungus also act as virulence factors. Urease is an enzyme which catalyses the breakdown of urea to ammonia and carbon dioxide. The production of ammonia raises phagolysosome pH which promotes non-lytic exocytosis and replication by *C. neoformans*. In turn, this limits permeation of the phagolysosome membrane which is believed to facilitate *C. neoformans* passage across the blood brain barrier. Additionally, a *C. neoformans* strain lacking urease is unable to grow on urea as a sole nitrogen source. Together with the fact that pigeon guano is rich in uric acid, uric acid can be degraded by other catabolic enzymes to form urea (**Figure 17**) (Lee *et al.*, 2013), it has been hypothesized that urease aids *C. neoformans* survival in the environment (Fu *et al.*, 2018). Phospholipases, cell membrane degrading enzymes, aid host infection by promoting attachment to host cells (Barrett-Bee *et al.*, 1985) and by inducing invasive growth (Santangelo *et al.*, 2004). Phosphatases and proteases have also been implicated in promoting the attachment to host cells and invasion of host cells respectively (Collopy-Junior *et al.*, 2006) (Chen *et al.*, 1997).

A morphological related virulence factor is the production of titan cells which have been isolated from the lungs of patients (Zaragoza *et al.*, 2010). Titan cells are enlarged cryptococcal cells which measure 50 to 100 μM in diameter (Okagaki *et al.*, 2010) and are, therefore, too large to be phagocytosed (Okagaki and Nielsen, 2012). Muramyl dipeptide, a bacterial peptidoglycan subunit found in serum, and bronchial alveolar lavage fluid has recently been identified as an agent which promotes the yeast to titan

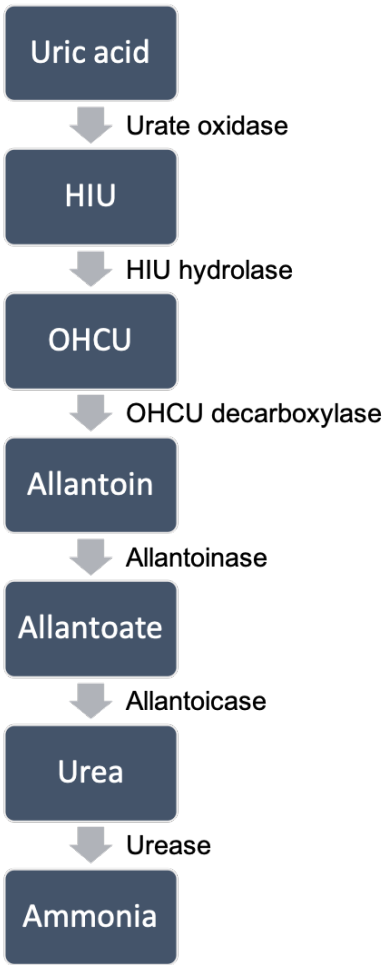

Figure 17: Uric acid degradation pathway in C. neoformans. *Uric acid is degraded by a series of catabolic enzymes to the end product ammonia.*

cell transition in the lungs (Dambuza *et al.*, 2018). In addition to their enlarged sized, titan cells are characterised by their highly cross linked capsule, thicker cell wall, reduced susceptibility to oxidative stress (Okagaki *et al.*, 2010) and increased polyploidy (Gerstein *et al.*, 2015). A mutant harbouring a mutation that reduces titan cell formation exhibits weakened virulence and diminished dissemination (Crabtree *et al.*, 2012).

1.7 Aims and context

Distinct members of the Amt/Mep/Rh superfamily (ammonium transceptors) in fungi regulate morphological change in response to ammonium availability. However, the underlying signalling mechanisms are unknown. Two models have been proposed: the conformational change model, whereby Mep2 acts like a G-protein coupled receptor to interact with a downstream signalling partner, and the pH model, which is dependent on the pathway the proton follows after NH_4^+ deprotonation. This study aims to enhance current knowledge on how ammonium signalling is generally conserved throughout fungi. To address this aim two divergent fungi will be investigated. The wheat pathogen, *Zymoseptoria tritici*, and the human pathogen, *Cryptococcus neoformans* serotype D JEC20/JEC21. Both are dimorphic fungi which are ubiquitous in the environment but belong to different phyla. First, phenotypic studies on different levels of ammonium will be conducted to see if morphological change is induced by ammonium availability. Specifically, established *C. neoformans* phenotypes will be investigated. Next, homology searches will be conducted to identify putative ammonium transporters. These homologues will subsequently be tested for both transport and signalling functions in yeast through complementation studies. Any transporters which are found to have a signalling role will be assayed for separation of function to confirm if they are transceptors. These findings will additionally help increase our understanding of the molecular basis of ammonium signalling. Moreover, the roles of these proteins in their own organism will be explored by generating mutants and undertaking phenotypic studies. In *Z. tritici*, we are also interested in establishing if the ammonium transporters are required for *Z. tritici's* pathogenicity of wheat. The location of these permeases makes them accessible drug targets. Therefore, if any of the *Z. tritici* ammonium transporters are found to be important for virulence fungal drugs could be developed against these transporters.

2 Materials and Methods

2.1 Reagents and chemicals

The chemicals for the media used in this study are listed in **Table 1.** For media containing dextrose, the dextrose was added after autoclaving unless otherwise stated. For solid media, 20 g/l agar was added unless otherwise stated.

Media	Chemicals	Supplier
Luria Bertani (LB)	Tryptone 10 g/l, NaCl 10 g/l, yeast extract 5 g/l	Formedium
2XL	Yeast extract 10 g/l, tryptone 20 g/l, NaCl 1 g/l	Formedium
Calcium/Manganese Medium – pH 5.5	100 mM $CaCl_2$, 70 mM $MnCl_2$, 40 mM sodium acetate	Sigma Aldrich
Yeast Peptone Dextrose (YPD)	Yeast extract 10 g/l, peptone 20 g/l, 2 % dextrose	Formedium
Synthetic Dextrose – Uracil (SD-URA)	Complete synthetic medium – uracil (CSM-URA) 0.77 g/l, yeast nitrogen base (YNB) without amino acids* 6.9 g/l, 2 % dextrose	Formedium, *Melford
0.1 % Proline	0.1 % L-Proline, YNB without amino acids and ammonium sulphate* 1.7 g/l , 2 % dextrose	Ducehfa Biochemie, *Melford
SLAD (low ammonium)	50 μM ammonium sulphate, YNB without amino acids and ammonium sulphate* 1.7 g/l, 2 % dextrose	Sigma Aldrich, *Melford

SHAD (high ammonium)	5 mM ammonium sulphate, YNB without amino acids and ammonium sulphate* 1.7 g/l, 2 % dextrose	Sigma Aldrich, *Melford
SD-URA + 0.1 % Glutamate	CSM-URA 0.77 g/l, YNB without amino acids and ammonium sulphate* 1.7 g/l, 0.1 % glutamic acid*, 2 % dextrose	Formedium, *Sigma Aldrich
SD + 1 mM Ammonium Sulphate	1 mM ammonium sulphate, YNB without amino acids and ammonium sulphate* 1.7 g/l, 2 % dextrose	Sigma Aldrich, *Melford
LB Mannitol	Tryptone 10 g/l, yeast extract 5 g/l, NaCl 2.5 g/l, mannitol* 10 g/l	Formedium, *Sigma Aldrich
Stock A	$MgSO_4$ 10 g/l, KH_2PO_4 29 g/l, NaCl 3 g/l (not autoclaved)	Sigma Aldrich
Stock B	K_2HPO_4 40.5 g/l, $(NH_4)SO_4$ 10 g/l (not autoclaved)	Sigma Aldrich
Stock C	$CaCl_2$ 2 g/l (not autoclaved)	Sigma Aldrich
Completed stock	5 % stock A, 5 % stock B, 5 % stock C, 2.5 g/l $FeSO_4$ (not autoclaved, kept for one week)	Sigma Aldrich
1 M MES (pH 5.3)	1M MES (pH adjusted with 5M KOH, filter sterilised and stored at 4 °C)	Sigma Aldrich
Induction Medium (IM)	10 mM glucose (added before autoclaving), 40 mM MES (pH 5.3), 0.5 % glycerol*, agar 13 g/l	Formedium, *Sigma Aldrich

20x Salts	$NaNO_3$ 120 g/l, KCl 10.4 g/l, $MgSO_4.7H_2O$ 10.4 g/l, KH_2PO_4 30.4 g/l	Sigma Aldrich
Trace elements	$ZnSO_4.7H_2O$ 22 g/l, H_3BO_3 11 g/l, $MnCl_2.4H_2O$ 5 g/l, $FeSO_4.7H_2O$ 5 g/l, $CoCl_2.5H_2O$ 1.6 g/l, $CuSO_4.5H_2O$ 1.6 g/l, $(NH_4)_6Mo_7O^{24}.4H_2O$ 1.1 g/l, Na_4EDTA 50 g/l (heat to boiling and cool to 60 °C before adjusting pH to 6.5 with 5M KOH, then autoclave and store in the dark)	Sigma Aldrich
Aspergillus nidulans Minimal Medium (MM)	5 % 20x salts, 0.1 % trace elements, glucose 10 g/l (added before autoclaving), agar 10 g/l	Formedium

Table 1: Media used in this study.

The buffers used for DNA gel electrophoresis, SDS-PAGE and western blotting are listed in **Table 2**. All buffers were not autoclaved and were kept at room temperature unless otherwise stated.

Buffers	**Chemicals**	**Supplier**
5x TBE	Tris base 54 g/l, boric acid 27.5 g/l, 20 mM EDTA pH 8.0	Sigma Aldrich
5x Running Buffer	Tris base 16 g/l, glycine 94 g/l (kept at 4 °C)	Sigma Aldrich
1x SDS Running Buffer	20 % 5x Running buffer, 1 % SDS	Melford

Western Transfer Buffer	Tris base 3.03 g/l, glycine 14.4 g/l, 20 % methanol*	Melford, *Fisher Scientific
10x PBS	Na_2HPO_4 11.6 g/l, KH_2PO_4 2 g/l, NaCl* 80 g/l, KCl 2.23 g/l (autoclaved)	Sigma Aldrich, *Formedium
1x PBS Tween	10 % 10x PBS, 0.1 % tween	Fisher Scientific
EB Buffer	10 mM Tris pH 7.5, 1 mM $MgCl_2$, 270 mM sucrose	Melford, *Sigma Aldrich, **Fisher Scientific
10x TBS (pH 7.6)	Tris base 24 g/l, NaCl* 80 g/l (autoclaved)	Melford, *Formedium
1x TBST	10 % 10x TBS, 0.1 % tween	Fisher Scientific

Table 2: Buffers used in this study.

The component chemicals of the reagents used in this study are listed in **Table 3**. All reagents were filter sterilised unless otherwise stated.

Reagents	**Chemicals**	**Supplier**
Lysis Buffer	100 mM Tris-HCl* pH 7.5, 0.15 M NaCl, 5 mM EDTA*, 0.5 mM PMSF	Sigma Aldrich, *Melford
Sample Loading Buffer	100 mM Tris-HCl* pH 6.8, 4 mM EDTA*, 4 % SDS, 20 % glycerol, 0.02 % bromophenol blue, 2 % 2-mercaptoethanol (added fresh on day of use)	Sigma Aldrich, *Melford

Chemiluminescent Solution A	100 mM glycine PH 10, 0.4 mM luminol*, 8 mM 4-iodophenol**, (store at 4 °C in dark)	Melford, Fluka analytical, **Sigma Aldrich
Chemiluminescent Solution B	0.12 % hydrogen peroxide, (store at 4 °C)	Fisher Bioreagents
ECL Solution	50 % chemiluminescent solution A, 50 % chemiluminescent solution B, (mix immediately prior to use)	
STET Buffer	8 % sucrose*, 50 mM Tris pH 8.0, 50 mM EDTA, 5 % Triton X-100**	Melford, *Fisher Scientific, **USB
TE Buffer	10 mM Tris-HCl pH 8.0, 1 mM EDTA	Melford

Table 3: Reagents used in this study.

2.2 Strains list

All the strains used in this study are listed in **Table 4 - Table 7**.

2.2.1 Bacterial strains

Strain	Genotype	Reference
SURE *E.coli* cells	e14-(McrA-) Δ*(mcrCB-hsdSMR-mrr)171 endA1 gyrA96 thi-1 supE44 relA1 lac recB recJ sbcC umuC*::Tn*5* (Kanr) *uvrC* [F´ *proAB lacI*qZΔ*M15* Tn*10* (Tetr)]	Stratagene
AGL1	C58 RecA (rif R/carbR) Ti pTiBo542DT-DNA (strepR) Succinamopine	Lazo *et al*., (1991)
LBA4404	Ach5 (RIF R) Ti pAL4404 (strepr) Octopine	Hoekema *et al*., (1983)

Table 4: Bacterial strains used in this study.

2.2.2 Fungal strains

Strain	Genotype	Reference
MLY61a/α	*MATa/α ura3-52/ura3-52*	Lorenz and Heitman., (1997)
MLY108a/α	*MATa/α mep2::LEU2/mep2::LEU2 ura3-52/ura3-52 leu2::hisG/leu2::hisG*	Lorenz and Heitman, (1998)

31019b	*MATa mep1Δ mep2Δ::LEU2 mep3Δ::KanMX2 ura3*	Marini *et al*., (1997)
31021c	*MATa mep1Δ mep2Δ::LEU2 ura3*	Marini *et al*., (1997)
*mep2Δ*Kan	*MATa his3Δ1 leu2Δ0 met15Δ0 ura3Δ0 mep2Δ::KanMX4*	*Sacchromyces* Genome Deletion Project

Table 5: Saccharomyces cerevisiae strains used in this study.

Strain	**Genotype**	**Reference**
IPO323	*MAT1-1*	Goodwin *et al.,* (2011)
IPO323 *Ztmep2Δ* 1	*MAT1-1 Ztmep2::HYG*	This study
IPO323 *Ztmep2Δ* 2*	*MAT1-1 Ztmep2::HYG*	This study
IPO323 *Ztmep2Δ* 3*	*MAT1-1 Ztmep2::HYG*	This study
IPO323 *Ztmep3Δ* 1	*MAT1-1 Ztmep3::HYG*	This study
IPO323 *Ztmep3Δ* 2	*MAT1-1 Ztmep3::HYG*	This study
IPO323 *Ztmep3Δ* 3	*MAT1-1 Ztmep3::HYG*	This study
IPO323 *Ztmep2Δ/Ztmep3Δ* 1*	*MAT1-1 Ztmep2::HYG Ztmep3::GEN*	This study
IPO323 *Ztmep2Δ/Ztmep3Δ* 2*	*MAT1-1 Ztmep2::HYG Ztmep3::GEN*	This study
IPO323 *Ztmep2ΔZztmep3Δ* 3*	*MAT1-1 Ztmep2::HYG Ztmep3::GEN*	This study

Table 6: Zymoseptoria tritici strains used in this study. *ZtMEP2 is disrupted.

Strain	Genotype	Reference
JEC20	*MATa*	Kwon-Chung *et al*., (1992)
JEC21	*MAT*α	Kwon-Chung *et al*., (1992)
JEC20 *amt2Δ*	*MATa amt2::GEN*	This study
JEC21 *amt2Δ*	*MAT*α *amt2::GEN*	This study
JEC20 *amt2Δ* + *AMT2*	*MATa amt2::GEN AMT2::HYG*	This study
JEC21 *amt2Δ* + *AMT2*	*MAT*α *amt2::GEN AMT2::HYG*	This study

Table 7: Cryptococcus neoformans strains.

2.3 Manipulation of bacterial strains

All the bacterial strains used in this study are listed in **Table 4**.

2.3.1 Preparation of Escherichia coli competent cells

SURE competent cells were used as the starting culture for the production of competent cells. Previously prepared competent cells were streaked for single colonies on a Luria-Bertani (LB) agar plate and incubated at 37 °C overnight. A single colony was inoculated into 2 ml of LB medium and incubated overnight with shaking (37 °C, 180 rpm). The 2 ml culture was inoculated into a flask containing 200 ml of 2XL medium and incubated with shaking (30 °C, 180 rpm). At OD_{595} 0.2, sterile magnesium chloride (20 mM) was added to the culture. At OD_{595} 0.5, the flask was placed in an ice-water bath on the bench. After 2 hours, the cells were transferred to four 50 ml falcon tubes and pelleted in a Hermle Z 326 K centrifuge (3000 rpm, 5 min, 4 °C). The supernatant was removed and the cells were gently resuspended in 100 ml of ice cold calcium/manganese medium in a 4 °C cold room using sterile filter tips. The cells were left overnight in the cold room before being pelleted as previously

described. In the cold room, the supernatant was discarded and the cells were resuspended in 10 ml of calcium/manganese medium with glycerol (15 % v/v). The competent cells were finally aliquoted into 50 1.5 ml micro centrifuge tubes, flash frozen in liquid nitrogen and stored in a -80 °C freezer.

2.3.2 Transformation of E.coli competent cells by the heat shock method

Competent cells were removed from the -80 °C freezer and thawed on ice. 50 μl of thawed cells were incubated with 1 μl of plasmid DNA (usually produced by 'Miniprep' section 2.4.11) on ice for 30 min. The mixture was then heat shocked in a 42 °C heat block for 45 seconds. Following a 2 min cool on ice, 800 μl of LB medium was added, and the mixture was incubated in a 37 °C water bath for 60 min. Cells were pelleted in a Progen GenFuge 24D microfuge (10,000 rpm, 1 min) and the supernatant was removed. The pellet was resuspended in 200 μl of LB medium before being inoculated onto an LB agar plate supplemented with the appropriate antibiotic (generally 100 μg ml^{-1} Carbenicillin or 50 μg ml^{-1} Kanamycin) and incubated overnight at 37 °C.

2.3.3 Preparation of Agrobacterium tumefaciens competent cells

A. tumefaciens cells were streaked for single colonies on LB agar plates. The AGL-1 and LBA4404 strains were used for subsequent work in *Zymoseptoria tritici* and *Cryptococcus neoformans* respectively. For LBA4404, LB medium was supplemented with Rifampicin (100 μg ml^{-1}) and Tetracycline (5 μg ml^{-1}) to reduce bacterial contamination. A single colony of *A. tumefaciens* was inoculated into 5 ml LB and incubated overnight with shaking (28 °C, 250 rpm). 2 ml of this overnight culture was used to inoculate a 250 ml flask with 50 ml of LB medium which was incubated with shaking (28 °C, 250 rpm) grown to OD_{600nm} 0.6. Cells were chilled on ice for 5 min, pelleted by centrifugation (3,000 rpm, 5 min, 4 °C), and resuspended in 1 ml of 20 mM $CaCl_2$. Resuspended cells were divided into 100 μl aliquots, flash frozen in liquid nitrogen and stored long term at -80 °C.

2.3.4 Transformation of A. tumefaciens competent cells by the freeze thaw method

A. tumefaciens competent cells were removed from the -80 °C freezer and thawed on ice. 50 μl of thawed competent cells were mixed with 10 μl of plasmid DNA (usually produced by 'Miniprep' section 2.4.11) in a 1.5 ml micro centrifuge tube by gentle tapping. 10 μl of double deionised water (ddH_2O) was mixed with cells for a negative control. The tubes were flash frozen in liquid nitrogen until the bubbling subsided. Tubes were immediately thawed at 37 °C for 5 min. 500 μl of LB medium was added to each tube and the cells were incubated with shaking (28 °C, 250 rpm) for 2 – 3 hours. Cells were then pelleted by centrifugation (10,000 rpm, 2 min), resuspended in 150 μl of LB medium and plated onto LB plates supplemented with kanamycin (50 μg ml^{-1}). For LBA4404, LB plates were also supplemented with rifampicin (100 μg ml^{-1}) and tetracycline (5 μg ml^{-1}). After 2 days incubation at 28 °C, a single transformant was used to inoculate 5 ml of LB medium, supplemented with the appropriate antibiotic(s). Cultures were incubated overnight with shaking (28 °C, 250 rpm). The overnight culture was used to make 15 % glycerol stocks; one 1 ml master stock, and five 75 μl working stocks, which were flash frozen in liquid nitrogen and stored long term at -80 °C (An *et al.*, 1988).

2.4 DNA cloning procedures

All primers and plasmids used in this study are listed in **Table 8 - Table 17**.

2.4.1 High fidelity amplification of DNA by polymerase chain reaction for plasmid preparation

The following reagents were mixed in 0.2 ml polymerase chain reaction (PCR) tubes and $ddH_2O$was added to bring the total volume to 50 μl: 5 μl of NEBioLabs ThermoPol Reaction Buffer (10X), 1 μl of Promega PCR Nucleotide Mix (10 mM), 10 μM of each primer (forward and reverse), template DNA (typically 1 μl of plasmid 'miniprep' section 2.4.11), and 1 unit of NEBiolab vent polymerase. PCR reactions were performed in a TaKara PCR Thermal Cycler or a Labnet Multigene™ Mini under the following conditions: initial denaturation (95 °C, 10 min), denaturation (95 °C, 1 min), annealing

(55 - 65 °C, 1 min), extension (72 °C, 1 min kb^{-1}) and final extension (72 °C, 10 min). Apart from the initial and final conditions, all conditions were cycled 35 times. PCR tubes were then left in the PCR machine at 4 °C until being removed for analysis, short term storage at 4 °C, or long term storage at -20 °C. All primers were purchased from Sigma-Aldrich.

2.4.2 Low fidelity amplification of DNA by polymerase chain reaction for diagnostic purposes

Reagents were mixed in 0.2 ml PCR tubes as stated in section 2.4.1 with the following exceptions: 10 μl of Promega GoTaq Reaction Buffer (5X) and 2.5 units of Promega GoTaq DNA Polymerase were used instead of the NEBioLabs ThermoPol Reaction Buffer (10X) and NEBiolab vent polymerase respectively, and part of a colony (*E. coli, C. neoformans, Z. tritici or S. cerevisiae*) was used as template.

2.4.3 Generation of codon optimised plasmids

Genes of interest were codon optimised to *S. cerevisiae* using Eurofins Genomics GENEius optimisation software. The resulting sequence was cloned into a plasmid by Eurofins Genomics and dispatched in a lyophilised format. Lyophilised DNA pellets were resuspended in TE buffer at a concentration of 100 ng ml^{-1}. 1 μl of resuspended DNA was transformed into *E. coli* to amplify the plasmid (section 2.3.2).

2.4.4 Restriction digestion of PCR products and plasmid DNA

Promega restriction enzymes with their respective buffers were used according to the manufacturer's instructions to digest PCR products and plasmid DNA. For DNA requiring digestion at two sites, a double digest was performed if an appropriate buffer for both enzymes was available; the Promega Restriction Enzyme Tool was used to determine this. Where an appropriate buffer was not available, sequential digests were performed. Typically, a double digest in pCHYG was performed sequentially unless the restriction sites were greater than 10 base pairs apart. The Sigma-Aldrich GenElute™ PCR Clean-Up Kit was used to purify digested DNA after each digest, according to manufacturer's instructions. For plasmid DNA (typically pRS316) being

linearised for subsequent yeast homologous recombination, this purification step was eliminated (section 2.4.9).

2.4.5 Visualisation of DNA by agarose gel electrophoresis

PCR products and plasmid DNA were separated according to size and charge on a 1 % agarose, Tris/Borate/EDTA (TBE) gel supplemented with 0.5 μg ml^{-1} ethidium bromide, in TBE buffer. DNA was separated at 120 V and visualised using ultraviolet light (BioRad Gel Doc™ XR+ Gel Documentation System, and Image Lab™ software).

2.4.6 Extraction of DNA from an agarose gel

DNA separated by size and charge in section 2.4.5, where appropriate, was extracted from the agarose gel using the Sigma-Aldrich GenElute™ Gel Extraction Kit according to the manufacturer's instructions.

2.4.7 Ligation of restriction digested insert DNA into linearised vector DNA

Promega T4 DNA ligase reagents were used to ligate restriction digested PCR fragments (section 2.4.4) or DNA excised from a plasmid into the linearised vector (sections 2.4.4 - 2.4.6). DNA concentrations of insert and vector were quantified using a NanoDrop spectrophotometer (ND-1000, NanoDrop). Approximately 75 ng of vector DNA was used for ligation reactions. The quantity of insert DNA was calculated using the insillico online ligation calculator, with parameters set at a 3:1 insert to vector ratio. Insert and vector DNA were mixed in a 1.5 ml micro centrifuge tube with 1 μl of Ligase 10X Buffer and 1 μl of T4 DNA Ligase. ddH_2O was used to bring the total reaction volume to 10 μl. Additionally, a no insert DNA control reaction was made. Typically, ligation reactions were incubated at 4 °C overnight, according to the manufacturer's instructions. *E. coli* competent cells were transformed with 5 μl of each mixture (section 2.3.2). Where multiple ligations were required, plasmids were sequenced after each ligation reaction.

2.4.8 Gibson assembly of DNA fragments into pCGEN

The NEBiolabs Gibson Assembly® Cloning system was used to ligate PCR fragments (section 2.4.1) purified using the Sigma-Aldrich GenElute™ PCR Clean-Up Kit, and gel extracted GEN (antibiotic resistance marker excised from pCGEN) into linear pCGEN (lacking GEN) (sections 2.4.4 – 2.4.6). The NEBioCalculator was used to determine the fentimolar (fmol) concentrations of each DNA reagent. Approximately 23.5 fmol of vector DNA was mixed with 94 fmol (4X excess) of each DNA fragment, ddH_2O was used to bring the total volume to 10 μl. 2 μl of the DNA mixture was combined with 2 μl of Gibson Assembly Master Mix (2X) in a 0.2 ml PCR tube, incubated in a Labnet Multigene™ Mini thermal cycler (50 °C, 60 min), and chilled at 4 °C overnight. *E. coli* competent cells were transformed with 2 μl of the chilled assembly mixture (section 2.3.2).

2.4.9 Yeast homologous recombination

The haploid *mep2ΔKan* (**Table 5**) was transformed (section 2.5.1) with 10 μl of each PCR product (section 2.4.1) and 10 μl of linearised plasmid DNA (2.4.4) to generate a novel plasmid.

2.4.10 Plasmid DNA recovery from yeast

Single yeast transformants (section 2.4.9) were inoculated into 5 ml of SD-URA medium and incubated overnight at 30 °C on a rotary wheel. Cells were pelleted in a non-sterile 2 ml ribolyser tube (10,000 rpm, 1 min). The supernatant was removed and the cells were resuspended in 200 μl of STET buffer. Following the addition of an equal volume of glass beads, cells were disrupted (Biospec Products Mini-Beadbeater 16) for 30 seconds. The tubes were immediately chilled on ice for 2 min before undergoing more disruption for a further 30 seconds. Cell lysates were collected into 1.5 ml micro centrifuge tubes by centrifugation (3000 rpm, 1 min). The ribolyser tubes were discarded and the cell lysates were incubated at 100 °C for 3 min before being cooled on ice for 2 min. After centrifugation (13,000 rpm, 10 min), the supernatant was added to a fresh micro centrifuge tube containing 100 μl of 7.5 M ammonium acetate, vortexed and freeze precipitated in a -20 °C freezer for 2 hours. The tubes were then

centrifuged (13,000 rpm, 10 min), the top layer was transferred to a fresh micro centrifuge tube and vortexed with 500 μl of ice cold 100 % ethanol. Plasmid DNA was then pelleted by centrifugation (13,000 rpm, 10 min), the supernatant was discarded and the DNA was washed with 500 μl of ice cold 70 % ethanol. DNA was again pelleted by centrifugation (13,000 rpm, 10 min) and the supernatant was discarded. The plasmid DNA pellet was air dried at 65 °C and then resuspended in 30 μl of ddH_2O. *E. coli* were transformed with 15 μl of recovered plasmid DNA (section 2.3.2) (Robzyk and Kassir, 1992).

2.4.11 Isolation of plasmid DNA from E. coli *by 'Miniprep'*

A single colony from the *E. coli* transformation (section 2.3.2) plate was inoculated into 5 ml of LB medium, supplemented with the appropriate antibiotic, and incubated overnight with shaking (30 °C, 180 rpm). Plasmid DNA was isolated from 2 ml of overnight culture using the Sigma-Aldrich GenElute™ Plasmid Miniprep Kit according to the manufacturer's instructions. 100 μl of ddH_2O was used to elute plasmid DNA.

2.4.12 Sequencing of DNA

Novel plasmids prepared in section 2.4.11 or PCR products purified using the Sigma-Aldrich GenElute™ PCR Clean-Up Kit were sequenced by GATC at Eurofins Genomics, using their Supreme Run Tube option.

2.5 Fungal genetic modification

All the fungal strains used in this study are listed in **Table 5**, **Table 6** and **Table 7**.

2.5.1 Saccharomyces cerevisiae yeast transformation

Yeast cells from a Yeast Peptone Dextrose (YPD) agar plate were inoculated into 5 ml YPD medium and incubated on a rotary wheel at 30 °C. The overnight culture was used to inoculate 50 ml of YPD medium in a 250 ml flask to an OD_{595nm} 0.15 – 0.35. Yeast cells were grown to mid log phase (OD_{595nm} 0.50 – 0.85) with orbital shaking (30 °C , 180 rpm). Mid log phase cells were pelleted by centrifugation in a MSE Mistral

2000 centrifuge (3,000 rpm, 3 min) and washed with dH_2O three times before being resuspended in 100 mM Lithium Acetate (300 μl for OD_{595nm} 0.7). 50 μl of cells were mixed in a 1.5 ml micro centrifuge tube with 240 μl of 50 % Poly(ethylene)glycol 4000, 3 μl of plasmid DNA (typically prepared by 'mini-prep' section 2.4.11), 10 μl of salmon sperm DNA and 32 μl of 1 M Lithium Acetate, before being incubated at the following temperatures (30 °C, 20 min) (42 °C, 15 min). Transformed cells were pelleted by centrifugation (10,000 rpm, 30 seconds) and washed once in dH_2O before being resuspended in 1 ml of dH_2O. 200 μl of resuspended cells were spread onto SD-URA agar plates. Transformed colonies appeared after 2 days incubation at 30 °C (Schiestl and Gietz, 1989).

2.5.2 Agrobacterium mediated transformation of Zymoseptoria tritici

Genes in IPO323 were deleted or disrupted using AGL-1 *A. tumefaciens* transformed with a deletion cassette (sections 2.4.7 and 2.4.8) as previously described (Motteram *et al.*, 2009). To achieve gene deletion approximately 1 kb of DNA flanking the gene of interest was ligated either side of the resistance cassette. For gene disruption approximately 1 kb of flanking DNA before the start codon of the gene of interest and 1 kb of DNA after transmembrane domain three of the protein of interest were ligated either side of the resistance cassette. 50 μl of transformed AGL-1 (section 2.3.4) were removed from the -80 °C freezer and plated onto an LB agar plate supplemented with kanamycin (50 μg ml^{-1}) and incubated at 28 °C. After three nights, one 5 μl loop of cells were inoculated into a 250 ml flask containing 40 ml of LB mannitol medium supplemented with kanamycin (50 μg ml^{-1}) and shaken for one night (28 °C, 250 rpm). The following morning 2 ml of cell culture was pelleted in a sterile ribolyser tube by centrifugation (2 min, 13,000 rpm) and washed with 400 μl of IM medium (made one day before transformation) supplemented with acetosyringone (AS) (200 μM). Cells were pelleted by centrifugation and resuspended in 1 ml IM medium + AS supplemented with kanamycin (50 μg ml^{-1}). The resuspended cells were used to inoculate 10 ml IM + AS + kanamycin in a fresh 250 ml flask to $0D_{660nm}$ 0.15, approximately 270 μl of culture was required to achieve this starting optical density. After approximately 3 hours incubation (28 °C, 250 rpm), at $0D_{660nm}$ 0.19 - 0.26, five large 5 μl loops of six day old *Z. tritici*, from a YPD agar plate grown at 16 °C, was resuspended in 30 ml IM + AS + kanamycin medium. 600 μl of *Z. tritici* was mixed with

600 μl of *A. tumefaciens* and supplemented with 6 μl of AS. 200 μl of mixed cells were spread onto a cellophane disc (325 P Cellulose 80 mm. diameter disc produced by A.A. Packaging Limited) on an IM agar (made fresh on day of transformation) plate supplemented with AS. This was repeated on four additional plates. 100 μl of *Z. tritici* was plated as a control. The plates were taped together and left in the dark at room temperature for two nights. Cellophane discs were subsequently transferred to Aspergillus MM agar (made fresh on day of use) plates supplemented with timentin (100 μg ml^{-1}) and hygromycin (100 μg ml^{-1}) or G418 (200 μg ml^{-1}) for pCHYG and pCGEN based transformations respectively, and left under the same conditions until small white colonies appeared, approximately after three weeks. Five to ten colonies from each plate were selected using a sterile cocktail stick, stabbed six times into YPD agar supplemented with timentin and hygromycin or G418 and incubated for six nights at 16 °C. Surviving colonies were then tested by colony PCR for integration of the resistance cassette at the correct locus (section 2.4.2). Positive colonies were streaked for single colonies twice on YPD agar plates supplemented with timentin and hygromycin or G418 before being re-tested by PCR for integration of the resistance cassette and absence of the target gene. Primers used in PCR reactions are listed in **Table 12**. Correct transformants were spread onto YPD hygromycin or G418 plates and incubated for 6 nights at 16 °C. Cells were scraped into 2 ml ribolyser tubes containing 50 % glycerol, flash frozen in liquid nitrogen and stored at -80 °C.

2.5.3 Transformation of Cryptococcus neoformans through electroporation

Electroporation was used to transform *C. neoformans* as previously described (Lin *et al.*, 2015). *C. neoformans* yeast cells were inoculated into 30 ml of YPD medium and incubated overnight (30 °C, 180 rpm). The overnight culture was diluted to OD_{600nm} 0.3 in a 100 ml total volume and grown for an additional three hours, until the density was OD_{600nm} 0.6 to 1.0. Cells were pelleted by centrifugation (3,000 rpm, 5 min) and washed twice with 50 ml of EB buffer. Cells were then resuspended in 50 ml of EB buffer, supplemented with 1 mM DTT, and chilled on ice for 30 – 60 min. Chilled cells were then pelleted by centrifugation and washed with 50 ml of EB buffer before being resuspended in 300 μl of EB buffer. 45 μl of resuspended cells were mixed with 5 μl of DNA (100 – 400 ng) in a 0.2 cm electroporation cuvette and electroporated (BTX ECM 630 Electroporation System). DNA used for the transformation included the

neomycin resistance cassette flanked by the genomic DNA either side of the Amt2 gene. This was initially cloned into pRS316 by yeast homologous recombination (section 2.4.9) and then gel extracted after restriction digestion (section 2.4.4 - 2.4.6). 5 μl of ddH_2O was used as a control. Cells were electroporated (0.45 kV, 125 μF, 400 – 600 Ω) and then immediately resuspended in 1 ml of YPD medium before being incubated at 30 °C for 90 min. Incubated cells were pelleted by centrifugation (10,000 rpm, 1 min) and resuspended in 200 μl of YPD medium before being plated onto YPD agar plates supplemented with G418 (200 μg ml^{-1}). After 2 nights incubation at 30 °C, transformed colonies appeared. Transformants were tested by colony PCR for integration of the neomycin resistance cassette (provides resistance to G418) at the correct locus. Colonies identified as having integrated the resistance cassette at the correct locus were streaked for single colonies twice. New colonies were re-tested for integration of the neomycin resistance cassette and tested for absence of the WT allele by colony PCR. Primers used in PCR reactions are listed in **Table 12**. Positive colonies were inoculated into 5 ml of YPD medium and grown overnight at 30 °C on a rotary wheel. The overnight culture was used to make 15 % glycerol stocks in 2 ml ribolyser tubes which were flash frozen in liquid nitrogen and stored at -80 °C.

2.5.4 *Agrobacterium mediated transformation of C. neoformans*

Reconstituted strains were generated by reintegrating *AMT2* into *C. neoformans* using the LBA4404 *A. tumefaciens* strain transformed with the Amt2 R- pPZPHYG construct (section 2.3.4) as previously described (McClelland *et al.*, 2005). Transformed LBA4404 cells were inoculated into 40 ml of LB mannitol medium and incubated overnight with shaking (28 °C, 250 rpm). LBA4404 cells were pelleted by centrifugation (2 min, 13,000 rpm) and washed twice in dH_2O before being resuspended in IM medium (made one day before transformation) supplemented with acetosyringone (100 μM) at OD_{600nm} 0.15 in a total volume of 8 -12 ml. Resuspended LBA4404 cells were incubated for 6 hrs with shaking (28 °C, 250 rpm). *C. neoformans* cells from a 5 ml overnight YPD culture were washed and diluted to 10^7 cells ml^{-1} in IM medium; a haemocytometer was used to determine cell numbers. LBA4404 and *C. neoformans* were mixed in a micro centrifuge tube at a 1:1 ratio. 200 μl of mixed cells were plated onto IM agar (made fresh on day of transformation) plates supplemented with acetosyringone (100 μM) and left at room temperature for 3 days. 100 μl of *C. neoformans* cells were plated as a control. After 3 days, dH_2O was pipetted on the

plates and the cells were dislodged from the surface using a spreader. The cells were washed three times with dH_2O and transferred onto YPD agar plates supplemented with hygromycin (100 μg ml^{-1}) and cefotaxime (100 μg ml^{-1}) and incubated at 30 °C until colonies appeared. Colonies were streaked for single colonies onto YPD + hygromycin + cefotaxime agar plates and inoculated into 5 ml of YPD medium and grown overnight on a rotary wheel at 30 °C. The overnight culture was used to make 15 % glycerol stocks which were flash frozen in liquid nitrogen and stored at -80 °C.

2.6 Experimental procedures

2.6.1 S. cerevisiae growth assays

The haploid strains 31019b and 31052c were transformed with the plasmids of interest (section 2.5.1) (**Table 17**). A single colony from each transformation plate was inoculated into 5 ml of SD-URA medium and rotated overnight at 30 °C. Cell densities were measured at OD_{595nm}. An equivalent number of cells were pelleted by centrifugation (10,000 rpm, 0.5 min) and washed three times in dH_2O. Cells were resuspended in 500 μl of dH_2O before being serially diluted 10 fold four times. 10 μl of cells were then spotted onto SD – URA + 0.1 % glutamate agar plates and 1 mM ammonium sulphate agar plates at each dilution.

2.6.2 S. cerevisiae pseudohyphal growth assays

The diploid strain MLY108 was transformed with the plasmids of interest (section 2.5.1) (**Table 17**). Single colonies were streaked for single colonies onto SLAD agar plates. Plates were incubated at 30 °C for five to six nights before being visualised and photographed using a Euromex Oxion optical microscope. Single colonies were visualised at 40 X magnification, whereas the edge of a streak of cells was visualised at 100 X magnification.

2.6.3 Preparation of membrane proteins and western blotting

MLY108 was transformed with the plasmids of interest (section 2.5.1) (**Table 17**). Single colonies were inoculated into 5 ml of SD + 0.1 % proline medium and rotated

overnight at 30 °C. The overnight culture was used to inoculate a 250 ml flask with 50 ml of SD + 0.1 % proline medium at OD_{595nm} 0.1 – 0.15. Cells were incubated with shaking (30 °C, 180 rpm) until OD_{595nm} 0.5, when cells were pelleted by centrifugation (3 min, 3,000 rpm) in 50 ml falcon tubes. The supernatant was discarded and the pellet was flash frozen in liquid nitrogen before being stored in a -20 °C freezer. Cell pellets were removed from the freezer and thawed on ice. Thawed cells were washed with 1 ml of dH_2O and transferred to a 1.5 ml micro centrifuge tube. Washed cells were pelleted by centrifugation (1 min, 12,000 rpm), the supernatant was removed and the cells were resuspended in 200 μl of lysis buffer. An equal volume of glass beads (0.45 μM in diameter) were added and the cells were vortexed vigorously for 5 min, with brief interruptions to be chilled on ice. An additional 500 μl of lysis buffer was added to the lysed cells which were then pelleted by centrifugation (3 min, 3,000 rpm). The supernatant was transferred to a clean 1.5 ml micro centrifuge tube and the plasma-membrane enriched fraction was collected by centrifugation (45 min, 13,000 rpm, 4 °C). The supernatant was discarded and the pelleted plasma-membrane was resuspended in 100 μl of 10 % tricholroacetic acid and 900 μl of lysis buffer and chilled on ice for 5 min. The plasma-membrane was precipitated by centrifugation (10 min, 13,000 rpm, 4 °C) and then neutralised with 20 μl of 1 M Tris Base and 80 μl of sample loading dye and incubated (37 °C, 15 min). For *Z. tritici* proteins expressed in *S. cerevisiae*, precipitates were incubated at room temperature for 20 min. After centrifugation (30 seconds, 10,000 rpm), the supernatant was transferred to a fresh 1.5 ml micro centrifuge tube; 5 -10 μl of each sample were loaded onto a 10 % SDS-polyacrylamide gel (Rutherford *et al.*, 2008a). Proteins were run at 120 V for 135 min. Proteins were transferred onto a methanol activated Immobilon-P PVDF membrane using a semi-dry transfer system (21 V, 60 min). The membrane was subsequently blocked with 10 % BSA/TBST for 30 min (if FLAG or Myc tagged proteins or Pma1 were being detected), or 5 % milk/PBST for 60 min (if HIS tagged proteins or Pma1 were being the detected) and cut at the 80 kDa mark to separate the proteins of interest from the loading control (Pma1). Membranes were then incubated overnight at 4 °C with their appropriate antibody (1:5000 Anti-His_6-Peroxidase (Roche), 1:2500 Anti-FLAG (Sigma Aldrich), 1:2500 Anti-Myc (Sigma Aldrich), 1:2500 Anti-Pma1(Thermo Fisher Scientific)) suspended in either 5 % milk/PBST or 5 % BSA/TBST. The following morning the membranes were washed three times with either PBST or TBST (the same as used previously). For FLAG or Myc tagged proteins and Pma1, membranes were incubated for an additional 1 hour at room temperature with an Anti-Mouse IgG

monoclonal horseradish peroxidase conjugated secondary antibody (Sigma Aldrich) (1:5000 suspended in either 5 % milk/PBST or 5 % BSA/TBST), before being washed three times as previously described. Membranes were then incubated at room temperature with ECL solution for 5 min before being exposed to X-ray film and developed using an automatic developer (Xography Imaging Systems Compact X4).

2.6.4 Z. tritici pre-growth procedure

Z. tritici cells taken from a -80 °C glycerol stock were streaked onto a YPD plate and incubated for five to six days at 16 °C. Using a pipette tip, a small scraping of cells were inoculated into 5 ml of YPD medium and incubated over three nights with orbital shaking (18 °C, 180 rpm).

2.6.5 Z .tritici growth assays

Z. tritici was pre-grown as previously described (section 2.6.4). Cell densities of each strain were measured at OD_{595nm}. An equivalent number of cells, were pelleted by centrifugation (10,000 rpm, 1 min). Cells were washed three times in dH_2O and resuspended in 500 μl of dH_2O. Each strain was serially diluted tenfold four times. 10 μl of each dilution was pipetted onto an agar plate and incubated at 18 °C for 1 week before being photographed with a Nikon camera using Robosoft Software.

2.6.6 Z. tritici phenotypic analysis

Z. tritici was pre-grown as previously described (section 2.6.4). Cell densities of each strain were measured at OD_{595nm}. An equivalent number of cells were pelleted by centrifugation (10,000 rpm, 1 min). Cells were washed three times in dH_2O and resuspended in 500 μl of dH_2O. 5 μl of each strain was pipetted into the centre of an agar plate and incubated at 18 °C for at least 1 week before being photographed with a Nikon camera using Robosoft Software and photographed at higher magnification using a microscope. For single colony analysis, cells from YPD plates were streaked onto agar plates using flat tooth picks and then incubated at 18 °C for at least 1 week before being photographed using a microscope.

2.6.7 Gene expression analysis in Z. tritici

2.6.7.1 Culturing of cells

Z .tritici was pre-grown as previously described (section 2.6.4). 2 ml of culture was inoculated into 25 ml of YPD medium in a 250 ml flask and incubated for an additional 2 nights (18 °C, 250 rpm). Cells were then pelleted by centrifugation (3,000 rpm, 5 min), washed three times in 25 ml dH_2O and resuspended in 5 ml dH_2O. Cells were inoculated into 50 ml of the medium of interest at OD_{595nm} 2 and incubated with shaking (18 °C, 180 rpm). For analysis of virulence genes, cells were incubated for 2 hours. For analysis of *MEP* genes, cells were incubated for 8 hours. After the appropriate incubation time, cells were harvested by centrifugation (3,000 rpm, 5 min) in 50 ml falcon tubes. The supernatant was removed and the cells were washed in dH_2O before being flash frozen in liquid nitrogen and stored at -20 °C.

2.6.7.2 Extraction of RNA

A pestle and mortar were pre cooled with liquid nitrogen. Frozen cell pellets (prepared in section 2.6.7.1) were ground to a fine powder in the mortar with the pestle. The mortar was constantly replenished with liquid nitrogen to prevent the cells thawing. Ground cells were poured into a fresh 50 ml falcon tube, pre chilled in liquid nitrogen, and placed on ice. After the liquid nitrogen had evaporated off, the lid was tightly screwed onto the tube and the tube was placed in liquid nitrogen. RNA was extracted from the ground cells by the addition of 2 ml of trizol (Sigma Aldrich). After 5 min, 400 μl of chloroform was added and the whole mixture was hand shaken for 30 seconds. After dividing the mixture between two 1.5 ml micro centrifuge tubes and leaving to settle for 3 min, the tubes were centrifuged (10,000 rpm, 15 min). The upper aqueous phase was pipetted evenly into two new 1.5 ml micro centrifuge tubes; care was taken to not disrupt the interphase. 500 μl of isopropanol was added to each tube, and the tubes were inverted gently three times to mix before being incubated for 10 min at room temperature. After centrifugation (10,000 rpm, 10 min), the supernatant was poured onto absorbent paper. The RNA pellets were combined into one tube and washed with 500 μl of 70 % ethanol and centrifuged (10,000 rpm, 10 min). The supernatant was discarded onto absorbent paper and the RNA pellets were air dried

and resuspended in 50 μl of ddH_2O. RNA concentration was determined using a NanoDrop spectrophotometer.

2.6.7.3 DNAse treatment of RNA

The Primer Design Precision DNase kit was used to remove genomic DNA from the RNA (section 2.6.7.2). For 50 μl of RNA, 5 μl of 10 X buffer and 0.6 μl of DNase were added. The RNA DNase mixture was incubated at 30 °C for 30 min to remove DNA, and 55 °C for 5 min to inactive the DNase.

2.6.7.4 Preparation of cDNA

DNase treated RNA (section 2.6.7.3) was converted to cDNA using the Promega GoScript™ Reverse Transcription System according to the manufacturer's instructions. Up to 5 μg of RNA was incubated with 1 μl of random primer and 1 μl of $oligo(dT)_{15}$ primer in a 5 μL total volume at 70 °C for 5 min and then chilled on ice for 5 min. On ice, 4 μl of GoScript™ 5X reaction buffer, 3.8 μl of $MgCl_2$, 1 μl of dNTP, and 1 μl of GoScript™ reverse transcriptase were mixed in a 1.5 ml micro centrifuge tube, ddH_2O was used to bring the final volume to 15 μl. 15 μl of the reverse transcription mix were combined with the RNA primer mix and heated at 25 °C for 5 min and then 42 °C for 1 hour. The reverse transcriptase was heat inactivated at 70 °C for 15 min. cDNA was diluted 1 in 20 (if 5 μg of RNA was converted to cDNA) and stored at -20 °C.

2.6.7.5 qPCR

The Sigma-Aldrich KAPA SYBR® FAST Universal kit was used to carry out qPCR reactions. The following reagents were added to Qiagen 0.1 ml strip tubes on ice: 5 μl of 2 X KAPA SYBR® FAST mix, 2.8 μl of ddH_2O, 2 μl of diluted cDNA (section 2.6.7.4) and 0.2 μl of 10 μM primer mix. The primer mix consisted of a forward and reverse primer for the gene of interest and are listed in **Table 14**. Primer pairs were designed to have an equivalent annealing temperature of approximately 60 °C. qPCR reactions were run for 50 cycles in triplicate in a Corbett Rotor Gene 6000 real-time rotary analyser, using a 2 step programme with melt. The Ct threshold was set at the half

way point on the exponential phase of the graph and the Ct values were normalised to the housekeeping gene actin. Microsoft Excel was used to analyse Ct values, calculate error bars and perform a 2 tailed Student T test.

2.6.8 Wheat infection assay

Wheat infection assays were carried out by Dr Jason Rudd at Rothamsted Research. Three independent isolates for each *Z. tritici* mutant were spread onto YPD agar plates from -80 °C glycerol stocks. Plates were immediately dispatched for testing. Upon arrival at Rothamsted Research, YPD agar plates were incubated at 16 °C for four to five days. Fungal spores were harvested and resuspended in water containing 0.1 % (v/v) Tween-20 at a density of 10^7 spores ml^{-1}. Wheat leaves were inoculated with spores using a swab stick attached to a cotton sterile tip. Control wheat leaves were inoculated with water containing 0.1 % (v/v) Tween-20 without fungal spores. Inoculated plants were incubated in the dark and at high relative humidity for 48 hr in plastic trays with plastic lids. Conditions were achieved by covering the plants with black plastic sheeting. Plants were then incubated in the light and at high humidity for up to 21 days (Keon *et al.*, 2007) (Orton *et al.*, 2017).

2.6.9 C. neoformans confrontation assay

C. neoformans cells of opposite mating type were patched onto low ammonium (50 μM) and high ammonium (5 mM) agar 1 mm apart from each other, using flat toothpicks and incubated in the dark for 3 weeks. Cells were observed for hyphal growth visually with the naked eye and under the microscope.

2.6.10 C. neoformans fruiting assay

Both *C. neoformans* mating types were patched onto low ammonium and high ammonium agar in the absence of their opposite mating type using flat toothpicks and incubated in the dark for 3 weeks. Cells were observed for hyphal growth visually with the naked eye and under the microscope.

2.6.11 C. neoformans invasive growth assay

Surface cells from the confrontation assay (section 2.6.9) and fruiting assay (section 2.6.10) were washed off with dH_2O and gentle rubbing. The plates were left to air dry before being photographed and observed under the microscope. For microscopy, a cover slip was placed onto the agar and a 1000 X oil immersion lens was used.

2.7 Bioinformatics

2.7.1 Retrieval of fungal sequences

Sequences were retrieved from the *Z. tritici* and *C. neoformans* (JEC21) EnsemblFungi websites using the BLAST search tool. The protein sequence of the homologue in *S. cerevisiae* was inputted into the protein sequence data box. *S. cerevisiae* protein sequences were initially downloaded from the *Saccharomyces* Genome Database. The parameters were set to Protein database and BLASTP.

2.7.2 Sequence alignment

DNA was sequenced by GATC Biotech (a Eurofins Genomics company) using their Supreme Run tube service. Returned sequences were inputted into the online EMBOSS Needle tool along with the expected sequences. The abi traces were analysed using the GATCViewer software.

https://www.ebi.ac.uk/Tools/psa/emboss_needle/

2.7.3 Transmembrane domain prediction

Protein sequences in the FASTA format were inputted into the TMHMM Server v. 2.0 online software tool to predict the transmembrane domains present.

http://www.cbs.dtu.dk/services/TMHMM/

2.8 Plasmids and primers list

Plasmids and primers used this study are listed in **Table 8 - Table 17**

2.8.1 Primers

Plasmid	Primer	Primer Sequence 5'-3'
ZtMep2 pCHYG	ZtMep2 -1kb SacI F	GCATCGGAGCTCCATCAAGTAGATCC ATCATG
	ZtMep2 -1kb KpnI R	GATCAGGGTACC CTGCCTTGGTCGGTCGACAT
	ZtMep2 +1kb Xba1 F	GTCGAGTCTAGAGAGAGGTCGGAGG TGCAGAC
	ZtMep2 +1kb Hpa1 R	GTATCGGTTAACGGCTTCGACCTTGT GATCGAC
ZtMep2 Dis - pCHYG	ZtMep2 -1kb SacI F	GCATCGGAGCTCCATCAAGTAGATCC ATCATG
	ZtMep2 -1kb KpnI R	GATCAGGGTACC CTGCCTTGGTCGGTCGACAT
	ZtMep2 D +750 SpeI F	GTCGAGACTAGTGAACGAGGTAAACT CCTC
	ZtMep2 D +750 HpaI R	GGATCGGTTAACCCATTCCAGTAACG CTATCG

ZtMep3 pCHYG	ZtMep3 -1kb ApaI F	GTCGAAGGGCCCGATAGCCGTGGTCAGAATGC
	ZtMep3 -1kb KpnI R	CACCGTGGTACCCCGACGAAGAAGTATGACAT
	ZtMep3 +1kb XbaI F	CAGTCATCTAGAGAGAAGCGCAAGCTGGTGG
	ZtMep3 +1kb HpaI R	GCGTACGTTAACGAGGCAAAGTCAGTCGAAAGG

Table 8: Primers used to clone DNA to be ligated into pCHYG.

Plasmid	**Primer**	**Primer Sequence 5'-3'**
ZtMep3 pCGEN	ZtMep3-GEN -1KB F	AGGCCACCATGTTGGGCCCGGCGCGCCGAATTCGATAGCCGTGGTCAGAATGC
	ZtMep3-GEN -1KB R	TGGTGGAGTGAGGGGTACCGAGCTCCCGACGAAGAAGTATGACAT
	ZtMep3-GEN+1KB F	GTCTACTGCTGGCGTCGACCTAGGGGAGAAGCGCAAGCTGGTGG
	ZtMep3-GEN+1KB R	GCATGCCTGCAGGTCGACTCTAGAGGATCCGAGGCAAAGTCAGTCGAAAGG

Table 9: Primers used to clone DNA for Gibson Assembly.

Plasmid	Primer	Primer Sequence 5'-3'
Amt2 Dis NEO pRS316	Amt2 KO -1kb KpnI	GCTGCAGGAATTCGATATCAAGCTTA TCGATACCGGTACCGAGGCTGGAGA TGGAAGGTGTATCC
	Amt2 KO -1kb	GGGCGAATTCCAGCACACTGGCGCA TTAGAATAAGTATTGGGCCTGG
	Amt2 KO NEO -1kb	CCAGGCCCAATACTTATTCTAATGCG CCAGTGTGCTGGAATTCGCCC
	Amt2 D NEO +1kb	CCGATACGAGACCGTTCAGCGGGAT ATCTGCAGAATTCGC
	Amt2 D +1Kb	GCGAATTCTGCAGATATCCCGCTGAA CGGTCTCGTATCGG
	Amt2 D XbaI	GGAACAAAAGCTGGGTACCGGGCCC CCCCTCGAGTCTAGAGAAAAGTCAGT GGGAACGTTC

Table 10: Primers used to make Amt2 disruption vector using yeast homologous recombination.

Primer	Primer Sequence 5'-3'
pCHYG -1kb F	GGCAGGATATATTGTGGTG
pCHYG -1kb R	GAACCATCTTGTCAAACGACAC
pCGEN -1kb R	GGCAGAGAAATCGCAACCTCGGCC
pCHYG +1kb F	GCGGCCGTCTGGACCGATGG
pCGEN +1kb F	GCGGAGGAGTTCTTCGTTGCGGG
pCHYG +1kb R	GACCGGCAACAGGATTCAATC

Table 11: Primers used to diagnose and sequence deletion cassette vectors.

Diagnose	Primer	Primer Sequence 5'-3'
IPO323 *Ztmep2Δ* (Left)	ZtMep2 Diag F	CAAGCGGATCATCGCGAAG
	HygTrpC R	CCACTAGCTCCAGCCAAGCC
IPO323 *Ztmep2Δ* (Right)	PCHYG +1KB Diag 1F	GACCAACTCTATCAGAGCTTG
	ZtMep2 DiagR R	GGCTTGGCTGGAGCTAGTGG
	*ZtMep2 DiagR Dis R	GAACCTTCTTGGACGGAAGATTC
IPO323 Ztmep2Δ (WT allele)	IPO323 MEP2 F	CGTCTTCTACAATGCCGGAG
	IPO323 MEP2 R	GACAGCATACATCAAATCCGG
IPO323 *Ztmep3Δ* (Left)	ZtMep3 diag F	CTCCGCTGTCAACGATCGAG
	HygTrpC R	CCACTAGCTCCAGCCAAGCC
IPO323 *Ztmep3Δ* (Right)	PCHYG +1KB Diag 1F	GACCAACTCTATCAGAGCTTG
	ZtMep3 DiagR R	GATCAGCAGGCATGGTCTTG
	ZtMep3 exon 2 F	GACTACGGTGGTGATTCTGCCACCGA GAACGTCAACGG

IPO323 Ztmep3Δ (WT allele)	ZtMep3 exon 2 R	GTGACAGCGCAGAATTGCATCTGGTAGAAAGCGTAGAG
IPO323 *Ztmep2Δ/ Ztmep3Δ* (Left)	ZtMep3 Diag 2 F	GTATGGATCTAGCTCAATGC
	pCGEN -1kb R	GGCAGAGAAATCGCAACCTCGGCC
IPO323 *Ztmep2Δ/ Ztmep3Δ* (Right)	PCGEN +1KB 2 F	CCTGTCAGACACTCTAGTTG
	ZtMep3 DiagR R	CAAGACCATGCCTGCTGATC
IPO323 *Ztmep2Δ/ Ztmep3Δ* (WT allele)	ZtMep3 exon 2 F	GACTACGGTGGTGATTCTGCCACCGAGAACGTCAACGG
	ZtMep3 exon 2 R	GTGACAGCGCAGAATTGCATCTGGTAGAAAGCGTAGAG
Jec21 *amt2Δ* (Left)	AMT2 Diag F	GGGTCCGATGTTGTTCGATG
	NEO Diag R primer	GTCTCTGAAACCAGGAAGC
Jec21 *amt2Δ* (WT allele)	Amt2 Dis Diag 1F	CCGTCTCGCACTACAACAAC
	Amt2 Dis Diag 1R	CACTGGAAAGACCCGACGGC

Table 12: Diagnostic primers to confirm integration of the antibiotic resistance cassette and absence of the WT allele in mutants. **Primer used for disruption mutant.*

Plasmid	Primer	Primer Sequence 5'-3'
ZtMep1 CO pRS316	M13 F	GTAAAACGACGGCCAGTG
	ZtMep1 CO 1R	CTTCTGCCGGAGAGGACATTGTTGATATTGTATTG
	ZtMep1 CO 1F	CAATACAATATCAACAATGTCCTCTCCGGCAGAAG
	ZtMep1 CO 2R	CAGAACACCAGTGGAAGCAGC
	ZtMep1 CO 2F	GCTGCTTCCACTGGTGTTCTG
	ZtMep1 CO 3R	CATTAGTGATGGTGATGGTGATGCACCATTGCTCTGCCTGG
	ZtMep1 CO 3F	CCAGGCAGAGCAATGGTGCATCACCATCACCATCACTAATG
	M13 R	CAGGAAACAGCTATGACC
ZtMep2 CO pRS316	M13 F	GTAAAACGACGGCCAGTG
	ZtMep2 CO ScMep2 prom R	CGGCAAACTTCCTTGATCCGTTGACATTGTTGATATTGTATTGTAATATATTAAG
	ZtMep2 CO ScMep2 prom F	CTTAATATATTACAATACAATATCAACAATGTCAACGGATCAAGGAAGTTTGCCG
	ZTMep2 CO M R	GGTTATGCATACCAATCCGG

	ZtMep2 CO M F	CC GGA TTG GTA TGC ATA ACC
	ZtMep2 CO His tag R	TTAGTGATGGTGATGGTGATGCATGG CATACCCAGTTTG
	ZTMep2 CO His tag F	CAA ACT GGG TAT GCC ATGCATCACCATCACCATCACTAA
	M13 R	CAGGAAACAGCTATGACC
ZtMep3 CO pRS316	M13 F	GTAAAACGACGGCCAGTG
	ZtMep3 CO 1R	CCAACAAAGAAGTAGCTCATTGTTGA TATTGTATTG
	ZtMep3 CO 1F	CAATACAATATCAACAATGAGCTACTT CTTTGTTGG
	ZtMep3 CO 2R	GCCATTACAGCTCTCAGATTAGCTCC
	ZtMep3 CO 2F	GGAGCTAATCTGAGAGCTGTAATGGC
	ZtMep3 CO 3R	TTAGTGATGGTGATGGTGATGATGCC CACCAGCTTGAGCTTC
	ZtMep3 CO 3F	GAAGCTCAAGCTGGTGGGCAT CATCACCATCACCATCACTAA
	M13 R	CAGGAAACAGCTATGACC
Amt2 CO pRS316	M13 F	GTAAAACGACGGCCAGTG

	Amt2 CO ScProm 1R	GGTATATGTGACATTGACCATTGTTG ATATTGTATTGTAATATATTAAG
	Amt2 CO ScProm 1F	CTTAATATATTACAATACAATATCAAC AATG GTCAATGTCACATATACC
	Amt2 CO 2R	GCGGAAAGAGCGGAACCACC
	Amt2 CO 2F	GGTGGTTCCGCTCTTTCCGC
	Amt2 CO FLG ScT 3R	CGTCGTCATCCTTGTAATCTACGTCA ACTCTGCCTCC
	Amt2 CO FLG ScT 3F	GGAGGCAGAGTTGACGTAGATTACAA GGATGACGACG
	M13 R	CAGGAAACAGCTATGACC
H191A	M13 F	GTAAAACGACGGCCAGTG
	Amt2 CO ScProm 1R	GGTATATGTGACATTGACCATTGTTG ATATTGTATTGTAATATATTAAG
	Amt2 CO ScProm 1F	CTTAATATATTACAATACAATATCAAC AATGGTCAATGTCACATATACC
	Amt2 CO H191A R	CTGAACTAATAGCAACAGGTGTAC
	Amt2 CO H191A F	GTACACCTGTTGCTATTAGTTCAG
	Amt2 CO FLG ScT 3R	CGTCGTCATCCTTGTAATCTACGTCA ACTCTGCCTCC

	Amt2 CO FLG ScT 3F	GGAGGCAGAGTTGACGTAGATTACAA GGATGACGACG
	M13 F	CAGGAAACAGCTATGACC
H191E	M13 F	GTAAAACGACGGCCAGTG
	Amt2 CO ScProm 1R	GGTATATGTGACATTGACCATTGTTG ATATTGTATTGTAATATATTAAG
	Amt2 CO ScProm 1F	CTTAATATATTACAATACAATATCAAC AATGGTCAATGTCACATATACC
	Amt2 CO H191E R	CTGAACTAATTTCAACAGGTGTAC
	Amt2 CO H191E F	GTACACCTGTTGAAATTAGTTCAG
	Amt2 CO FLG ScT 3R	CGTCGTCATCCTTGTAATCTACGTCA ACTCTGCCTCC
	Amt2 CO FLG ScT 3F	GGAGGCAGAGTTGACGTAGATTACAA GGATGACGACG
	M13 R	CAGGAAACAGCTATGACC
N241A	M13 F	GTAAAACGACGGCCAGTG
	Amt2 CO ScProm 1R	GGTATATGTGACATTGACCATTGTTG ATATTGTATTGTAATATATTAAG
	Amt2 CO ScProm 1F	CTTAATATATTACAATACAATATCAAC AATGGTCAATGTCACATATACC

	Amt2 CO N241A R	CGGAACCACCAGCAAAACCAAAC
	Amt2 CO N241A F	GTTTGGTTTTGCTGGTGGTTCCG
	M13 R	CAGGAAACAGCTATGACC
H342A	M13 F	GTAAAACGACGGCCAGTG
	Amt2 CO ScProm 1R	GGTATATGTGACATTGACCATTGTTG ATATTGTATTGTAATATATTAAG
	Amt2 CO ScProm 1F	CTTAATATATTACAATACAATATCAAC AATGGTCAATGTCACATATACC
	Amt2 CO 2R	GCGGAAAGAGCGGAACCACC
	Amt2 CO 2F	GGTGGTTCCGCTCTTTCCGC
	Amt2 CO H342A R	CACCAATACCAGCAGAGGC
	Amt2 CO H342A F	GCCTCTGCTGGTATTGGTG
	M13 R	CAGGAAACAGCTATGACC
G343C	M13 F	GTAAAACGACGGCCAGTG
	Amt2 CO ScProm 1R	GGTATATGTGACATTGACCATTGTTG ATATTGTATTGTAATATATTAAG
	Amt2 CO ScProm 1F	CTTAATATATTACAATACAATATCAAC AATGGTCAATGTCACATATACC
	Amt2 CO 2R	GCGGAAAGAGCGGAACCACC

Amt2 CO 2F	GGTGGTTCCGCTCTTTCCGC
Amt2 CO G343C 2R	CATACCACCAATACAATGAGAGGCAAATAC
Amt2 CO G343C 2F	GTATTTGCCTCTCATTGTATTGGTGGTATG
M13 R	CAGGAAACAGCTATGACC

Table 13: Primers used to create codon optimised plasmids using yeast homologous recombination.

Primer	**Primer Sequence 5'-3'**
ACT1 F	TCGTGATTTGACCGACTAC
ACT1 R	GGATCTCCTGCTCAAAGTC
3LYSM F	GGCATCGATAACCCAGAC
3LYSM R	GGTGTTCGTAATCACTGGG
IPO323 MEP2 F	CGTCTTCTACAATGCCGGAG
IPO323 MEP2 R	GACAGCATACATCAAATCCGG
IPO323 MEP3 4F	GTCATACTTCTTCGTCGGGC
IPO323 MEP3 4R	GGTTGTTCGTAGCGTATCGAG

Table 14: Primers used for qPCR.

Primer	Primer Sequence 5'-3'
H99/KN99 ACTIN F*	CCTGACGGTCAGGTCATCAC
H99/KN99 ACTIN R*	GAACCACCGATCCAGACACTG
JEC21 AMT2 F	CCTGTCTATGGCTGGTGTTGC
JEC21 AMT2 R	CAAAGTCGAGACCGCCCATG

Table 15: Primers used for reverse transcription PCR. *The same actin primers can be used for both H99/KN99 and JEC20/JEC21 strains

Primer	Primer Sequence 5'-3'
ZtMep1 Mep1 F	GTTCAGCGTCACTGGGGCTTG
ZtMep1 transposon R	GGACTCGAAGTTTAATGTGGCG
ZtMep1 transposon F	CCTCTTAGAGCACACCGTC
ZtMep1 Mep1 R	CGTGGAGCTTGAAGACATCG

Table 16: Primers to identify ZtMep1 transposon.

2.8.2 Plasmids list

The plasmids used in this study are listed in **Table 17** while the plasmid maps of plasmids generated in this study, along with their codon optimised sequence, where appropriate, are depicted in **Figure 18 - Figure 30**.

Plasmid	Construct	Reference
pRS316	*URA3*-CEN	(Sikorski and Hieter, 1989)
pJRH7	Mep2-N4Q-FLAG *URA3-CEN*	Rutherford *et al.,* (2008)
ScMep2 WT HIS	Mep2-N4Q-HIS *URA3-CEN*	Rutherford lab
pCHYG	*TrpC–Hph*	Motteram *et al.,* (2009)
pCGEN	*Pgpd1-Gen*	Motteram *et al.,* (2011)
ZtMep2-pCHYG	*ΔZtmep2::TrpC–Hph*	This study
ZtMep2-pCHYG (disruption)	*ΔZtmep2::TrpC–Hph*	This study
ZtMep3-pCHYG	*ΔZtmep3::TrpC–Hph*	This study
ZtMep3-pCGEN	*ΔZtmep3::Pgpd1-Gen*	Rutherford lab
pJAF1	*Neo^r*	Fraser *et al.* (2003)
Amt2-NEO-pRS316	*Δamt2::Neo^r*	This study
pPZP-Hyg	*Hyg^r*	Walton *et al.* (2005)
Amt2 R–pPZP-Hyg	*AMT2::Hyg^r*	Rutherford lab
ZtMep1-pRS316	ZtMep1-HIS *URA3*-CEN	This study
ZtMep2-pRS316	ZtMep2-HIS *URA3*-CEN	This study

ZtMep3-pRS316	ZtMep3-HIS *URA3*-CEN	This study
Amt2-pRS316	Amt2-FLAG *URA3*-CEN	This study
$Amt2^{H191A}$-pRS316	Amt2-H191A-FLAG *URA3*-CEN	This study
$Amt2^{H191E}$-pRS316	Amt2-H191E-FLAG *URA3*-CEN	This study
$Amt2^{N241A}$-pRS316	Amt2-N241A-FLAG *URA3*-CEN	This study
$Amt2^{H342A}$-pRS316	Amt2-H342A-FLAG *URA3*-CEN	This study
$Amt2^{G343C}$-pRS316	Amt2-G343C-FLAG *URA3*-CEN	This study
$Amt2^{S282A}$-pRS316	Amt2-S282A-FLAG *URA3*-CEN	This study
$Amt2^{S282D}$-pRS316	Amt2-S282D-FLAG *URA3-CEN*	This study

Table 17: Plasmids used in this study.

```
ATG TCC TCT CCG GCA GAA GTG TAT TCC GAT ATG TTC CCA GTT CCT GAA
TAC GAC CCA TCT ATG CCT AGA GGT GGG AAT ACG TTG GAA GTA AAC GTA
AAC GAC CAA TAT ACT GGC CAT GAG TTT CAC TAC GTG TAT CTA ACC GTG
TGT GCC TTC TTA GTT TGG ATG ATC ATT CCT GGA ATT GGA CTG TTG TAC
TCG GGG TTG GCT AGA AGA AAA TCT TCC CTT GCT CTG TTG TTT CAG ACA
TTA ATG GTA ATC GCT ATT GTG ACT TTT CAA TGG ATG TTT TGG GGT TAT
TCT CTA GCC TAT TCT AGA ACT GGT AAT GCG TTC ATT GGC AAT TTG GAC
AAT TTT GGT CTA ATG GGA GTT AGG GTG GCT CCA TCT CCA GGA AAT GCC
TTT CTT CCC GAA ATT ATC TTC TGC TTC TAT CAG CTG TTA TTC TGC GCT
GTT ACC GTT CAA CTT GTC ATT GGT GGA GCC TTT GAA AGA GGC GGT ATA
TTG GCC AGT CTG TTA TTT TCC TTT ATA TGG GCA ACA ATT GTC TAC TGT
CCT GTA GCA AAT TGG ACC TGG AAT AGC AAT GGT TGG TTG TAC AAC TTA
GGT GAA CTA GAT TTT GCA GGA GGT GGC CCG GTT CAC ATA GCA TCA GGT
TGT GCT TCA TTG GCC TAT GCG TTG ATT TTA GGC AAA CGT CAA GTG AAA
TCA GAG ATA GGT AGA GGT AGA ACA AAA CCC CAT AAT GCC TCA TTG GTT
TGG TTA GGA ACT ATG TTG ATA TGG TTC GGA TGG TTT GGA TTC AAT GGT
GGT TCA GCC CTG AAT GCT TCG GTA AGA TCG CTT TAT GTC GTC TTT AAC
ACG AAT ACT GCT GCT TCC ACT GGT GTT CTG GGT TGG GTC CTT GTC GAT
ATG GTT AGG AAC AAG GGC AAG TTT TCA GTA ACA GGT GCA TGC GAA GGA
GCC ATT GCT GGC TTA GTT GGA ATC ACT CCA GCT GCC GGT TAC GTT AAT
TTC TGG TTA GCT GCA CTT ATC GGG TTC TTA ACG GGC ATA GTC TGT AGT
AGC CTA CAT GAT TTG AAC GAT TTG TTG AAT ATC GAC GAA GGC TTG GAT
GTC TTT AAG CTT CAC GGT ATA GGT GGT ATG GTT GGT TCT TTC TTA ACA
GGT ATA TTC GCG GAT GCA CCT ATC GGT GCA TTG GAC TAC GAA CTA GAG
ATT GCG GGT GCG ATT AAC GGT AAC GGT GTG CAA ATT GGG TAC AAC TTA
GCT GGG ATC GTA GCT ATA GCA GCA TAT AGC TTT ACT GTA ACC TCA ATT
ATC TTA CTA GTC TTA AGG TAT ATT CCA GGT GTT GGC TTG AGA GTT TCA
GCT GAA GAT GAA ATG ATG GGC TTG GAT GCT GTT CAT TTT GCA GAC GAA
GAG ATT GGG GAT TGG GAA TAT ATG AAA GAA GCT CGT AGT ACC TTA AAC
GGA CAT GAT GGG ACA GAG CAA AGT AGG AGA GTT AGT TCC GCT GGA AGT
AAG GAG AGA GAA GTA GAG AGC ACA TCT GCA ACT TCT CCA GGC AGA GCA
ATG GTG TAA
```

Figure 18: ZtMEP1 codon optimised sequence. *Sequence generated by Eurofins Genomic GENEius software.*

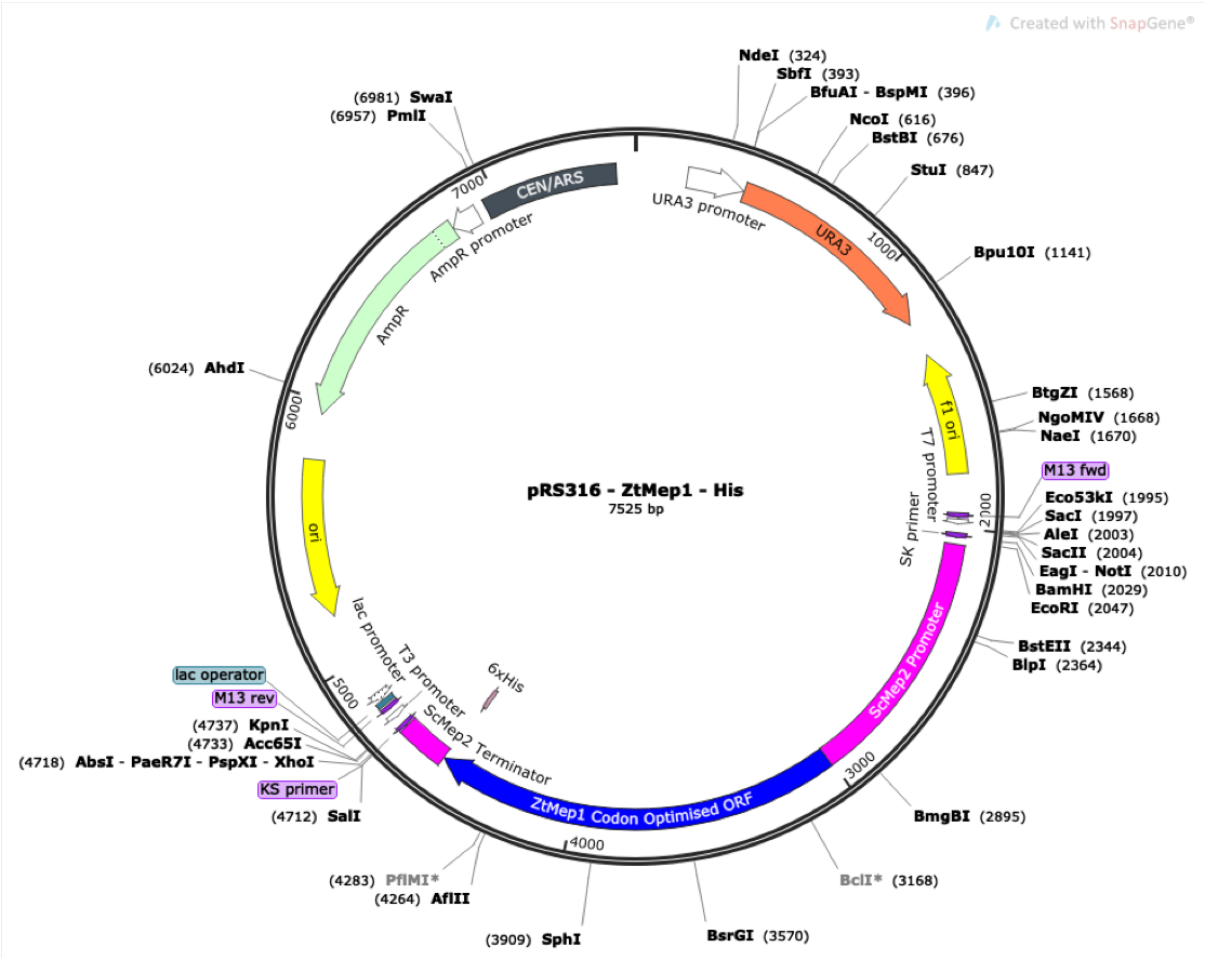

Figure 19: ZtMep1 codon optimised plasmid map. *A plasmid containing the 1E4 ZtMEP1 open reading frame (ORF) codon optimised to S. cerevisiae was generated by Eurofins Genomics. Yeast homologous recombination was used to clone the ORF and the ScMEP2 promoter and terminator into pRS316. A His tag was introduced for western analysis. The plasmid map was created in SnapGene.*

```
ATG TCA ACG GAT CAA GGA AGT TTG CCG TAT GTT CCG CTA GTT GAG TAC
AAC GGT ACT GCC GAT AGC ACT GGT GGA GAC TCT CTG ACT CAA GAC CTT
AAC GTC TTT TAT AAT GCC GGC GAT ATT GCA TGG ATG TTG ACT GCA ACA
GCT CTT GTA TGC CTA ATG GTA CCA GGC GTC GGT TTC TTT TAC AGC GGT
TTG GCA AGA AGA AAA TCT GCA CTT TCT TTG ATC TGG TTA TCA GTG ATG
TCC ACA GCA GTC GTG AGC TTT CAA TGG TTC TTT TGG GGA TAT AGC CTG
GCC TTT TCT CAT ACT GCG ACG AAT GGT TTT ATA GGT GAT CTA GAC TCA
TTC GGT TTA AAA GGT GTA TTA GGC GCT CCT TCG TTA GGC TCA GCA AAG
ATT CCC GAT TTG ATG TAT GCT GTT TAT CAA GGA ATG TTC GCG TGT ATG
ACG ATG GCA TTA TTG ACC GGT GCG GTT TCC GAA AGG GGC AAG TTA TTG
CCC TGT GTT ATA TTC ATG TTT ATC TGG ACG ACA ATC GTG TAT GAT CCT
ATA GCC TGT TGG ACT TGG AAT CCA AAT GGA TGG TCT TAC AAA TTG GGT
GGT CTG GAT TTA GCA GGA GGC ACA CCT GTC CAC ATT GCT TCA GGT ACT
GCA GCA CTG GCT TAT TCC TAC ATG TTG GGT CCA AGA ACC GGT CAT GGT
ACA CCC GCT TTA AAC TAC AGG CCA CAC AAT GTT ACC CAT ATT GTG ATA
GGT ACT GTA TTC TTA TGG GTT GGT TGG TTT GGA TTC AAT GCC GGT AGT
GCT CTT GGT GCT AAC TTG AGA GCC ATT ATG GCA GCT GTA GTG ACA AAT
CTT GCT GCC GGA GTT GGT GGT ATA ACA TGG TGT CTT GTC GAT TAC AGG
TTA GAG GCT AAA TGG AGT ACA GTG GGA TTC TGT TCA GGT GTT ATT TCC
GGA TTG GTA TGC ATA ACC CCA GGT AGT GGC TAT GTT CCA GCG TGG GCT
GCC GTT ATT TAT GGC ATT TGT GCT GGT ATA GGG TGC AAC TTT GCC ACT
CAG CTG AAA TTT TGG ATG AAT GCT GAT GAC GCT CTG GAT ATC TTC GCC
GTT CAT GGT GTT GGA GGC TTT ATC GGG AAC TTA TTG ACC GGG ATA TTT
GCT GCT GAT TGG ATT GCA CAC TTG GAC GGT TTT ACC GAA ATA CAA GGA
GGC TGG TTG AAT AGA CAT TGG ATT CAA CTA GCA ATT CAG TTA GCG GAT
AGT GTG ACT GGC ATG GTT TAC TCC TTT ACC ATG ACG ATT GCG ATT CTA
TTC TTG ATG AAT TTA CTA GGG AGA AAG ATT CCT GCT TTA CGT CTT AGA
GCA TCT GCA GAA GAG GAA TTG GCT GGA ATC GAC GAC GTA GAA ATC GGT
GAA TTT GCC TAT GAT TAC GTC GAA TTG ACT AGA GAT GTA CGT CCT GCT
GAT GCT CTA GAA GGG GTT AAT GAC GGT TAT GCC ACA GAC GAT GCA AGA
TCG ACA AGA TCT TCG TTG GTC TTT GGG AGA GCT CAG TAC GTC AGA TCA
GAG AGA AGG GAG AAG AAC GAT ATC CCA ATG AGA GAA TTC GAA CGT TCT
GAA GTG CAA ACT GGG TAT GCC ATG TAA
```

Figure 20: ZtMEP2 codon optimised sequence. *Sequence generated by Eurofins Genomic GENEius software.*

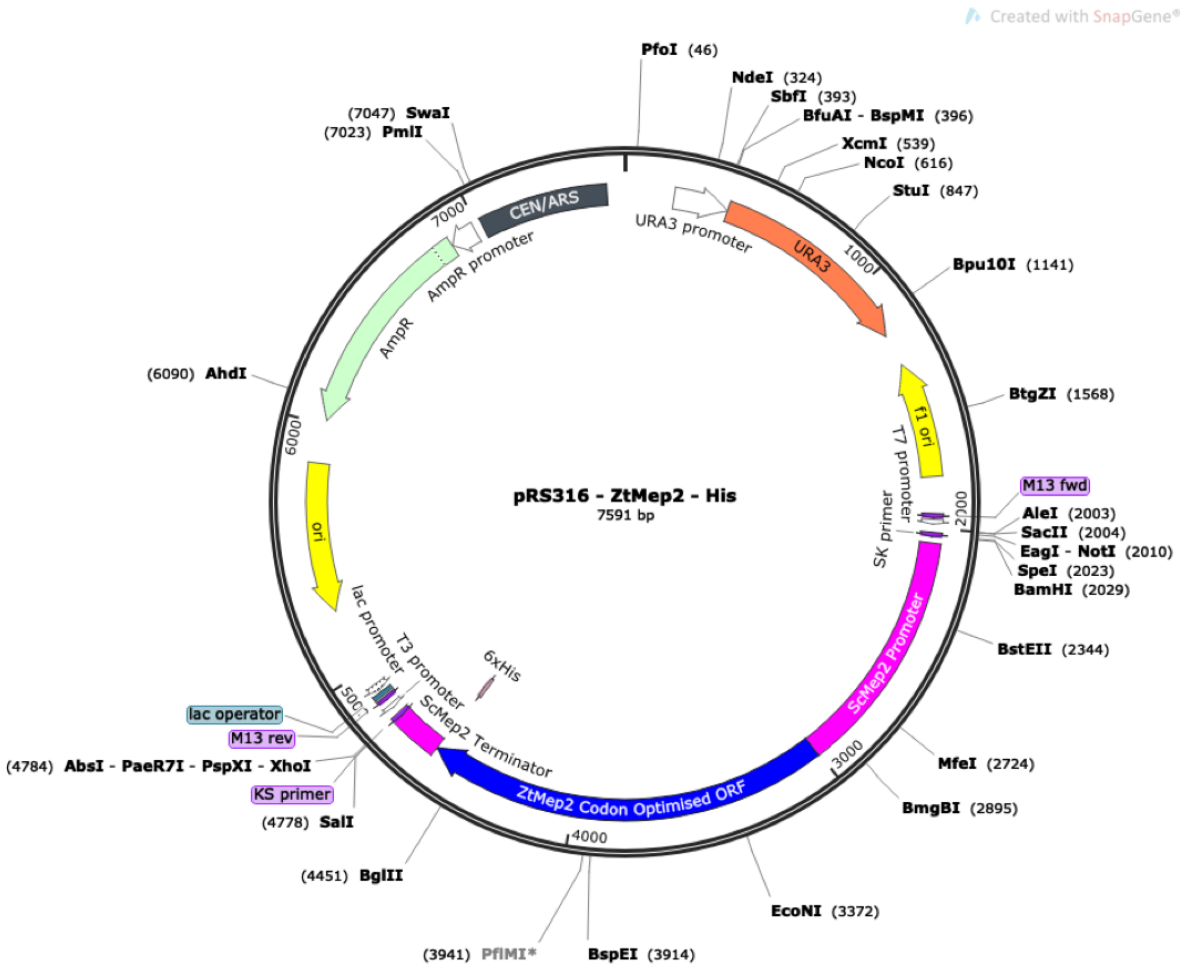

Figure 21: ZtMep2 codon optimised plasmid map. *A plasmid containing the IPO323 ZtMEP2 open reading frame (ORF) codon optimised to S. cerevisiae was generated by Eurofins Genomics. Yeast homologous recombination was used to clone the ORF and the ScMEP2 promoter and terminator into pRS316. A His tag was introduced for western analysis. The plasmid map was created in SnapGene.*

ATG AGC TAC TTC TTT GTT GGT CCA CCC GTT CCC TTT AAC GGA ACT AAC
GCA GAT TAT GGC GGT GAC AGT GCT ACA GAG AAT GTG AAT GGA TGG TTT
TCG TCG GGT GAT CAA GCG TAC ATC ATA GTC GCA TCA GCC ATG GTT ATG
GTT ATG GTA CCA GGT CTA GGT TTT CTG TAT AGC GGA TTA GCT AGA AGG
AAA TCT GCT TTG ACA ATG ATT ATG GCC TGT CTT GCC AGT AGC TCT GTG
ATT ACG TTT CAG TGG TAC TTT TGG GGT TAT AGT TTG GCC TTT TCT AGG
TAT GCC ACT AAT AAT CCT TTC ATT GGT GAT CTG CAA CAA TTC GGC TTG
TTG AAA ACT TTA GCA GTG CCA TCT CAA GGC TCT CCG TTG GTA CCT GAC
TTA TTA TAT GCG TTT TAT CAG ATG CAA TTT TGC GCA GTT ACT GGT GCC
ATA ATA ATG GGT GCA ATT GCG GAA AGA GGA AGA ATA GTT CCT GCA ATG
GTG TTT ATC TTT GCA TGG GCC ACT ATA GTT TAC TGC CCT ATT GCA TAT
TGG GTG TGG AAT GCA AAT GGA TGG GCT TTC AAG TTA GGC GTA TTA GAC
TAT GCC GGA GGT GGA CCA GTC GAA ATT GGG TCA GGT CTA AGC GCA TTA
GCT TAT TCT ATG GTT CTG GGT AGA CGT CAA GAA AAG ATG ATG TTA AAC
TTT AGA CCC CAC AAT GTC TCC CTG ATT ACC CTA GGC ACG ATA TTG CTT
TGG TTC GGC TGG TTG GGC TTC AAT GGT GGT TCT TCT TTC GGA GCT AAT
CTG AGA GCT GTA ATG GCA TGT TGG AAC TCC AAC TTG ACA GCC ATG TTC
GCC GCT ATG ACA TGG GTT CTA CTT GAC TGG AGA TTA GCA AGG AAG TGG
TCC ATG GTA GGT TGG TGT TCT GGC ACC ATT AGT GGT TTA GTC GCT GCG
ACT CCA GCT TCA GGT TTC ATT CCA CCA TGG GCC TCA GTG ATA CTA GGT
ATC ACC ACA GGT GTG GTC GCA AAT TTT GCA ACC AAA ATC AAG TAT TGG
ATT AAG ATC GAT GAT TCC ATG GAT GTT TTC GCA GAA CAT GGT GTT GCT
GGC ATT GTC GGC TTG GTC TTT AAC GGG TTC TTT GCT GCA AAG TAT GTG
ATA GGA TTA GAC GGG GTA AAC ACG GGA CTA TTT GAT GGT GGG TGG ATT
CAT GGG AAT TAC ATC CAG ATG GGA TAC CAG ATC GCG TTC ATT GTT GCT
GCT TGT GCT TGG TCA TTC GTT GTT TCC GCT ATC TTG GCA TAT GCG ATT
AAC TTT ATC CCA GGA TTG AAA TTG AGA GCT TCG GAA GAG GCG GAG CTT
TTA GGT ATG GAT GAT GAT CAA CTT GGC GAG TTT GCT TAC GAT TAC GTC
GAA GTT AGA CGT GAC TAT TTG GCC TGG ACT CCT GCT AAA GCC GAA CAA
GAA GGT GAA GGT CAT TCA ATT CCT AAT GGT GAG AGA TAC GGT ATT CAA
GAG CAC AGT GAA ATG TTG GAA GGG AAA GAT CCG GTA GGA TCC GAA GGT
TCA AGT AAC GGC CAT GAA CAC ACA GGA ATA GGT GGT GAC AGA CAT GGG
GTA GCT TAC GAA GAA ATG GAG AAA TCA AGG AGA GAA GCT CAA GCT GGT
GGG CAT TAA

Figure 22: ZtMEP3 codon optimised sequence. *Sequence generated by Eurofins Genomic GENEius software.*

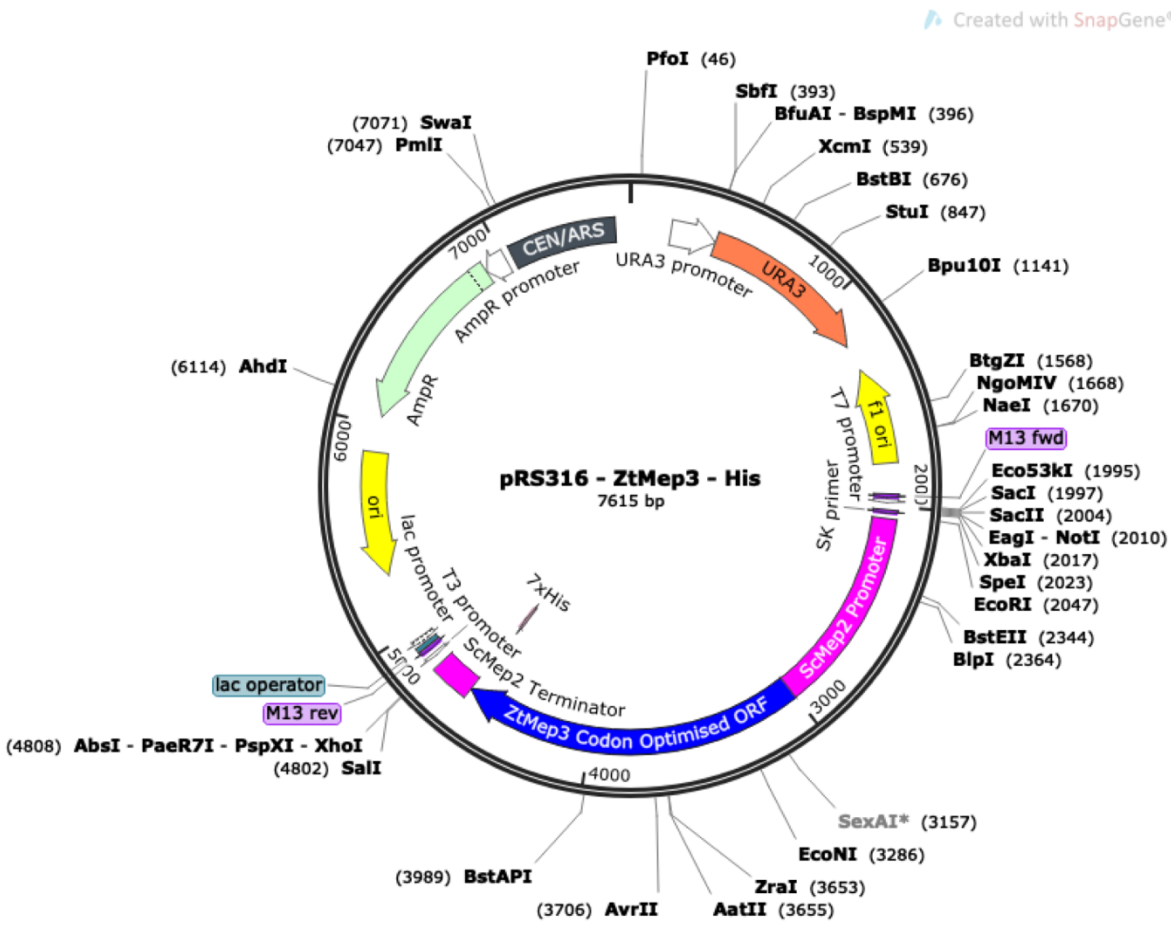

Figure 23: ZtMep3 codon optimised plasmid map. *A plasmid containing the IPO323 ZtMEP3 open reading frame (ORF) codon optimised to S. cerevisiae was generated by Eurofins Genomics. Yeast homologous recombination was used to clone the ORF and the ScMEP2 promoter and terminator into pRS316. A His tag was introduced for western analysis. The plasmid map was created in SnapGene.*

H191A = GCT
H191E = GAA
N241A = GCT
H342A = GCT
G343C = TGT

```
ATG GTC AAT GTC ACA TAT ACC GAT TCA TCA TCT GAC ATG ATA TAC
ACA GCG GAC GAT GGT ACG CAG TAC CTG TAC AAT TTA GGA GAT ATG
TCA TTC GTC ATA GCA GCT ATG GCC TTA GTT TGG ATT ATG GTT CCT
GGT GTA GGC TTA TTC TAT TCT GGG CTA TTA AGG CGT AAG AAC GCA
TTG TCT ATG ATC TTC TTG AGC ATG GCT GGC GTT GCC GTA GGT TCG
TTC CAA TGG TTC TTT TGG GGT TAT TCT TTA GCA TTT TCG GAC ACA
GGC AGT AAA TAT ATC GGC GAT TTG AGA TAC TTT GGT CTA AAA GGG
GTA TTA GCT GAA CCA TCA GCC GGT TCC GAT AGA ATT CCT GCC TTG
CTG TTT TGC GTC TAT CAG TGT ATG TTT TGC CTT ATT ACG GGC GTT
TTG GCT ATT GGT GGT TTT GCT GAG AGA TCC AGA ATA GGT CCG GTT
ATG GTT TTC TTG TTT TGT TGG TTG ACG CTG GTA TAT TGT CCA CTT
GCT TGT TGG ACT TGG AAC CCA AAT GGC TGG TCC TTC GTG ATG GGA
GGT TTG GAC TTT GCT GGA GGT ACA CCT GTT CAC ATT AGT TCA GGT
ACT GCA AGT CTA GCT ATA GCG TTG TAT TTA GGG AAA AGA CGT GGA
TAT GGA ACT GAG AGA TTG GCA TAC AAA CCC CAC AAC ACT GCA TTC
GTT GTT ATC GGT ACT GTC TTT CTA TGG TTT GGA TGG TTT GGT TTT
AAC GGT GGT TCC GCT CTT TCC GCA AAC TTG AGA GCA GTT CAA GCG
TGT ATA GTG ACC AAT TTA TCG GCT AGT GTG GGA GGC TTG GTG TGG
ATG TTT CTG GAC TAC AGG TTG GAA AGG AAA TGG AGT GCT GTT GGG
TTC TGT TCA GGT GCA ATA TCT GGT TTA GTA GGT ATT ACT CCT GCG
GCT GGG TAT GTC GGT TCT CCA GCC GCA CTT GCA ATT GGC GCT ATC
ACT GCG ATT GCC TGC AAT TTC GCT ACT AAG TTA AAG TTT CTA ATT
GGG GTT GAC GAA ACC TTG GAT GTA TTT GCC TCT CAT GGT ATT GGT
GGT ATG GTA GGT TGC TTC CTA ACA GGG CTA TTC GCC CAA GGA AGC
GTT GCT GGC TTT GAT GGT ATC ACC GAT ATT CCA GGA GGT TGG GTG
AGT CAT TAT TGG ATA CAA GCT GGA TAC CAA ATG GCA GAT CTT ACC
GCT GGT TTC GCC TAT ACA TTT GTC ATG ACT ACG ATA ATC TGT TGG
TTA TTG CAC TTC ATA CCT GGA TTG AGG TTA AGA GCC TCT GAA GAA
GCA GAG ATC ATC GGC ATT GAT GAT GCT TAT CTT GGG GAA TTT GCC
TAC GAT TAC GTG GGA ACT GAT CCC GAA TTA AGA CTG CAT AGA ATT
GAC AGC AAA CCA CAA TTT ACC TCA GGC GAT GTG ATT GCC GAA GTC
TCA GCA TCT AAT GGT CAT GAA AGC TCC ACA ACA GAG AAG GTT GAT
CCG CAT GCA ACA GGT AAT GCT GCG GCT GGT GGA GGC AGA GTT GAC
GTA TAA
```

Figure 24: C. neoformans serotype D (JEC21) AMT2 codon optimized sequence. *The codon optimised sequence was generated using Eurofins GENEius software. Codons highlighted in cyan, green and yellow correspond to the twin histidine motif, the asparagine reside adjacent to the proposed deprotonation site and a glycine residue next to the second histidine of the twin histidine motif respectively. Highlighted codons were point mutated to generate mutant Amt2 plasmids. The nucleotides underlined correspond to the nucleotide switches made.*

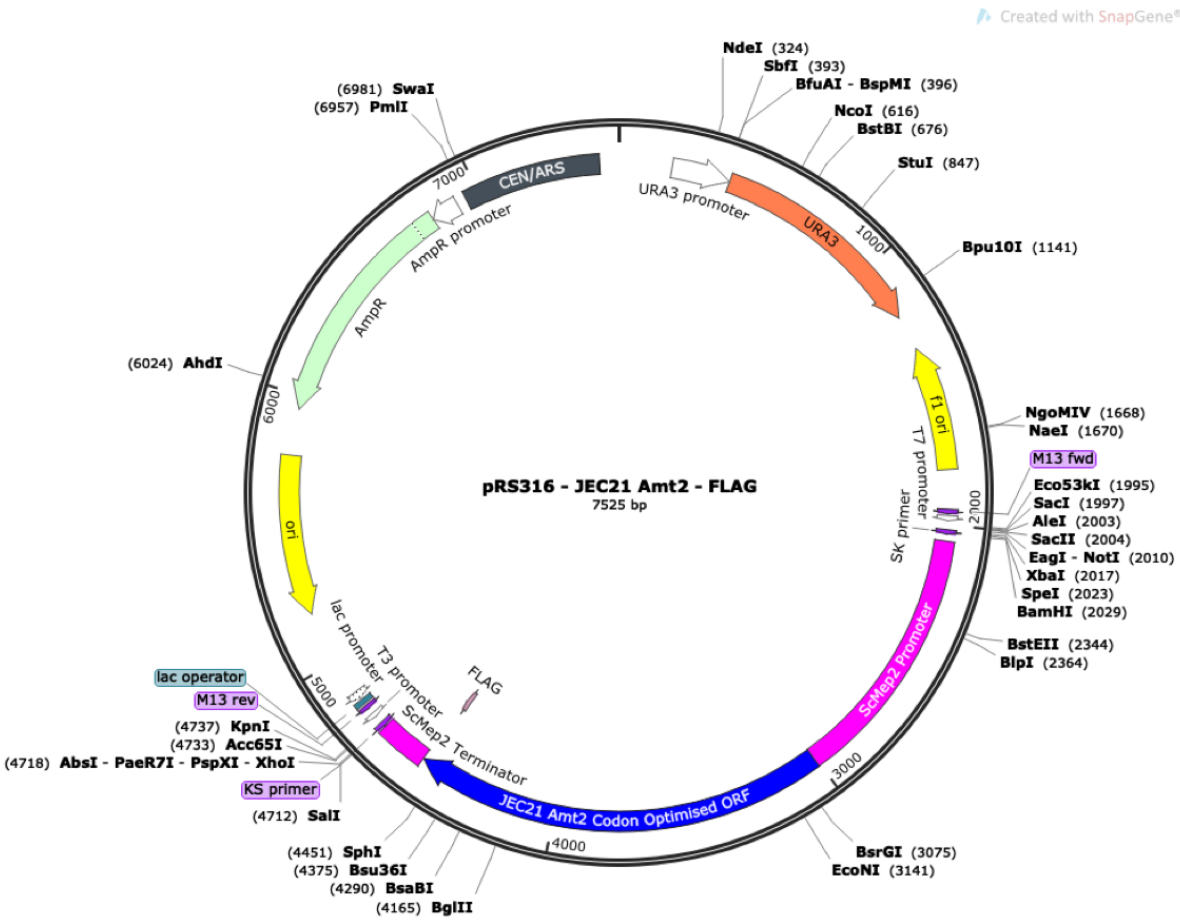

Figure 25: Amt2 codon optimised plasmid map. *A plasmid containing the JEC21 AMT2 open reading frame (ORF) codon optimised to S. cerevisiae was generated by Eurofins Genomics. Yeast homologous recombination was used to clone the ORF and the ScMEP2 promoter and terminator into pRS316. A FLAG tag was introduced for western analysis. The plasmid map was created in SnapGene.*

ZtMep2 Left Flank

CATCAAGTAGATCCATCATGACGGATGGACCCATCGCTGTGATCACGACTCCCAGCAAAGCGGGCGCACTCCTGCA
GGCTGCCGGTTGAAGGAACAAGTCAATTCCGCCCTGATCTGTCGTCGCAGAAAGCGGCAGTGCCTGCATTGGTGGC
GTCGATTCATATGCACCCTAAAACAAGGCCATCACATCTCTCGACACCATTCCCATCATCGAATGCTTGAGAACCT
GCGACGGCGTGTTCCTCCTCGGCGTGGATATCGTTTTGGTGTGAGTTGTGTGTACTGTCAAGACTGAAAGACCTTG
AGACGAAGAAGAACATGGCGTTTCTCCCGGATTGCTCCGACGGAAGACAATTCTCCGGGACCCACCAGAACGGACT
TCACTTGTGCCGTCTCAATCATTGGCTCACTTCGGTCTTTATCTATTCCTTCCCAGTGGAGACATTGCTCAACATG
GAACTCACTGCGGACATGGATCCATCAATATTCTGGAGGCGACACCAAATTGTCAAAGGCAGTGCCCACGCCCGGC
CGAGAGTCCGAGACTAGAACTAACATCCCACGCAAATTTCCGTGTCTGGCTGAGATGAGGACGCCATGGGCCCATG
GCCATGCAATTGCAGGGGAAAATTCATCGCATTTGCGTGCTCAGAGACATGCGAGTTCCACGATGGCCTCCTCCAG
CTTTACCCCAAGCGGAAACACAAATGCAGCTCTCTCGATCGGTCTGGAACACACCCTGATCCGCGACCCAATGAAG
TCGACTGCGATGGACCGATAAGAGCATTGGTATCCGGAAGATCGTCCCAAGAGCATCCTTCGCATGTGCACTTCAT
GAGCTTATTCGGATCTCTGGTATCTCTGGGATTACTTTCGACGCCGGCGACGTTTGACTCTTTCGCGCTTGTGCTT
GAAAATACAGAGTCGCAAGCGG

ZtMep2 Right Flank

TGACCACACAATGCGCCTCGCCAGATTCCTCTCGCTTCATCTACCTGGAAAGCACCCCCTTCACGGTCCCCACCAA
CTCCACATTCCCCGGCACAACCGACTCCGTAATGCCATTCTCCGGCGTACACCCCTCCTGCAACCACCTCGCCAAC
AGATCATTCGACTCCTTCGGCTTGATGTCCTGATTCGCCGTGCCCACCGTAACATGCGGCACTTTATTCGTGCTCT
GGAACACCTCCGCACCAGCTCCCGCGGGACTCAGCCGAACGAGGAAAGCCATCACGCGAGAGTCCCAAATAAGCCG
CTCAAGGCGGACGTTGCAGTCGCCGATCTTGGGCGTTGGCAGAGGGTAGGCGGCGGAAGCGGTGGGTTGGGAGTAG
TGCGTGTGGAGTTCTGTTAGGCGGTCCCAGATGTTCTGGAACTCGGAGGATTGGGCGCGGTGGACGAGGGTGACGT
GGAATTCGTTTTGGATGCGGTGTTGAGCGCGGAGGGTGTTGTAGATGCGGGCGGTGTCGGGCGAGGCGGAGGAGAA
CATGGCGTGGAGGATGCGGGAGACTTGGTCTGCGGGGATCTGGACGGCGAAGTATTCGAGTTTGCGTTCTTTGGGT
TTGGCGCCGTTGGATTGAGCGGTGAAGTTGTTGTTTGGCTTGTTGCCTTGCTTCTTTGAGCGGTCGTCGCGGGCTT
TGATCTCGTGTTTGATGTCGACGGTATATTCCGAGAGGGCTGCTTGAATCGCGTTGTCCATTTCATCGGGTGACGG
CATGTCTTGTCCACCGAAAAGCTTAGGGTATTCGTTGTACATCCGCGTGATCACCGCCTCCAAGTTCTCCCTCGAT
GAGGCGATGGGATCCAGGTCGATCACAAGGTCGAAGCC

Figure 26: ZtMep2 deletion vector map. *Flanking DNA was amplified by PCR and ligated into the pCHYG binary vector. Restriction sites highlighted in orange indicate the sites used for ligation. Vector map was created using SnapGene. Sequencing results of left flank and right flank shown.*

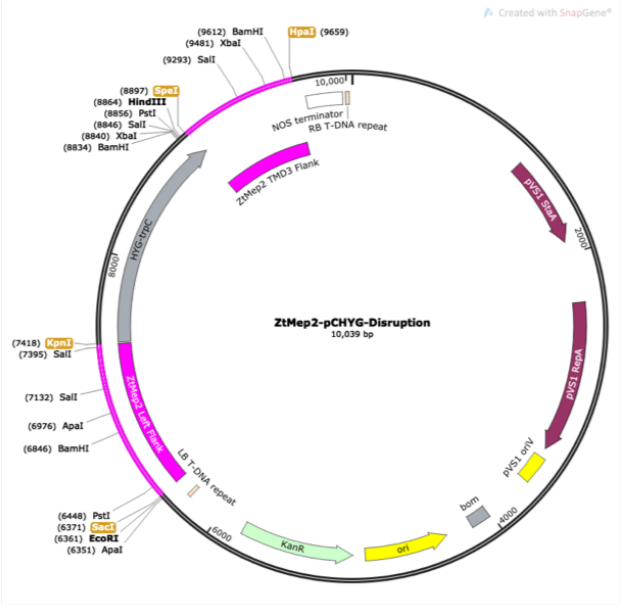

ZtMep2 Left Flank

CATCAAGTAGATCCATCATGACGGATGGACCCATCGCTGTGATCACGACTCCCAGCAAAGCGGGCGCACTCCTGCA
GGCTGCCGGTTGAAGGAACAAGTCAATTCCGCCCTGATCTGTCGTCGCAGAAAGCGGCAGTGCCTGCATTGGTGGC
GTCGATTCATATGCACCCTAAAACAAGGCCATCACATCTCTCGACACCATTCCCATCATCGAATGCTTGAGAACCT
GCGACGGCGTGTTCCTCCTCGGCGTGGATATCGTTTTGGTGTGAGTTGTGTGTACTGTCAAGACTGAAAGACCTTG
AGACGAAGAAGAACATGGCGTTTCTCCCGGATTGCTCCGACGGAAGACAATTCTCCGGGACCCACCAGAACGGACT
TCACTTGTGCCGTCTCAATCATTGGCTCACTTCGGTCTTTATCTATTCCTTCCCAGTGGAGACATTGCTCAACATG
GAACTCACTGCGGACATGGATCCATCAATATTCTGGAGGCGACACCAAATTGTCAAAGGCAGTGCCCACGCCCGGC
CGAGAGTCCGAGACTAGAACTAACATCCCACGCAAATTTCCGTGTCTGGCTGAGATGAGGACGCCATGGGCCCATG
GCCATGCAATTGCAGGGGAAAATTCATCGCATTTGCGTGCTCAGAGACATGCGAGTTCCACGATGGCCTCCTCCAG
CTTTACCCCAAGCGGAAACACAAATGCAGCTCTCTCGATCGGTCTGGAACACACCCTGATCCGCGACCCAATGAAG
TCGACTGCGATGGACCGATAAGAGCATTGGTATCCGGAAGATCGTCCCAAGAGCATCCTTCGCATGTGCACTTCAT
GAGCTTATTCGGATCTCTGGTATCTCTGGGATTACTTTCGACGCCGGCGACGTTTGACTCTTTCGCGCTTGTGCTT
GAAAATACAGAGTCGCAAGCGGAGGGAGGTTGACATAAaGCCGTAtATTCACTCCTCCCGCCATCCCATCGGCGGC
TAGTGTAAACGGCTACCGGACTTCTCACCAATATGTC

ZtMep2 TMD3 Right Flank

GAAGCTGCGCGTCATATATCCTTTCGGAAGGGCGGACGAGGCCATCCGGAGCTTGGCAGGGATCACGGCCTTCCGG
GCGTAATATGCTCGCATGTCTTGACCACTCTTATTCAGAGCTTGGTGACCGCCAATTTTCGATGATGCAGCTTGGG
CGCAGGGTCGATGCGACGCAATCGTCCCGATCCGGAGCCCGGGACTGTCGGGCGTACACAAATCGCCCGCAGAAGC
GCGGCCGTCTGGACCCGATGGCTGTGTAGAAGTACTCGCCGATAGTGGAAACCGACGCCCCAGCACTCGTCCGAGG
GCAAAGGAATAGAGTAGATGCCGACCGGGAACCAGTTGGGGATCCTCTAGAGTCGACCTGCAGGCATGCAAGCTTT
AAGAGGAGTCCACCATGGTAGATCTGACTAGTGAACGAGGTAAACTCCTCCCCTGCGTGATCTTCATGTTCATCTG
GACCACCATCGTCTACGACCCGATCGCCTGCTGGACCTGGAACCCAAATGGCTGGTCCTACAAACTCGGCGGCCTC
GACCTCGCAGGTGGCACGCCAGTACACATCGCATCCGGCACCGCGGCTCTAGCATACAGCTACATGCTTGGTCCAC
GCACTGGACACGGCACACCAGCTCTGAACTACCGTCCACACAACGTCACGCACATCGTTATTGGTACTGTCTTCCT
CTGGGTTGGCTGGTTCGGCTTCAACGCCGGATCTGCTCTCGGTGCAAACCTCCGAGCGATAATGGCGGCGGTGGTG
ACCAACCTGGCCGCAGGCGTCGGTGGTATCACATGGTGCCTCGTCGACTACCGCCTCGAAGCGAAATGGTCCACAG
TCGGCTTCTGCTCCGGTGTCATCTCAGGTCTTGTCTGCATCACTCCAGGCTCAGGATATGTGCCCGCGTGGGCTGC
TGTAATTTACGGCATCTGCGCGGGTATCGGCTGCAACTTCGCCACGCAGCTCAAATTCTGGATGAACGCCGACGAT
GCTCTAGACATCTTCGCCGTACATGGTGTGGGTGGCTTCATCGGCAATCTCCTCACGGGCATATTCGCAGCCGACT
GGATCGCACATCTCGACGGCTTCACGGAAATCCAAGGCGGCTGGCTCAACCGCCACTGGATCCAGCTCGCGATCCA
ACTCGCCGATAGCGTTACTGGAATGG

Figure 27: ZtMep2 disruption vector map*. Flanking DNA was amplified by PCR and ligated into the pCHYG binary vector. Restriction sites highlighted in orange indicate the sites used for ligation. Vector map was created using SnapGene. Sequencing results of left flank and right flank shown.*

ZtMep3 Left Flank

GATAGCCGTGGTCAGAATGCACCTCTGGGCGTGGAAAGAAGACGGCTTGGAGTCATGGAGTGCATGTGTGAGGAGT
GCAGGATGTGAGATCCAAGAGCAGTTCGGTGACACTGCGTGGTTTCTGTGTGTGCCTCAGAACGGCTTACAGGGTC
CTAACTTTGGCAAATCTCCAAGGTTTGAAGGATGGGGGTGGAGCCACACTCGGTCCATGTGCAACGTGGAACAGAG
TGCAAGCGCCAACAAAGAACATGGAGATATTGCCTATGGATACACTCCTTGTCACAGGATCAGTCAAGGCAATGGG
AGGCTGAACGGGAAGCAATGCGGCCACTTTGAGGCGACTCATCAAGCGAACACCACGAGATAGAGGCGTTCGTCCA
CGACCTTGATCGTACCCGAAGCAGCGGTGCACGCGATCGATGCAGGCATGCCGTAGGCCAAGGGTGTTGGGGTTTA
GAGTGTTGGGGGTTGAAGCTGGGTGCGTGTTGGTGCTGCCAATGGAAAGCCTGCGGAGCGGACGTTGTCTCTTACT
AGGAGCTCTCGGCACGCGCAGCGCGGGCGCCCCAGTGTCTGGCTAGGCTAAGATAGCTTCCGCGAGAGATAAGAAA
ACAATCCATGTCAAAGGTCGGCTCGTTGTGGTGGGTTGCCCTTGCCCTTGATTCCACTTG

ZtMep3 Right Flank

GAGAAGCGCAAGCTGGTGGTCATTGATCATAGAGCGATGTTTTGCGACTTGAAATTTCTTGGACACCTTTACACGT
GTGGCGTTTTCCACTATTTTGTTTCATATGCTTGTGATACCAGACGGAGCAGGAAGTGCTCGTTCGACGATGGAGA
TTTGTAGAGTTGAGAGAGACGACGTGGCTGGCGTGATTACCACGGTCGTGTGAAGATAGATCAGATCTGCAGAGAT
ATATACCAACGACATTCACCATCACCACAGTCTGGCTTCTGCTTCCCACACTCATGCCAACATCAATGTTTGACTC
ATCTGGAGCATCTACAGATCTCACTGCGAGAGAACTCTCAATCAAAACGAAGTCCCACCTCAACCAAGCAAGACCA
TCATCAAGCACCACGCTCAAGCACCCTCCCCTCGCTCGCTGGAAGGCTTCACACCCGCACGAGCAGAGTGGAGCCC
ACGCAAGGGAAGGGAACAGACAATGCTAGTCCGTTCACTCGAACCCGGTTACCTCAATCAATGAATTCTCGGAATC
GCATGGCTCGAACAAGGATCCTTATCAGCGCCCTTGAGAGATAGATGCAAGATTGACCGTTCTCGTCTCCCTTGTC
TGCTTGGTCCCTGGGTGCCGCGTGGAAACGTTGAGCAAGGTGTGCAACGCTCGAGCCCAGGTGCCGCACCACTGCT
GTTGCTTGGGTCTTATCTTTGAGAGTTCCTTATCTGGTTCGATGGCTTGTACATACCTGTATGACTTCCTTGTTGA
TGCCCAAGCTCCCTCAGTCCCAGGAACTGGGGGTTGCGGATCGGAGGACATCGTGCAGTTGTGGATCGGAGGACAT
CGAGCATCGTTG

***Figure 28: ZtMep3 deletion vector map**. Flanking DNA was amplified by PCR and ligated into the pCHYG binary vector. Restriction sites highlighted in orange indicate the sites used for ligation. The vector map was created in SnapGene.*

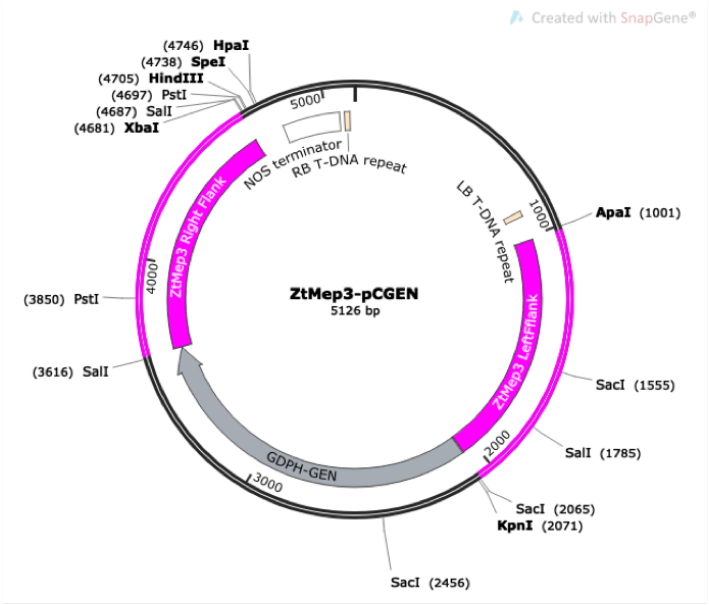

ZtMep3 Left Flank

GATAGCCGTGGTCAGAATGCACCTCTGGGCGTGGAAAGAAGACGGCTTGGAGTCATGGAGTGCATGTGTGAGGAGT
GCAGGATGTGAGATCCAAGAGCAGTTCGGTGACACTGCGTGGTTTCTGTGTGTGCCTCAGAACGGCTTACAGGGTC
CTAACTTTGGCAAATCTCCAAGGTTTGAAGGATGGGGGTGGAGCCACACTCGGTCCATGTGCAACGTGGAACAGAG
TGCAAGCGCCAACAAAGAACATGGAGATATTGCCTATGGATACACTCCTTGTCACAGGATCAGTCAAGGCAATGGG
AGGCTGAACGGGAAGCAATGCGGCCACTTTGAGGCGACTCATCAAGCGAACACCACGAGATAGAGGCGTTCGTCCA
CGACCTTGATCGTACCCGAAGCAGCGGTGCACGCGATCGATGCAGGCATGCCGTAGGCCAAGGGTGTTGGGGTTTA
GAGTGTTGGGGGTTGAAGCTGGGT

ZtMep3 Right Flank

ACCACGGTCGTGTGAAGATAGATCAGATCTGCAGAGATATATACCAACGACATTCACCATCACCACAGTCTGGCTT
CTGCTTCCCACACTCATGCCAACATCAATGTTTGACTCATCTGGAGCATCTACAGATCTCACTGCGAGAGAACTCT
CAATCAAAACGAAGTCCCACCTCAACCAAGCAAGACCATCATCAAGCACCACGCTCAAGCACCCTCCCCTCGCTCG
CTGGAAGGCTTCACACCCGCACGAGCAGAGTGGAGCCCACGCAAGGGAAGGGAACAGACAATGCTAGTCCGTTCAC
TCGAACCCGGTTACCTCAATCAATGAATTCTCGGAATCGCATGGCTCGAACAAGGATCCTTATCAGCGCCCTTGAG
AGATAGATGCAAGATTGACCGTTCTCGTCTCCCTTGTCTGCTTGGTCCCTGGGTGCCGCGTGGAAACGTTGAGCAA
GGTGTGCAACGCTCGAGCCCAGGTGCCGCACCACTGCTGTTGCTTGAGTCTTATCTTTGAGAGTTCCTTATCTGGT
TCGATGGCTTGTACATACCTGTATGACTTCCTTGTTGATGCCCAAGCTCCCTCAGTCCCAGGAACTGGGGGTTGCG
GATCGGAGGACATCGTGCAGTTGTGGATCGGAGGACATCGAGCATCGTTGCGATCGAGCAGGAGCATGTCGCGTGG
TGAGCAGCTGACGTCGTTACGGAGATGGGATATGTTTTTTTTTTGTTGATGCCTGAGGCACCTATCAGCAGTGCAT
CGATTTCCGGAGCCTCGTCCTTTTACTGTCGTGATTAGATGCCAAGTGCATGCACGAAGGAGTCAAATCATACCAG
ACCTTTCGACTGACTTTGCCTC

Figure 29: ZtMep3 deletion vector map to generate double mutant. *Flanking DNA was amplified by PCR and ligated into the pCGEN binary vector using the Gibson Assembly kit. GEN was initially excised from pCGEN using the EcoRI and BamHI restriction enzymes before being used in the assembly reaction. The vector map was created in SnapGene. The DNA sequencing results are shown below. Red and yellow highlighting correspond to point and insertion mutations respectively.*

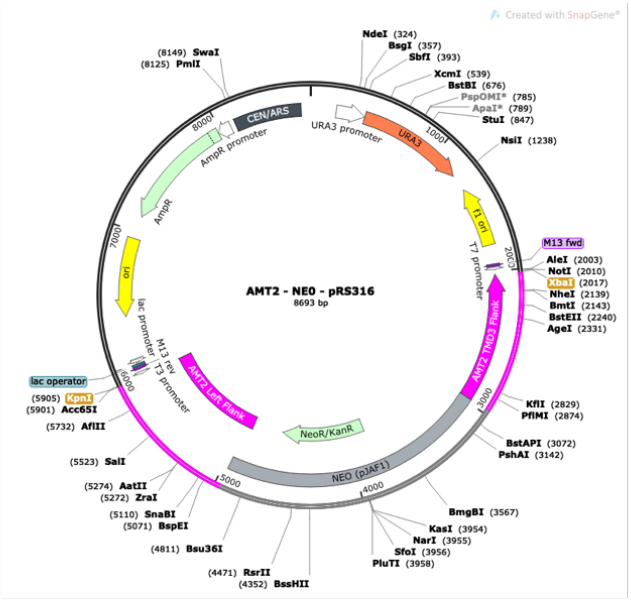

Amt2 Left Flank

GAGGCTGGAGATGGAAGGTGTATCCCGGAAGGTCTCATTTCCCCCGGAGCTCCTCTCTACGCATTGAGAAGAAGAA
AAGTCAAGTCTGGGGACCGAGCTCGCTGTTCGTCCAGTCTGATCGAGATTAGTAGACGGCGGAGATCAGCAGTGCA
CTAGCGCTCAGCTTAAGCTCGGTCTCGCACTTTGCATCATCCATCACGGATCAAGCGAAGACTTCCAGCAGCATAT
TCATCCATTGAGCATGGACTGGTGTTGCCCATATTTTTCCAGCAAGTCGCCCTTATTTGTCATGTTTTGAGGAATA
AAAAGTGATTAGCGATTTACACGGCTAAAATACGTGCACCCTAATACGACTGATTATGCCATCCTCTCGTCGACCT
ATCCCAGAGCCGCAAGCTATCAGTTATCAGTTACATACTACTCGAACTCTGAGACCGTTTATCTCCACCAACCACG
GCGCGTGATGGCGCATAATTTCGGTTCCGATTTACAACCACCCTCAGCGCTTCCGCCAGCAATCGGCCTGCGCCGC
ATCCTTGGTTCAGGACGCGGCAATTCAATTCACCAGTCTTTTTTATCCTGGGCAAATGAGTACGCGTCATGAGGCT
GATAGCTCATAGATAAGGACGTCCGCGGCAGAGTAGTGCGACAAGGTCTTGGCGTATCTTCTTTTGCAGGTTCTCT
AATCTCTTCATGCTCTGCGTTTGCGTGTTCGGTCGTGCACTCGTGTTTTGCAATTTCCCTATTCTGTCGGTTCGCC
GTTTGCAGTTGACTGAAGCGAATGCAATACGTAATAACATTAAGACGCGTAAATGCTAGTCGCCTCCGGAGCTCAG
AAGATGAGGCATCTTTCAACGCGGGGATAGATAAGGATTGACTGGCCAATGAGGGGCAGCCGTCTTGTTGTGGTAT
CTACCCCCTTTCTCTTTCATCTTCCGATTCCTTCCCCCTTTATCGTTCTCCCAGGCCCAATACTTATTCTAA

Amt2 TMD3 Flank

TGCTGGCTCACCCTCGTCTACTGCCCTCTCGCTTGCTGGACATGGAACCCCAACGGCTGGTCTTTTGTCATGGGCG
GTCTCGACTTTGCTGGTGGGACCCCCGTTCACATCTCTTCTGGTACTGCCTCTCTGGCTATCGCCTTGTACCTCGG
CAAGCGTCGAGGCTACGGCACTGAACGACTCGCCTACAAGCCCCACAACACTGCTTTCGTTGTTATCGGCACCGTT
TTCCTCTGGTTCGGTTGGTTCGGCTTCAATGGTGGTTCCGCTCTTTCTGCCAACTTGAGGGCTGTTCAGGCTTGTA
TCGTCACCAACCTTTCTGCCTCTGTCGGTGGTTTGGTCTGGATGTTCTTGGACTACAGGCTTGAACGCAAATGGTC
CGCTGTTGGCTTCTGCTCCGGTGCTATTTCTGGTTTGGTCGGTATCACCCCTGCTGCTGGCTACGTCGGTTCCCCA
GCTGCTCTTGCCATCGGTGCGATTACCGCCATCGCCTGTAACTTTGCCACCAAGCTCAAGTTTCTCATTGGCGTTG
ATGAGACTCTCGATGTCTTTGCTTCTCACGGGATTGGCGGCATGGTCGGTTGCTTCCTTACCGGTCTCTTCGCCCA
AGGTTCTGTGGCCGGCTTTGACGGTATCACCGATATCCCCGGTGGCTGGGTCAGCCATTACTGGATACAGGCTGGT
TACCAGATGGCCGATTTGACCGCTGGTTTCGCTTACACCTTTGTCATGACCACCATCATCTGCTGGTTACTTCACT
TCATCCCTGGATTGAGGTTGAGGGCTAGCGAAGAGGCCGAAATCATCGGTATTGACGATGCTTACCTCGGCGAATT
TGCTTACGACTATGGCAAGTTTTTTTTTTTAGTTCTCTACCTTTTTCTTGAACGTTCCCACTGACTTTTC

Figure 30: Generation of Amt2 disruption mutant. *DNA flanking the first 3 transmembrane domains of the AMT2 gene and the neomycin resistance cassette from pJAF1 were cloned into pRS316 at the SalI restriction site by yeast homologous recombination (left). The Amt2 – NEO DNA segment (right) was excised from Amt2 – NEO – pRS316 using the restriction enzymes highlighted in orange (KpnI and XbaI) and used to disrupt the AMT2 gene in JEC21 by electroporation. DNA maps were created in SnapGene. Sequencing results are shown below for flanking DNA. The region of sequencing highlighted in yellow indicates the loss of two T nucleotides.*

3 Ammonium Signalling in *Zymoseptoria tritici*

3.1 *Z. tritici* introduction

Z. tritici can transition from yeast-like growth to filamentous growth and is therefore a dimorphic fungus. In several fungi, members of the Amt/Mep/Rh superfamily have been identified as ammonium sensors (transceptors) which are responsible for this dimorphic switch in limiting ammonium conditions (Lorenz and Heitman, 1998). For some pathogenic fungi this dimorphic switch is critical for infection. As *Z. tritici* is responsible for devastating crop losses globally, and anti-fungal resistance is on the rise (Hayes *et al.*, 2016), new fungicides need to be developed. Proteins on the plasma membrane serve as very good targets for anti-fungal drugs as their location makes them easily accessible. If *Z. tritici* possesses an ammonium sensor, the crystal structure of the transceptor could be solved and used for the development of new anti-fungal drugs. However, the main aim is to address the conservation of ammonium signalling. The identification of an ammonium sensor in *Z. tritici* could help in understanding the signalling mechanism of transceptors, which is currently unknown.

3.2 *Z. tritici* displays an ammonium dependent phenotype

Several fungi undergo a morphological switch in response to changes in ammonium levels. To determine if *Z. tritici* exhibits this switch, filamentation was assayed when cells were spotted onto low (50 μM) and high (5 mM) ammonium medium (**Figure 31**). On high ammonium, *Z. tritici* remained pink with minimal filamentation, whereas on low ammonium *Z. tritici* became melanised and displayed extensive filamentation around the edge of the colony. Furthermore, scavenging morphologies consisting of aerial hyphae (which have a 'white fluffy' appearance on the top of the cell spot), and cell invasion (visible on the underside of the agar plate) were observed. In liquid media, *S. cerevisiae* arrests growth in low ammonium, but grows in high ammonium or 0.1 % proline (a poor nitrogen source which also induces pseudohyphal growth). Identical growth phenotypes were observed when *Z. tritici* was inoculated into the same liquid media (**Figure 32**). In liquid high ammonium medium, yeast-like cells consisting of

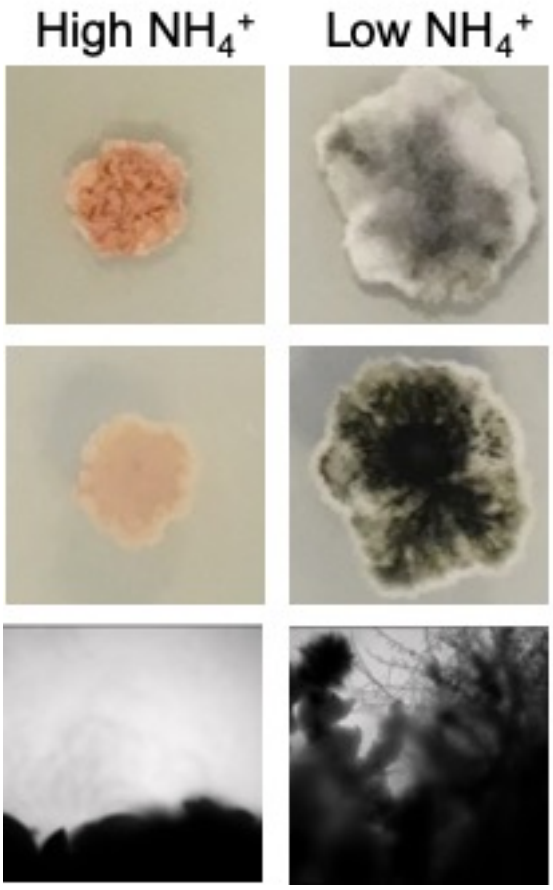

Figure 31: Z. tritici phenotypic analysis. *Z. tritici was grown in YPD for 3 days at 18 ºC before being washed and spotted onto high (5 mM) (left) and low (50 μM) (right) ammonium agar plates. After 5 weeks, the plates were photographed from above (top panel), on the underside of the agar plate (middle panel) and the edge of the colony was photographed under the microscope at 40 x magnification..*

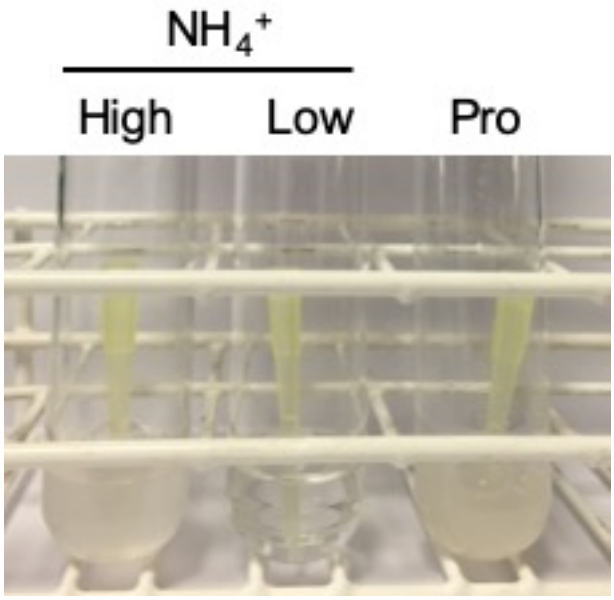

Figure 32: IPO323 liquid culture growth. *Cells were inoculated from 6 day old YPD agar plates into high ammonium, low ammonium, and 0.1 % proline liquid medium and incubated at 18 °C at 250 rpm for 6 nights, before being photographed.*

micropycnidiospores budding off the multicellular macropycnidiospores were visible under the microscope. In 0.1 % proline medium, hyphae were present (**Figure 33**). This is a vegetative growth morphology formed when the macropycnidiospores extend in a polarised fashion from the tip into very elongated, narrow cells. Thus, *Z. tritici* switches from yeast-like growth to filamentous growth in limiting nitrogen conditions and is unable to grow in liquid low ammonium.

3.3 Identification of putative ammonium transporters in *Z. tritici*

Ammonium is an important source of nitrogen for may organisms, therefore, ammonium transporters, which are part of the Amt/Mep/Rh superfamily, are found in both eukaryotes and prokaryotes. All fungi contain at least two of these proteins, with *S. cerevisiae* containing three where ScMep2 possesses an additional role as an ammonium sensor (transceptor) (Lorenz and Heitman, 1998).

3.3.1 Retrieval of sequences

To determine how many ammonium transporters *Z. tritici* contains in its genome a homology search using ScMep2 was conducted in the IPO323 genome database. 17 results were returned containing four different genes. Mycgr3G91450, Mycgr3G35079 and Mycgr3G73144 were recorded by the database to contain domains associated with ammonium transporters. Mycgr3G32616 was recorded to be a putative uncharacterised protein containing major facilitator superfamily (MFS) domains and a sugar transporter conserved site. All ammonium sensors to date contain the conserved twin histidine motif, whereas non signalling versions possess a glutamate residue in the equivalent position of the first histidine (Boeckstaens *et al.*, 2008). Mycgr3G91450 and Mycgr3G35079 protein sequences, when aligned with ScMep2, contain the twin histidine motif, whereas Mycgr3G73144 contains the glutamate histidine motif. Moreover, Mycgr3G35079 exhibits the highest identity and similarity percentages and score value when aligned with ScMep2, as stated in (**Table 18**). These genes were, therefore, selected as putative ammonium transporters and were designated as ZtMep1, ZtMep2 and ZtMep3 as identified in (**Table 18**). The sequence alignment between ScMep2 and all the *Z. tritici* putative ammonium transporters

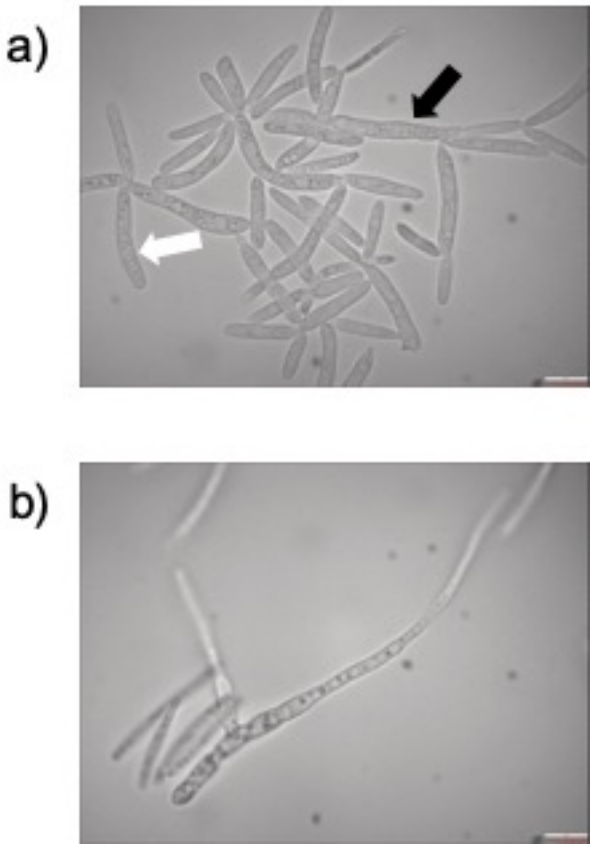

Figure 33: 1000 x microscope images of IPO323 grown in liquid media. *a) Cells inoculated into high ammonium (5 mM) medium. Black arrow indicates macropycnidiospores and white arrow indicates micropycnidiospores. b) Cells inoculated into 0.1 % proline medium display hyphal growth.*

highlighted that the ExxGxD motif was conserved as were functional residues, including two phenylalanine residues which form the Phe gate, and an asparagine residue adjacent to the second phenylalanine. As ZtMep1 and ZtMep2 possess the conserved twin histidine motif they are the most likely candidates for being ammonium sensors (**Figure 34**). However, the ZtMep3 transcript has previously been found to be highly expressed at day 13 of the infection cycle, suggesting that ZtMep3 plays an important role in virulence (Yang *et al.*, 2013).

Name	*Z.tritici* Gene ID	UniProtKB/TrEMBL Accession Number	Identity %	Similarity %	Score
ZtMep1	Mycgr3G91450	F9X7M3_ZYMTI	37.5	52.7	869.5
ZtMep2	Mycgr3G35079	F9X1I0_ZYMTI	44.6	58.9	1219.0
ZtMep3	Mycgr3G73144	F9XDE7_ZYMTI	42.9	58.2	1139.0

Table 18: Z. tritici MEP genes

3.3.2 IPO323 is a ZtMep1 null strain

Alignment between ScMep2 and all three *Z. tiritici* ammonium transporters revealed a large gap of 46 amino acids after glutamate 303 (E303) in ZtMep1 (**Figure 34**). Firstly, to investigate this difference the protein sequences were analysed by a transmembrane domain (TMD) prediction site. ScMep2 is predicted to contain 11 TMDs, which is consistent with the published structure (van den Berg *et al.*, 2016). Equally, ZtMep2 and ZtMep3 are predicted to contain 11 TMDs, however, ZtMep1 is predicted to contain merely 9 TMDs (**Figure 35**). The *ZtMEP1* genomic sequence, according to the IPO323 genome database, is forecast to contain four exons and three introns with intron three containing 4219 bp. However, the *ZtMEP1* gene has additionally been annotated by Rothamsted Research (RRes) which anticipates that *ZtMEP1* contains 11 exons and 10 introns (**Figure 36**). Exons one and two, in the RRes annotation, are identical to the original prediction. Whereas exons three and 11, according to the RRes annotation, are 82 bp and 223 bp longer than exons three and four from the original projection respectively. The RRes annotation envisages that

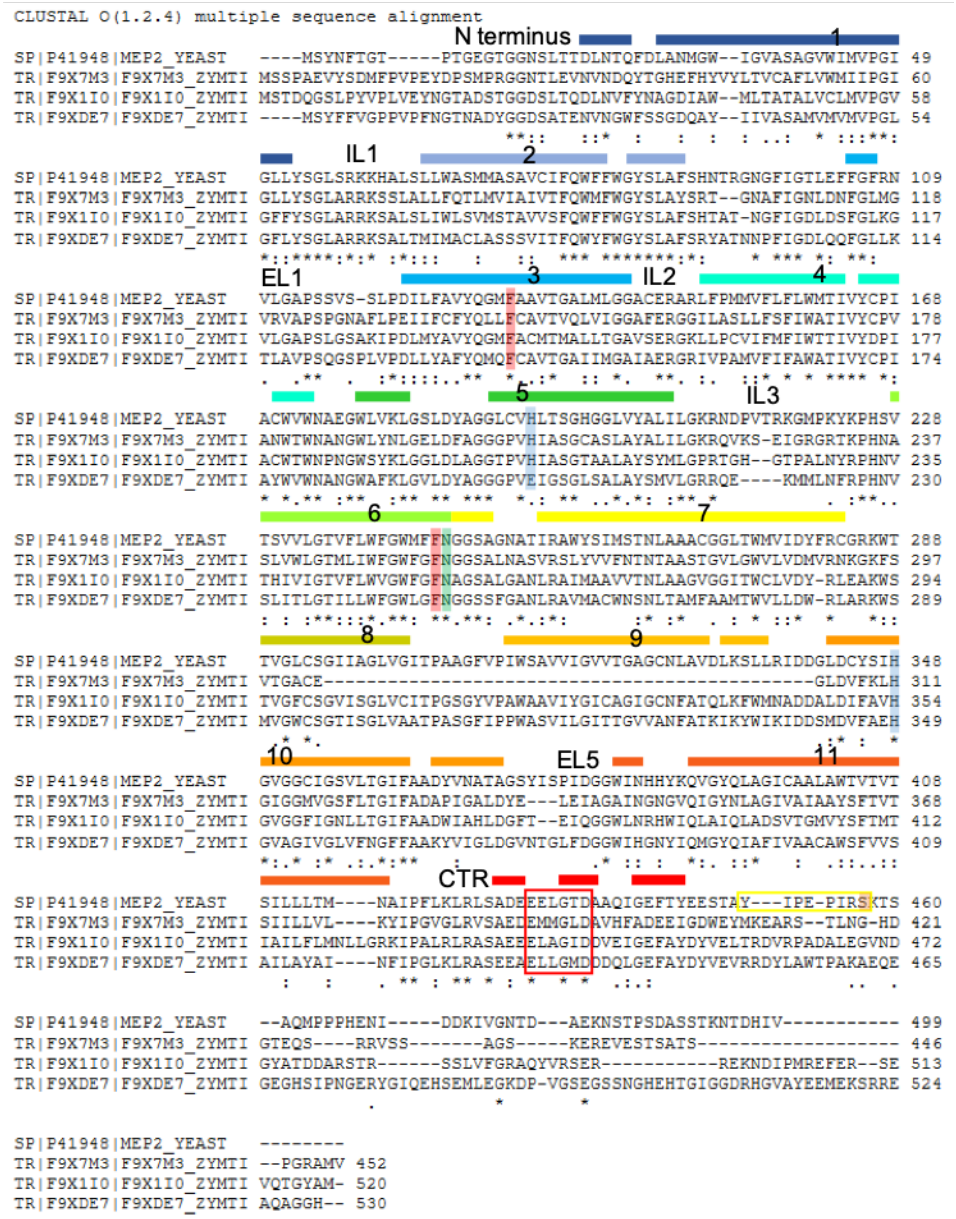

Figure 34: CLUSTAL O protein sequence alignment of ScMep2, ZtMep1, ZtMep2 and ZtMep3*. The conserved ExxGxD motif is boxed in red. The AI region found in ScMep2 is boxed in yellow, with the Npr1 kinase phosphorylation site highlighted in orange. Red highlighted residues correspond to the Phe gate, while blue highlighted residues correspond to the twin – His motif, or Glu – His motif. A conserved asparagine residue adjacent to the proposed deprotonation site is highlighted in green. The secondary structure elements are based on the figure in(van den Berg et al., 2016) and are indicative of ScMep2. The centre of the transmembrane domain is indicated with the number.*

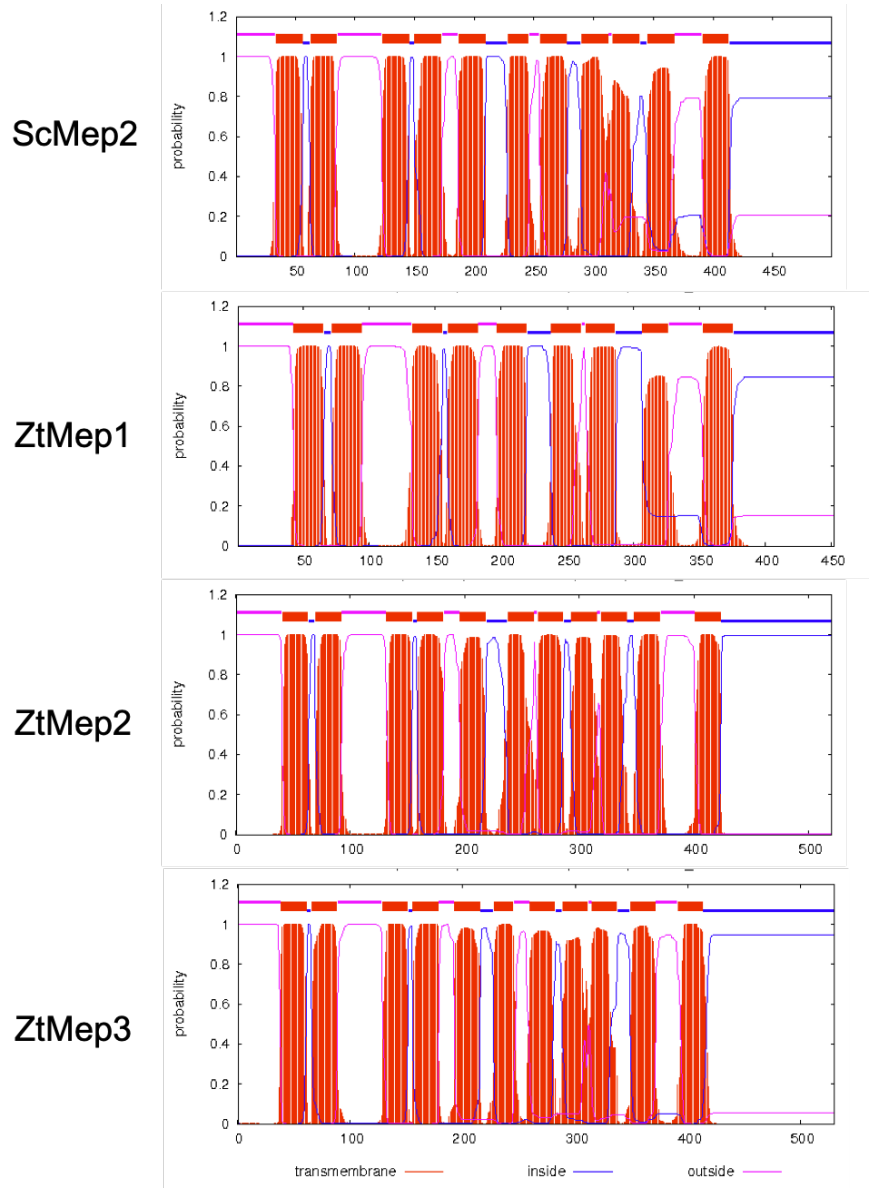

Figure 35: TMD predictions. *Protein sequences for ScMep2 and ZtMep1, ZtMep2 and ZtMep3 from IPO323 were analysed by the TMHMM Server v. 2.0 online software tool. The returned graphs depict the predicted transmembrane domains (TMDs). Pink and blue lines indicate extracellular and intracellular loops respectively, while red boxes indicate TMDs.*

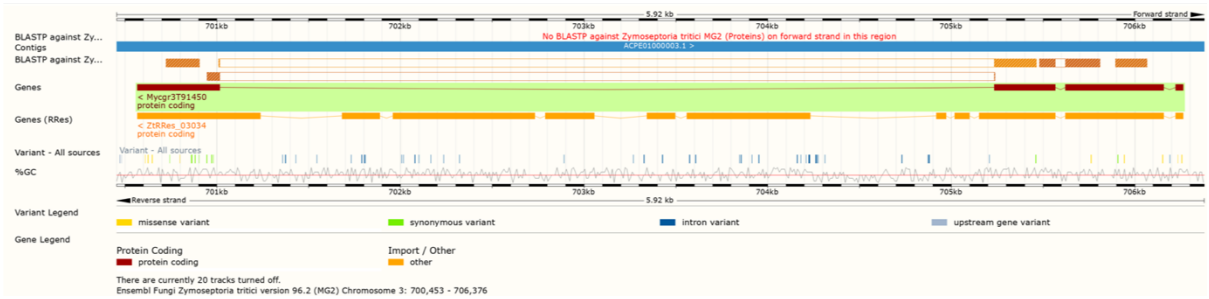

Figure 36: Schematic of ZtMEP1. *Image imported from the IPO323 genome database. Red indicates the original intron exon prediction. Orange indicates the Rothamsted Research (RRes) exon intron prediction.*

ZtMep1 contains 1168 amino acids; 716 bp more than the original prediction. To see if *ZtMEP1* was conserved within the *Z. tritici* population, a *ZtMEP1* homology search was conducted in three other *Z. tritici* strains, ST99CH_3D7 (3D7), ST99CH_1A5 (1A5) and ST99CH_1E4 (1E4). A 46 amino acid gap is not observed when ZtMep1 from 3D7, 1A5 or 1E4 are aligned with ScMep2. This demonstrates that ZtMep1 in IPO323 is predicted to be different to the homologues in the other *Z. tritici* strains inspected. Comparison between IPO323, 3D7, 1A5, and 1E4 *ZtMEP1* revealed repeat sequences in IPO323 *ZtMEP1* which are consistent with the insertion of a transposable element (Kazazian, 2004). Flanking direct repeats, composed of 8 nucleotides with the sequence CGGCTGGC, and terminal inverted repeats, composed of 21 nucleotides, were identified within intron three of the original (not annotated by RRes) IPO323 *ZtMEP1* sequence (**Figure 37**). The newly predicted IPO323 *ZtMEP1* sequence, lacking the transposon, was translated into a protein sequence and aligned with ZtMep1 from the 3D7, 1A5 and 1E4 *Z. tritici* strains (**Figure 38**). Apart from five resides, all the ZtMep1 sequences are identical. However, the newly forecast IPO323 ZtMep1 protein sequence, along with ZtMep1 from 1E4, are projected to contain one TMD less than ScMep2 according to the TMD prediction site (**Figure 39**). To confirm that the IPO323 strain used in our lab contained this transposon, regions overlapping the *ZtMEP1* transposon borders were amplified by high fidelity PCR and sequenced. Sequencing results verified that *ZtMEP1*, in the IPO323 strain used in our lab, was disrupted by a transposon. Therefore, IPO323 is essentially a *Ztmep1Δ* null strain (**Figure 40**).

3.4 Ammonium dependent expression of *ZtMEP2* and *ZtMEP3*

Ammonium transporter expression is under the control of nitrogen catabolite repression in several fungi. Limiting ammonium enhances their expression while high levels of ammonium represses them (Rutherford *et al.*, 2008a). To determine if *ZtMEP2* and *ZtMEP3* exhibit ammonium dependent expression, mRNA, extracted from IPO323 WT cells grown in low and high ammonium, was analysed by qPCR. *ZtMEP2* and *ZtMEP3* were expressed 4.06 and 6.26 fold more in low ammonium compared to high ammonium media respectively. A 2 tailed student T test confirmed that both results were statistically significant, as indicated by *p-value* 0.0002

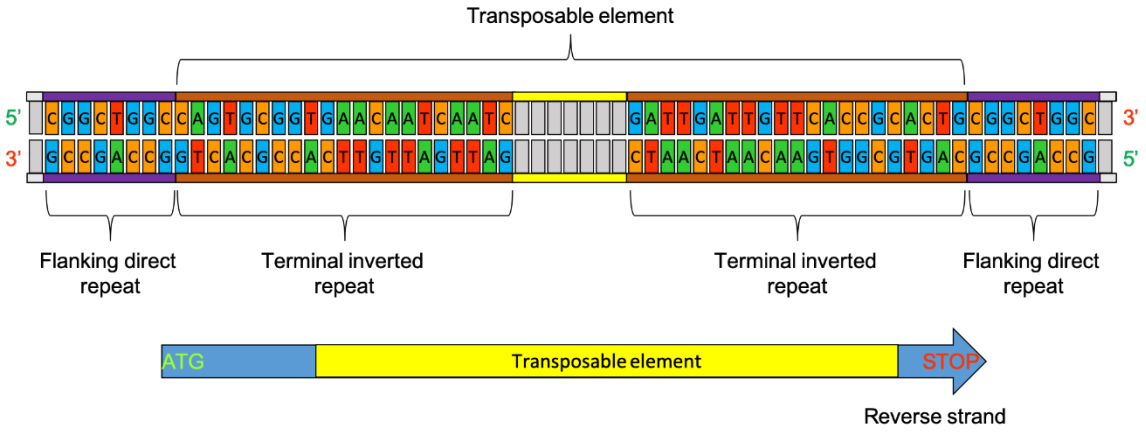

Figure 37: ***Schematic of transposable element integrated into ZtMEP1****. The IPO323 ZtMEP1 sequence was analysed for flanking direct repeats and terminal inverted repeats, coloured in purple and brown respectively. The middle grey nucleotides correspond to 4001 bp within the transposable element. ZtMEP1 is present on the reverse strand, however the sequence is shown in the forward direction for ease, as indicated by the arrow below. The location of the transposable element is depicted on the arrow. Adapted from Pierce, Benjamin. Genetics: A Conceptual Approach, 2nd ed.*

```
IPO323      MSSPAEVYSDMFPVPEYDPSMPRGGNTLEVNVNDQYTGHEFHYVYLTVCAFLVWMIIPGI      60
3D7         MSSPAEVYSDMFPVPEYDPSMPRGGNTLEVNVNDQYTGHEFHYVYLTVCAFLVWMIIPGI      60
1A5         MSSPAEVYSDMFPVPEYDPSMPRGGNTLEVNVNDQYTGHEFHYVYLTVCAFLVWMIIPGI      60
1E4         MSSPAEVYSDMFPVPEYDPSMPRGGNTLEVNVNDQYTGHEFHYVYLTVCAFLVWMIIPGI      60
            ************************************************************

IPO323      GLLYSGLARRKSSLALLFQTLMVIAIVTFQWMFWGYSLAYSRTGNAFIGNLDNFGLMGVR      120
3D7         GLLYSGLARRKSSLALLFQTLMVIAVVTFQWMFWGYSLAYSRTGNAFIGNLDNFGLMGVR      120
1A5         GLLYSGLARRKSSLALLFQTLMVIAIVTFQWMFWGYSLAYSRTGNAFIGNLDNFGLMGVR      120
1E4         GLLYSGLARRKSSLALLFQTLMVIAIVTFQWMFWGYSLAYSRTGNAFIGNLDNFGLMGVR      120
            ************************:***********************************

IPO323      VAPSPGNAFLPEIIFCFYQLLFCAVTVQLVIGGAFERGGILASLLFSFIWATIVYCPVAN      180
3D7         VAPSPGNAFLPEIIFCFYQLLFCAVTVQLVIGGAFERGGILASLLFSFIWATIVYCPVAN      180
1A5         VAPSPGNAFLPEIIFCFYQLLFCAVTVQLVIGGAFERGGILASLLFSFIWATIVYCPVAN      180
1E4         VAPSPGNAFLPEIIFCFYQLLFCAVTVQLVIGGAFERGGILASLLFSFIWATIVYCPVAN      180
            ************************************************************

IPO323      WTWNANGWLYNLGELDFAGGGPVHIASGCASLAYALILGKRQVKSEIGRGRTKPHNASLV      240
3D7         WTWNANGWLYNLGELDFAGGGPVHIASGCASLAYALILGKRQVKSEIGRGRTKPHNASLV      240
1A5         WTWNANGWLYNLGELDFAGGGPVHIASGCASLAYALILGKRQVKSEIGRGRTKPHNASLV      240
1E4         WTWNSNGWLYNLGELDFAGGGPVHIASGCASLAYALILGKRQVKSEIGRGRTKPHNASLV      240
            *****:******************************************************

IPO323      WLGTMLIWFGWFGFNGGSALNASVRSLYVVFNTNTAASTGVLGWVLVDMVRNKGKFSVTG      300
3D7         WLGTMLIWFGWFGFNGGSALNASVRSLYVVFNTNTAASTGVLGWVLVDMVRNKGKFSVTG      300
1A5         WLGTMLIWFGWFGFNGGSALNASVRSLYVVFNTNTAASTGVLGWVLVDMVRNKGKFSVTG      300
1E4         WLGTMLIWFGWFGFNGGSALNASVRSLYVVFNTNTAASTGVLGWVLVDMVRNKGKFSVTG      300
            ************************************************************

IPO323      ACEGAIAGLVGITPAAGYVNFWLAALIGFLTGIVCSSLHDLNDWLNVDEGLDVFKLHGIG      360
3D7         ACEGAIAGLVGITPAAGYVNFWLAALIGFLTGIVCSSLHDLNDLLNIDEGLDVFKLHGIG      360
1A5         ACEGAIAGLVGITPAAGYVNFWLAALIGFLTGIVCSSLHDLNDLLNIDEGLDVFKLHGIG      360
1E4         ACEGAIAGLVGITPAAGYVNFWLAALIGFLTGIVCSSLHDLNDLLNIDEGLDVFKLHGIG      360
            ****************************************  **:**************

IPO323      GMVGSFLTGIFADAPIGALDYELEIAGAINGNGVQIGYNLAGIVAIAAYSFTVTSIILLV      420
3D7         GMVGSFLTGIFADAPIGALDYELEIAGAINGNGVQIGYNLAGIVAIAAYSFTVTSIILLV      420
1A5         GMVGSFLTGIFADAPIGALDYELEIAGAINGNGVQIGYNLAGIVAIAAYSFTVTSIILLV      420
1E4         GMVGSFLTGIFADAPIGALDYELEIAGAINGNGVQIGYNLAGIVAIAAYSFTVTSIILLV      420
            ************************************************************

IPO323      LKYIPGVGLRVSAEDEMMGLDAVHFADEEIGDWEYMKEARSTLNGHDGTEQSRRVSSAGS      480
3D7         LRYIPGVGLRVSAEDEMMGLDAVHFADEEIGDWEYMKEARSTLNGHDGTEQSRRVSSAGS      480
1A5         LRYIPGVGLRVSAEDEMMGLDAVHFADEEIGDWEYMKEARSTLNGHDGTEQSRRVSSAGS      480
1E4         LRYIPGVGLRVSAEDEMMGLDAVHFADEEIGDWEYMKEARSTLNGHDGTEQSRRVSSAGS      480
            *:**********************************************************

IPO323      KEREVESTSATSPGRAMV          498
3D7         KEREVESTSATSPGRAMV          498
1A5         KEREVESTSATSPGRAMV          498
1E4         KEREVESTSATSPGRAMV          498
            ******************
```

Figure 38: ZtMep1 alignment between Z. tritici strains. *ZtMep1 from IPO323 (new sequence generated from factoring in the transposon), 3D7, 1A5 and 1E4 were aligned. The sequence highlighted in yellow corresponds to the 46 amino acids missing from the original IPO323 ZtMep1 sequence.*

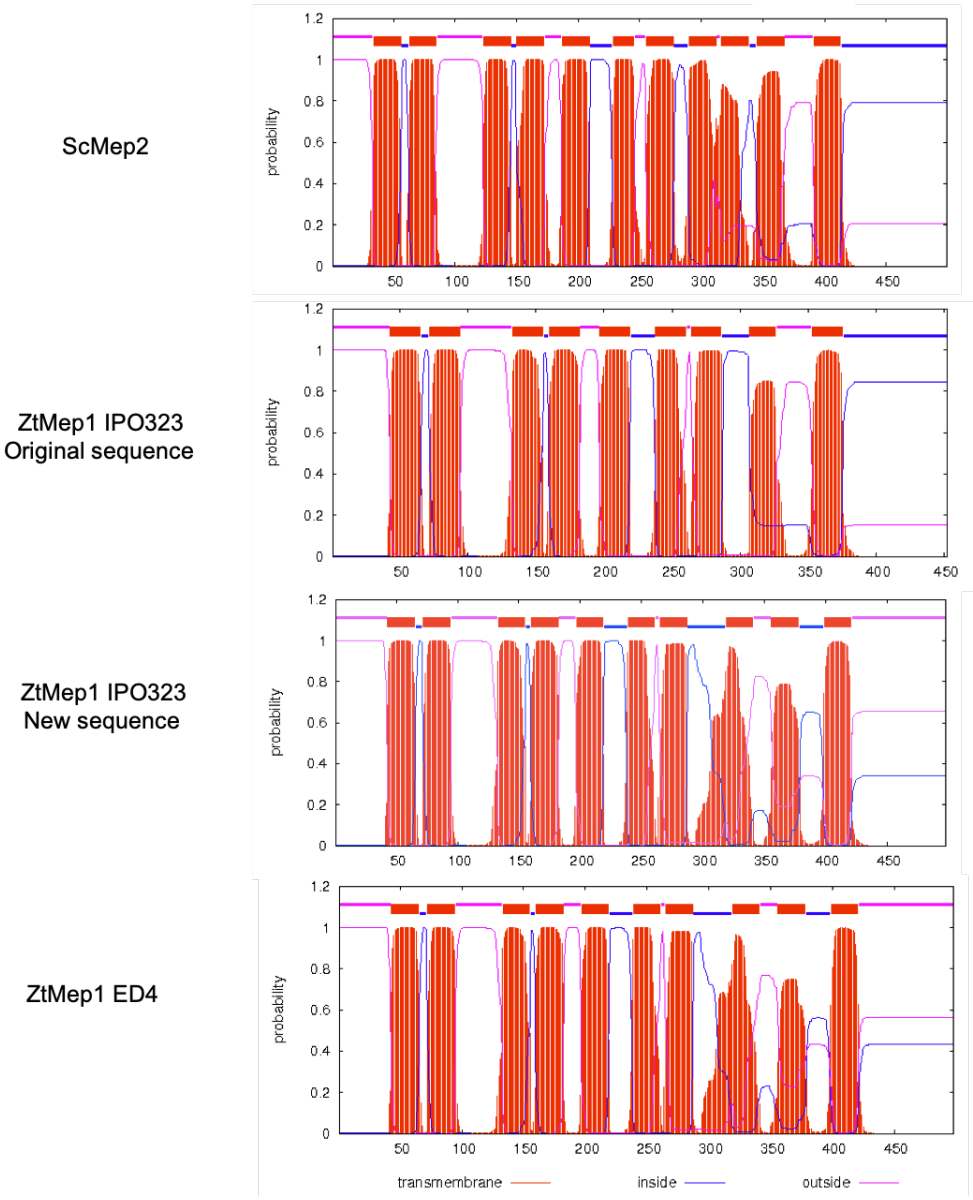

Figure 39: TMD predictions. *Protein sequences for ScMep2 and ZtMep1 from the IPO323 and ED4 strains were analysed by the TMHMM Server v. 2.0 online software tool. The returned graphs depict the predicted transmembrane domains (TMDs). Pink and blue lines indicate extracellular and intracellular loops respectively, while red boxes indicate TMDs. The original sequence is the protein sequence available from the IPO323 genome database, which was not based on the RRes annotation. The new sequence is the sequence created by factoring in the transposon.*

Figure 40: ZtMEP1 contains a transposon. *a) Schematic of the ZtMEP1 gene downloaded from the Z. tritici genome database including the annotation from RRes. The black lines labelled A and B indicate the regions amplified by PCR. b) DNA gel of PCR product A and the returned sequencing result. c) DNA gel of PCR product B and the returned sequencing result. Red annotation in the sequencing indicates the region is part of ZtMEP1, whereas blue and grey indicate exon and intron regions (according to the RRes annotation) within the transposon respectively. The sequences highlighted in orange and yellow correspond to the direct flanking repeats and the inverted terminal repeats respectively.*

and *p-value* 0.0000007 for *ZtMEP2* and *ZtMEP3* results respectively (**Figure 41**). This data confirms that the *ZtMEP2* and *ZtMEP3* expression is induced in response to limiting ammonium conditions which is consistent with nitrogen catabolite repression.

3.5 Expression of *Z. tritici* ammonium transporters in *S. cerevisiae*

A diploid *S. cerevisiae* strain lacking ScMep2 (*mep2Δ/mep2Δ*) is unable to undergo pseudohyphal growth in response to limiting ammonium (Lorenz and Heitman, 1998) , whereas lack of all three ammonium transporters (*mep123Δ*) renders the yeast unable to grow on medium with ammonium as the sole nitrogen source (Marini *et al.*, 1997). *S. cerevisiae* can therefore be utilised as a model for testing putative ammonium transporters for growth and signalling functions. *Z. tritici* ammonium transporters were hence codon optimised to *S. cerevisiae* and expressed in the appropriate *S. cerevisiae* strains to verify that they are ammonium transporters and to test if they act as ammonium sensors. ZtMEP2 and ZtMEP3 were cloned from the IPO323 strain whereas ZtMEP1 was cloned from the 1E4 strain as ZtMEP1 in IPO323 is disrupted by a transposon. All codon optimised genes were cloned into the low copy shuttle plasmid pRS316 (Sikorski and Hieter, 1989).

3.5.1 ZtMep1, ZtMep2, and ZtMep3 are ammonium transporters

Transformation of *mep123Δ* with all three ammonium transporters supported growth on 0.1 % glutamate. Glutamate is a positive control as this is a preferred source of nitrogen. On 1 mM ammonium sulphate, a limiting concentration of ammonium, ZtMep2 and ZtMep3 restored growth to the same level as the ScMep2 positive control. The amount of restored growth achieved by ZtMep1 was more than the negative vector control, but considerably less than the ScMep2 (**Figure 42**). These findings confirm that ZtMep1, ZtMep2 and ZtMep3 are ammonium transporters, but suggest that ZtMep2 and ZtMep3 are more efficient transporters than ZtMep1. ScMep2 transport activity is regulated by the TOR regulated kinase Npr1 in *S. cerevisiae* by phosphorylation. Therefore, in a strain lacking all three ammonium transporters, and Npr1 (*mep123Δ/npr1Δ*), ScMep2 is not activated and the strain cannot grow on low ammonium (Boeckstaens *et al.*, 2014). To test if the *Z. tritici* ammonium transporters were regulated by Npr1 in yeast, the *mep123Δ/npr1Δ* strain was transformed with the

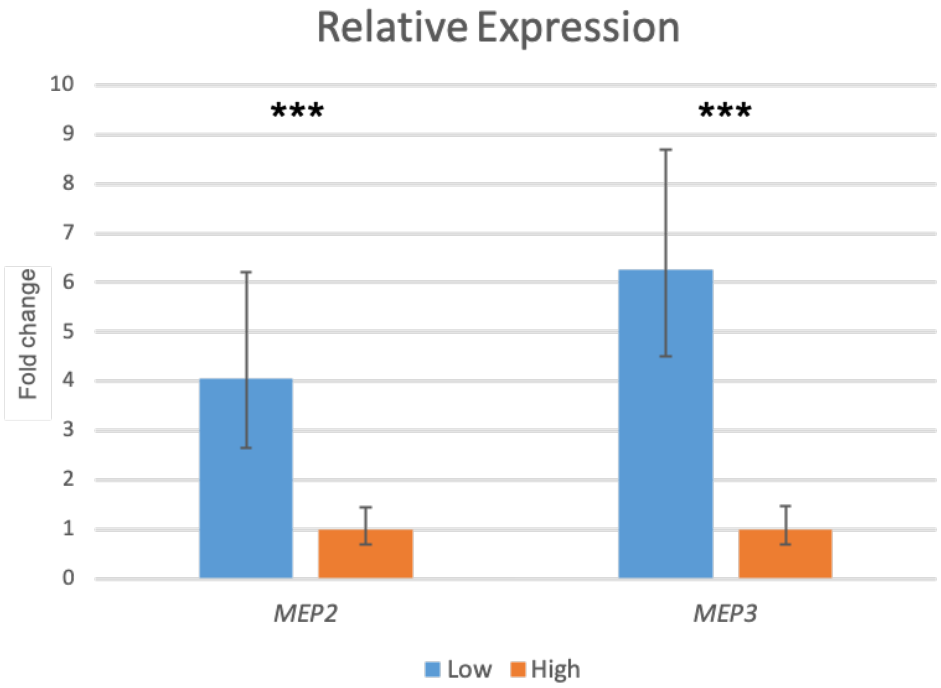

Figure 41: Expression analysis of ZtMEP2 and ZtMEP3. *IPO323 cells pre-grown in YPD were washed and inoculated into low and high NH_4^+ liquid medium at OD_{595nm} 2. Cells were harvested after 8 hours growth at 18 °C. RNA extracted from the cells was converted to cDNA to be used as template for qPCR. The $^{2-\Delta Ct}$ method was used to calculate relative expression to cultures grown in high NH_4^+. Actin was used as a reference gene. A 2 tailed Student T test was used to calculate significance. *** p-value <0.001*

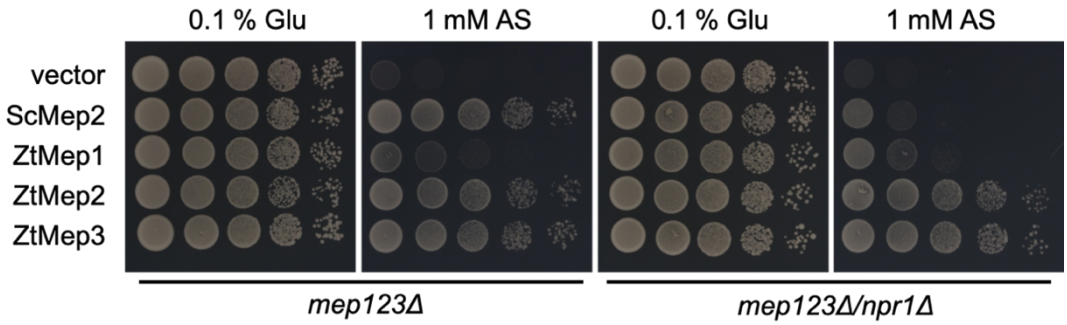

Figure 42: Growth analysis of Z. tritici ammonium transporters expressed in yeast . *Haploid mep123Δ and mep123Δ/npr1Δ S. cerevisiae cells containing the plasmids of interest were grown in SD-URA medium overnight, washed, and 10 fold serially diluted before being spotted onto 0.1 % glutamate or 1 mM ammonium sulphate agar.*

same codon optimised plasmids and the growth assay was repeated. Interestingly, in contrast to ScMep2, which does not restore growth to WT levels in *mep123Δ/npr1Δ*, ZtMep2 and ZtMep3 do complement the growth defect on low ammonium. Moreover, there was no difference in the level of restored growth by ZtMep1 between *mep123Δ* and *mep123Δ/npr1Δ* (**Figure 42**). This data confirms that the transport activity of ZtMep1, ZtMep2 and ZtMep3 is not regulated by Npr1 when expressed in yeast.

3.5.2 ZtMep3 acts as an ammonium sensor in S. cerevisiae

Transformation of *mep2Δ/mep2Δ* with ZtMep1 or ZtMep2 did not restore the pseudohyphal growth defect as the edge of their colonies were smooth and not dissimilar to the negative vector control. On the contrary, ZtMep3 did complement the pseudohyphal growth defect of the *mep2Δ/mep2Δ* strain. Both invasive and surface pseudohyphae were observed on the edge of ZtMep3 single colonies and streaked cells. (**Figure 43**). When analysing the pseudohyphae on the edge of the single colonies, the ZtMep3 filaments did not extend as far as the ScMep2 positive control filaments, however no discrepancy was observed between ScMep2 and ZtMep3 when comparing the pseudohyphae on the edge of the streaks of cells. Thus, ZtMep3 acts as an ammonium sensor when expressed in yeast.

3.5.3 ZtMep3 is expressed to a lower level than ZtMep1 and ZtMep2 in S. cerevisiae

The pseudohyphal growth assays suggest that only ZtMep3, and not ZtMep1 nor ZtMep2 are ammonium sensors in *S. cerevisiae*. However, a reduction in the protein expression of Mep2 can impact on pseudohyphal growth. Protein expression of each *Z. tritici* transporter was therefore analysed by western blotting. The expected molecular weights of each protein were 53616 Da, 56218 Da, and 57617 Da for ZtMep1, ZtMep2, and ZtMep3 respectively. ZtMep1 and ZtMep2 were expressed to similar levels to each other, however, ZtMep3 expression was substantially lower (**Figure 44**). Therefore, the lack of pseudohyphal growth by ZtMep1 and ZtMep2 cannot be attributable to reduced expression, as their expression was higher than ZtMep3.

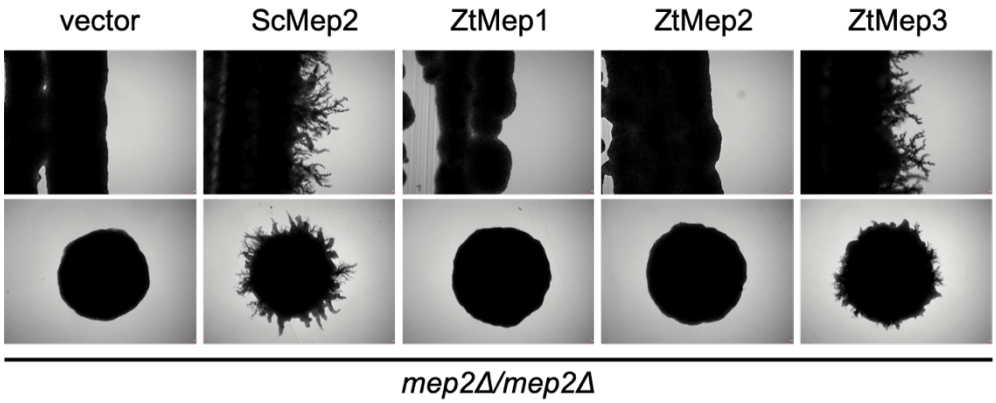

Figure 43: Pseudohyphal growth analysis of Z. tritici ammonium transporters expressed in yeast . *Diploid mep2Δ/mep2Δ S. cerevisiae cells containing the plasmids of interested were streaked for single colonies on low ammonium sulphate medium (50 μM). After 6 days growth, cells were photographed under the microscope at 100 x (top panel) and 40 x (bottom panel) respectively.*

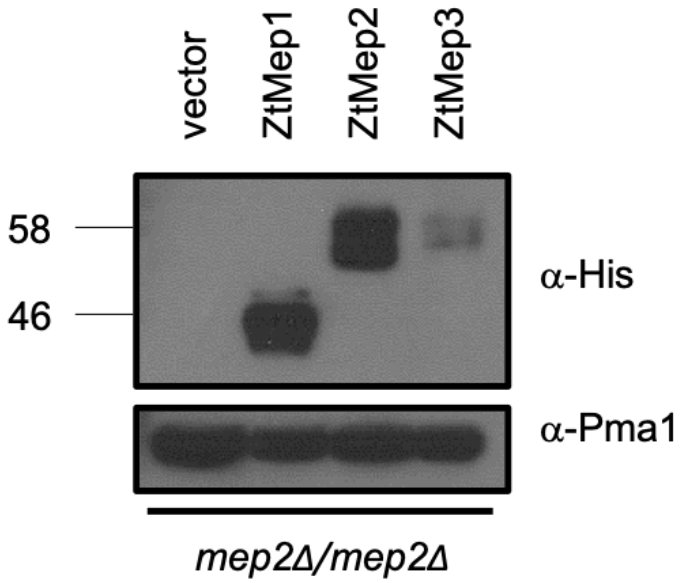

Figure 44: Western analysis of Z. tritici ammonium transporters expressed in yeast. *Diploid mep2Δ/mep2Δ S. cerevisiae cells containing the plasmids of interested were grown to mid-log phase in 0.1 % proline medium. Membrane proteins were extracted and assayed by western blotting. Pma1 was used as a loading control to compare protein expression levels.*

3.6 Generation of *Z. tritici* mutants

Ammonium dependent filamentation in several fungal species is dependent on members of the Mep/Amt/Rh family. To determine if the ammonium dependent filamentation exhibited by *Z. tritici* (**section 3.2**) is dependent on ammonium transporters, *ZtMEP2* and *ZtMEP3* were deleted from the IPO323 genome by agrobacterium mediated transformation, before being analysed in later experiments for filamentation. *ZtMEP1* was not selected for deletion as the gene has already been disrupted in IPO323 by a transposable element (**section 3.3.2**). As the 3' end of *ZtMEP2* is very close to the 3' UTR of another gene (Mycgr3T67486). *ZtMEP2* was therefore disrupted in addition to being deleted. For the deletion *Ztmep2Δ* mutant, the left side flanking DNA was chosen so that the adjacent gene would not be disrupted. *ZtMEP3* is not in close proximity to its adjacent genes, therefore *ZtMEP3* was deleted rather than disrupted (**Figure 45**).

3.6.1 Deletion and disruption of ZtMEP2

Upon agrobacterium mediated transformation, the Hygromycin-trpC resistance cassette was successfully integrated into the IPO323 genome at the *ZtMEP2* locus (**Figure 46**). The deletion construct exhibited 10 % targeting efficiency (4 out of 40 mutants tested), whereas the disruption construct displayed 40 % targeting efficiency (23 out of 49 mutants tested) as confirmed by diagnostic colony PCR. PCR primers annealing to genomic DNA adjacent to the deletion and disruption cassette and primers targeted to the hygromycin-trpC cassette were used to confirm successful integration at the correct locus. Absence of the WT allele verified that the mutants had been generated (**Figure 47**). One deletion mutant and two disruption mutants were used for further investigation.

3.6.2 Deletion of ZtMEP3

The hygromycin-trpC resistance cassette was integrated into the IPO323 genome at the *ZtMEP3* locus by agrobacterium mediated transformation with a 47 % targeting efficiency (18 out of 45 mutants tested) (**Figure 48**). Colony PCR was used to diagnose successful integration, as previously described (section 3.6.1) (**Figure 49**). Three independent isolates were used for subsequent experiments.

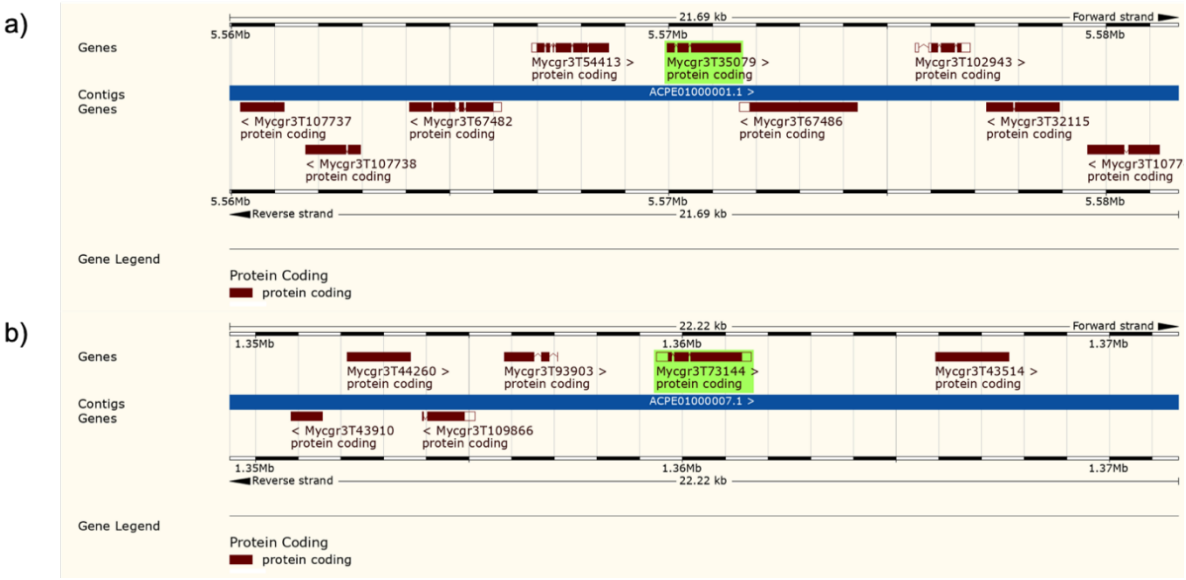

Figure 45: Schematic of ZtMEP2 and ZtMEP3 genomic locations. *Images exported from the IPO323 genome database depict a) ZtMEP2 and b) ZtMEP3 location. Regions highlighted in green indicate the genes of interest. Red boxes and lines correspond to exons and introns respectively, while red outlines white boxes indicate 5' or 3' UTRs.*

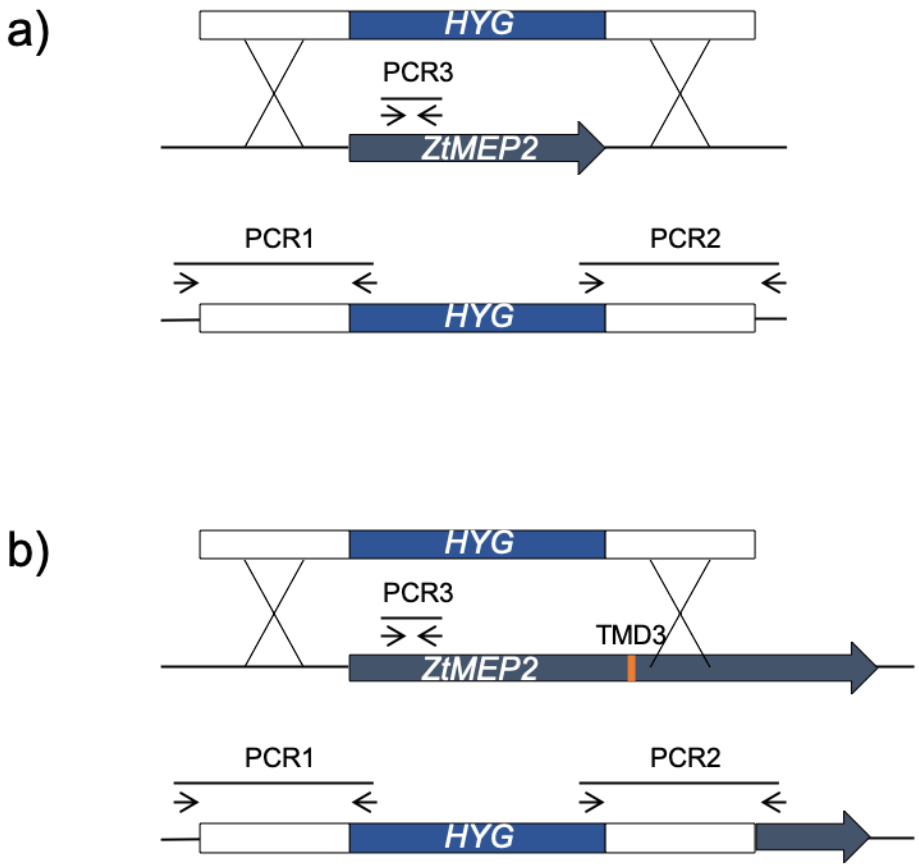

Figure 46: Schematic of homologous recombination to delete and disrupt ZtMEP2*. a) Homologous recombination event to delete ZtMEP2. b) Homologous recombination event to disrupt ZtMEP2. PCR1, PCR2 and PCR3 correspond to diagnostic PCRs*

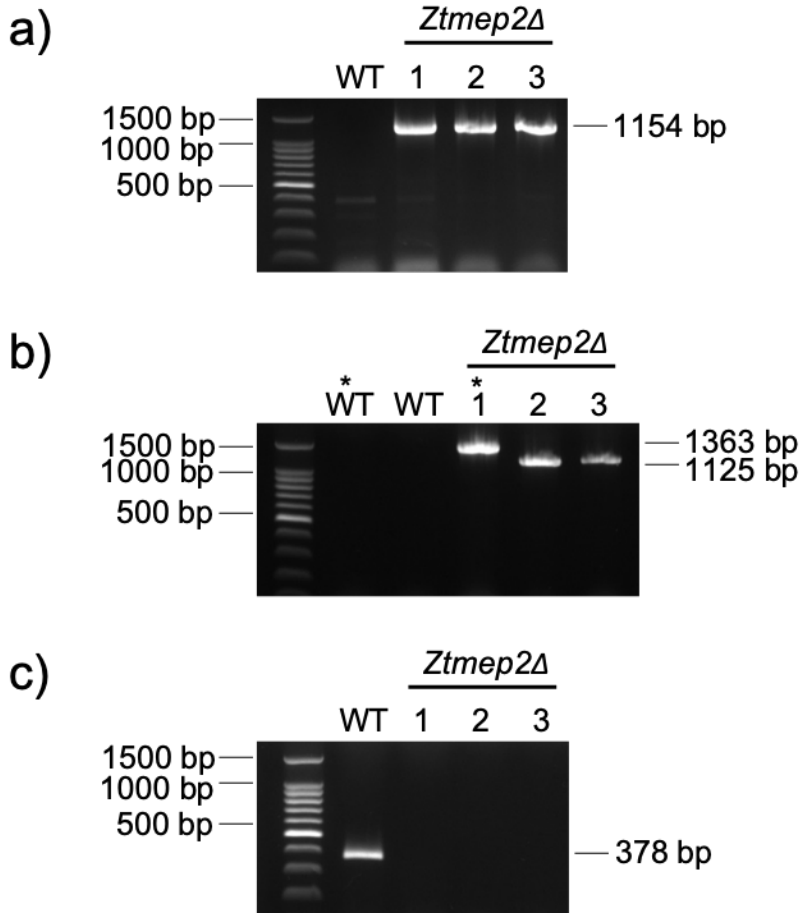

Figure 47: Diagnostic Z. tritici colony PCRs to confirm Ztmep2Δ mutants. *The WT colony along with three independent mutant isolates were tested for targeted integration of the resistance cassette and for the presence of the WT allele. a) PCR1: results from the left hand side HYG integration. b) PCR 2: results from the right hand side HYG integration (* primers to detect HYG in the deletion mutant were used). c) PCR 3: results from the WT allele PCR. Lanes labelled 1, 2 and 3 identify which Ztmep2Δ independent isolate is being tested.*

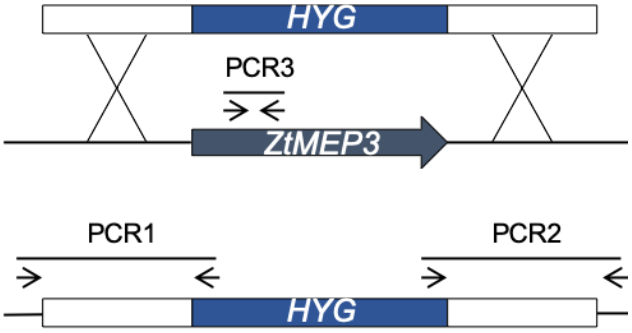

Figure 48: Schematic of homologous recombination to delete ZtMEP3*. a) Homologous recombination event to delete ZtMEP3. PCR1, PCR2 and PCR3 correspond to diagnostic PCRs*

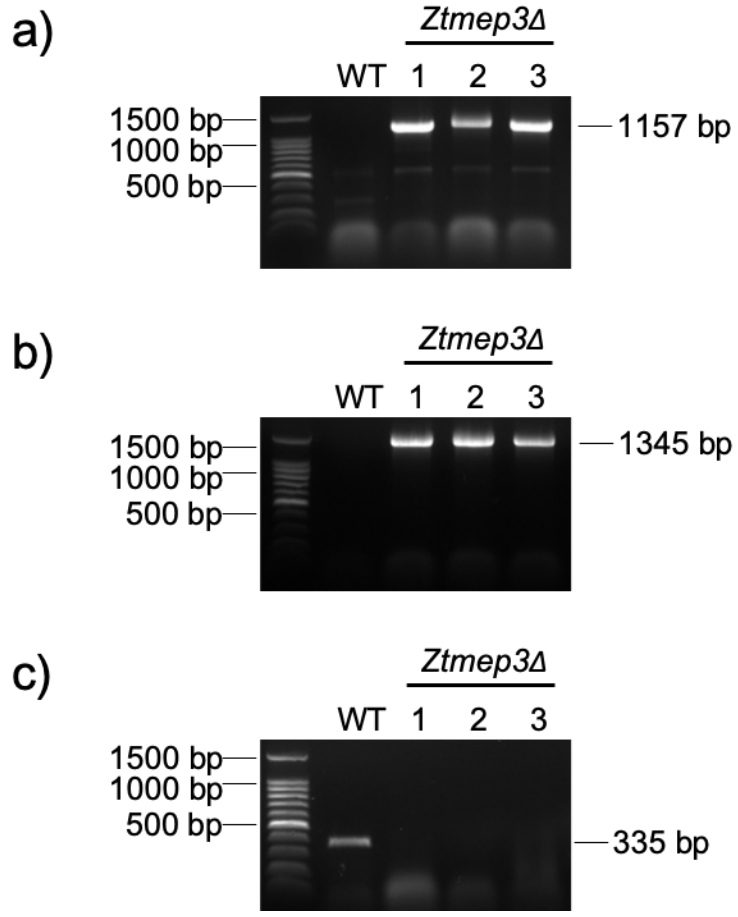

Figure 49: Diagnostic Z. tritici colony PCRs to confirm Ztmep3Δ mutants. *The WT colony along with three independent mutant isolates were tested for targeted integration of the resistance cassette and for the presence of the WT allele. a) PCR1: results from the left hand side HYG integration. b) PCR2: results from the right hand side HYG integration. c) PCR3: results from the WT allele PCR. Lanes labelled 1, 2 and 3 identify which Ztmep3Δ independent isolate is being tested.*

3.6.3 Generation of ZtMep2/ZtMep3 double mutant

To test if both ZtMep2 and ZtMep3 were required for the ammonium dependent switch, yeast to filamentous growth, *ZtMEP3* was deleted from the *Ztmep2Δ* #2 strain and assayed for filamentation. The GEN resistance cassette was integrated into the IPO323 *Ztmep2Δ* #2 genome at the *ZtMEP3* locus by agrobacterium mediated transformation with a 13 % targeting efficiency (9 out of 70 mutants tested) (**Figure 50**). Colony PCR was used to diagnose successful integration, as previously described (**section 3.6.1**) (**Figure 51**). Three independent isolates were used for subsequent experiments.

3.7 Phenotypic analysis of mutants

3.7.1 IPO323 Ztmep3Δ and Ztmep2Δ/Ztmep3Δ mutants display a growth defect on high ammonium

As ammonium is such an important source of nitrogen for many fungi, the loss of an ammonium transporter has the potential to impact on growth (Marini *et al.*, 1997), therefore, a growth assay was performed with the mutants on different solid media. On rich YPD medium, there was no difference between the WT cells and the mutants. On high ammonium, the *Ztmep2Δ* single mutants grew like WT cells, whereas the *Ztmep3Δ* single mutants and *Ztmep2Δ*/*Ztmep3Δ* double mutants barely grew. Interestingly the growth defect of the double mutants was slightly less severe than the growth defect of the *Ztmep3Δ* single mutants. Both WT cells and the mutants displayed a growth defect on low ammonium compared to high ammonium, however, the growth defects were slightly more severe with the *Ztmep3Δ* single mutants and *Ztmep2Δ*/*Ztmep3Δ* double mutants. On 0.1 % proline medium (a non-preferred source of nitrogen), the *Ztmep2Δ* and *Ztmep3Δ* single mutants grew like the WT cells, however although growth was not impaired in the double mutants, they were melanised, whereas the WT cells and single mutants remained pink (**Figure 52**). Hence, *Ztmep3Δ* single mutants and *Ztmep2Δ*/*Ztmep3Δ* double mutants show a growth defect at levels of ammonium sufficient for growth for WT cells, while *Ztmep2Δ* single mutants show no difference to WT cells.

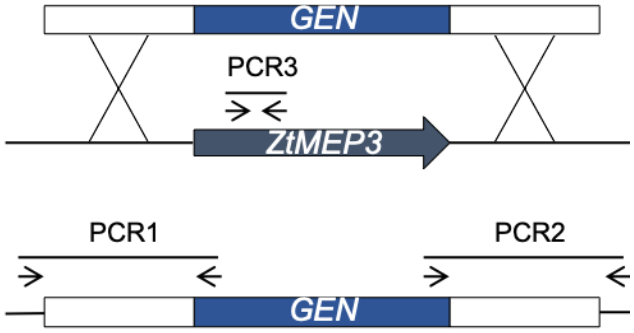

Figure 50: Schematic of homologous recombination to delete ZtMEP3 in Ztmep2Δ #2*. a) Homologous recombination event to delete ZtMEP3. PCR1, PCR2 and PCR3 correspond to diagnostic PCRs*

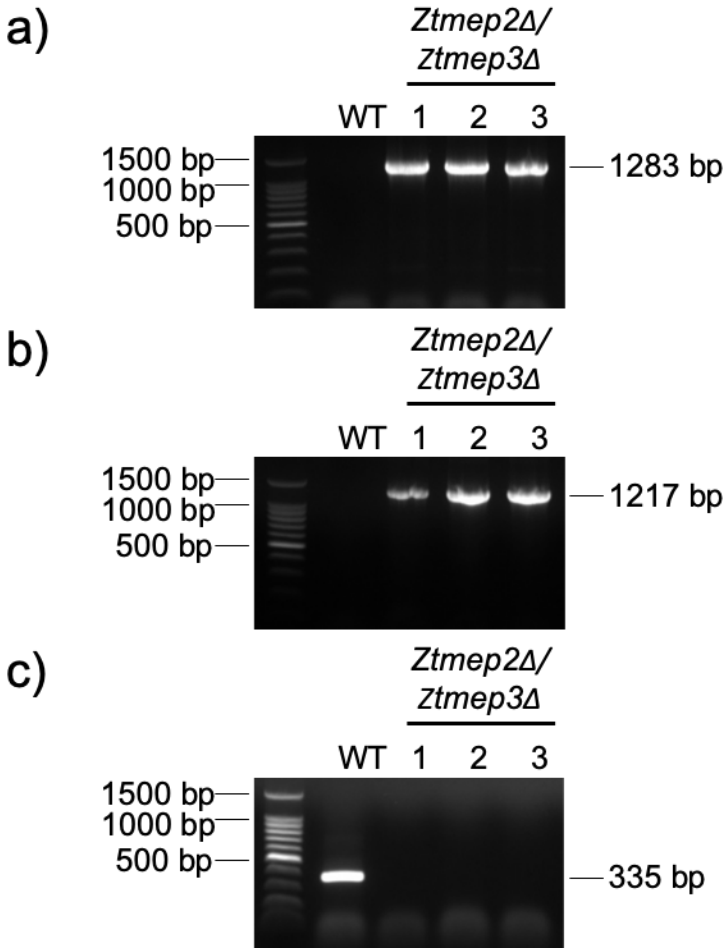

Figure 51: Diagnostic Z. tritici colony PCRs to confirm Ztmep2Δ/ Ztmep3Δ mutants. *The WT colony along with three independent mutant isolates were tested for targeted integration of the resistance cassette and for the presence of the WT allele. a) PCR1: results from the left hand side GEN integration. b) PCR2: results from the right hand side GEN integration. c) PCR3: results from the WT allele PCR. Lanes labelled 1, 2 and 3 identify which Ztmep2Δ/Ztmep3Δ independent isolate is being tested.*

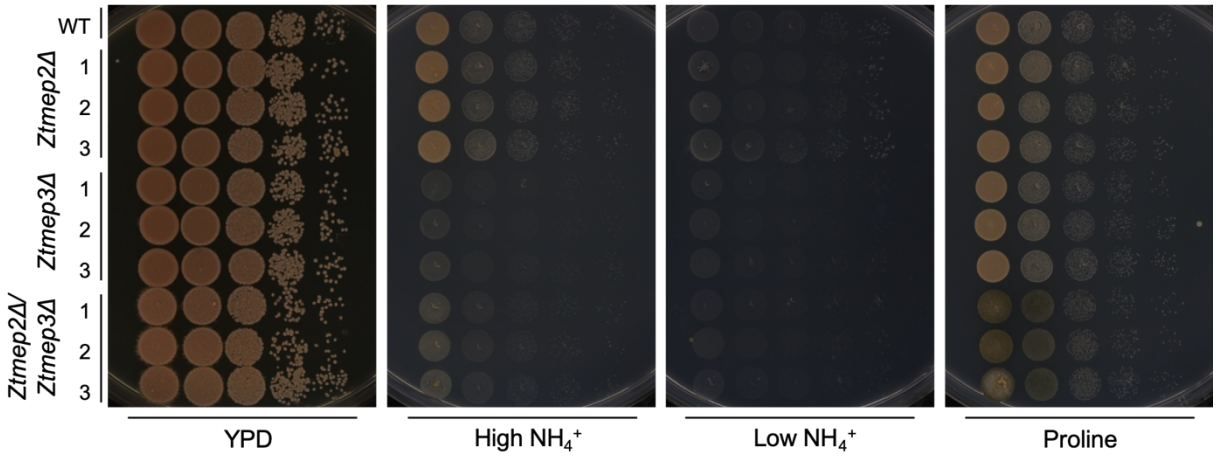

Figure 52: Growth analysis of IPO323 mutants. *Cells were grown in YPD medium over three nights, washed, and 10 fold serially diluted before being spotted onto YPD, high ammonium (5 mM), low ammonium (50 μM) and 0.1 % proline agar. Cells were photographed after 1 week incubation at 18 °C.*

The growth defects on solid media were consistent with growth in liquid media. WT and *Ztmep2Δ* single mutants grew in high ammonium, however the *Ztmep3Δ* single mutants and *Ztmep2Δ*/*Ztmep3Δ* double mutants did not grow. All strains did, however, grow in 0.1 % proline medium (**Figure 53**). Together, these findings are consistent with the possibility that ZtMep3 is a high capacity transporter.

3.7.2 IPO323 Ztmep3Δ and Ztmep2Δ/Ztmep3Δ mutants display interesting filamentation on high ammonium

Certain fungal species possess one ammonium transporter that senses ammonium availability in addition to their role as a transporter, hence, acting as a transceptor (Lorenz and Heitman, 1998). This sensing function triggers a signalling cascade to allow the cells to change morphology if required. To test if ZtMep2 and/or ZtMep3 are ammonium sensors in *Z. tritici*, WT and mutant strains were streaked for single colonies on different solid media and observed for filamentation by microscopy. On YPD, very few filaments emanated from their central colonies, however, some mutants had substantially more, especially *Ztmep2Δ*/*Ztmep3Δ #3* and *Ztmep2Δ #2*. On high ammonium medium all the strains displayed more filamentation compared to on YPD. However, the appearance of the *Ztmep3Δ* and *Ztmep2Δ*/*Ztmep3Δ* filaments differed from the WT and *Ztmep2Δ* filaments. Firstly, WT and *Ztmep2Δ* filaments emanated evenly around the whole circumference of their colonies, while *Ztmep3Δ* and *Ztmep2Δ*/*Ztmep3Δ* filaments emanated sporadically around the centre of their colonies. Secondly, the WT and *Ztmep2Δ* filaments had a 'wispy' appearance and did not extend out of the photographed frame, whereas the *Ztmep3Δ* and *Ztmep2Δ*/*Ztmep3Δ* filaments had a thicker 'barbed wire-like' appearance with some filaments extending out of the photographed frame. On low ammonium medium, the WT and *Ztmep2Δ* mutants filamented more than on high ammonium, and thicker filaments were present within the 'wispy' filaments. Both types of filaments extended out of the photographed frame and were evenly distributed around the centre of their colonies. Again, the *Ztmep3Δ* and *Ztmep2Δ/Ztmep3Δ* filaments were sporadically distributed around the centre of their colonies, and although thicker than the WT and *Ztmep2Δ* filaments, they were thinner than when extending on high ammonium

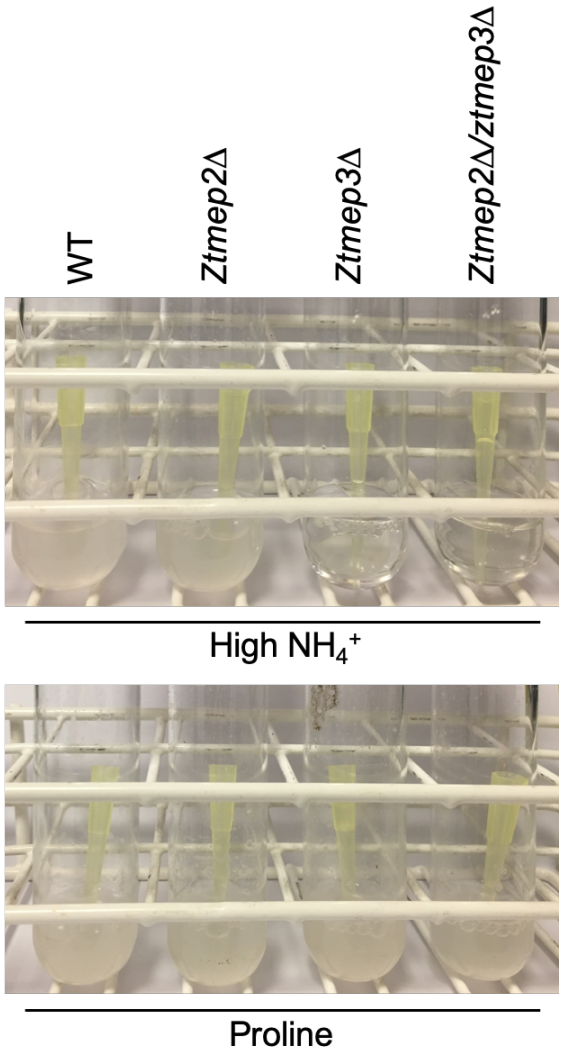

Figure 53: Analysis of IPO323 mutants in liquid culture. *Cells were inoculated into high ammonium (5 mM) (top panel) and 0.1 % proline medium (bottom panel). Tubes were photographed after 3 nights incubation at 18 °C.*

medium. Furthermore, *Ztmep3Δ* and *Ztmep2Δ/Ztmep3Δ* central colonies were barely visible; the filaments extended from a central point, like a pin wheel, rather than from a mass of cells. This phenotype is consistent with the growth defect of *Ztmep3Δ* and *Ztmep2Δ/Ztmep3Δ* being more severe on low ammonium as opposed to high ammonium medium. On 0.1 % proline medium all the strains exhibited the 'wispy' filaments evenly distributed around their central colonies, however the filaments extended slightly further from the *Ztmep3Δ* and *Ztmep2Δ/Ztmep3Δ* colonies compared to the other strains. No difference in size or shape of the central colonies was visible (**Figure 54**). The yeast to filamentous switch under ammonium limiting conditions is, therefore, ZtMep2 and ZtMep3 independent. To further analyse filamentation WT and mutant cells were spotted onto different solid media. After one weeks growth on YPD there was no difference in the size of the colonies between all the strains. The double mutants and *Ztmep2Δ* #2 did, however, display minimal filamentation around their colony giving a 'halo-like' appearance. On high and low ammonium medium, after two weeks growth, a difference in spot size was clearly visible; the *Ztmep3Δ* and *Ztmep2Δ/Ztmep3Δ* central colonies were smaller in diameter. While the filaments were evenly distributed around the WT and *Ztmep2Δ* mutant colonies, forming 'halos', this morphology was absent in the *Ztmep3Δ* and *Ztmep2Δ/Ztmep3Δ* mutants. Instead 'hair-like' filaments were visible emanating sporadically from the edge of the colonies; consistent with the growth assay and single colony analysis. The loss of the 'halo' in these mutants could be indicative that ZtMep3 is required for filamentation. The colour of the central spots were also different for Ztm*ep3Δ* and *Ztmep2Δ/Ztmep3Δ*. While the WT and *Ztmep2Δ* mutants remained pink, the *Ztmep3Δ* and *Ztmep2Δ/Ztmep3Δ* mutants displayed a 'rusty' colour. Analysis of the spots on a white background, as opposed to a black background, revealed another colour discrepancy. Some of the filaments extending from the *Ztmep3Δ* and *Ztmep2Δ/Ztmep3Δ* mutants appeared green, indicating that they were melanised, while the 'halo' of filaments around the WT and *Ztmep2Δ* mutants were white. After five weeks growth on 0.1 % proline medium all the spots appeared a similar size in diameter to each other and were melanised. Most of the mutants also displayed some degree of aerial hyphae which appeared as a smooth 'cotton wool-like" structure on the surface of the spot. The most aerial hyphae was present on the surface of the *Ztmep2Δ/Ztmep3Δ* mutants and *Ztmep2Δ* #2. Nevertheless, the aerial hyphae present on the *Ztmep2Δ/Ztmep3Δ* mutants did not have a smooth surface. Instead, the aerial hyphae was clumped (**Figure 55**).

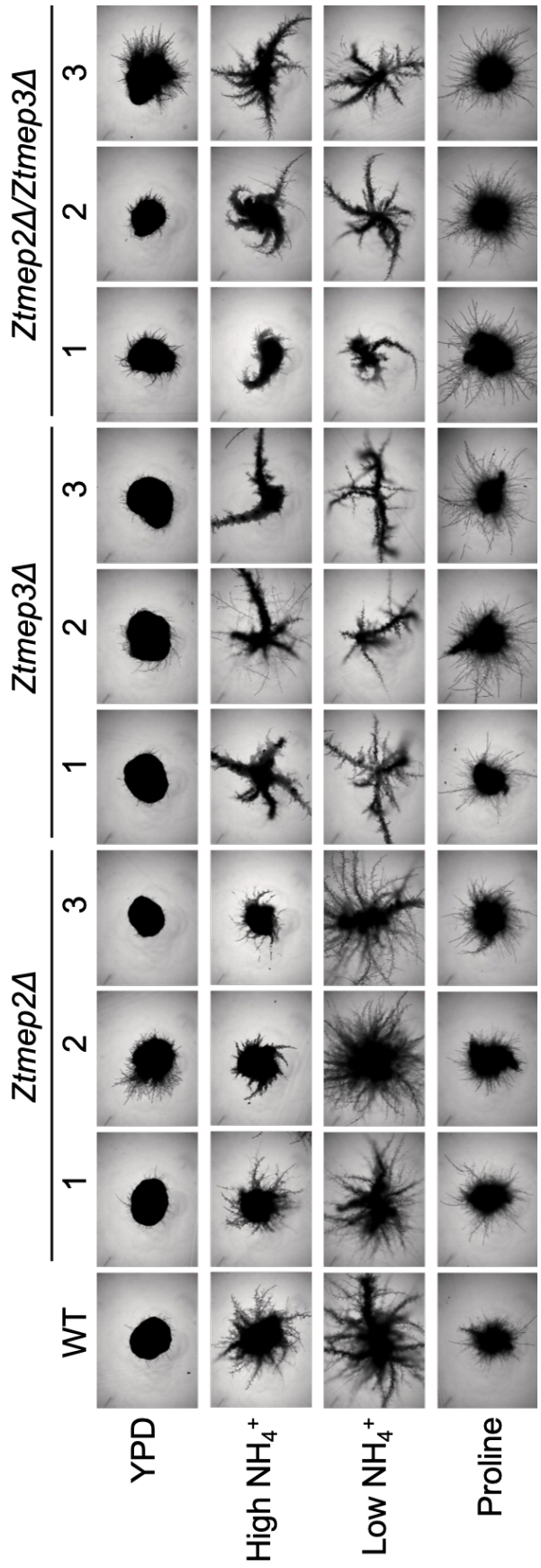

Figure 54: Analysis of morphology by the IPO323 mutant single colonies. *Cells were streaked for single colonies onto YPD, high ammonium (5 mM), low ammonium (50 μM) and 0.1 % proline agar. Cells were photographed after 1 week under the microscope at 40 x magnification.*

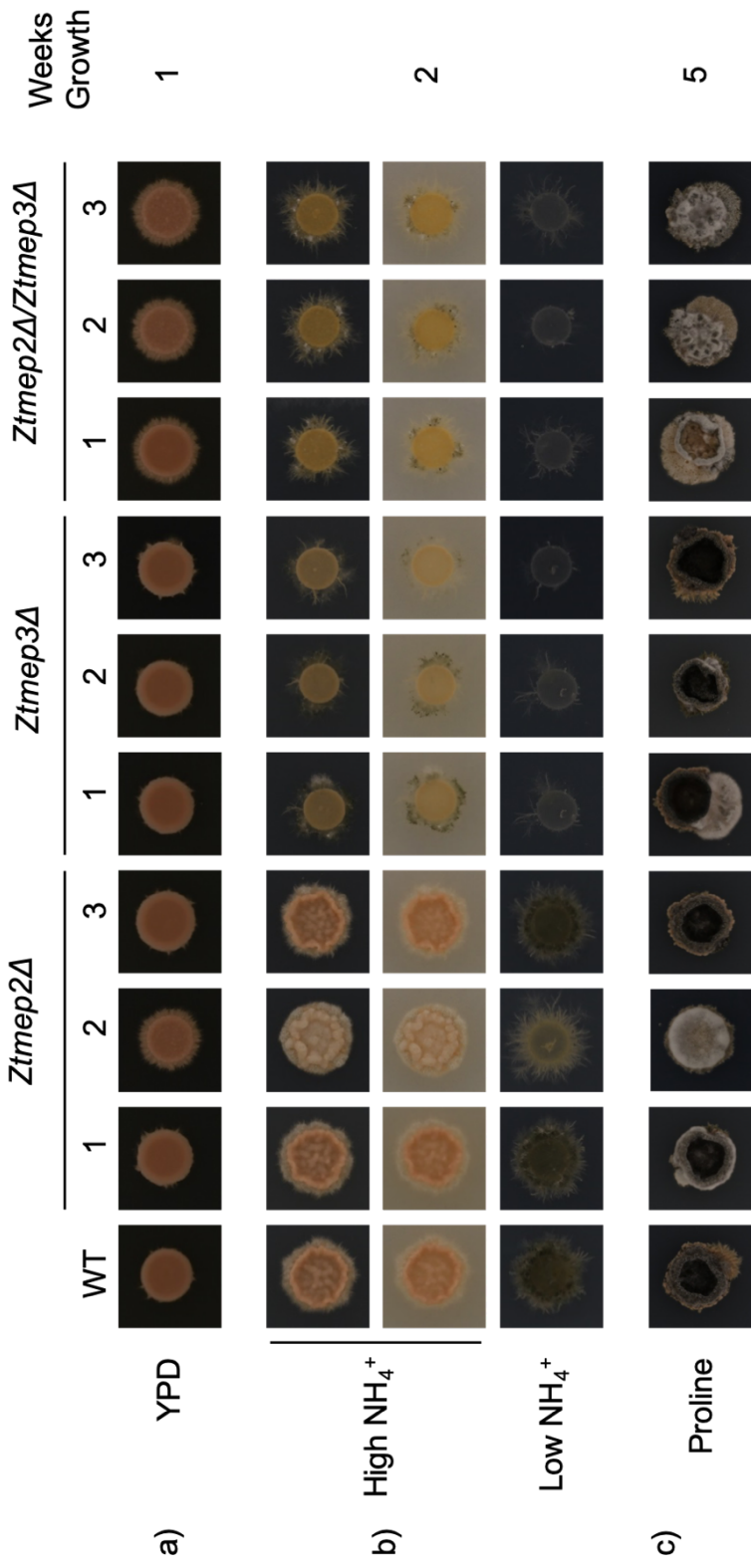

Figure 55: 5 μl spot assay. *WT and mutant cells were grown in YPD medium over three nights, washed, and spotted onto YPD, high ammonium (5 mM), low ammonium (50 μM) and 0.1 % proline agar. Cells grown on a) YPD were photographed after 1 weeks growth, cells grown on b) high and low ammonium were photographed after 2 weeks growth, and cells grown on c) proline were photographed after 5 weeks growth. For high ammonium colonies cells were photographed twice on black (top panel) and white (bottom panel) backgrounds.*

Consistent with the previous filamentation assay, ZtMep2 is not responsible for the yeast to filamentous dimorphic switch under ammonium limiting conditions. However, ZtMep3 may be required for some degree of filamentation, as indicated by the loss of the 'halo'.

3.8 IPO323 *Ztmep2Δ/Ztmep3Δ* double mutants are hypervirulent

In order for the smut fungus *Ustilago maydis* to infect maize, the fungus must first switch to a filamentous growth form. Under limiting ammonium conditions, *U. maydis* switches from budding to filamentous growth, and this switch is Ump2 dependent; Ump2 is the high affinity ammonium transporter in *U. maydis*. Ump2 is, hence, important for pathogenicity (Smith *et al.*, 2003). We were, therefore, interested to assess if the *Z. tritici* ammonium transporters are important for pathogenicity.

3.8.1 IPO323 Ztmep2Δ and Ztmep3Δ single mutants show do difference in virulence compared to WT IPO323

To test if ZtMep2 or ZtMep3 are important for the pathogenicity of *Z. tritici*, the single mutants were tested in a wheat infection assay by our collaborators at RRes. No differences between the infectivity of the WT or the mutants were visible 14 days post infection (DPI) (**Figure 56**). From images of the wheat leaves photographed 21 DPI, pycnidia were counted from sample areas. No significant difference between the WT and single mutants was calculated (**Figure 57**). These findings confirm that a lack of ZtMep2 or ZtMep3 does not impact on *Z. tritici's* ability to infect wheat.

3.8.2 IPO323 *Ztmep2Δ/Ztmep3Δ double mutants infect wheat sooner than WT IPO323*

To assess if ZtMep2 and ZtMep3 together are important for virulence, the double mutants were tested in the wheat infected assay. 14 DPI, the wheat leaves infected with the *Ztmep2Δ*/*Ztmep3Δ* double mutants showed visible signs of disease, whereas the leaves infected with the WT strain barely showed any disease symptoms. 17 DPI the leaves infected with the *Ztmep2Δ/Ztmep3Δ* double mutants were dead, whereas the leaves infected with the WT strain were alive but showing greater signs of disease. 21 DPI the leaves inoculated with the WT strain were almost dead (**Figure 58**). The

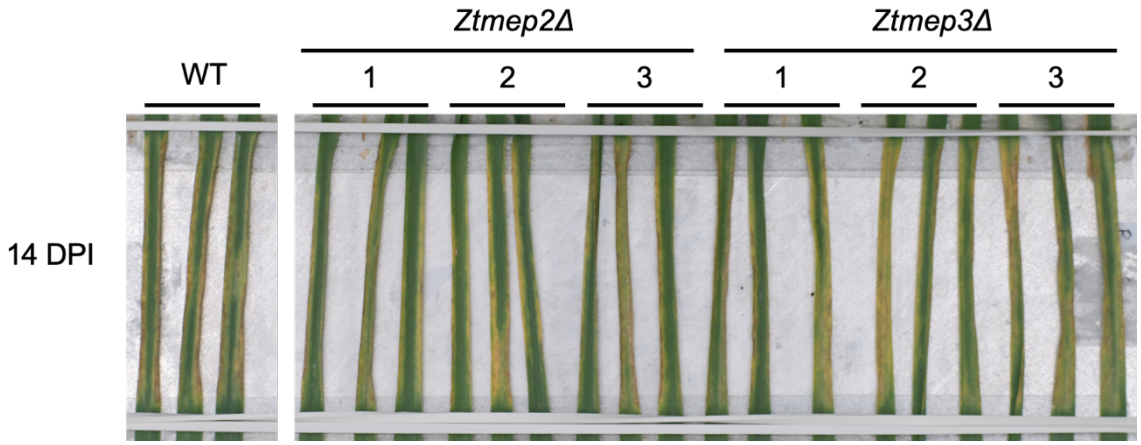

Figure 56: IPO323 Ztmep2Δ and Ztmep3Δ mutants what infection assay. *WT and mutant cells were assayed for their ability to infect wheat by Rothamsted Research. Wheat leaves were photographed 14 days post infection (DPI).*

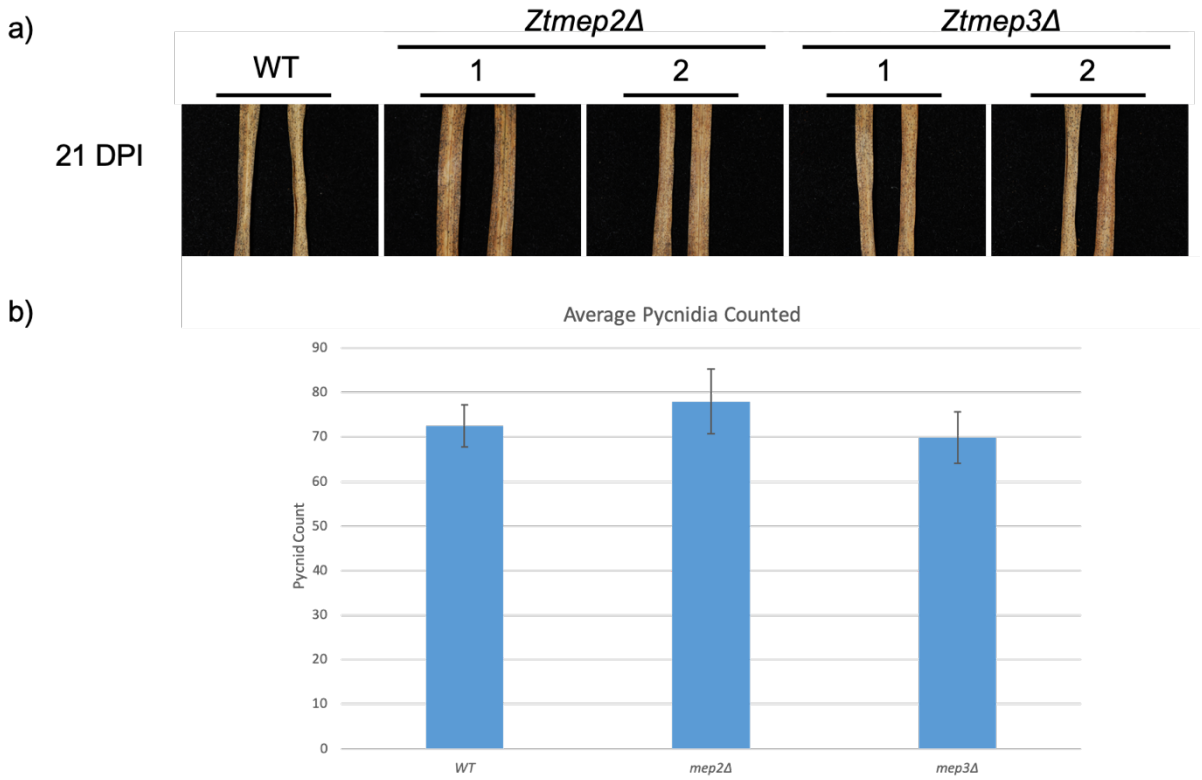

Figure 57: Analysis of pycnidia on wheat leaves 21 days post infection. *a) Images of wheat leaves 21 DPI. Black spots are pycnidia. b) Pycnidia were counted from sample areas on each leaf and a mean was calculated for each strain. Error bars represent standard error of the mean (SEM).*

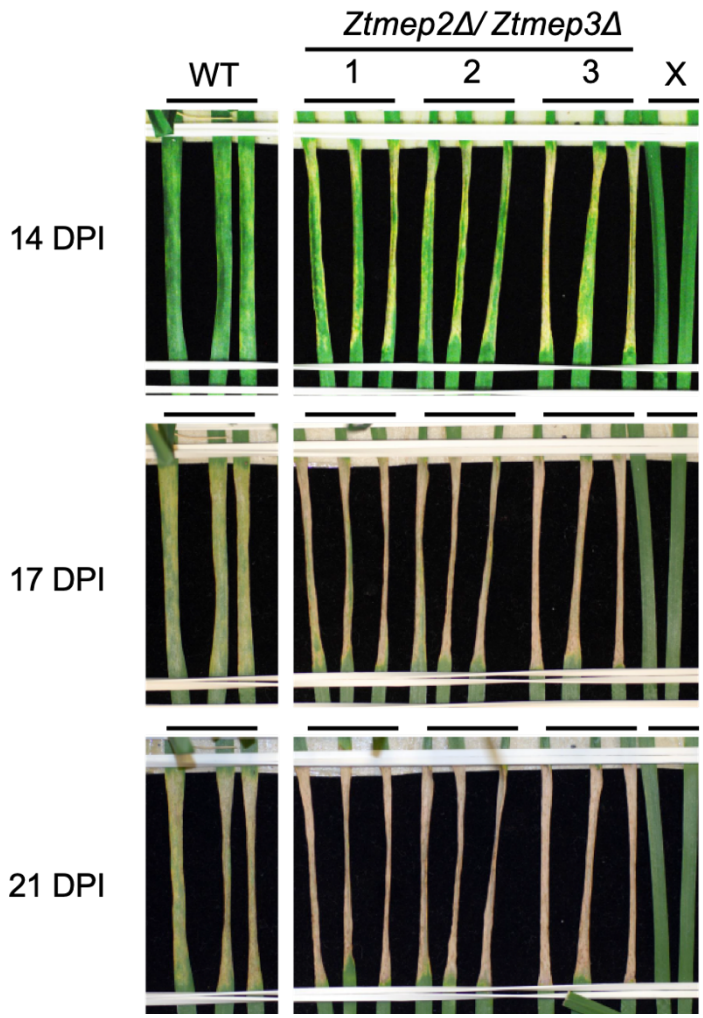

Figure 58: IPO323 Ztmep2Δ/Ztmep3Δ double mutants wheat infection assay. *WT and mutant cells were assayed for their ability to infect wheat by Rothamsted Research. Wheat leaves were photographed 14 days post infection (DPI), 17 DPI and 21 DPI. X indicates leaves not infected with WT or mutant IPO323.*

Ztmep2Δ/Ztmep3Δ double mutants infected the leaves sooner than the WT strain, thus, the *Ztmep2Δ/Ztmep3Δ* double mutants are hypervirulent.

3.8.3 Analysis of virulence gene expression by the double mutants

As the *Ztmep2Δ/Ztmep3Δ* double mutants are hypervirulent, in comparison to the WT strain, qPCR of a known virulence gene was carried out on both strains grown in high ammonium medium. *Zt3LYSM* gene expression was enhanced 2.83 fold in the *Ztmep2Δ*/*Ztmep3Δ* double mutant compared to the WT strain. This result was statistically significant (*p-value* 0.0046) (**Figure 59**). Consistent with the wheat infection assay, the expression of the *Zt3LYSM* virulence gene is upregulated in the *Ztmep2Δ*/*Ztmep3Δ* double mutant.

3.9 *Z. tritici* discussion

Z. tritici undergoes a morphological switch in response to ammonium availability. During ammonium limiting conditions, this pathogenic fungus melanises and displays extensive filamentation. A Mep2 homology search identified three putative ammonium transporters which were designated as ZtMep1, ZtMep2 and ZtMep3. The twin-histidine motif, believed to be critical in signalling ammonium availability, is conserved in ZtMep1 and ZtMep2. ZtMep3 contains the glutamate-histidine motif, which is associated with non-signalling ammonium transporters.

Mep/Amt proteins contain 11 TMDs while the human Rh protein contains 12 TMDS (Andrade *et al.*, 2005) (Zheng *et al.*, 2004) (van den Berg *et al.*, 2016) (Gruswitz *et al.*, 2010). Analysis of ZtMep1 highlighted a 46 amino acid gap compared to ScMep2, ZtMep2 and ZtMep3. This could be due to an incorrect assignment of intron/exon borders by the software used to predict the coding sequence. Nonetheless, this

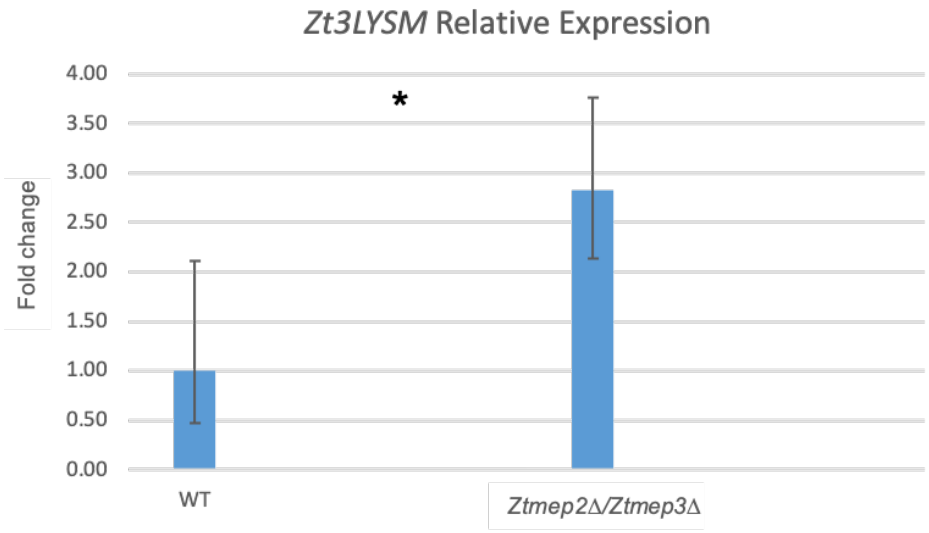

Figure 59: Expression of Zt3LSYM. *IPO323 WT and* Ztmep2Δ/Ztmep3Δ cells pre-grown in YPD were washed and inoculated into high NH_4^+ liquid medium at OD_{595nm} 2. Cells were harvested after 2 hours growth at 18 °C. RNA extracted from the cells was converted to cDNA to be used as template for qPCR. The $^{2-\Delta Ct}$ method was used to calculate relative expression to WT. Actin was used as a reference gene. A 2 tailed Student T test was used to calculate significance. **p-value* <0.005

predicted coding sequence, when analysed by a TMD prediction tool, projects ZtMep1 to contain two fewer TMDs than ScMep2. Further investigation revealed the presence of a transposable element within a large intron of ZtMep1. Removal of the transposable element provides a sequence with high identity and similarity to ZtMep1 orthologues, in other *Z. tritici* strains, while excluding the 46 amino acid gap. However, the new IPO323 ZtMep1 sequence is still predicted to contain fewer TMDs than ScMep2, albeit, one more than the original prediction. Analysis of the graph, produced by the TMD prediction software, does show lower probability scores for TMD8 and TMD9 within the new sequence and 1E4 ZtMep1 sequence. Moreover, double peaks are depicted for TMD8 which could be indicative of two TMDs. ZtMep1 may, therefore, have the same number of TMDs as other ammonium transporters. To confirm how many TMDs ZtMep1 contains cDNA, generated from 3D7, 1AS or 1E4 RNA, would need to be sequenced to verify the coding sequence. This sequence could then be cloned into a yeast expression vector for crystal studies. If ZtMep1 does indeed contain one less TMD than the other *Z. tritici* ammonium transporters, this could explain why ZtMep1, from 1E4, does not restore growth, in yeast lacking all three ammonium transporters, to the same level as ZtMep2 and ZtMep3. The loss of just one TMD could be crucial in its ability to transport ammonium and, hence, restore growth in the growth assay.

All *Z. tritici* ammonium transporter sequences were codon optimised to achieve optimal expression in *S. cerevisiae*. Eukaryotic and prokaryotic genomes exhibit codon usage bias. Condon usage bias is the non-proportionate use of synonymous codons. There are more tRNAs for preferred codons, thus, highly expressed genes are encoded by the preferred codons (Akashi, 1994) (Sharp *et al.*, 1986). However, the type of codon used, preferred or non-preferred, has been correlated with secondary structures. Preferred codons promote simple β-sheets, and α-helixes, while non-preferred codons promote more complex coiled structures; α-helixes are also associated with non-preferred codons (Pechmann and Frydman, 2013). Linked with the finding that non-preferred codons and preferred codons increase and decrease elongation rates respectively, complex structures require longer time periods than simpler structures to co-translationally fold (Yu *et al.*, 2015). The protein expression level of ZtMep1 in yeast was higher than ZtMep3, which was found to signal for pseudohyphal growth, suggesting that ZtMep1 was expressed to sufficient levels to function. The significant reduction in ZtMep1 transport activity could be attributable to incorrect folding as a

result of the use of preferred codons in regions where non-preferred codons would be favoured. For example within the TMDs. As all three ammonium transporters show reasonable identity and similarity to each other it would be expected that a significant reduction in growth would have been observed in ZtMep2 and ZtMep3 expressing cells if the introduction of preferred codons, into regions where non-preferred codons are more appropriate, was responsible. Methylammonium uptake studies should be carried out in IPO323 *Ztmep2Δ*/*Ztmep3Δ* reconstituted with *ZtMEP1* from 1E4, and *ZtMEP2* and *ZtMEP3* from IP0323; the codon usage by both species should be similar. This would rule out the possibility that codon optimised residues have been introduced into regions where non-preferred codons are more appropriate, thus, allowing extra time for co-translational folding of more complex structures. If methylammonium uptake levels by ZtMep1 are significantly less, than ZtMep2 and ZtMep3, this would confirm that ZtMep1 is a less efficient transporter. It is not inconceivable that ZtMep1 could be a very efficient ammonium transporter *per se* and codon optimisation lead to expression levels higher than in nature giving rise to ammonium toxicity. Nonetheless, if ZtMep1 is a poor transporter of ammonium it may be that ZtMep1 is a non-transporting transceptor on the evolutionary journey from transporter to receptor. ZtMep1 could be analogous to the non-transporting transceptors, Ssy1, Snf3 and Rgt2, which induce the transcriptional expression of their respective binding nutrient transporters (Poulsen *et al.*, 2005) (Ozcan *et al.*, 1996). To test this hypothesis ZtMep1 would need to be deleted from 1E4, 3D7 or 1A5 and screened for changes in many different phenotypes, including the expression of *ZtMEP2* and *ZtMEP3*. Complementation of pseudohyphal growth was not achieved with ZtMep1 in diploid yeast lacking Mep2. Although transport is not sufficient for signalling, by ammonium sensors, no mutation to date has been identified which supports signalling but not transport (Boeckstaens *et al.*, 2008). This favours the hypothesis that if ZtMep1 is a non-transporting transceptor it may be signalling for something other than filamentation.

All identified ammonium sensors, to date, possess the conserved twin-histidine motif believed to be important for their signalling function. Moreover, a reduction in Mep2 expression is correlated with a reduction in filamentation (Biswas and Morschhauser, 2005). The observation that ZtMep3 acts as an ammonium sensor in yeast was, therefore, an intriguing finding on two parts. Firstly, ZtMep3 does not possess the conserved twin-histidine motif, thus, this is not a defining feature of an ammonium

transceptor. Interestingly, minimal filamentation was induced in *S. cerevisiae* cells lacking Mep2 which expressed FfMepC which does not possess the twin-histidine motif (Teichert *et al.*, 2008). Secondly, ZtMep3 was expressed to considerably lower levels than ZtMep1 and ZtMep2; ZtMep1 nor ZtMep2 complemented the pseudohyphal growth defect of a diploid yeast strain lacking Mep2. It may be that any ammonium transporter has the ability to complement the pseudohyphal growth defect of the *mep2Δ/mep2Δ* strain if the protein expression and activity levels are balanced. This would favour the pH model of signalling. If ZtMep3 is highly active this could compensate for it being expressed to a low level in yeast.

Deletion of *ZtMEP3* in IPO323 did not completely abolish filamentation. Instead a different type of filamentation was displayed. As the filament 'halo', exhibited by the WT and *Ztmep2Δ* strains under high and low ammonium conditions in the spot assay, was absent when Ztmep3 was lacking, this could suggest that ZtMep3 is a transceptor regulating ammonium dependent filamentation natively. However, a significant growth defect was displayed by these mutants, therefore, the lack of the filament 'halo' could be due to ammonium starvation rather than a lack of transceptor mediated ammonium signalling. ZtMep3 did act as a transceptor when expressed in yeast, thus, if filamentation is not regulated by ZtMep3 in IPO323, ZtMep3 could signal for something other than filamentation natively. An array of transceptors, including Mep2, reactivate the PKA pathway upon re-addition of their respective starved nutrient in yeast (Holsbeeks *et al.*, 2004). For example, supplementation of ammonium to nitrogen staved fermenting yeast cells reverses the PKA activity to high; this is a Mep2 dependent phenotype. A readout of PKA activity is phosphorylation of trehalase (Van Nuland *et al.*, 2006). Thus, comparing the phosphorylation statuses of putative trehalase in IPO323, during and after nitrogen starvation, would be an ideal preliminary experiment to identify a potential signalling role for ZtMep3 in *Z. tritici*. However, if ZtMep3 is not a transceptor then using *S. cerevisiae* as a model for testing ammonium transceptors is not an appropriate strategy. Instead, all further experiments into putative ammonium permeases should be carried out in their native organism. The affinity and capacity of ZtMep3 should be determined in *Z. tritici* by expressing *ZtMEP3* in IPO323 *Ztmep2Δ*/*Ztmep3Δ* and measuring methylammonium uptake. The H194E separation of function allele renders ScMep2 hyperactive for transport (Boeckstaens *et al.*, 2008). It would be beneficial to reconstitute IPO323 *Ztmep2Δ*/*Ztmep3Δ* with ZtMep3^{E201H} to test if the introduction of histidine limits transport activity. Equally,

methylammonium uptake by IPO323 *Ztmep2Δ/Ztmep3Δ* reconstituted with all three ammonium transporters should be assayed to test if their capacities and affinities are comparable. Moreover, optimum pH (pH_{opt}) could simultaneously be determined to address the dependence of pH on transport activity. The signalling transporter in *S. cerevisiae* has a substantially lower pH_{opt} than the non-signalling homologues (Boeckstaens *et al.*, 2008) which would suggest that ZtMep3 would have a lower pH_{opt} than ZtMep2. However, when considering the twin-histidine motif it could equally be argued to be the opposite. ZtMep3 does not possess the twin-histidine motif and is, thus, genetically more similar to the non-signalling homologues which have a higher pH_{opt}.

ScMep2 transport activity is regulated by Npr1 kinase phosphorylation. Each *Z. tritici* Mep is immunodetected as a doublet by western blotting in *S. cerevisiae*. The higher molecular weight band could be indictive of a phosphorylated version of the protein. In ScMep2, the higher molecular weight band is due to phosphorylation by Npr1 kinase and is sensitive to lambda (λ) phosphatase but not alkaline phosphatase treatment (Boeckstaens *et al.*, 2014). As a preliminary experiment protein extracts should be treated with λ phosphatase, and alkaline phosphatase, to confirm if the higher molecular weight band is phosphorylated. If so, phosphatase treatment should lead to loss of the higher molecular weight band. None of the ZtMeps lost their ability to restore growth on limiting ammonium when Npr1 kinase was lacking from the strain. This suggests that Npr1 kinase is not responsible for the higher molecular weight band and is not required for the ZtMeps to function in *S. cerevisiae*. However, *Z. tritici* is an organism which is typically grown at 18 ºC in the laboratory (Zhan *et al.*, 2016) (Yemelin *et al.*, 2017) whereas *S. cerevisiae's* optimal growth temperature is 30 ºC. All the growth assays were performed at 30 ºC. *Neuhäuser et al.*, (2011) observed that at higher temperatures CaMep2 activity is rendered Npr1 kinase independent (Neuhauser *et al.*, 2011). At higher temperatures, bonds which maintain ZtMep3's quaternary structure may be disrupted generating a constitutively open transporter or fashioning a dynamically fluid protein. Therefore, the growth assays should be performed at a range of lower temperatures to test their dependence on Npr1 kinase in yeast. Moreover, to aid with immunodetection a 6X His tag was introduced to the C-terminal tail. This could equally have created interactions between the C-terminal tail with the rest of the transporter, thereby, rendering ZtMep3 Npr1 kinase independent. These interactions are believed to be vital for Mep/Amt proteins to

transport their substrate (van den Berg *et al.*, 2016) (Neuhauser *et al.*, 2007) (Ludewig *et al.*, 2003). An Npr1 kinase homology search in the IPO323 genome database does identify a putative Npr1 kinase orthologue. Notably, a database which predicts interactions between proteins predicts an interaction between putative Npr1 kinase and ZtMep3 but not ZtMep2 (**Figure 60**). Additionally, there is a putative phosphorylation site in the CTR of ZtMep3 as identified by a phosphorylation site prediction tool. Serine 531, within the EMEKSRREA motif, is positioned nine residues from the C-terminus, which is considerably closer to the C-terminal end than in ScMep2. If transport activity by ZtMep3 is found to be regulated by Npr1 kinase, at 18 ºC in yeast, then the S531A and S531D mutations should be made. These mutants should be tested in *mep123Δ* strain possessing and lacking Npr1 kinase respectively to verify, if like the equivalent mutation in ScMep2, abolishes and restore growth respectively. As the putative phosphorylation site is considerably closer to the C-terminus in ZtMep3, than it is in ScMep2, the His tag may prevent Npr1 kinase from interacting with ZtMep3. This would abolish transport in both growth assay strains at 18 ºC if transport activity is Npr1 kinase dependent at this lower temperature. Furthermore, the putative Npr1 kinase in IPO323 should be deleted from the IPO323 *Ztmep2Δ*/*Ztmep3Δ* double mutant and *ZtMEP1*, *ZtMEP2* and *ZtMEP3* should be reconstituted into this triple mutant strain independently. Methylammonium uptake assays should then be performed to compare the transport activity of each ammonium permease with and without Npr1 kinase. If methylammonium uptake is inhibited, or significantly reduced, in the strain lacking Npr1 kinase this would indicate that the ammonium permeases are regulated by Npr1 kinase in IPO323. As this finding would contradict the result in *S. cerevisiae,* this would strengthen the argument for only using native organisms to test ammonium permease function.

Pseudohyphal growth in *S. cerevisiae*, during limiting ammonium conditions, is a Mep2 regulated process. Despite ZtMep3 acting as an ammonium sensor in yeast, to induce pseudohyphal growth, a loss of ZtMep3 did not abolish filamentation on low ammonium in *Z tritici* nor did a loss of ZtMep2. A dramatic growth defect was, however, observed in the *Ztmep3Δ* single mutants and the *Ztmep2Δ*/*Ztmep3Δ* double mutants on high ammonium. Reconstitution of the *Ztmep2Δ*/*Ztmep3Δ* double mutants and *Ztmep3Δ* single mutants should complement this growth defect. This is a future experiment to verify that the growth defects are due to the loss of ZtMep3. Interestingly, the growth defect appeared to be more severe for the *Ztmep3Δ* single mutants than the

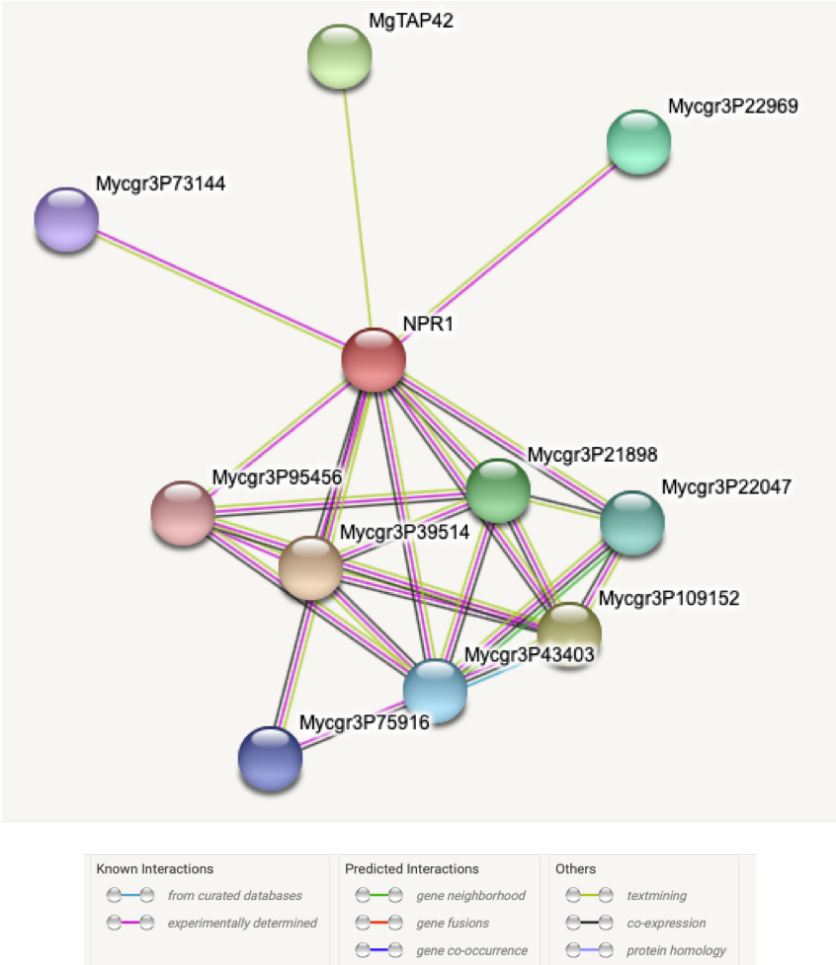

Figure 60: Protein-Protein interactions for NPR1. *Predicted protein interaction network for NPR1according to the STRING database. Mycgr3P73144 represents ZtMep3. Image imported from the STRING database: https://string-db.org/network/1047171.Mycgr3P75925.*

Ztmep2Δ/*Ztmep3Δ* double mutants. It is possible that ZtMep2 is overexpressed in the *Ztmep3Δ* single mutants to compensate for the lack of ZtMep3. If ZtMep2 is analogous to ScMep2, and is a high affinity transporter, overexpression would lead to a higher volume of ammonium entering the cell. Too much ammonium can be cytotoxic, therefore, this could explain why the growth defect is less severe in the *Ztmep2Δ*/*Ztmep3Δ* double mutants. qPCR experiments should be undertaken to confirm this hypothesis. The *Ztmep3Δ* single mutants and *Ztmep2Δ*/*Ztmep3Δ* double mutants produced filaments that were not evenly distributed around the centre of their colonies on both low and high ammonium medium. Additionally, these mutants were melanised on high ammonium while the WT and *ztmep2Δ* single mutant colonies remained pink. These findings suggest a starvation response rather than a signalling response and are consistent with ZtMep3 being the low affinity, high capacity transporter. Methylammonium uptake assays using the IPO323 *Ztmep2Δ*/*Ztmep3Δ* double mutants reconstituted with all three ZtMeps independently would confirm this. Thus, filamentation during ammonium limitation is not an ammonium transceptor regulated morphology in *Z. tritici*.

Proline grown *S. cerevisiae* cells import proline through the high affinity proline permease Put4 (Jauniaux *et al.*, 1987) but simultaneously leak ammonium. To maintain ammonium homeostasis, ScMep1, and ScMep2 re-import the excreted ammonium; ammonium import through ScMep2 induces pseudohyphal growth (Boeckstaens *et al.*, 2007). On proline medium the *Ztmep2Δ/Ztmep3Δ* double mutant cells were melanised in the growth assay while the other strains were not. Furthermore, the *Ztmep2Δ/Ztmep3Δ* double mutants displayed the most aerial hyphae, when spotted onto proline, which is additionally clumped. As there are no ammonium transporters in the double mutant strain, *Ztmep2Δ/Ztmep3Δ* will be more starved of ammonium, than the single mutants and WT cells, which could explain why *Ztmep2Δ/Ztmep3Δ* is melanised on proline medium. Consistent with the *Ztmep2Δ*/*Ztmep3Δ* double mutants being more starved than the single mutants, the *Ztmep2ΔZtmep3Δ* double mutants caused disease symptoms sooner in the wheat infection assay than the WT cells suggesting that nitrogen starvation is the signal for virulence. Moreover, the expression of the *Zt3LYSM* virulence gene was more highly induced in the *Ztmep2Δ*/*Ztmep3Δ* double mutants as opposed to in the WT cells grown in high ammonium medium.

In *S. cerevisiae*, ScMep2 is transcriptionally regulated by Gln3 and Gat1 (Scherens *et al.*, 2006). These are zinc finger transcription factors which bind to GATA upstream activation sequences (5'-GATAAG-3') (Cunningham *et al.*, 1996) (Coffman *et al.*, 1996). Both ZtMep2 and ZtMep3 possess one of these GATA upstream activation sequences (**Figure 61Figure 62**). Putative Gln3 has already been assigned by the IPO323 genome database. It would be beneficial to see the impact of *ZtGLN3* deletion on the expression of *ZtMEP2* and *ZtMEP3*. If similar to ScMep2, another transcription factor may compensate for *ZtMEP2* and/or *ZtMEP3* expression, therefore, a double mutant may be required to abolish *ZtMEP2* and/or *ZtMEP3* gene expression. If this is the case, it would be anticipated that this mutant could behave like the *Ztmep2Δ*/*Ztmep3Δ* double mutants in all experiments tested. Furthermore, point mutations should be made in the putative UAS sequence to confirm if these are the transcription factor binding sites.

ACGGATGGACCCATCGCTGTGATCACGACTCCCAGCAAAGCGG
GCGCACTCCTGCAGGCTGCCGGTTGAAGGAACAAGTCAATTCC
GCCCTGATCTGTCGTCGCAGAAAGCGGCAGTGCCTGCATTGGT
GGCGTCGATTCATATGCACCCTAAAACAAGGCCATCACATCTC
TCGACACCATTCCCATCATCGAATGCTTGAGAACCTGCGACGG
CGTGTTCCTCCTCGGCGTGGATATCGTTTTGGTGTGAGTTGTG
TGTACTGTCAAGACTGAAAGACCTTGAGACGAAGAAGAACATG
GCGTTTCTCCCGGATTGCTCCGACGGAAGACAATTCTCCGGGA
CCCACCAGAACGGACTTCACTTGTGCCGTCTCAATCATTGGCT
CACTTCGGTCTTTATCTATTCCTTCCCAGTGGAGACATTGCTC
AACATGGAACTCACTGCGGACATGGATCCATCAATATTCTGGA
GGCGACACCAAATTGTCAAAGGCAGTGCCCACGCCCGGCCGAG
AGTCCGAGACTAGAACTAACATCCCACGCAAATTTCCGTGTCT
GGCTGAGATGAGGACGCCATGGGCCCATGGCCATGCAATTGCA
GGGGAAAATTCATCGCATTTGCGTGCTCAGAGACATGCGAGTT
CCACGATGGCCTCCTCCAGCTTTACCCCAAGCGGAAACACAAA
TGCAGCTCTCTCGATCGGTCTGGAACACACCCTGATCCGCGAC
CCAATGAAGTCGACTGCGATGGACCGATAAGAGCATTGGTATC
CGGAAGATCGTCCCAAGAGCATCCTTCGCATGTGCACTTCATG
AGCTTATTCGGATCTCTGGTATCTCTGGGATTACTTTCGACGC
CGGCGACGTTTGACTCTTTCGCGCTTGTGCTTGAAAATACAGA
GTCGCAAGCGGAGGGAGGTTGACATAAAGCCGTATATTCACTC
CTCCCGCCATCCCATCGGCGGCTAGTGTAAACGGCTACCGGAC
TTCTCACCAAT**ATG**

Figure 61: GATA UAS sequence in ZtMEP2 promoter. *1000 bp of genomic DNA before the START codon (ATG) OF ZtMEP2 is depicted. The GATA sequence in highlighted in yellow and the START codon is listed in bold.*

CTGGGCGTGGAAAGAAGACGGCTTGGAGTCATGGAGTGCATGT
GTGAGGAGTGCAGGATGTGAGATCCAAGAGCAGTTCGGTGACA
CTGCGTGGTTTCTGTGTGTGCCTCAGAACGGCTTACAGGGTCC
TAACTTTGGCAAATCTCCAAGGTTTGAAGGATGGGGGTGGAGC
CACACTCGGTCCATGTGCAACGTGGAACAGAGTGCAAGCGCCA
ACAAAGAACATGGAGATATTGCCTATGGATACACTCCTTGTCA
CAGGATCAGTCAAGGCAATGGGAGGCTGAACGGGAAGCAATGC
GGCCACTTTGAGGCGACTCATCAAGCGAACACCACGAGATAGA
GGCGTTCGTCCACGACCTTGATCGTACCCGAAGCAGCGGTGCA
CGCGATCGATGCAGGCATGCCGTAGGCCAAGGGTGTTGGGGTT
TAGAGTGTTGGGGGTTGAAGCTGGGTGCGTGTTGGTGCTGCCA
ATGGAAAGCCTGCGGAGCGGACGTTGTCTCTTACTAGGAGCTC
TCGGCACGCGCAGCGCGGGCGCCCCAGTGTCTGGCTAGGCTAA
GATAGCTTCCGCGAGAGATAAGAAAACAATCCATGTCAAAGGT
CGGCTCGTTGTGGTGGGTTGCCCTTGCCCTTGATTCCACTTGG
CATAACCCCAAAAAGAACCCGTTCTCGTCCGCCGCTCGCTCCA
CCAGAATAATGATTAGACTCCCACCCACGCCTTGTGAGATGCC
CTTGCCGTCCCCGGTCGACTTCTGGTACTAATCTGCACACTGT
CGCACTCTTTTATAACCATTCCTCTCTCTTCCGACCTCACCTC
TTCTCTCGCGTCCCCATCTCTGTCTCCGCTTCTTGTGTGCATC
TACTGCTATCCCTTGCCCCACCCAGTCGGCACGTGGAATACGT
CGGTCTTGCATAACATCCGACAGACGTCAACACCGCCTGGTCT
TGGACAGCCACACCCATCCAGAGCACCTCGCCGCTTTCGAGCA
TCTCTTTCATC**ATG**

Figure 62: GATA UAS sequence in ZtMEP3 promoter. *1000 bp of genomic DNA before the START codon (ATG) OF ZtMEP3 is depicted. The GATA sequence in highlighted in yellow, the 5' UTR is represented in red, and the START codon is listed in bold.*

4 Ammonium Signalling in *Cryptococcus neoformans*

4.1 *C. neoformans* introduction

C. neoformans is a fungal pathogen which primarily infects immunocompromised patients but is ubiquitous in the environment. The fungus exists as haploid yeast cells of opposite mating type: MATa and MATα with the latter being immensely more prevalent (Kwon-Chung and Bennett, 1978). Under nitrogen limiting conditions, the fungus undergoes a morphological switch from yeast to hyphae to allow the fusion of two cells of opposite mating type and the formation of a dikaryon (Kozubowski and Heitman, 2012). Moreover, the same conditions induce fruiting and haploid invasive growth. The H99/KN99 strain (serotype A) possesses two ammonium permeases: Amt1 and Amt2 which are low and high affinity transporters respectively. *AMT2*, but not *AMT1*, is transcriptionally induced during limiting nitrogen conditions, consistent with nitrogen catabolite repression, whereas the latter is constitutively expressed. Although a double *amtΔ* mutant is unable to grow on low ammonium medium both single and double *amtΔ* mutants remain virulent. However, haploid invasive growth and mating, during nitrogen limitation, are Amt2 dependent processes. Thus, Amt2 is an ammonium sensor in the H99/KN99 strain (Rutherford *et al.*, 2008b).

4.2 *C. neoformans* displays an ammonium dependent phenotype

Haploid cells of the H99/KN99 strain mate, undergo invasive growth, and produce dikaryon and basidiospores from basidium (fruiting body) in response to limiting ammonium (Rutherford *et al.*, 2008b). The JEC21/JEC20 strain is known to produce hyphae in a confrontation assay on filament agar (Wang *et al.*, 2000). To determine if hyphal growth by JEC20 (MATa) and JEC21 (MATα) is ammonium dependent, JEC20 and JEC21 were patched in close proximity to one another on high and low ammonium medium and assayed for hyphal growth. On low ammonium medium, extensive hyphal growth was observed around the edge of the patched cells of both mating types, with the filaments extending further from MATα in comparison to MATa. Hyphal growth was also observed in the region between the cells, but this was at a much lower frequency compared to the hyphal filaments extending away from the outer edges. No

hyphal growth from either mating type was established on high ammonium medium, however the density of growth was greater. Therefore, hyphal growth is induced by limiting ammonium (**Figure 63a**). In addition to dikaryotic hyphae, produced during sexual growth, *C. neoformans* is documented to produce monokaryotic hyphae (fruiting-like structures) in the absence of the opposite mating type; this is most associated with MATα rather than MATa. Hence, this is referred to as monokaryotic fruiting (Wickes *et al.*, 1996). To test if this phenotype is dependent on limiting ammonium, JEC20 and JEC21 cells were patched onto low and high ammonium medium in the absence of their opposite mating partner in fruiting assays. MATα but not MATa formed hyphal filaments on low ammonium medium, however this was at a much lower frequency than when MATa was present. As with the confrontation assays, no hyphal growth was established in the fruiting assays when patched onto high ammonium medium, but the density of growth was again greater. Therefore, hyphal growth is induced in JEC21 under limiting ammonium conditions in a fruiting assay, but not in JEC20 (**Figure 63b**).

Invasive growth by JEC21 has been documented under low ammonium (Rutherford *et al.*, 2008b). To determine if cell invasion is exhibited during the confrontation and fruiting assays, the surface cells, from both assays, were washed away and assayed for invasive growth. For the confrontation assays, cell invasion was established on both low and high ammonium, however, microscopic inspection revealed that the appearance of embedded cells was different. In addition to yeast cells, enlarged cells were visible within the low ammonium agar; only yeast cells were observed within the high ammonium agar (**Figure 64**). In the fruiting assays, despite WT MATa not displaying hyphal growth or producing enlarged cells on low ammonium, the cells succeeded in invading the agar, as did the MATα cells. Invasive growth is therefore independent on the presence of the opposite mating type. However, invasive enlarged cells are dependent on the presence of the opposite mating type. Furthermore, in addition to the presence of yeast cells in the MATα fruiting assay, hyphal filaments were observed embedded within the agar (**Figure 65**). Similar to the confrontation assays, both mating types displayed invasive growth on high ammonium, nevertheless, only yeast cells were present. JEC20 and JEC21, therefore, display invasive growth during confrontation and fruiting assays, but this is independent on ammonium levels. Moreover, the presence of enlarged cells, embedded within the

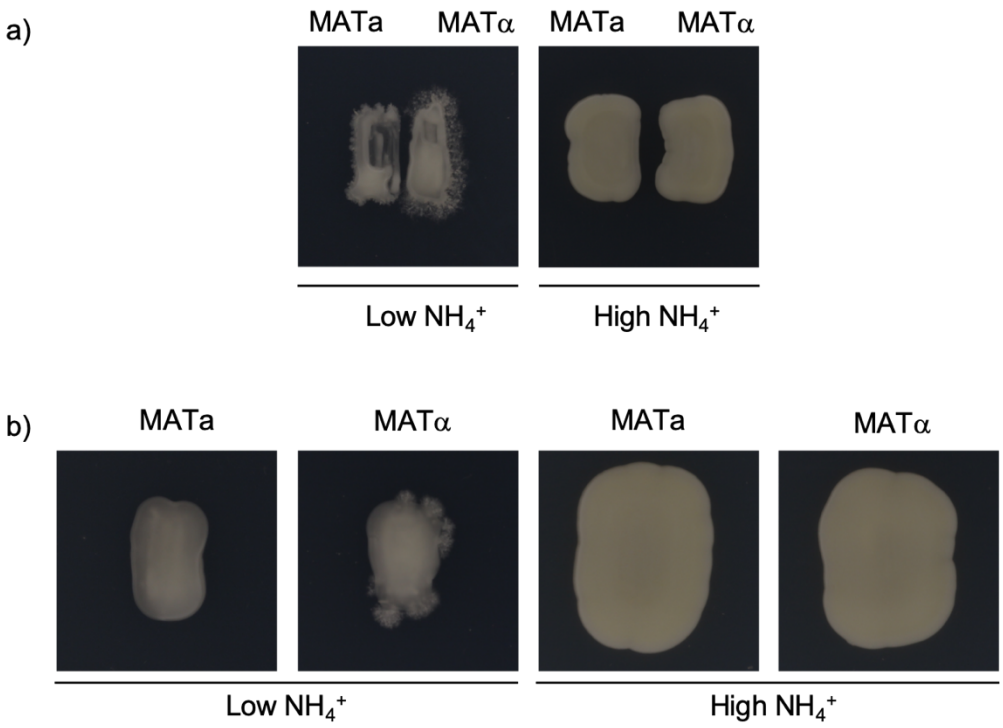

Figure 63: Ammonium dependent hyphal growth. *a) C. neoformans serotype D (JEC20/JEC21) cells of opposite mating type were confronted on low (50 μM) and high (5 mM) ammonium medium. b) Cells were patched in the absence of their mating partner onto low and high ammonium medium in fruiting assays. Images were taken after 3 weeks growth in the dark at room temperature.*

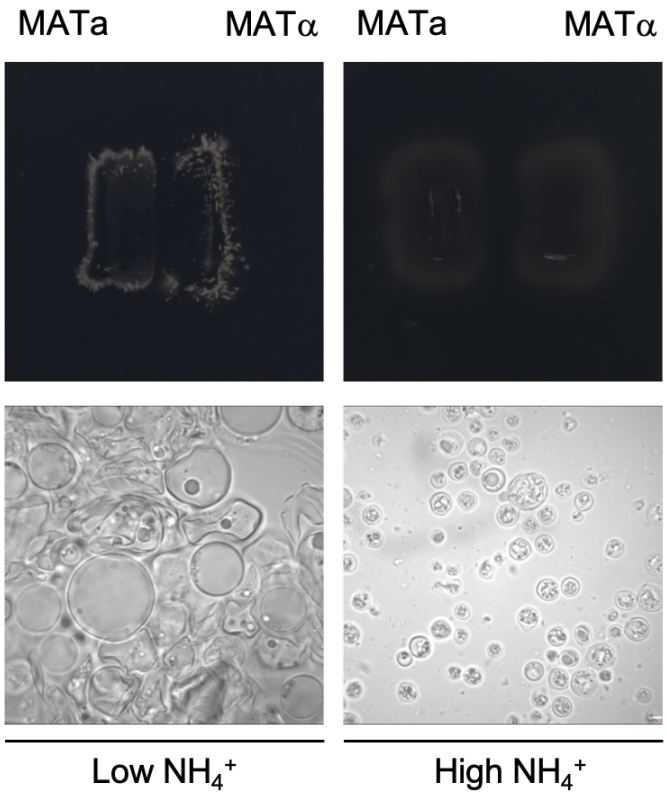

Figure 64: Images of invasive cells. *The surface cells were washed off the confrontation assays (top panel). Embedded cells were observed under the microscope at 1000 x magnification using an oil emersion lens.*

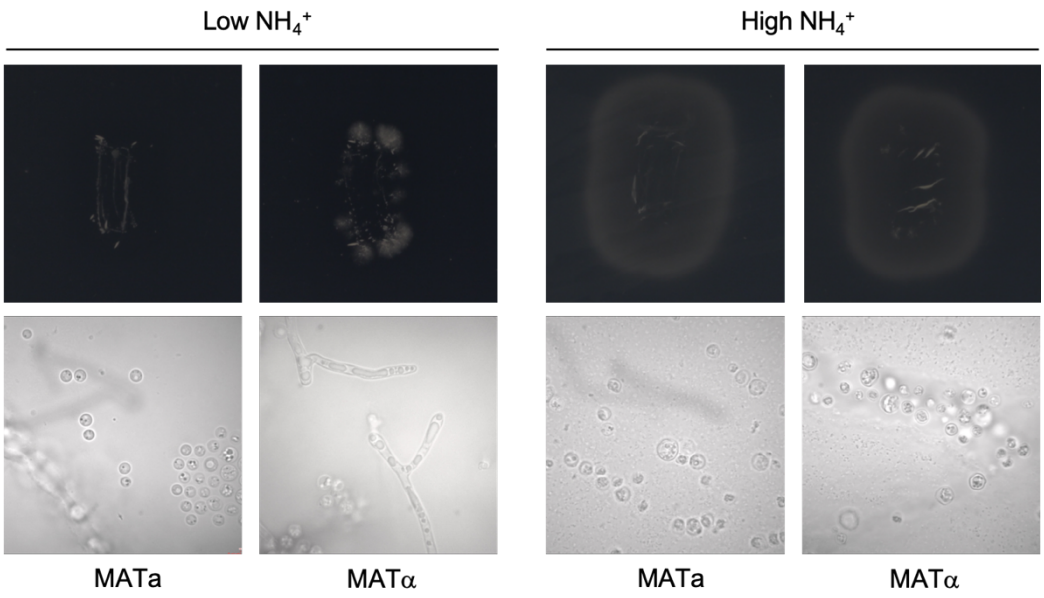

Figure 65: Images of invasive cells. *The surface cells were washed off the fruiting assays (top panel). Embedded cells were observed under the microscope at 1000 x magnification using an oil emersion lens.*

agar, is stimulated by limiting ammonium and is dependent on the presence of the opposite mating type.

4.3 Identification of putative ammonium transporters in *C. neoformans* serotype D (JEC20/JEC21)

In some fungi, members of the Amt/Mep/Rh family are responsible for an ammonium dependent dimorphic switch. For example, Mep2 in *S. cerevisiae* is responsible for the induction of pseudohyphal growth during ammonium limitation (Lorenz and Heitman, 1998). To identify ammonium transporters in JEC20 and JEC21 a Mep2 homology search was conducted. 10 search results were returned containing two different genes (CNJ01880 and CNA02250). Both genes were described as encoding putative ammonium transporters in the database used for the search. The presence of only two ammonium transporters in the genome is consistent with the *C. neoformans* H99/KN99 strain (Rutherford *et al.*, 2008b). Previously identified ammonium sensors possess the conserved twin histidine motif, believed to be important for ammonium transceptor function, whereas non signalling versions contain a glutamate residue at the equivalent position of the first histidine. Alignment between both protein sequences with ScMep2 revealed that CNJ01880 contains the conserved twin histidine motif while CNA02250 contains a glutamate histidine motif similar to Mep1 in *S. cerevisiae* (Boeckstaens *et al.*, 2008). Furthermore, CNJ01880 was calculated to have the higher identity, similarity and score values compared to CNA02250 (**Table 19**). CNA02250 and CNJ01880 were therefore designated as Amt1 and Amt2 respectively.

Name	JEC21 Gene ID	UniProtKB/TrEMBL Accession Number	Identity %	Similarity %	Score
Amt1	CNA02250	Q5KPM5 (Q5KPM5_CRYNJ)	36.6	53.1	998.0
Amt2	CNJ01880	Q5KAF6 (Q5KAF6_CRYNJ)	45.2	60.9	1121.0

Table 19: C. neoformans serotype D AMT genes

The sequence alignment between ScMep2 and both putative *C. neoformans* ammonium transporters highlighted that the ExxGxD motif was conserved but the autoinhibitory (AI) region, containing the Npr1 kinase phosphorylation site in ScMep2, was not. However, functional residues including the Phe gate, and an asparagine residue adjacent to the proposed deprotonation site were preserved (**Figure 66**). When Amt1 and Amt2 protein sequences were analysed by a TMD prediction site, both putative ammonium transporters were predicted to be composed of 11 TMDs (**Figure 67**), the same as ScMep2. Amt2 was therefore chosen for future analysis as this was the most likely candidate to be responsible for the ammonium dependent phenotypes.

4.4 Ammonium dependent expression of *AMT2*

AMT2 expression is induced under limiting ammonium and repressed under ammonium sufficient conditions in the *C. neoformans* H99/KN99 strain (Rutherford *et al.*, 2008b). We were, therefore, interested to assess if *AMT2* expression is ammonium dependent in the JEC20/JEC21 strain. Cells of both mating type were grown to mid log phase in high and low ammonium medium. Reverse transcriptase PCR revealed that under low ammonium *AMT2* is expressed in both mating types to similar levels. Conversely, under high ammonium *AMT2* is not expressed. (**Figure 68**). Consistent with *AMT2* expression in *C. neoformans* H99/KN99, *AMT2* expression in JEC20/JEC21 is regulated by ammonium availability as the gene is induced under limiting ammonium but repressed under sufficient ammonium conditions.

4.5 Analysis of Amt2 expressed in yeast

Growth and pseudohyphal growth assays in *S. cerevisiae* are a useful model to test putative ammonium permeases for transport and signalling function respectively. Codon optimised CnAmt2, from *C. neoformans* JEC21, was therefore tested for both functions. Codon optimised *CnAMT2* was cloned into the low copy shuttle plasmid pRS316 (Sikorski and Hieter, 1989).

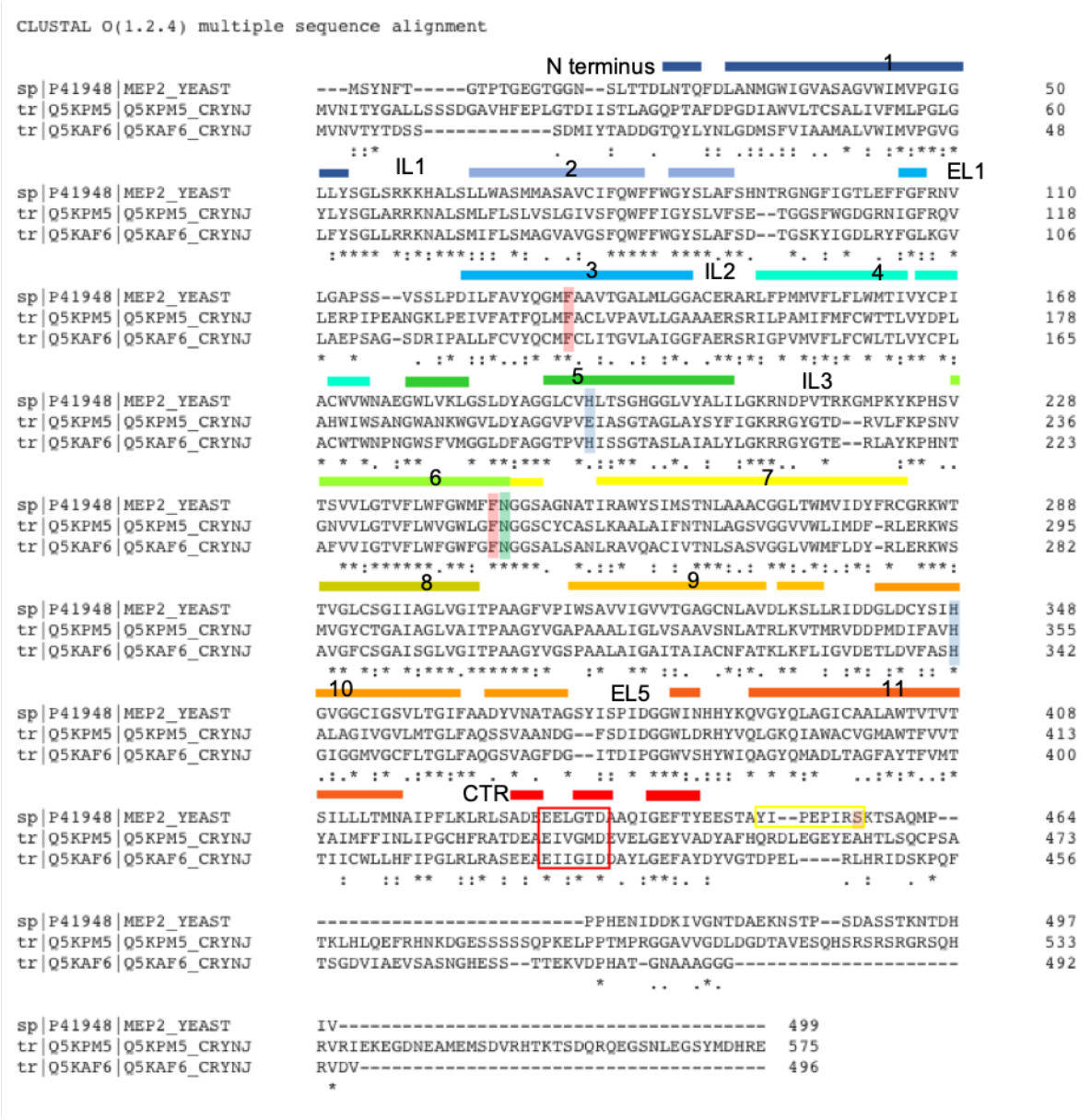

Figure 66: CLUSTAL O protein sequence alignment between ScMep2, CnAmt1 and CnAmt2. *Secondary structure elements are based on the figure published in (van den Berg et al., 2016), and correspond to ScMep2. The conserved ExxGxD motif is boxed in red. The AI region found in ScMep2 is boxed in yellow, with the Npr1 kinase phosphorylation site highlighted in orange. The twin – His motif is highlighted in blue and the Phe gate is highlighted in red. The conserved asparagine residue adjacent to the proposed deprotonation site is highlighted in green. The centre of each transmembrane domain is indicated with a number.*

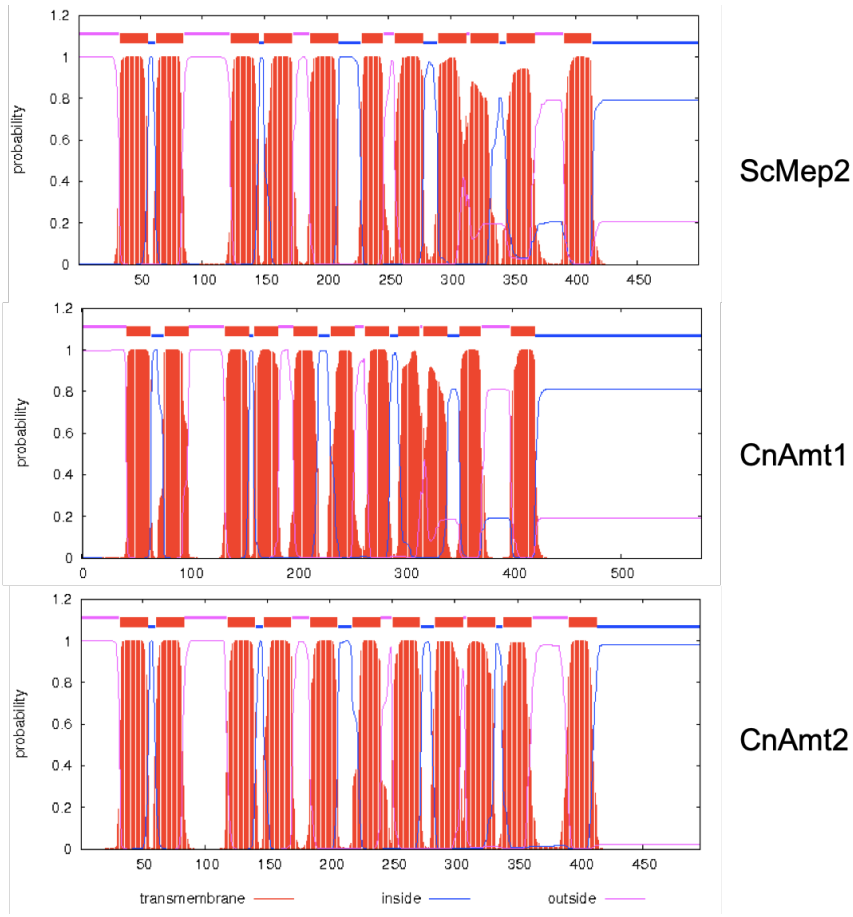

Figure 67: TMD predictions. *Protein sequences for ScMep2 and CnAmt1 and CnAmt2 from JEC21 were analysed by the TMHMM Server v. 2.0 online software tool. The returned graphs depict the predicted transmembrane domains (TMDs). Pink and blue lines indicate extracellular and intracellular loops respectively, while red boxes indicate TMDs.*

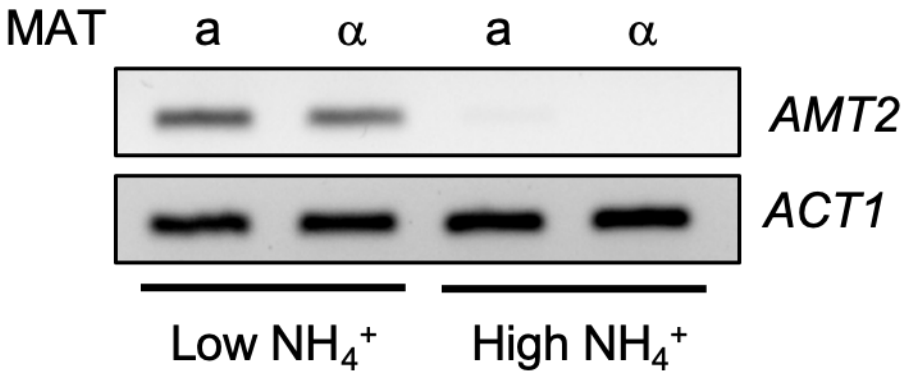

Figure 68: AMT2 expression is ammonium dependent. *Cells of opposite mating type were grown in high ammonium (5 mM) medium to OD_{595nm} 0.3. Cells were then switched to fresh high ammonium medium or low (50 μM) ammonium medium and grown until OD_{595nm} 0.5. RNA was extracted and converted to cDNA to be used as template to amplify AMT2 by PCR. The housekeeping gene ACT1 was used to confirm equal loading.*

4.5.1 Amt2 is an ammonium transporter in yeast

A *S. cerevisiae* strain lacking all three ammonium transporters is unable to grow on media containing ammonium as the sole nitrogen source (Marini *et al.*, 1997). To assess if CnAmt2 transports ammonium, the haploid *mep123Δ S. cerevisiae* strain was transformed with CnAmt2 and assayed for growth. All the transformed cells grew on 0.1 % glutamate which is a good source of nitrogen for fungi. On 1 mM ammonium sulphate, a limiting concentration of ammonium, CnAmt2 restored growth as well as the positive control ScMep2. Hence, CnAmt2 is an ammonium transporter. Furthermore, the *mep123Δ* strain was transformed with the CnAmt2 mutants. In *S. cerevisiae*, mutation of the first histidine (H194), of the twin histidine motif, to alanine abolishes the ability of Mep2 to transport ammonium while mutation of the same reside to glutamate does not. Equally, mutation of the second histidine of the twin histidine motif (H348), or the asparagine residue adjacent to the proposed deprotonation site (N246), to alanine, in ScMep2, has no impact on transport proficiency. Nor does mutation of the glycine residue neighbouring the second histidine (G349) to cysteine. Analogous to ScMep2, transformation of the *mep123Δ* strain with the CnAmt2 mutants resulted in the same phenotypes respectively. Specifically, CnAmt2^{H191A} did not restore growth, while CnAmt2^{H191E}, CnAmt2^{H342A}, CnAmt2^{N241A} and CnAmt2^{G343C} did. (**Figure 69**). Thus, residues important for transport in ScMep2 are conserved in CnAmt2.

4.5.2 Amt2 is an ammonium sensor in yeast

A diploid *S. cerevisiae* strain lacking Mep2 (*mep2Δ/mep2Δ)* will not undergo pseudohyphal growth during ammonium limiting conditions (Lorenz and Heitman, 1998). Expression of CnAmt2 in the *mep2Δ/mep2Δ* strain complemented the pseudohyphal growth defect as well as ScMep2. Invasive and surface pseudohyphae were observed on the edge of the single colonies and streaked cells. Thus, CnAmt2 acts as a signalling molecule in *S. cerevisiae*. On the contrary, expression of CnAmt2^{H191A}, CnAmt2^{H191E}, CnAmt2^{H342A} and CnAmt2^{N241A} did not restore pseudohyphal growth, while CnAmt2^{G343C} did (**Figure 70**), which is consistent with the equivalent mutations in ScMep2. Together with the growth assay findings, transport and signalling function can be separated in CnAmt2 confirming that CnAmt2 is a transceptor.

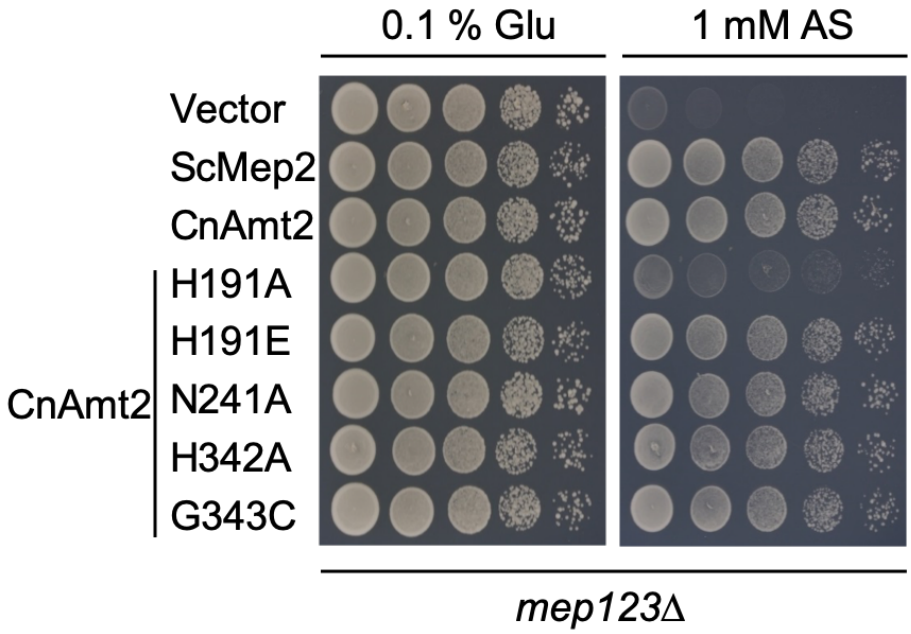

Figure 69: Growth analysis of Amt2 mutants expressed in yeast. *Haploid mep123Δ S. cerevisiae cells containing the plasmids of interest were grown in SD-URA medium overnight, washed, and 10 fold serially diluted before being spotted onto 0.1 % glutamate or 1 mM ammonium sulphate agar.*

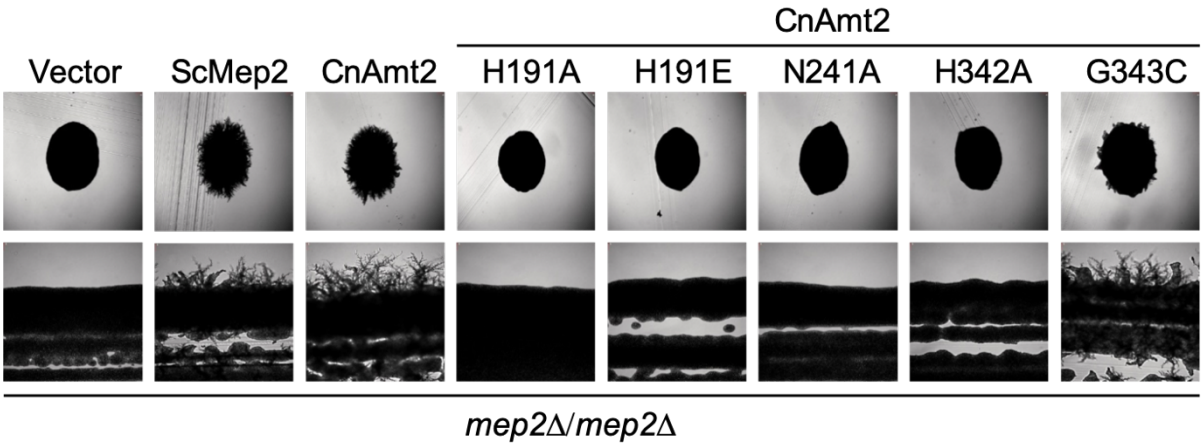

Figure 70: Pseudohyphal growth analysis of Amt2 mutants expressed in yeast. *Diploid mep2Δ/mep2Δ S. cerevisiae cells containing the plasmids of interest were streaked for single colonies on low ammonium sulphate medium (50 μM). After 6 days growth, cells were photographed under the microscope at 100 x (top panel) and 40 x (bottom panel) magnification respectively.*

4.5.3 Reduced protein expression is displayed by some CnAmt2 mutants

A reduction in the protein expression level of ScMep2 is known to impact on filamentous growth (Biswas and Morschhauser, 2005). To confirm that the separation of function observed by CnAmt2 is due to the mutations and not reduced protein expression, protein levels were assayed by western blotting in the *mep2Δ/mep2Δ* strain. CnAmt2 was expressed to a similar level as ScMep2. CnAmt2^{N241A} and CnAmt2^{G343C} were expressed to a slightly lower level than CnAmt2, but to the same level as each other. As CnAmt2^{G343C} still complemented the pseudohyphal growth defect of the strain, the expression level of this mutant could be used as a threshold to assess the protein levels of other mutants. A faint band was detected for the CnAmt2^{H191A} and no bands were detected for CnAmt2^{H191E} and CnAmt2^{H342A} mutants (**Figure 71**). Thus, as the CnAmt2^{H191A} and CnAmt2^{H342A} mutants are expressed to lower levels than the CnAmt2^{G343C} mutant the lack of pseudohyphal growth cannot be confirmed to be attributable to the mutations. However, as CnAmt2^{N241A} was expressed to a similar level as CnAmt2^{G343C}, N241A is regarded as a mutation which can uncouple transport from signalling.

4.5.4 Amt2 is not regulated by Npr1 in yeast

ScMep2 transport activity is regulated by Npr1 kinase (Boeckstaens *et al.*, 2014). Therefore, ScMep2 cannot restore growth in a haploid strain lacking all three ammonium transporters and Npr1 kinase (*mep123Δ/npr1Δ)* on low ammonium. To determine if CnAmt2 activity is regulated by Npr1 kinase when expressed in yeast, growth assays using the *mep123Δ* and *mep123Δ/npr1Δ* strains were performed. CnAmt2 restored growth on 1 mM ammonium sulphate regardless of whether Npr1 kinase was present or not. Hence, CnAmt2 activity is Npr1 kinase independent when expressed in yeast (**Figure 72**). In cells containing Npr1 kinase, ScMep2 is detected as a doublet, with each band being of equivocal intensity and detached by a ~6-8 kDa shift. In contrast, in cells lacking Npr1 kinase, ScMep2 appears as a single band with a greater intensity and at the lower molecular weight position. To test if Npr1 kinase phosphorylates CnAmt2 in yeast for a purpose other than transport CnAmt2 was expressed in *mep123Δ* and *mep123Δ/npr1Δ* and band intensity and position were analysed by western blotting. CnAmt2 did not appear as a doublet in cells possessing

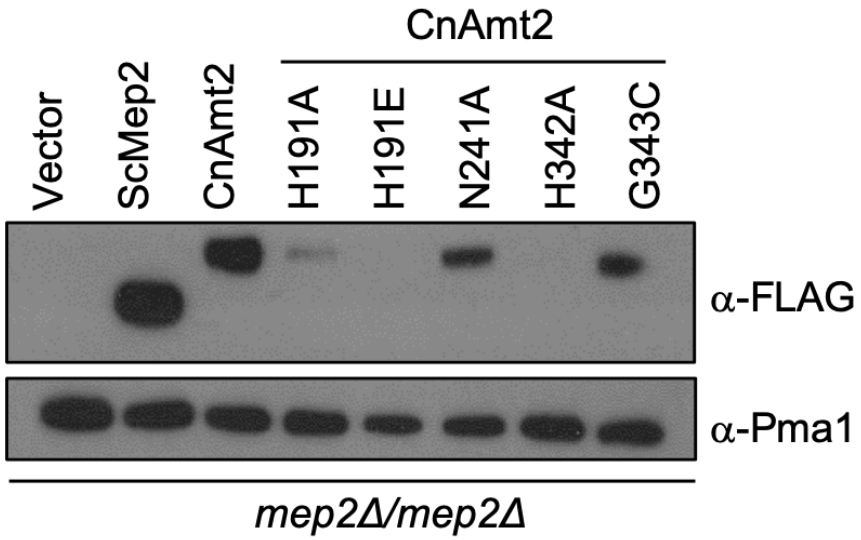

Figure 71: Western analysis of Amt2 mutants expressed in yeast. *Diploid mep2Δ/mep2Δ S. cerevisiae cells containing the plasmids of interest were grown to mid-log phase in 0.1 % proline medium. Membrane proteins were extracted and assayed by western blotting and detected with an α-FLAG antibody. Pma1 was used as a loading control to compare levels.*

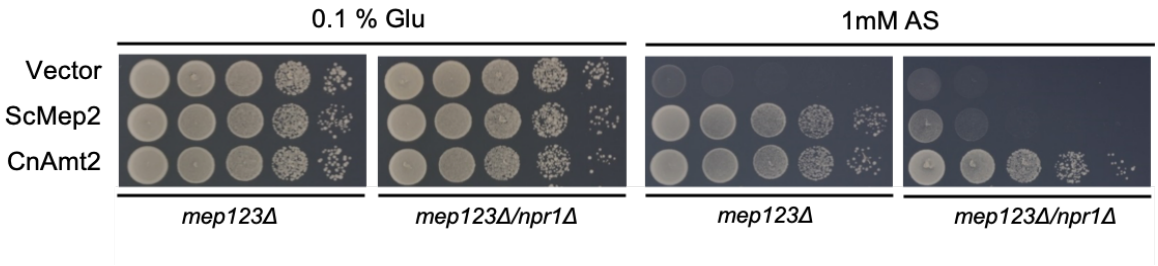

Figure 72: Effect of Npr1 kinase on growth of Amt2 expressed in yeast. *Haploid mep123Δ and mep123Δ/npr1Δ S. cerevisiae cells containing the plasmids of interest were grown in SD-URA medium overnight, washed, and 10 fold serially diluted before being spotted onto 0.1 % glutamate or 1 mM ammonium sulphate agar.*

Npr1 kinase, nor was a shift in the position of the band detected when Npr1 kinase was lacking from the strain. The band intensity was, however, greater despite less protein being loaded, as indicated by the levels of Pma1 (**Figure 73**). Therefore, when CnAmt2 is expressed in yeast Npr1 kinase does not phosphorylate CnAmt2 for any purpose.

4.6 Generation of *C. neoformans* MATα *amt2Δ* mutant

The 3' UTR of another gene on the forward strand overlaps with the 3' UTR of *AMT2* which resides on the reverse strand. To avoid altering the 3' UTR of the other gene (CNJ01870), only the first three transmembrane domains of Amt2 were deleted. Disruption of Amt2 in the *MATα* strain, with the GEN resistance cassette, was achieved via electroporation (**Figure 74**). Out of more than 50 mutants tested only one mutant was confirmed by PCR resulting in a targeting efficiency of < 2 %. PCR primers annealing to genomic DNA adjacent to the integrated disruption cassette and primers targeted to the neomycin resistance cassette were used to confirm successful integration at the correct locus. Absence of the WT Amt2 allele verified that the mutants had been generated. The *MATa* strain was also subjected to electroporation mediated transformation, however, no *MATa amt2Δ* mutants were confirmed (**Figure 75**). The *MATa amt2Δ* mutant was subsequently generated by genetic backcross, using the *MATα amt2Δ* mutant, by another lab member and gifted for future experiments. To confirm that Amt2 was no longer present in the *MATa amt2Δ* strain, *AMT2* expression under limiting ammonium conditions was tested by reverse transcriptase PCR. In contrast to the WT cells, *AMT2* was not expressed in both *amt2Δ* mutant mating types verifying that *AMT2* was disrupted (**Figure 76**).

4.7 *C. neoformans* hyphal growth under limiting ammonium is Amt2 dependent

To determine if Amt2 is responsible for the ammonium dependent hyphal growth previously described, confrontation assays and fruiting assays were performed with the WT and *amt2Δ* mutant strains. When observing the region between the patches, under the microscope, *amt2Δ* mutants of opposite mating type patched in a bilateral

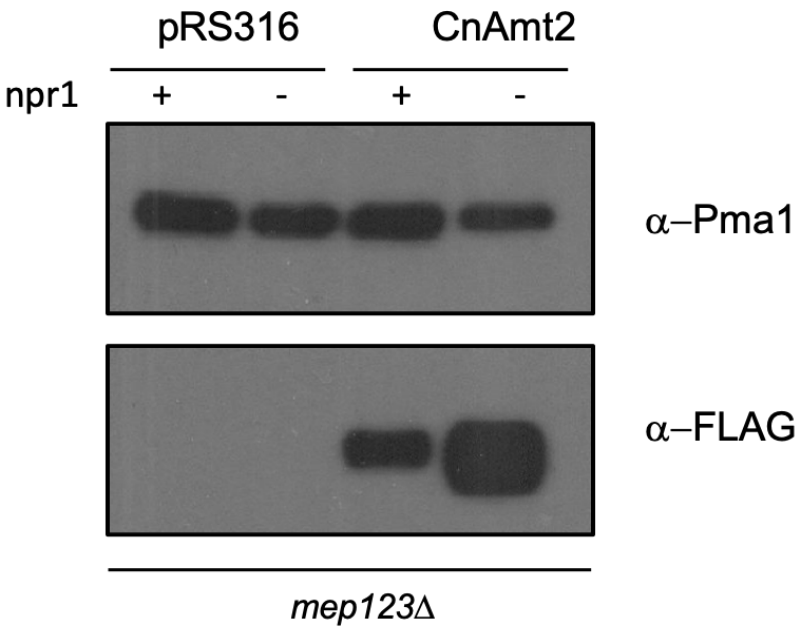

Figure 73: Western analysis of Amt2 expressed in yeast possessing and lacking Npr1 kinase. *Haploid mep123Δ and mep123Δ/npr1Δ S. cerevisiae cells containing the plasmids of interest were grown to mid-log phase in 0.1 % proline medium. Membrane proteins were extracted and assayed by western blotting. Pma1 was used as a loading control to compare levels.*

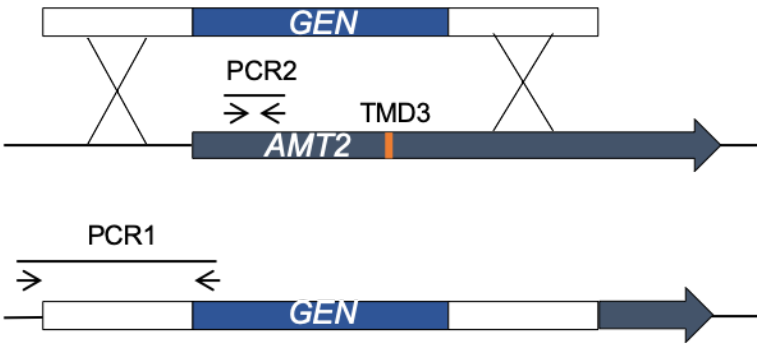

Figure 74: Schematic of homologous recombination to disrupt AMT2*. Homologous recombination event to disrupt AMT2. PCR1 and PCR2 correspond to diagnostic PCRs shown in the next figure.*

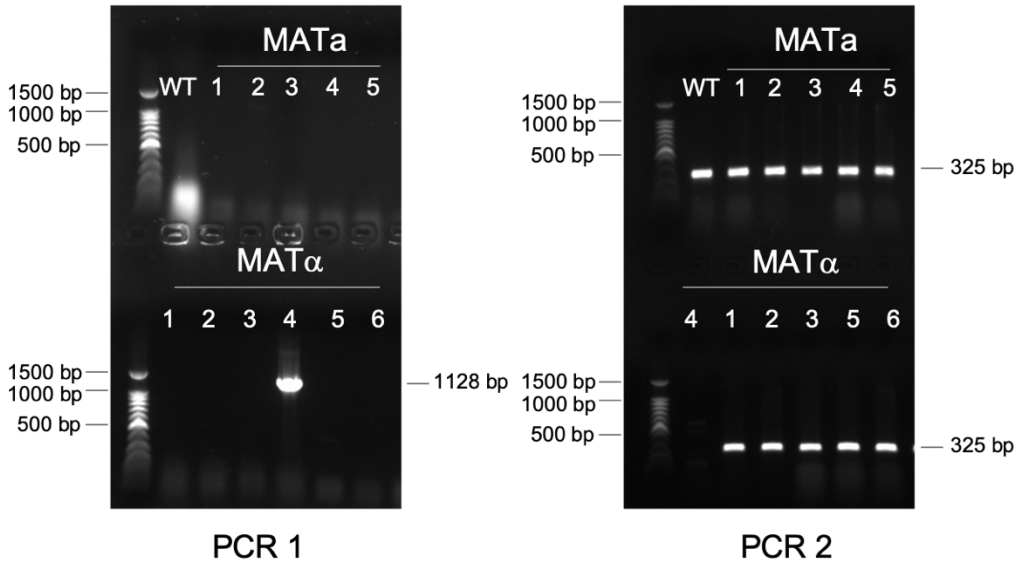

Figure 75: Diagnostic PCRs to confirm generation of MATα amt2Δ mutant. *The WT colony along with five MATa and 6 MATα independent mutant isolates were tested for targeted integration of the resistance cassette and for the presence of the WT allele. PCR 1 corresponds to left hand side GEN integration, whereas PCR 2 corresponds to the WT allele PCR. Numbers listed below MATa or MATα correspond to the independent isolate being tested.*

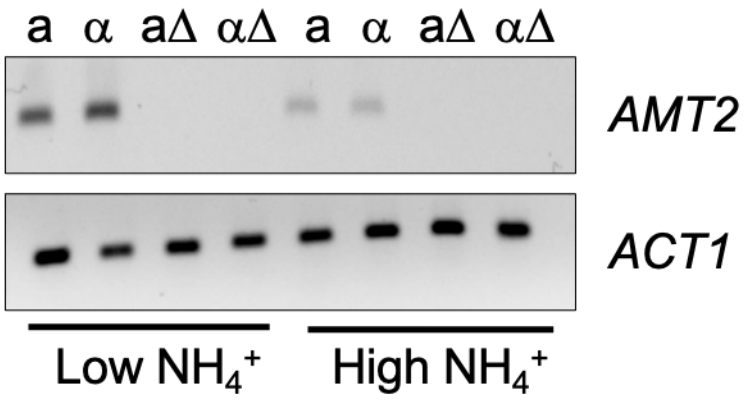

Figure 76: Amt2 disruption mutant diagnostic reverse transcriptase-PCR. *RNA extracted from the amt2Δ mutants was converted to cDNA and used as template to amplify AMT2 by reverse transcriptase-PCR. WT but not amt2Δ mutants transcribe AMT2.*

confrontation assay showed a complete loss of hyphal growth on low ammonium. Hyphal growth under these conditions is therefore Amt2 dependent. When the mutants were analysed with the WT version of their opposite mating type, in unilateral confrontation assays, the WT strain was not defective in hyphal growth despite its mating partner being unable to produce hyphal filaments. Therefore, hyphal growth in a confrontation assay, under ammonium limiting conditions, is not dependent on the opposite mating type possessing Amt2. Regardless of whether MATα was confronted with a WT or *amt2Δ* mutant mating partner, MATα still produced substantially longer hyphal filaments than MATa and produced chlamydospores. Hence, the lack of Amt2 in MATa is not required to induce longer hyphal filaments in MATα, nor is it required to promote chlamydospore formation. Moreover, the enlarged cells on the outer edge of MATa, which were observed previously in the WT confrontations assay, were observed on the edge of the MATa patch when analysed with WT or *amt2Δ* MATα. Thus, Amt2 does not need to be present in MATα to promote the formation of enlarged cells in MATa. On high ammonium, WT cells do not produce hyphal filaments and the same was observed for the *amt2Δ* mutants (**Figure 77**). In the fruiting assays, on low ammonium medium, no difference between the WT MATa and the MATa *amt2Δ* mutant was observed, which was expected, as the hyphal growth phenotype and production of enlarged cells was missing when the opposite mating type was not present. The MATα *amt2Δ* mutant was defective in displaying hyphal growth which was exhibited by WT MATα. Therefore, the induction of hyphal growth by MATα, in a fruiting assay under ammonium limiting conditions, is Amt2 dependent. No difference was observed between the WT strains and *amt2Δ* mutants when patched onto high ammonium medium (**Figure 78**) further verifying that hyphal growth is promoted by limiting ammonium.

4.8 Invasive growth is promoted by Amt2 on low ammonium

Amt2 in *C. neoformans* serotype H99/KN99 is responsible for invasive growth on low ammonium (Rutherford *et al.*, 2008b). To test if Amt2 controls the same phenotype in JEC20/JEC21, the surface cells on the confrontation assays and fruiting assays were washed away and assayed for invasive growth. On the low ammonium bilateral WT confrontation assay cells were embedded within the agar for both mating types. However, the volume of embedded cells was substantially greater on the outside edge

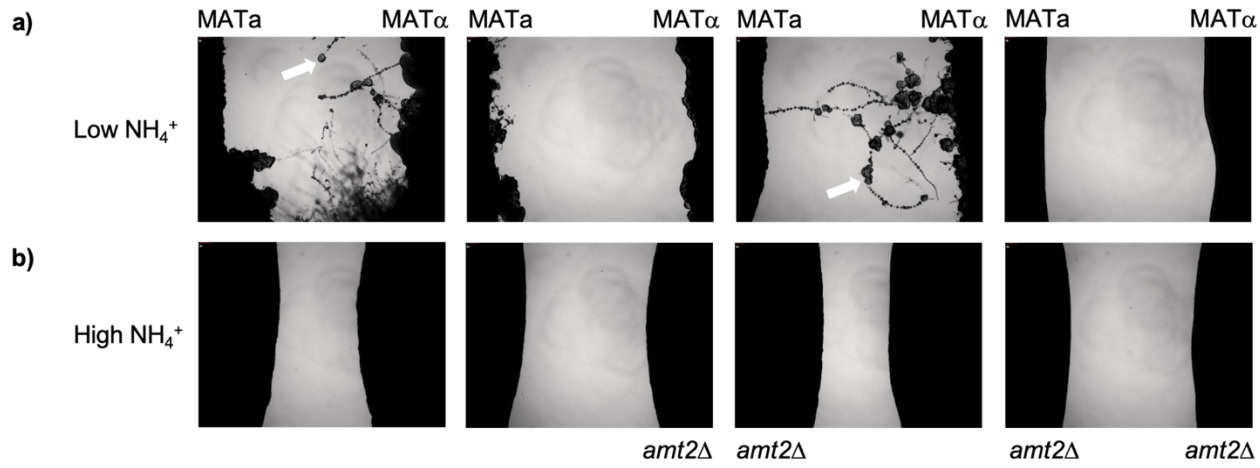

Figure 77: Ammonium and AMT2 dependent hyphal growth. *C. neoformans serotype D cells of opposite mating type were confronted on a) low (50 μM) and b) high (5 mM) ammonium medium. Images were taken of the region between the cells under the microscope at 40 x magnification after 3 weeks growth in the dark at room temperature. White arrows indicate chlamydospores.*

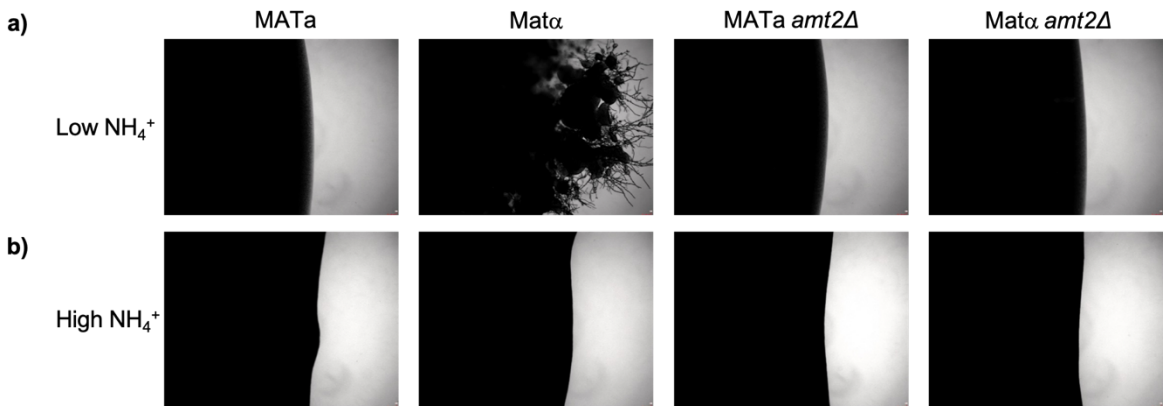

Figure 78: Ammonium and AMT2 dependent MATα hyphal growth*. Microscopic images of the edge of the fruiting assays at 40 x magnification on a) low (50 μM) and b) high (5 mM) ammonium medium.*

of each patch as opposed to the centre of the patches, as was observed previously. On the unilateral confrontation assays, invasive growth was displayed by the WT strains and to a much lesser extent by the *amt2Δ* mutants. When the *amt2Δ* mutants were confronted in a bilateral assay, embedded cells were barely visible (**Figure 79**). Out of the cells that did invade, enlarged cells were still present in the bilateral mutant confrontation assay (**Figure 80**). Thus, Amt2 is required to achieve a WT level of invasive growth under low ammonium, however, the production of enlarged embedded cells is promoted by cell invasion which is Amt2 independent. Interestingly, on high ammonium, regardless of whether cells possessed Amt2 or not, yeast cells invaded the agar in both confrontation and fruiting assays (**Figure 79 & Figure 81**). Hence, invasive growth on high ammonium is Amt2 independent. On the low ammonium fruiting assays a lack of Amt2 resulted in a reduction in invasive growth in both mating types (**Figure 81**). Therefore, in the absence of the opposite mating type, Amt2 is required to achieve a WT level of invasive growth under limiting ammonium conditions. Microscopic inspection revealed no difference between the size of the *MATa* WT or *amt2Δ* mutant embedded cells. However, embedded hyphal filaments, which are characteristic of the WT *MATα* cells, were lacking in the *MATα amt2Δ* cells; only yeast cells were observed (**Figure 82**). Thus, Amt2 is required for the presence of *MATα* hyphal filaments embedded within the agar.

4.9 Complementation of *amt2Δ* strains

To confirm that the hyphal growth and invasive growth defects exhibited by the *amt2Δ* mutants were due to the disruption of Amt2, *AMT2* was re-integrated randomly into the genome of each mating type by agrobacterium mediated transformation and assayed for hyphal and invasive growth. Reconstitution of Amt2 complemented the hyphal growth defect exhibited by each mating type in the confrontation assay (**Figure 83**). Notably, the extent of hyphal growth was greater in the reconstituted strains as opposed to the WT strains. Microscopic inspection confirmed that chlamydospores and enlarged cells were also visible on the reconstituted strain bilateral confrontation assay. Hence, hyphal growth along with chlamydospores and enlarged cells, observed on a low ammonium confrontation assay, are Amt2 dependent phenotypes. Reconstitution of Amt2 into the *MATα amt2Δ* strain complemented the hyphal growth defect displayed by the *MATα amt2Δ* mutant during the fruiting assay (**Figure 84**).

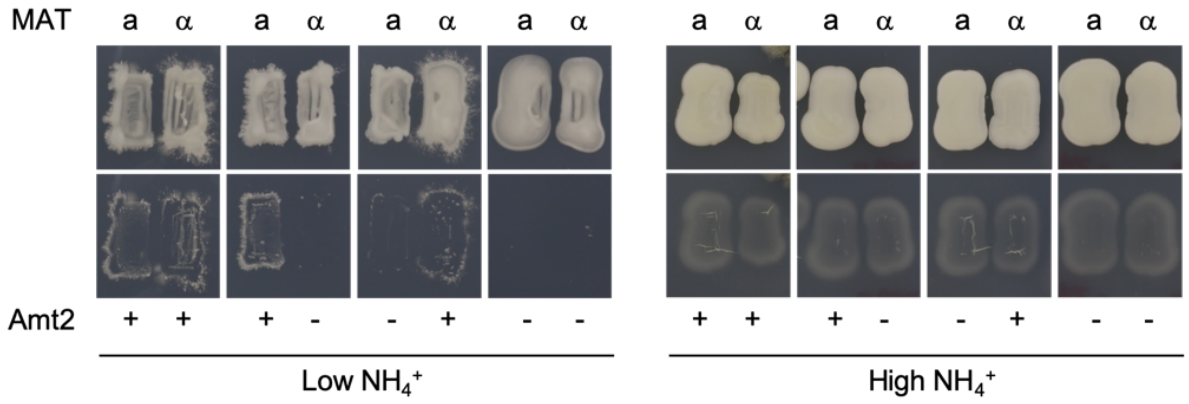

Figure 79: Confrontation assays invasive growth. *Surface cells from the confrontation assays on both low and high ammonium medium were washed away and the invasive cells were photographed. Top panel is before washing and bottom panel is after washing.*

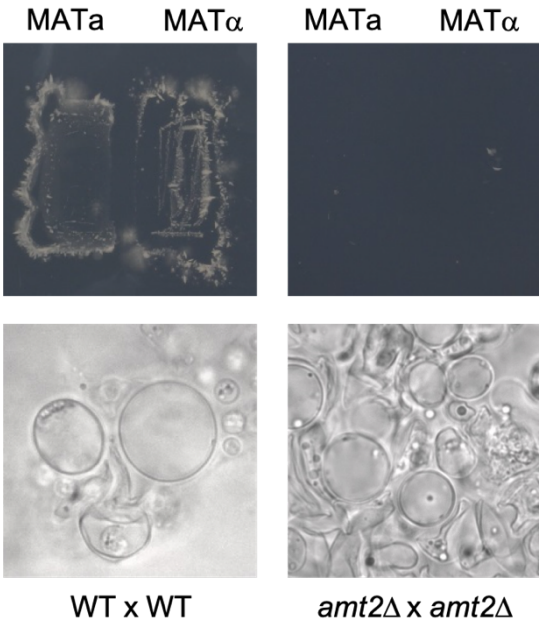

Figure 80: ***Confrontation assay invasive cells****. The surface cells were washed off the low ammonium confrontation assays (top panel). Embedded cells were observed under the microscope at 1000 x magnification using an oil emersion lens. Left panel corresponds to WT bilateral assay and right panel corresponds amt2Δ mutant bilateral assay****.*

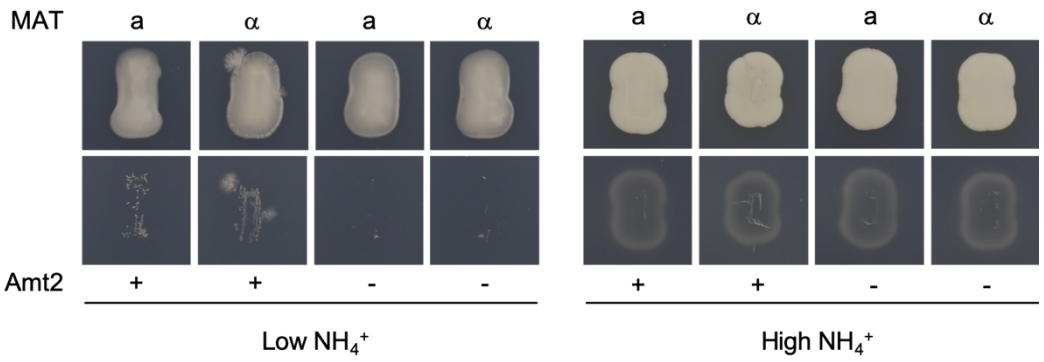

Figure 81: Fruiting assay invasive growth. *Surface cells from the fruiting assays on both low and high ammonium medium were washed away and the invasive cells were photographed. Top panel is before washing and bottom panel is after washing*

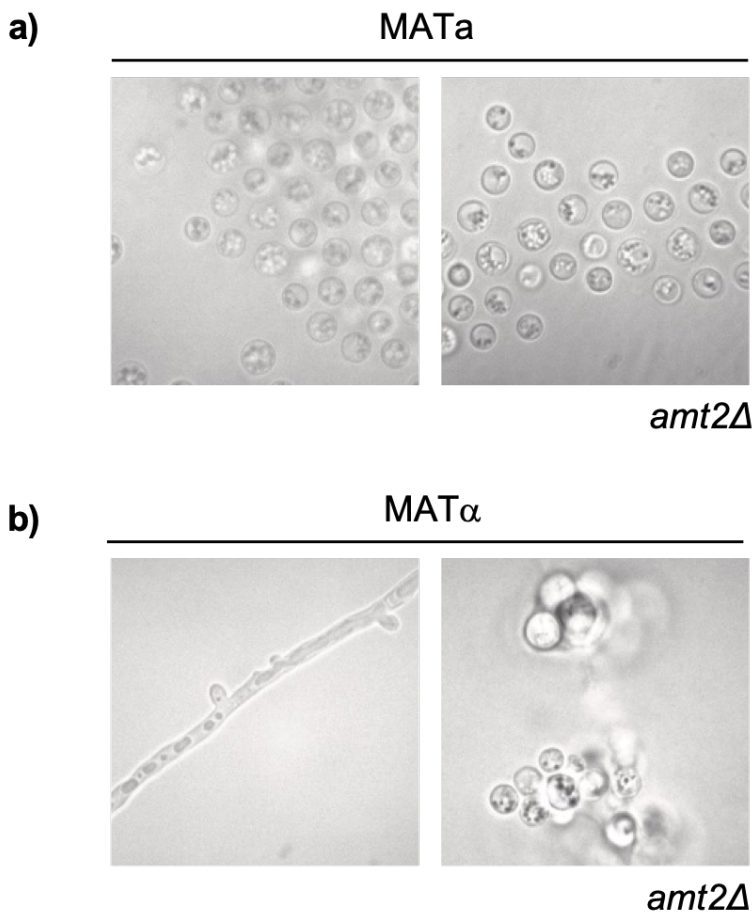

Figure 82: Fruiting assay invasive cells. *The embedded cells of both mating types a) MATa and b) MATα from the low ammonium fruiting assays were photographed under the microscope at 1000 x magnification.*

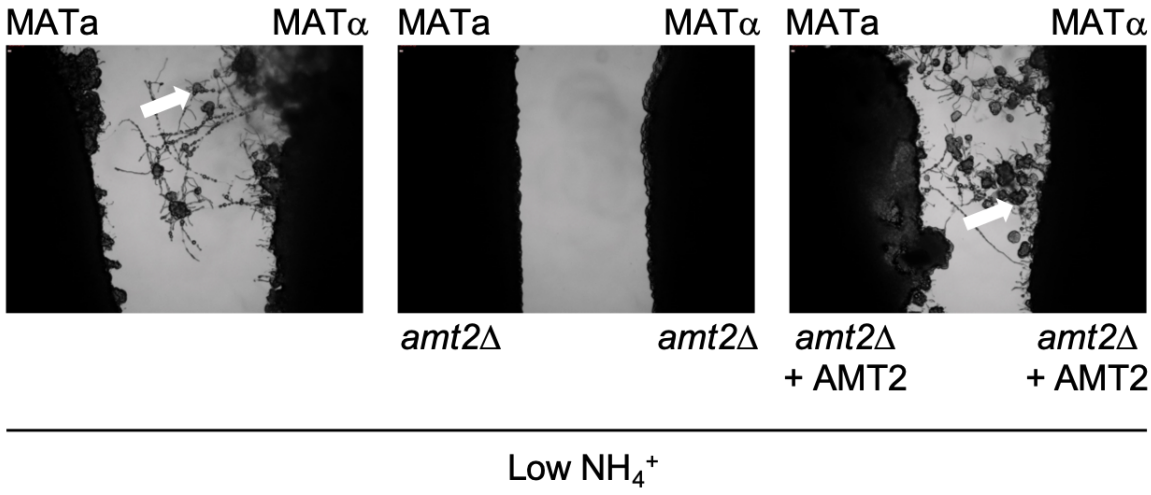

Figure 83: Reconstituted strains confrontation assays. *C. neoformans serotype D cells of opposite mating type were confronted on low (50 μM) ammonium medium. Images were taken of the region between the cells under the microscope at 40 x magnification after 3 weeks growth in the dark at room temperature. White arrows indicate chlamydospores.*

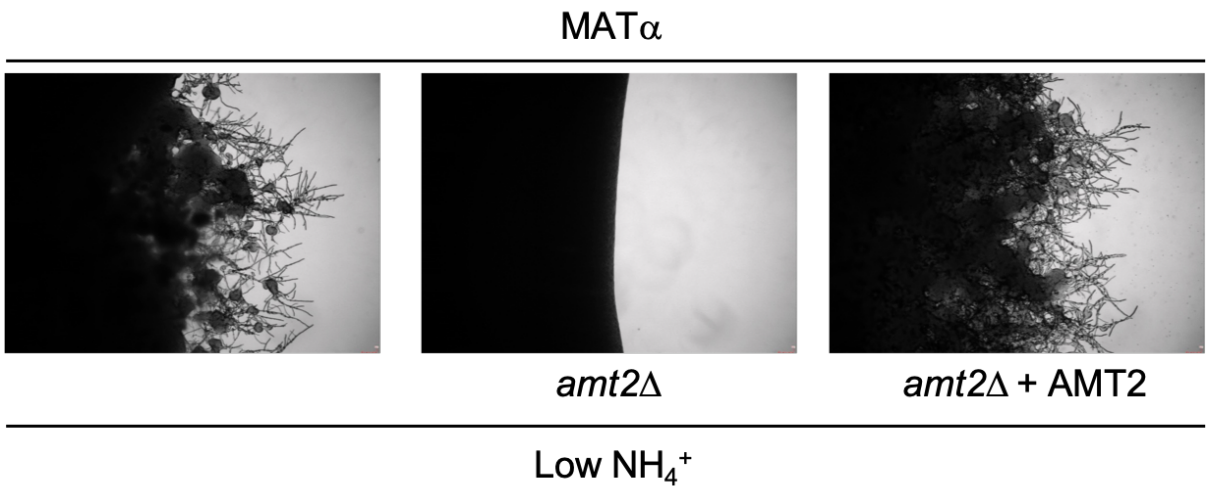

Figure 84: Reconstituted MATα fruiting assays. *Microscopic images of the edge of the fruiting assays on low ammonium (50 μM) medium at 40 x magnification.*

Thus, Amt2 regulates the hyphal growth displayed by *MAT*α cells on a low ammonium fruiting assay. Washing away the surface cells on the confrontation assays and the *MAT*α fruiting assays revealed that reintroduction of Amt2 complemented the invasive growth defect displayed by the *MAT*α *amt2*Δ mutants (**Figure 85 & Figure 86**). Markedly, the level of invasive growth was greater in the reconstituted strains than the WT strains. This difference was most striking for the fruiting assays where a substantial amount of invasive growth was visible in the centre of the patch. Invasive growth on low ammonium is dependent on Amt2 in both confrontation and fruiting assays.

4.10 *C. neoformans* discussion

C. neoformans undergoes a morphological switch in response to ammonium availability. During ammonium limiting conditions, JEC20 (MATa) and JEC21 (MATα) produced hyphal filaments in a confrontation assay. Hyphal filaments grew mostly away from the opposite mating type but some filaments were observed between the patched cells. In *S. cerevisiae*, growth is arrested in times of nitrogen starvation (Lorenz and Heitman, 1998). Hyphal growth is likely more repressed between the patched cells as there is a larger cell to nutrient ratio leading to greater ammonium limitation. It is presumed that where the filaments of opposite mating type meet mating occurs. Filaments produced by mating are functionally distinct to those produced by haploid cells. During nitrogen limitation *C. neoformans* must adapt to survive. If the opposite mating type is present two haploid cells can mate to form a dikaryon. In addition to foraging for nutrients (Phadke *et al.*, 2013), spores are produced in the terminal compartment of the dikaryon, the basidium. Spores are more resistant to starvation conditions and can be dispersed faraway by wind and rain (Botts *et al.*, 2009). In the absence of the opposite mating type, haploid cells can produce hyphal filaments to move away from the limiting environment, however, this phenotype is most associated with MATα (Wickes *et al.*, 1996). In this study, MATa but not MATα required its opposite mating type to undergo hyphal growth as only MATα produced hyphal filaments in the fruiting assay. This is consistent with *Shen et al's.*, (2002) findings. *Shen et al.,* (2002) found that MATa cells, grown on filament agar, will not produce hyphal filaments or enlarged cells when confronted with the congenic MATα strain lacking all three pheromone genes (*mf*α*123*Δ). However, reconstitution of just one pheromone gene complements both defects. Moreover, the authors observed that

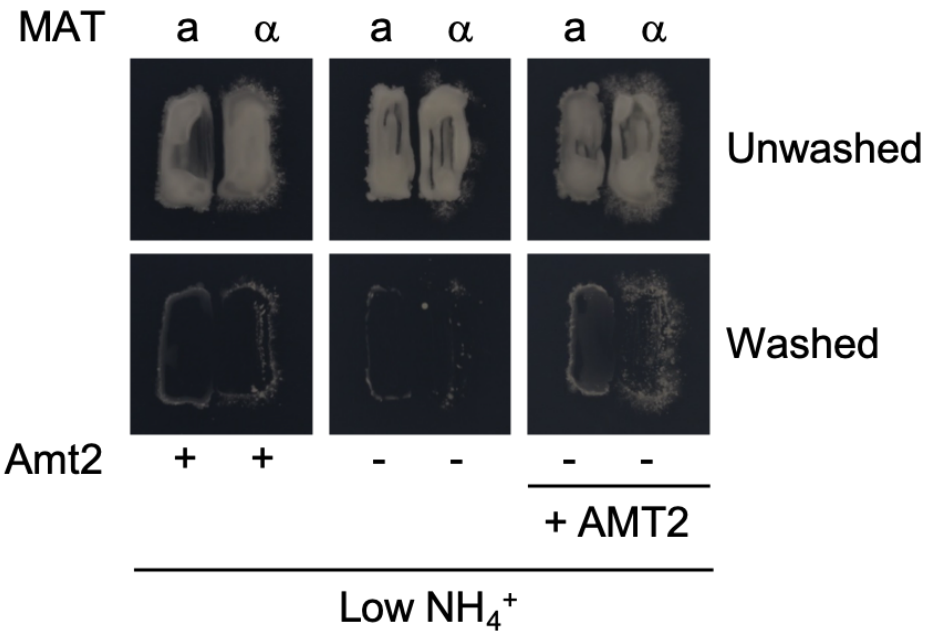

***Figure 85: Reconstituted strains invasive growth**. Confrontation assays were photographed before and after washing after 3 weeks incubation in the dark at room temperature. Washing revealed invasive cells.*

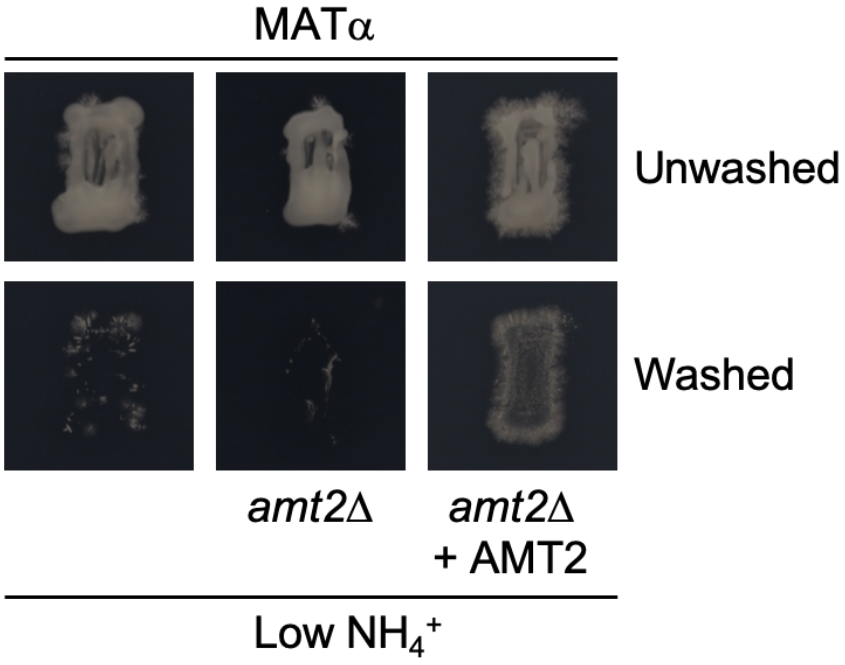

Figure 86: Reconstituted MATα invasive growth*. Fruiting assays were photographed before and after washing after 3 weeks incubation in the dark at room temperature. Washing revealed invasive cells.*

the *mfα123Δ* mutant strain fails to produce hyphal filaments in a fruiting assay on filament agar but will produce fewer filaments than the WT strain after prolonged incubation. Thus, *Shen et al.,* (2002) concluded than MATa cells rely on paracrine pheromone signalling to produce hyphal filaments, and enlarged cells, whereas MATα cells can support hyphal growth via autocrine pheromone signalling (Shen *et al.*, 2002). The hyphal growth exhibited by MATα in the fruiting assay is likely a scavenging response, analogous to pseudohyphal growth, allowing the strain to explore its environment in times of ammonium limitation. A Mep2 homology search identified two putative ammonium transporters. The H99/KN99 strain similarly contains two ammonium transporters in its genome (Rutherford *et al.*, 2008b). The twin-histidine motif, previously believed to be important for signalling, is conserved in Amt2 but not in Amt1. Amt1 contains the glutamate-histidine motif associated with the non-signalling members of the Mep/Amt/Rh superfamily. *AMT2* in both mating types is expressed under ammonium limiting conditions but repressed under ammonium sufficient conditions. This is consistent with *AMT2* expression being regulated by NCR and is equivalent to *AMT2* in the H99/KN99 strain. *AMT1* expression was not tested but this would be a future experiment to ascertain if, similar to the H99/KN99 strain, *AMT1* is constitutively expressed under ammonium limiting and sufficient conditions (Rutherford *et al.*, 2008b).

Amt2 was codon optimised and cloned into the yeast expression vector pRS316. Similar to ScMep2, CnAmt2 restored the growth defect of the *mep123Δ* strain verifying that CnAmt2 is an ammonium transporter. CnAmt2 additionally complemented the pseudohyphal growth defect of the *mep2Δ/mep2Δ* strain and, thus, acted as an ammonium sensor. To test if CnAmt2 acted, mechanistically, in the same way as ScMep2, the equivalent mutations which uncouple transport from signalling in ScMep2 were made in CnAmt2. Mutation of the first histidine of the twin-histidine motif to alanine abolished transport and signalling while mutation to glutamate only blocked the latter. Mutation of the second conserved histidine, or asparagine residue adjacent to the proposed deprotonation site, equally uncoupled transport from signalling as pseudohyphal growth was abolished. However, as the protein expression levels of the CnAmt2^{H194E} and CnAmt2^{H348A} mutants were less than the CnAmt2^{G343C} mutant, which induced pseudohyphal growth to WT levels, it could not be concluded that the lack of pseudohyphal growth was attributable to the mutations. A reduction in Mep2 protein expression is known to result in a reduction in filamentation (Biswas and

Morschhauser, 2005), therefore, the lack of pseudohyphal growth could be due to insufficient CnAmt2 expression. Despite no or very little CnAmt2^{H194E} and CnAmt2^{H348A} protein being immunodetected both mutants supported optimal growth in the *mep123Δ* strain, hence, they must have been expressed but to levels below the limit of detection by western blotting. It is possible that all the mutant proteins are expressed to the same level but the H194E and H348A mutations render the proteins less stable and sensitive to degradation during the membrane protein preparation procedure. The CnAmt2^{H194A} was expressed to a higher level than CnAmt2^{H194E} and CnAmt2^{H348A} but less than CnAmt2^{G343C}, thus, the H191A mutation could equally make the protein less stable. The CnAmt2^{N241A} mutant was expressed to equivalent levels to the CnAmt2^{G343C} mutant, therefore, the lack of pseudohyphal growth is due to the mutation. N241 is adjacent to the proposed deprotonation site which includes the first conserved histidine. It is plausible that NH_4^+ deprotonation occurs in CnAmt2^{N241A}, as the mutant supports growth and, thus, possesses transport activity. However, the route the proton follows, after deprotonation, may be altered. Alanine is a hydrophobic amino acid (Nilsson *et al.*, 2003) whereas asparagine is a larger polar residue (Thanki *et al.*, 1988). The N241A mutation could alter intermolecular interactions within this region of the pore, which could lead to conformational changes in the protein which in turn could impact on the pathway the proton follows. The fact that the same mutation uncouples transport from signalling suggests that the signalling mechanism is conserved between ScMep2 and CnAmt2.

The equivalent mutation to G343C in ScMep2 is hyperactive for transport and pseudohyphal growth. On the contrary, in *C. albicans* this mutation slightly reduces transport activity and abolishes filamentation (Van Nuland *et al.*, 2006) (Boeckstaens *et al.*, 2007) (Neuhauser *et al.*, 2011). Methylammonium uptake studies have not been performed to determine the affinity and capacity of CnAmt2. This would be a noteworthy study to undertake to confirm if the G343C mutation increases CnAmt2 transport activity. In parallel to this experiment the pH_{opt} could also be determined to address the pH model of ammonium sensing. If analogous to ScMep2 it would be expected that the pH_{opt} would be around 4. Non-signalling ammonium permeases, in *S. cerevisiae,* possessed higher optimum pHs than ScMep2. If signalling is dependent on pH it would be hypothesised that the pH_{opt} would be higher for the CnAmt2^{N241A} mutant as seen for the separation of function ScMep2^{H194E} mutant (Boeckstaens *et al.*, 2008). However, these experiments should be performed in *C. neoformans* rather than

in *S. cerevisiae*. *AMT1* would first need to be deleted from MATa *amt2Δ and* MATα *amt2Δ* to generate the double mutants with no functional ammonium transporters. The double mutants should then be reconstituted with the different tagged Amt2 mutants individually. Confrontation assays, between the mutant reconstituted strains, and growth assays should additionally be performed to test if separation of function occurs when the mutants are expressed natively. It could be possible that the mutants are all expressed to similar levels when expressed in *C. neoformans.* Moreover, GFP tagging of the mutants would allow localisation studies to be performed. Another reason for the low expression of certain mutants could be due to a lack of localisation to the membrane.

ScMep2 is immunodetected as a smear by western blotting. This is because an asparagine residue in native ScMep2 is glycosylated at the N-terminus. Mutation to this residue, N4Q, does not impact on ScMep2 function but does allow the protein to be visualised as a distinct band (Marini and André, 2000). Although CnAmt2 was not immunodetected as a smear, when expressed in yeast, this cannot rule out the possibility that CnAmt2 is indeed N-glycosylated in *C. neoformans*. Similar to ScMep2, RhCG is glycosylated, however, non-glycosylated Rh proteins also exist. In RhCG, the polysaccharide is proposed to protect a hydrophobic region within ICL1 from proteolytic degradation; ICL1 in the non-glycosylated versions is much shorter and postulated to be less prone to degradation (Gruswitz *et al.*, 2010). Native immunodetection of CnAmt2 would verify whether CnAmt2 is N-glycosylated in *C. neoformans*. If so, perhaps the mutations, which resulted in little or no immunodetection of CnAmt2, impacted on the conformation of ICL1, in CnAmt2, making the protein sensitive to proteolytic degradation. CnAmt2 possesses an asparagine residue near the start of its N-terminal end. This residue, N3, could be the glycosylation site if the protein is natively glycosylated.

Similar to the ZtMeps, CnAmt2 transport activity is not regulated by Npr1 kinase when expressed in yeast. An Npr1 kinase homology search identified several serine/threonine protein kinases but with low similarity to Npr1 kinase suggesting that there may not be an Npr1 orthologue in *C. neoformans*. Thus, if CnAmt2 is regulated by phosphorylation in *C. neoformans* it could to be by a protein kinase other than Npr1. There is a potential phosphorylation site in the CTR of CnAmt2, however, this is closer to the C-terminus than it is in ScMep2. Without a crystal structure of CnAmt2 we do

not know how the CTR is ordered. An interaction between the CTR and ICL3, as a result of phosphorylation, has been proposed to be important for the opening of ScMep2 (van den Berg *et al.*, 2016). Similar interactions between the CTR and ICL3 are believed to be important in other Amt orthologues to function (Loque *et al.*, 2007) (Severi *et al.*, 2007). With the CTR sequence of CnAmt2 being different to the ScMep2 CTR the same proposed mechanism, interaction between the CTR with ICL3 following phosphorylation and ammonium ion binding, may not occur. Perhaps these regions are already interacting and, thus, do not require phosphorylation for activation. Furthermore, although *C. neoformans* grows well at 30 °C, the temperature the growth assays were performed at, the fungus is ubiquitous in the environment which will inevitably be much cooler. *C. neoformans* is frequently associated with eucalyptus trees (Gugnani *et al.*, 2005). It is likely that ammonium would be limiting on the surface of the leaves and, thus, Amt2 would be highly expressed. In CaMep2, a shift from 30 °C to 37 °C made the transport activity Npr1 kinase independent (Neuhauser *et al.*, 2011). Perhaps at lower temperatures, CnAmt2 activity is dependent on Npr1 kinase in yeast. It is possible that at higher temperatures the intermolecular bonds holding the quaternary structure together denature slightly locking the transporter in a constitutively active conformation or render the pore more fluid.

In the western blots comparing band migration between CnAmt2 expressed in strains containing and lacking Npr1 kinase no difference was observed. This supports the conclusion that CnAmt2 is not phosphorylated by Npr1 kinase when expressed in yeast. The band intensity was, however, significantly greater in the strain lacking Npr1 kinase. The *ScMEP2* promoter and terminator were cloned before and after *CnAMT2* respectively. *ScMEP2* is transcribed by the Gln3 and Gat1 transcription factors which bind to the UAS in the *ScMEP2* promoter. Phosphorylated Npr1 kinase (inactive) is a negative regulator of Gln3 nuclear localisation as evidenced by the nuclear localisation in *npr1Δ* cells growing in ammonium replete conditions (Crespo *et al.*, 2004). Hence, in the *mep123Δ* cells lacking Npr1 kinase, Gln3 will be more active and upregulate transcription of CnAmt2. More CnAmt2 transcripts will lead to an increase in transcribed protein as observed. Two 5'-GATAAG-3' sequences, the sequences identified by Gln3 and Gat1 (Cunningham *et al.*, 1996) (Coffman *et al.*, 1996), are present in the region upstream of CnAmt2 (**Figure 87**). Moreover, there are three putative Gln3 or Gat1 transcription factors in the JEC20/JEC21 genome, hence, transcriptional regulation may be conserved in CnAmt2. To verify this, *AMT2* gene

GCTCGCTGTTCGTCCAGTCTGATCGAGATTAGTAGACGGCGGA
GATCAGCAGTGCACTAGCGCTCAGCTTAAGCTCGGTCTCGCAC
TTTGCATCATCCATCACGGATCAAGCGAAGACTTCCAGCAGCA
TATTCATCCATTGAGCATGGACTGGTGTTGCCCATATTTTTCC
AGCAAGTCGCCCTTATTTGTCATGTTTTGAGGAATAAAAAGTG
ATTAGCGATTTACACGGCTAAAATACGTGCACCCTAATACGAC
TGATTATGCCATCCTCTCGTCGACCTATCCCAGAGCCGCAAGC
TATCAGTTATCAGTTACATACTACTCGAACTCTGAGACCGTTT
ATCTCCACCAACCACGGCGCGTGATGGCGCATAATTTCGGTTC
CGATTTACAACCACCCTCAGCGCTTCCGCCAGCAATCGGCCTG
CGCCGCATCCTTGGTTCAGGACGCGGCAATTCAATTCACCAGT
CTTTTTTATCCTGGGCAAATGAGTACGCGTCATGAGGCTGATA
GCTCATAGATAAGGACGTCCGCGGCAGAGTAGTGCGACAAGGT
CTTGGCGTATCTTCTTTTGCAGGTTCTCTAATCTCTTCATGCT
CTGCGTTTGCGTGTTCGGTCGTGCACTCGTGTTTTGCAATTTC
CCTATTCTGTCGGTTCGCCGTTTGCAGTTGACTGAAGCGAATG
CAATACGTAATAACATTAAGACGCGTAAATGCTAGTCGCCTCC
GGAGCTCAGAAGATGAGGCATCTTTCAACGCGGGGATAGATAA
GGATTGACTGGCCAATGAGGGGCAGCCGTCTTGTTGTGGTATC
TACCCCCTTTCTCTTTCATCTTCCGATTCCTTCCCCCTTTATC
GTTCTCCCAGGCCCAATACTTATTCTAATGCAATTCCTGTTTT
CTCTTTTCCATCTTTCTTTCTTCCTTTTCTTTACTTGGACAAT
TATTGACCTTCCGTTTTCCGTCTCGCACTACAACAACAGCAAT
TCCCATTCAAT**ATG**

Figure 87: GATA UAS sequence in CnAMT2 promoter. *1000 bp of genomic DNA before the START codon (ATG) OF CnAMT2 is depicted. The GATA sequences are highlighted in yellow, the 5' UTR is represented in red, and the START codon is listed in bold*

expression should be assayed in mutants lacking the putative transcription factors. As Gln3 and Gat1 carry redundant functions, in *S. cerevisiae* (Scherens *et al.*, 2006), it is likely that double mutants may need to be generated to incur an effect on gene expression. Additionally, the UAS could be verified by making point mutations in the putative UAS sequences. Mutation to the UAS should prevent the transcription factors binding and, thus, inhibit *AMT2* expression under ammonium limiting conditions.

Disruption of *AMT2* in both MATa and MATα abolished hyphal growth under ammonium limiting conditions. Likewise, invasive growth was drastically reduced. Although Amt2 promotes invasive growth, during ammonium limiting conditions, enlarged cells were still observed suggesting these phenotypes can occur in a stochastic fashion which is not Amt2 dependent. The enlarged cells are speculated to be titan cells but this has not been confirmed. To confirm this the enlarged cells should be extracted from the agar and assayed for cell ploidy by fluorescence-activated cell sorting (FACS). Titan cells are known to exhibit increased ploidy (Gerstein *et al.*, 2015) in addition to a thicker cell wall and cross linked capsule (Okagaki *et al.*, 2010). On high ammonium *C. neoformans* invaded the agar in an Amt2 independent manner. This is consistent with *S. cerevisiae* haploid cells invading the agar of rich media (Roberts and Fink, 1994). However, enlarged cells were lacking in the pool of embedded cells. Moreover, the volume of growth was greater than on low ammonium. It is likely that another nutrient became limiting which could be responsible for the Amt2 independent growth; this nutrient could be carbon. Equally, on both high and low ammonium, the volume of invasive growth was greater on the outer edges of the patched cells as opposed to within the centre. Invasive growth is a scavenging response so will only occur when there are sufficient nutrients worth scavenging for. Cells will be more starved in the centre of the patch due to a higher cell to nutrient ratio, therefore, invasive growth may be partially repressed.

To confirm that the loss of hyphal growth and reduction in invasive growth were Amt2 dependent Amt2 was reconstituted into the *amt2*Δ mutant strains. Both invasive and hyphal growth were complemented by Amt2 to levels greater than the WT strains. The greatest increase in invasive growth was observed with the MATα reconstituted strain in the fruiting assay; the images taken before and after washing look very similar. As *AMT2* was reconstituted randomly into the genome it is possible that *AMT2* disrupted another gene which may be a negative regulator of both developmental processes.

After generating the reconstituted strains it was noticed that another gene (CNJ01885), residing on the forward strand, had been recently annotated on the database. This gene overlaps with most of the *AMT2* gene, however, CNJ01885 is only annotated as being a hypothetical protein, so may not code for a functional protein. If CNJ01885 does encode a functional protein it may not have any involvement in regulating morphology (**Figure 88**). To verify that the phenotypes are Amt2 dependent the *amt2Δ* mutant strains should be reconstituted with the *AMT2* upstream and downstream regions along with the *AMT2* open reading frame (ORF) sequence lacking introns. This would prevent the overlapping gene from simultaneously being reconstituted into the genome. If the new reconstituted strains undergo hyphal and invasive growth then it can be confirmed that they are Amt2 dependent processes and not dependent on the protein encoded by the overlapping gene.

The *amt2Δ* mutants have not been tested in a virulence assay, however, this would be a future experiment to undertake. Virulence assays include the murine nasal inhalation test (Nielsen *et al.*, 2003) and the wax moth assay (Mylonakis *et al.*, 2005). DME medium and Niger seed medium could additionally be utilised to test for the competency to produce capsule and melanin, respectively, which are both virulence traits. In the H99/KN99 strain, single and double Amt1/Amt2 mutants behaved like WT in all virulence assays, thus, the Amt permeases are not virulence factors in this strain. However, this does not rule out the possibility that Amt2 is a virulence factor in the JEC20/JEC21 strain. Ump2 is the ammonium transceptor in *U. maydis*. For *U. maydis* to infect its host, maize, the fungus must first mate to form a dikaryon. The dikaryon is the morphology which allows *U. maydis* to infect (Smith *et al.*, 2003). Thus, an ammonium transceptor is important for virulence in this fungus. In the confrontation assays, mating presumably occurs when the cells of opposite mating type meet. Mating by *C. neoformans* produces dikaryons (Kwon-Chung, 1975), similar to *U. maydis*, therefore CnAmt2 could also be important for virulence in JEC20/JEC21. If CnAmt2 is important for virulence this would provide a new target for antifungal drugs to treat cryptococcal infections. If the structure of Amt2 is solved this could be used to screen for potential drugs. Due to the similarity between Amt2 in H99/KN99 and JEC20/JEC21, it seems unlikely that Amt2 in the latter strain would be important for virulence. However, the crystal structure could aid in providing more breadth into the underlying signalling mechanism and molecular simulation studies could provide insight into the transported molecule.

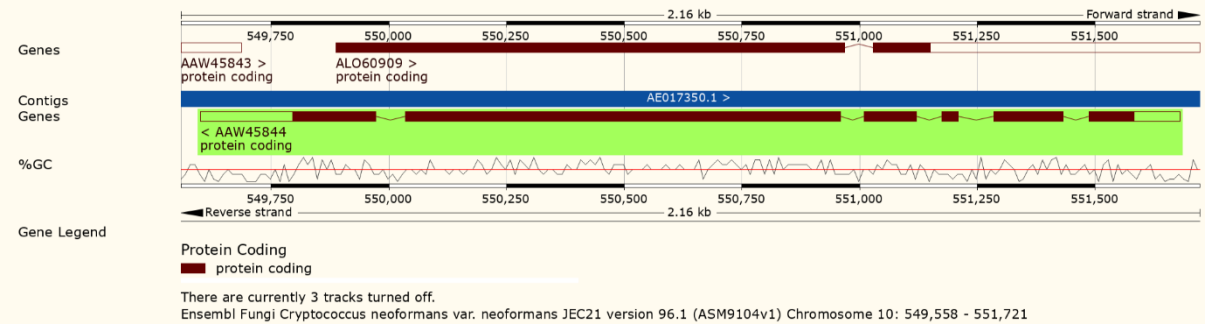

Figure 88: Location of AMT2 and overlapping genes. *The diagram was exported from the EnsembleFungi website. The red filled boxes and redlines indicate exons and introns respectively. The red outlined white boxes indicate UTR's. The gene highlighted in green depicts AMT2 on the reverse strand. The overlapping gene, on the forward strand, was added after the reconstituted strains were generated.*

5 Final discussion

5.1 Project summary

Nitrogen is an essential nutrient for many organisms and ammonium is a preferred source of nitrogen for fungi (Boer *et al.*, 2007). All fungal genomes encode at least two functional ammonium permeases which facilitate the transport of ammonium across the plasma membrane (Marini *et al.*, 1997). In four distinct fungi one of the encoded proteins serves an additional role as an ammonium sensor. ScMep2 and CaMep2 induce pseudohyphal growth and filamentation in *S. cerevisiae* and *C. albicans* (Lorenz and Heitman, 1998) (Biswas and Morschhauser, 2005) respectively, whereas, CnAmt2 and Ump2 regulate mating between haploid *C. neoformans* H99/KN99 and *U. maydis* cells respectively to generate a dikaryon and disperse spores (Smith *et al.*, 2003) (Rutherford *et al.*, 2008b). The ammonium sensors control these processes during ammonium limitation. Although these two developmental processes are distinct, they are both starvation responses which aid survival in times of limitation. Pseudohyphal growth and filamentation are non-motile morphologies which allow the yeast cells to forage for limiting ammonium. Hyphae production, following mating of two haploid cells, equally allows *C. neoformans* and *U. maydis* to explore their environments and scavenge for nutrients (Phadke *et al.*, 2013). Spores, which can withstand harsher conditions, are dispersed further afield by wind and water to potentially more favourable environments (Botts *et al.*, 2009). Furthermore, the production of spores involves recombination events which generate genetic variation and diversity which may introduce favourable traits to aid survival in shifting conditions (Lin *et al.*, 2005). Mutations that uncouple transport from signalling demonstrate that the physical act of transport triggers signalling as opposed to internal nutrient metabolism. Hence, these permeases are classified as transceptors; transporters which act like receptors (Van Zeebroeck *et al.*, 2014). However, the underlying molecular signalling mechanisms adopted by these ammonium transceptors is unknown. As sensing the environment is critical for all fungi, to adapt to changing niches, the aims of this study were to enhance current knowledge in how ammonium signalling is conserved. Investigation into ammonium signalling in two divergent fungi has identified that in *C. neoformans* JEC20/JEC21 an ammonium transceptor, Amt2, is important for the induction of hyphal growth during ammonium limitation. However,

ammonium permeases do not play the same role in regulating morphology in *Z. tritici*, instead ammonium starvation triggers a hypervirulent phenotype.

5.1.1 Nitrogen starvation induces virulence in Zymoseptoria tritici

In the wheat pathogen *Z. tritici*, a lack of ZtMep2 and ZtMep3 renders the fungus hypervirulent suggesting that nitrogen starvation is the stimulus for virulence. Nitrogen starvation as a trigger for virulence has previously been proposed for other pathogenic fungi including the vascular wilt fungus *Fusarium oxysporum*, the wheat head blight fungus *Fusarium graminearum*, and the rice blast fungus *Magnaporthe oryzae* (López-Berges *et al.*, 2010). An early study found a correlation between starvation induced genes and the expression of genes in planta (Coleman *et al.*, 1997). In this study, both *ZtMEP2* and *ZtMEP3* were expressed to higher levels during ammonium limitation as opposed to ammonium replete conditions. Moreover, *Yang et al.*, (2013) found *ZtMEP3* and the virulence gene *Zt3LYSM* to be highly expressed during the wheat infection cycle when the fungus switches to the necrotrophic phase (Yang *et al.*, 2013). Thus, the expression of *ZtMEP3* is correlated between starvation and infection. After penetration of the wheat leaf, through the stomata, *Z. tritici* colonises the substomatal space (Duncan and Howard, 2000). Despite colonisation, the biomass of *Z. tritici* does not significantly increase and *Z. tritici* is believed to rely on internal nutrient stores as well as soluble nutrients in the apoplast (Keon *et al.*, 2007) (Rohel *et al.*, 2001). However, upon the switch from biotrophy to necrotrophy, when pycnidia appear on the wheat leaves, *Z. tritici* proliferates more rapidly increasing its biomass (Duncan and Howard, 2000). Perhaps once *Z. tritici* has exhausted the internal nutrient stores, and hence become starved of nitrogen, high expression of *Zt3LYSM* and *ZtMEP3* are induced. An increase in virulence will provide plentiful nitrogen for *Z. tritici*, from wheat cell death, to be imported through ZtMep3 to support the rapid growth.

In *F. oxysporum*, a virulence associated phenotype is cellophane membrane penetration in the presence of sodium nitrate containing minimal medium (MM). The same phenotype is repressed in the presence of ammonium nitrate or ammonium tartrate. Repression of cellophane penetration was also observed with *F. graminearium* and *M. oryzae*, which like *F. oxysporum* are ascomycetes (López-Berges *et al.*, 2010). Ascomycetes form the Ascomycota phylum of the fungal kingdom and are defined by their production of spores in sac-like structures known as asci

during the sexual cycle (Bennett and Turgeon, 2016). Supplementation of the amino acid glutamine, which is a preferred source of nitrogen, to the growth media partially repressed cellophane penetration by *F. oxysporum*. Moreover, addition of l-methionine sulfoximine (MSX), a glutamine synthetase (Gln1) inhibitor, to ammonium nitrate containing medium, fully restored cellophane penetration. As glutamine synthetase converts ammonia to glutamine this suggested that glutamine was the repressing stimulus as opposed to ammonium (López-Berges *et al.*, 2010). The partial cellophane penetration observed, when MM medium was supplemented with glutamine, could be attributable to the instability of glutamine, which has a relatively short half-life in solution (Coster *et al.*, 2004), or due to inefficient uptake. Glutamine uptake is mediated by Gnp1, the high affinity glutamine permease capable of importing other amino acids: leucine, serine, threonine, cysteine, methionine and asparagine (Zhu *et al.*, 1996) (Regenberg *et al.*, 1999), Agp1, the low affinity amino acid permease (Schreve *et al.*, 1998) and Gap1 in *S. cerevisiae*. In *S. cerevisiae*, glutamine is a key regulator of the TOR pathway (Stracka *et al.*, 2014). Supplementation of rapamycin to ammonium containing medium reversed the repressive cellophane penetration phenotype establishing an involvement of the TOR pathway in regulating virulence in *F. oxysporum* (López-Berges *et al.*, 2010). Similar to *F. oxysporum*, *Z. tritici* is an ascomycete (Steinberg, 2015), therefore, the hypervirulence phenotype associated with the *Ztmep2Δ/Ztmep3Δ* double mutants could be due to glutamine starvation which inhibits the TOR pathway. If this theory is correct it would be hypothesised that treatment of high ammonium grown WT cells with rapamycin, or MSX, would mimic the starvation associated phenotypes displayed by the *Ztmep2Δ/Ztmep3Δ* double mutants on high ammonium. These phenotypes would include melanisation and sporadic distribution of 'barbed wire-like' filaments around the centre of the colony in the 5 μl spot and single colony analysis assays, and a lack of growth in high ammonium liquid medium and reduced growth on high ammonium solid medium. Furthermore, it would be postulated that the expression of *Zt3LYSM* by WT cells, grown in high ammonium medium supplemented with rapamycin or MSX, would be comparable to the expression of the virulence gene in the *Ztmep2Δ/Ztmep3Δ* double mutants. Treatment of WT cells with MSX and rapamycin should, therefore, be tested to investigate the underlying signalling mechanisms governing virulence in *Z. tritici*. Interestingly, a protein interaction prediction site does forecast an interaction between ZtMep3 and a putative glutamine synthetase. If glutamine starvation is found to the be

the trigger for virulence, putative Gln1 should be deleted from the WT strain to assay if this mutant also mimics the *Ztmep2Δ/Ztmep3Δ* double mutant phenotypes.

AreA is a GATA binding transcription factor that mediates NCR in ascomycetes by activating the transcription of genes which encode proteins that enable uptake and assimilation of less preferred nitrogen sources (Wong *et al.*, 2008) (Caddick *et al.*, 1986) (Fu and Marzluf, 1990). Thus, non-functional *areaΔ* mutants cannot utilise secondary nitrogen sources, other than ammonium and glutamine, for growth (Marzluf, 1997). AreA is an orthologue of Gln3/Gat1 in *S. cerevisiae* which transcriptionally induce *MEP2* during nitrogen limitation (Scherens *et al.*, 2006). In *Fusarium fujikuroi*, AreA induces the expression of all three ammonium permease genes (Teichert *et al.*, 2008) and glutamine synthetase (*gln1Δ*). Interestingly *AREA* expression is repressed by glutamine and ammonium, but expression is derepressed in a *gln1Δ* mutant regardless of the nitrogen source. This suggested that the *gln1Δ* mutant does not sense the repressive nitrogen sources to inhibit the expression of *AREA* and, thus, Gln1 regulates the expression of *AREA* (Wagner *et al.*, 2013) (Tudzynski, 2014). In some pathogenic fungi, *Colletotrichum lindemuthianum* and *F. oxysporum*, AreA has been found to be important for virulence (Pellier *et al.*, 2003) (Divon *et al.*, 2006). *ZtMEP3* and *Zt3LYSM* are highly expressed at day 14 of the infection cycle (Yang *et al.*, 2013), and in this study *ZtMEP3* is greater than six-fold more expressed during nitrogen limiting conditions as opposed to ammonium replete conditions; AreA could be the transcriptional regulator of both genes. To test this hypothesis *areaΔ* mutants and complemented strains should be generated. The *areaΔ* mutants should be tested in the wheat infection assay for their impact on virulence. Moreover, the expression levels of *ZtMEP2*, *ZtMEP3*, and *Zt3LSYM* between the strains containing and lacking AreA should be determined by qPCR. If the *areaΔ* mutants mimic the hypervirulent phenotype of the *Ztmep2Δ/Ztmep3Δ* double mutants on wheat, and show a lack of *ZtMEP2 and ZtMEP3* expression during ammonium limitation, but an induction of *Zt3LSYM*, this would suggest that the Meps are transcriptionally induced by AreA but AreA does not regulate the virulence pathway. If virulence is AreA dependent, RNAseq should be performed to assay which genes are regulated by AreA under low and high ammonium conditions. A model for the link between nitrogen availability, Gln1, TOR and AreA is depicted in (**Figure 89**).

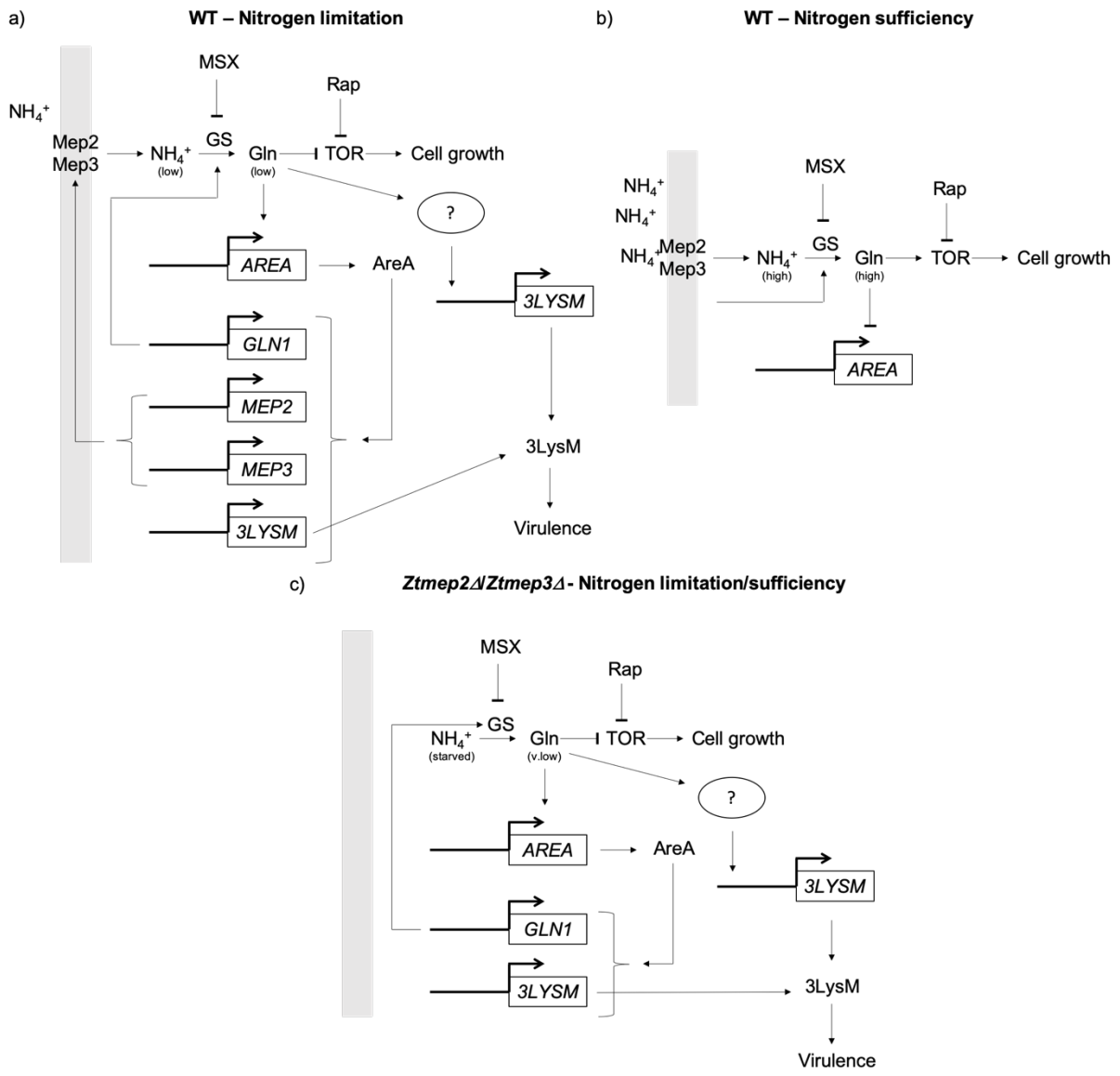

Figure 89: Model of nitrogen starvation induced virulence in Z. tritici. *a) During nitrogen limiting conditions low levels of NH_4^+ are imported through Mep2 and Mep3 in WT cells. NH_4^+ is converted to glutamine (Gln) by glutamine synthetase (GS). Limiting glutamine induces expression of AREA, GLN1, MEP2, MEP3 and 3LSYM. Or low glutamine induces 3LSYM expression by another route. 3LysM induces virulence. b) During nitrogen replete conditions high levels of NH_4^+ are converted to glutamine by GS in WT cells. Sufficient glutamine levels activate the TOR pathway and inhibit AREA expression. GLN1, MEP2, MEP3 AND 3LSYM are not transcriptionally induced. Virulence is not induced in Z. tritici. c) During nitrogen limiting or replete conditions Ztmep2Δ/Ztmep3Δ* cells are starved of *NH_4^+, thus, glutamine levels are very (v) low. Low levels of glutamine induce transcription of AREA which induces transcription of GLN1 and 3LSYM. Or low glutamine induces 3LSYM expression by another route. 3LysM induces hypervirulence. Lines with arrow heads indicate a positive relationship whereas T-lines represent inhibition.*

5.1.2 Cryptococcus neoformans hyphal growth is transceptor regulated

Amt2 is a transceptor in the H99/KN99 strain which controls mating and invasive growth in response to limiting ammonium (Rutherford *et al.*, 2008b). In this study we have identified an new phenotype governed by Amt2 in the JEC20/JEC21 strain. Hyphal growth exhibited by *C. neoformans* JEC20/JEC21, during a confrontation assay under ammonium limiting conditions, is dependent on the ammonium permease Amt2. Moreover, Amt2 controls hyphal growth exhibited by JEC21 in the absence of JEC20 in a low ammonium fruiting assay and Amt2 promotes invasive growth in both assays under the same conditions. Consistent with the H99/KN99 strain, *AMT2* expression is under the control of NCR. A mutation in Amt2, N241A, which uncouples transport from signalling, when expressed in *S. cerevisiae*, is consistent with the equivalent mutation, N246A in ScMep2 (Van Nuland *et al.*, 2006). This suggests that CnAmt2 and ScMep2 may be working mechanistically in the same way.

The underlying signalling mechanisms adopted by the ammonium transceptors is currently unknown, however, two models have been proposed. The conformational change model hypothesises that transport of ammonium induces a conformational change in the transporter, analogous to a G-protein coupled receptor, allowing the transporter to interact, or disengage interaction, with a downstream signalling partner (Rutherford *et al.*, 2008a). The pH model proposes that following NH_4^+ deprotonation, to NH_3 gas, the route the proton follows may impact on internal pH triggering a pH sensitive, filamentation inducing, signalling cascade (Wacker *et al.*, 2014) (Boeckstaens *et al.*, 2008). The N241A separation of function allele identified in CnAmt2 is located at an equivalent position to the proposed deprotonation site. N246A in ScMep2 likewise uncouples transport from signalling, thus, this is a conserved signalling residue (Van Nuland *et al.*, 2006). The transport mechanism adopted by ammonium transceptors is also unknown. The transported substrate could be NH_3, NH_4^+ or NH_3/H^+ symport, where the latter two would establish an electrogenic transport mechanism. Asparagine 241 in CnAmt2 could be essential in directing the pathway the proton follows succeeding deprotonation. If the transport mechanism is electroneutral, as has been confirmed for human RhCG (Baday *et al.*, 2015), the proton would leave CnAmt2 on the extracellular side. This would result in the NH_3 gas being solely imported into the cytosol where it would acquire a proton to form NH_4^+. This acquisition of a proton would, therefore, raise the cytosolic pH which could activate or

deactivate a pH responsive pathway. If transport is electroneutral, the N241A allele may direct the excess proton through the pore to combine with NH_3 to reconstitute NH_4^+. This would not result in a change in internal pH as the necessity to acquire a proton from the cytosol would be lacking. Another possibility is that the N241A mutation causes the NH_4^+ deprotonation event to be bypassed completely. In support of the conformational change model, perhaps the deprotonation event leads to a conformational change in the transporter or maybe relay of the excess proton, by the twin-histidine motif, induces a conformational change. The twin-histidine motif forms a charge delocalised structure (Wang *et al.*, 2012). During proton relay, the charge across the twin-histidine motif alters and could, thus, alter interactions with neighbouring residues which may incur a conformational change. If ammonium signalling occurs via the conformational change model, perhaps the N241A mutation prevents the relay of the excess proton by the twin-histidine motif resulting in no conformational change. Whichever signalling model is correct, the proposed deprotonation site is likely crucial for signalling by ScMep2 and CnAmt2.

5.2 Comparison between ammonium signalling in *Z. tritici* and *C. neoformans*

Deletion of ZtMep3 in *Z. tritici* does not abolish filamentation, however, ZtMep3 does complement the pseudohyphal growth defect of a *S. cerevisiae* strain lacking Mep2; as does CnAmt2. CnAmt2, alike with ScMep2, and all other identified ammonium sensors, to date, possesses the conserved twin-histidine motif; ZtMep3 does not. Glutamate is instead found at the equivalent position, in ZtMep3, to the first conserved histidine, which is comparable to the non-signalling homologues, ScMep1 and ScMep3. In ScMep2, substitution of the first histidine to glutamate blocks pseudohyphal growth but sustains transport which would suggest that the first histidine is functionally important for signalling (Boeckstaens *et al.*, 2008). The ability of ZtMep3 to work as an ammonium sensor, therefore, contradicts this theory. Furthermore, the expression level of CnAmt2 is comparable to the expression level of ScMep2, whereas, ZtMep3 is poorly expressed. A reduction in Mep2 protein expression is correlated with a reduction in filamentous growth (Biswas and Morschhauser, 2005). This poses the question how can ZtMep3 complement pseudohyphal growth when it does not possess the twin-histidine motif and is expressed to a low level? Pseudohyphal growth is a

process which occurs exclusively during ammonium limitation and not during ammonium starvation or ammonium replete conditions (Lorenz and Heitman, 1998) (Marini *et al.*, 1997) (Rutherford *et al.*, 2008a). Notably, the G349C allele is hyperactive in ScMep2 but slightly less active in CaMep2. ScMep2^{G349C} results in enhanced pseudohyphal growth in *S. cerevisiae* but CaMep2^{G349C} abolishes filamentation in *C. albicans* (Boeckstaens *et al.*, 2007) (Neuhauser *et al.*, 2011) suggesting that there could be a fine balance between too much or not enough ammonium entering the cell. Although not determined, the glutamate-histidine motif, together with the growth defect of the single *ztmep3Δ* mutants, suggest that ZtMep3 is the high capacity, low affinity transporter. If the balance between transport activity and expression is crucial in signalling for pseudohyphal growth, the high transport activity of ZtMep3 may compensate for its low protein expression resulting in the import of an inducing concentration of ammonium. This is consistent with minimal filamentation being induced in *C. albicans* by CaMep1 when placed under the control of the *CaMEP2* promoter; *CaMEP1* contains the glutamate-histidine motif. Northern analysis of *CaMEP1* and *CaMEP2* found *CaMEP2* to be highly expressed when grown in ≤10 mM ammonium, whereas *CaMEP1* was expressed to levels below the limit of detection. As CaMep1 could support growth of a strain lacking both functional ammonium transporters it was concluded that *CaMEP1* must have been expressed in these conditions to support growth. Thus, the *CaMEP2* promoter is more strongly induced during ammonium limitation. It was, therefore, anticipated that the expression of *CaMEP1*, under the control of the *CaMEP2* promoter, would be increased resulting in increased protein expression (Biswas and Morschhauser, 2005). Equally, substitution of the first histidine to glutamate in ScMep2 (H194E), to mimic ScMep1, incurred higher transport rates than WT ScMep2 but failed to induce pseudohyphal growth. ScMep1 was expressed to lower levels than ScMep2 but was more active (Boeckstaens *et al.*, 2008) (Marini *et al.*, 1997). The increase in expression of *CaMEP1*, incurred by being controlled by the *CaMEP2* promoter, could lead to more ammonium being imported bringing the concentration of ammonium into a range which supports pseudohyphal growth. Whereas, an increase in the activity of ScMep2, incurred by the H194E mutation, may push the concentration of imported ammonium above the optimum threshold for pseudohyphal growth to occur. The reason that ScMep2^{G349C} induced pseudohyphal growth, despite being hyperactive, may be because it has a lower V_{max} than ScMep2^{H194E} and is, thus, a lower capacity transporter (Boeckstaens *et al.*, 2007) (Marini and André, 2000). Perhaps the extra imported ammonium by ScMep2^{G349C}

does not push the concentration of imported ammonium above the optimum threshold. The K_m and V_{max} values published in other literature, which indicate affinity and capacity respectively, are listed in (**Table 20**).

Plasmid	**V_{max}** nmol min^{-1} mg^{-1} protein	**K_m** mM
YCp $Mep2^{N4Q}$	18.1[a]	0.6[a]
YCp $Mep2^{N4Q,G349C}$	55.8 ± 0.8[b]	1.12 ± 0.04[b]
YCp $Mep2^{H194E}$	64.0 ± 1.7[c]	3.46 ± 0.44[c]

***Table 20: Kinetic parameters of Mep2 variants**. The mep123Δ strain was transformed with the Mep2 variant plasmids listed. [^{14}C]-methylammonium uptakes rates, ranging from 0.1 – 5 mM were measured. Experiments were performed in duplicate. The measured values from both experiments were averaged to calculate V_{max} and K_m. All values listed are taken from the following literature. [a] values from (Marini and André, 2000), [b] values from (Boeckstaens et al., 2007), and [c] values from (Boeckstaens et al., 2008).*

Our findings, along with previously published results, allow us to propose that if the expression and transport activity levels of an ammonium permease are correctly balanced, so that an inducing concentration of ammonium is imported, any ammonium permease, from any organism, has the potential to function as an ammonium sensor. This theory favours the pH model of signalling. Moreover, the twin-histidine motif does not appear to be a defining feature of an ammonium sensor. A graphical representation of this model, where CnAmt2 and ZtMep3 are used as examples, is depicted in (**Figure 90**).

The transport activity of ZtMep3 and CnAmt2 is Npr1 kinase independent when expressed in yeast. As *Z. tritici* and *C. neoformans* are ubiquitous in the environment (Steinberg, 2015) (Gugnani *et al.*, 2005), they will frequently experience temperatures lower than 30 °C, the temperature the growth assays were incubated at. Npr1 kinase is indispensable for CaMep2 transport activity at 30 °C, but dispensable for transport at the higher temperature of 37 °C (Neuhauser *et al.*, 2011). As temperature impacts on the dependence on Npr1 kinase in CaMep2, the same may be occurring in ZtMep3 and CnAmt2 at 30 °C. In ScMep2, phosphorylation by Npr1 kinase causes conformational changes in the CTR which alleviates the autoinhibition of the AI domain (Boeckstaens *et al.*, 2014) (van den Berg *et al.*, 2016). The higher temperature, 30 °C, may impact on the conformation of ZtMep3 and CnAmt2 and/or the fluidity of their

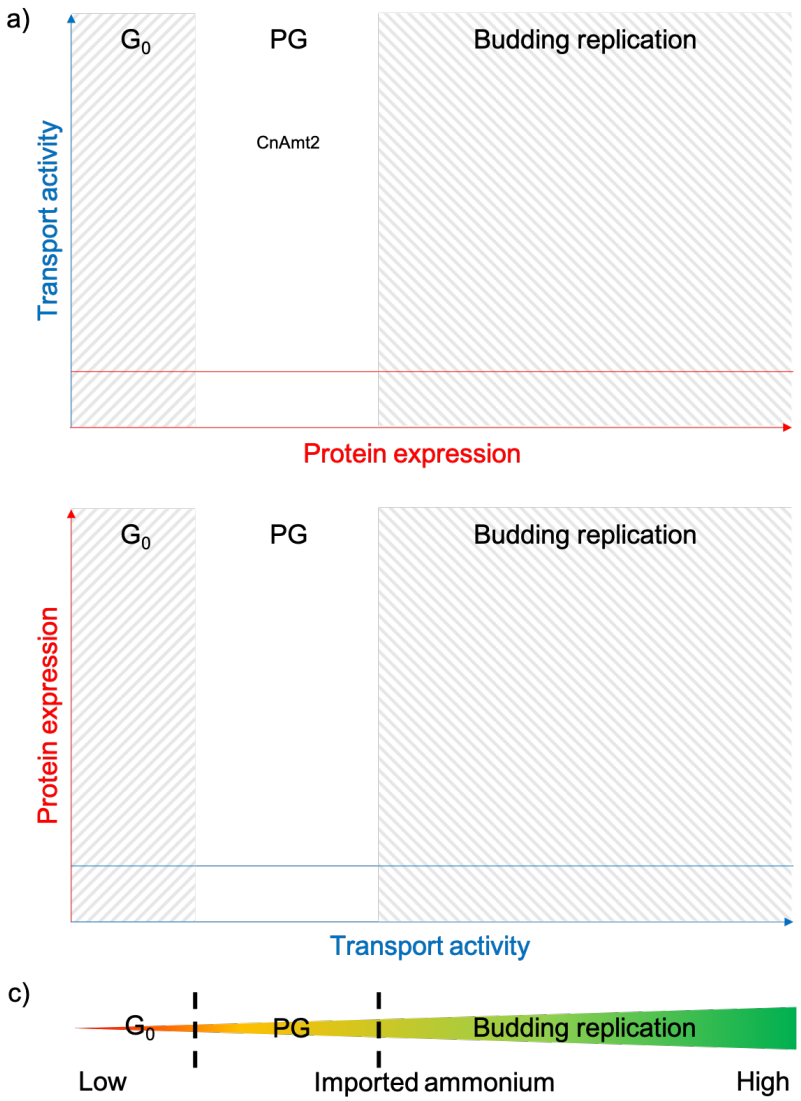

Figure 90: Graphical representation of ammonium signalling model based on the balance between transport activity and expression. *a) Increased expression of an ammonium transporter could compensate for its low activity, for example CnAmt2. b) Increased activity of an ammonium transporter could compensate for its low expression, for example ZtMep3. Transport activity is coloured blue and protein expression is coloured red. The colour of the line on the graph indicates the factor which is changing. Right slanted grey lines represent growth arrest (G_0) as a result of too little ammonium entering the cell. Left slanted grey lines represent replete ammonium conditions which induces budding replication. No grey lines represents ammonium limitation which induces pseudohyphal growth (PG). c) Concentration of imported ammonium based on the graphs above. The concentration of imported ammonium dictates the type of growth or lack of growth.*

transporting pores. If so, this could potentially prevent signalling; especially if signalling is dependent on the amount of ammonium entering the cell as this could alter transport rates. Thus, ammonium permeases could be rejected as ammonium sensors solely on experiments in yeast. This strengthens the notion that investigating ammonium permeases in *S. cerevisiae* may not be an appropriate strategy, or at least that experiments should additionally be performed natively.

5.3 Conclusion

In this study ammonium signalling has been investigated in two divergent fungi. We have identified a new phenotype regulated by CnAmt2 and discovered a new ammonium sensor ZtMep3. ZtMep3 regulates pseudohyphal growth in yeast but we cannot conclude that this regulates filamentation in *Z. tritici*; it is possible that ZtMep3 regulates a different process natively. In *C. neoformans* JEC20/JEC21, CnAmt2 is responsible for inducing the hyphal growth exhibited in the confrontation and fruiting assays on low ammonium. Moreover, CnAmt2 promotes invasive growth under the same conditions. In *Z. tritici*, nitrogen starvation, acquired by the lack of both functional ammonium permeases, induces hypervirulence. Virulence in the phytopathogen *F. oxysporum*, is also triggered by nitrogen starvation, however, glutamine, the product of ammonium metabolism catalysed by glutamine synthetase, is the sensed molecule (López-Berges *et al.*, 2010). Thus, we propose that a lack of internal ammonium metabolism may be the signal for virulence in *Z. tritici*. All identified ammonium transceptors, to date, contain the twin-histidine motif and, thus, this histidine pair was believed to be essential for signalling ammonium permeases (Boeckstaens *et al.*, 2008). As ZtMep3 can complement the pseudohyphal growth defect of a diploid *S. cerevisiae* strain lacking Mep2 (*mep2Δ/mep2Δ*), despite lacking the conserved twin-histidine motif, the twin-histidine motif is not a distinguishing feature of an ammonium sensor. Furthermore, we propose that any ammonium permease has the potential to complement the pseudohyphal growth defect of the *mep2Δ/mep2Δ* strain if the transport activity and expression levels are correctly balanced so that an inducing concentration of ammonium is imported into the cell to trigger a signalling cascade. Thus, studying ammonium permeases in *S. cerevisiae* may not be an appropriate strategy. Instead, research into these proteins should be performed natively. No investigations have been undertaken to establish whether transport by either transceptor is electroneutral or electrogenic. Crystal structures of both proteins, along

with molecular simulation studies, voltage clamp electrophysiology studies and N isotope discrimination experiments, would aid in determining the transported substrates and in establishing the underlying signalling mechanisms. The reasons why *C. neoformans* chooses to regulate filamentation, during nitrogen limitation, via a transceptor mediated process, while *Z. tritici* responds to nitrogen starvation by inducing virulence is unknown. However, whether ammonium availability is sensed by a transceptor on the surface of the cell or sensed internally, after ammonium metabolism, ammonium availability directs important developmental processes in both organisms. By investigating ammonium signalling in other fungi we will gain an understanding in how prevalent and conserved these starvation responses are and why different organisms adopt different modes of ammonium signalling.

6 References

Acosta, M.J., Marchal, J.A., Fernandez-Espartero, C.H., Bullejos, M. and Sanchez, A. (2008) 'Retroelements (LINEs and SINEs) in vole genomes: differential distribution in the constitutive heterochromatin', *Chromosome Res*, 16(7), pp. 949-59.

Akashi, H. (1994) 'Synonymous codon usage in *Drosophila melanogaster:* natural selection and translational accuracy', *Genetics*, 136(3), pp. 927-35.

Amara, I., Miled, W., Slama, R.B. and Ladhari, N. (2018) 'Antifouling processes and toxicity effects of antifouling paints on marine environment. A review', *Environ Toxicol Pharmacol*, 57, pp. 115-130.

An, G., Ebert, P., Mitra, A. and Ha, S. (1988) 'Binary vectors, pA3/1–19', *Plant molecular biology manual. Kluwer, Dordrecht*.

Analía Edith Perelló, M.V.M., Cecilia Mónaco, María Rosa Simón, Cristina Cordo, (2009) 'Biological control of Septoria tritici blotch on wheat by *Trichoderma spp*. under field conditions in Argentina', *BioControl*, 54(1), pp. 113–122.

Andrade, S.L., Dickmanns, A., Ficner, R. and Einsle, O. (2005) 'Crystal structure of the archaeal ammonium transporter Amt-1 from *Archaeoglobus fulgidus*', *Proc Natl Acad Sci U S A*, 102(42), pp. 14994-9.

Andrade, S.L.A. and Einsle, O. (2007) 'The Amt/Mep/Rh family of ammonium transport proteins (Review)', *Molecular Membrane Biology*, 24(5-6), pp. 357-365.

Antonenko, Y.N., Pohl, P. and Denisov, G.A. (1997) 'Permeation of ammonia across bilayer lipid membranes studied by ammonium ion selective microelectrodes', *Biophys J*, 72(5), pp. 2187-95.

Ariz, I., Boeckstaens, M., Gouveia, C., Martins, A.P., Sanz-Luque, E., Fernández, E., Soveral, G., von Wirén, N., Marini, A.M., Aparicio-Tejo, P.M. and Cruz, C. (2018) 'Nitrogen isotope signature evidences ammonium deprotonation as a common transport mechanism for the AMT-Mep-Rh protein superfamily', *Science Advances*, 4(9), p. eaar3599.

Arora, S., Olszewski, M.A., Tsang, T.M., McDonald, R.A., Toews, G.B. and Huffnagle, G.B. (2011) 'Effect of cytokine interplay on macrophage polarization during chronic pulmonary infection with Cryptococcus neoformans', *Infect Immun*, 79(5), pp. 1915-26.

Atkinson, M.R. and Ninfa, A.J. (1998) 'Role of the GlnK signal transduction protein in the regulation of nitrogen assimilation in Escherichia coli', *Molecular Microbiology*, 29(2), pp. 431-447.

Atkinson, M.R. and Ninfa, A.J. (1999) 'Characterization of the GlnK protein of *Escherichia coli*', *Molecular Microbiology*, 32(2), pp. 301-313.

Baday, S., Orabi, Esam A., Wang, S., Lamoureux, G. and Bernèche, S. (2015) 'Mechanism of NH_4^+ Recruitment and NH_3 Transport in Rh Proteins', *Structure*, 23(8), pp. 1550-1557.

Bar-Peled, L., Chantranupong, L., Cherniack, A.D., Chen, W.W., Ottina, K.A., Grabiner, B.C., Spear, E.D., Carter, S.L., Meyerson, M. and Sabatini, D.M. (2013) 'A Tumor suppressor complex with GAP activity for the Rag GTPases that signal amino acid sufficiency to mTORC1', *Science*, 340(6136), pp. 1100-6.

Barbet, N.C., Schneider, U., Helliwell, S.B., Stansfield, I., Tuite, M.F. and Hall, M.N. (1996) 'TOR controls translation initiation and early G1 progression in yeast', *Mol Biol Cell*, 7(1), pp. 25-42.

Barrett-Bee, K., Hayes, Y., Wilson, R.G. and Ryley, J.F. (1985) 'A comparison of phospholipase activity, cellular adherence and pathogenicity of yeasts', *J Gen Microbiol*, 131(5), pp. 1217-21.

Barwell, K.J., Boysen, J.H., Xu, W. and Mitchell, A.P. (2005) 'Relationship of DFG16 to the Rim101p pH Response Pathway in *Saccharomyces cerevisiae* and *Candida albicans*', *Eukaryotic Cell*, 4(5), p. 890.

Beck, T. and Hall, M.N. (1999) 'The TOR signalling pathway controls nuclear localization of nutrient-regulated transcription factors', *Nature*, 402(6762), pp. 689-92.
Bennett, R.J. and Turgeon, B.G. (2016) 'Fungal Sex: The Ascomycota', *Microbiol Spectr*, 4(5).

Bertram, P.G., Choi, J.H., Carvalho, J., Ai, W., Zeng, C., Chan, T.F. and Zheng, X.F. (2000) 'Tripartite regulation of Gln3p by TOR, Ure2p, and phosphatases', *J Biol Chem*, 275(46), pp. 35727-33.

Binda, M., Peli-Gulli, M.P., Bonfils, G., Panchaud, N., Urban, J., Sturgill, T.W., Loewith, R. and De Virgilio, C. (2009) 'The Vam6 GEF controls TORC1 by activating the EGO complex', *Mol Cell*, 35(5), pp. 563-73.

Biswas, K. and Morschhauser, J. (2005) 'The Mep2p ammonium permease controls nitrogen starvation-induced filamentous growth in *Candida albicans*', *Mol Microbiol*, 56(3), pp. 649-69.

Biswas, S., Van Dijck, P. and Datta, A. (2007) 'Environmental Sensing and Signal Transduction Pathways Regulating Morphopathogenic Determinants of *Candida albicans*', *Microbiology and Molecular Biology Reviews*, 71(2), p. 348.

Boeckstaens, M., Andre, B. and Marini, A.M. (2008) 'Distinct transport mechanisms in yeast ammonium transport/sensor proteins of the Mep/Amt/Rh family and impact on filamentation', *J Biol Chem*, 283(31), pp. 21362-70.

Boeckstaens, M., André, B. and Marini, A.M. (2007) 'The yeast ammonium transport protein Mep2 and its positive regulator, the Npr1 kinase, play an important role in normal and pseudohyphal growth on various nitrogen media through retrieval of excreted ammonium', *Molecular Microbiology*, 64(2), pp. 534-546.

Boeckstaens, M., Llinares, E., Van Vooren, P. and Marini, A.M. (2014) 'The TORC1 effector kinase Npr1 fine tunes the inherent activity of the Mep2 ammonium transport protein', *Nat Commun*, 5, p. 3101.

Boeckstaens, M., Merhi, A., Llinares, E., Van Vooren, P., Springael, J.-Y., Wintjens, R. and Marini, A.M. (2015) 'Identification of a Novel Regulatory Mechanism of Nutrient Transport Controlled by TORC1-Npr1-Amu1/Par32', *PLoS genetics*, 11(7), pp. e1005382-e1005382.

Boer, V.M., Tai, S.L., Vuralhan, Z., Arifin, Y., Walsh, M.C., Piper, M.D., de Winde, J.H., Pronk, J.T. and Daran, J.M. (2007) 'Transcriptional responses of *Saccharomyces cerevisiae* to preferred and nonpreferred nitrogen sources in glucose-limited chemostat cultures', *FEMS Yeast Res*, 7(4), pp. 604-20.

Botts, M.R., Giles, S.S., Gates, M.A., Kozel, T.R. and Hull, C.M. (2009) 'Isolation and characterization of *Cryptococcus neoformans* spores reveal a critical role for capsule biosynthesis genes in spore biogenesis', *Eukaryot Cell*, 8(4), pp. 595-605.

Boyd, C.A. (1979) 'Chemical neurotransmission: an hypothesis concerning the evolution of neurotransmitter substances', *J Theor Biol*, 76(4), pp. 415-7.

Brizendine, K.D., Baddley, J.W. and Pappas, P.G. (2011) 'Pulmonary cryptococcosis', *Semin Respir Crit Care Med*, 32(6), pp. 727-34.

Broach, J.R. (2012) 'Nutritional control of growth and development in yeast', *Genetics*, 192(1), pp. 73-105.

Caddick, M.X., Arst, H.N., Jr., Taylor, L.H., Johnson, R.I. and Brownlee, A.G. (1986) 'Cloning of the regulatory gene areA mediating nitrogen metabolite repression in *Aspergillus nidulans*', *Embo j*, 5(5), pp. 1087-90.

Cardenas, M.E., Cutler, N.S., Lorenz, M.C., Di Como, C.J. and Heitman, J. (1999) 'The TOR signaling cascade regulates gene expression in response to nutrients', *Genes & development*, 13(24), pp. 3271-3279.

Charlier, C., Nielsen, K., Daou, S., Brigitte, M., Chretien, F. and Dromer, F. (2009) 'Evidence of a role for monocytes in dissemination and brain invasion by *Cryptococcus neoformans*', *Infect Immun*, 77(1), pp. 120-7.

Chen, L.C., Pirofski, L.A. and Casadevall, A. (1997) 'Extracellular proteins of *Cryptococcus neoformans* and host antibody response', *Infection and Immunity*, 65(7), p. 2599.

Chen, T.L. and Manuelidis, L. (1989) 'SINEs and LINEs cluster in distinct DNA fragments of Giemsa band size', *Chromosoma*, 98(5), pp. 309-16.

Chen, Y., Farrer, R.A., Giamberardino, C., Sakthikumar, S., Jones, A., Yang, T., Tenor, J.L., Wagih, O., Van Wyk, M., Govender, N.P., Mitchell, T.G., Litvintseva, A.P., Cuomo, C.A. and Perfect, J.R. (2017) 'Microevolution of Serial Clinical Isolates of *Cryptococcus neoformans var. grubii* and *C. gattii*', *MBio*, 8(2).

Chothia, C. and Lesk, A.M. (1986) 'The relation between the divergence of sequence and structure in proteins', *The EMBO journal*, 5(4), pp. 823-826.

Chrisman, C.J., Albuquerque, P., Guimaraes, A.J., Nieves, E. and Casadevall, A. (2011) 'Phospholipids trigger *Cryptococcus neoformans* capsular enlargement during interactions with amoebae and macrophages', *PLoS Pathog*, 7(5), p. e1002047.

Cimprich, P., Slavík, J. and Kotyk, A. (1995) 'Distribution of individual cytoplasmic pH values in a population of the yeast *Saccharomyces cerevisiae*', *FEMS Microbiology Letters*, 130(2-3), pp. 245-251.

Coffman, J.A., Rai, R., Cunningham, T., Svetlov, V. and Cooper, T.G. (1996) 'Gat1p, a GATA family protein whose production is sensitive to nitrogen catabolite repression, participates in transcriptional activation of nitrogen-catabolic genes in *Saccharomyces cerevisiae*', *Mol Cell Biol*, 16(3), pp. 847-58.

Cogliati, M., D'Amicis, R., Zani, A., Montagna, M.T., Caggiano, G., De Giglio, O., Balbino, S., De Donno, A., Serio, F., Susever, S., Ergin, C., Velegraki, A., Ellabib, M.S., Nardoni, S., Macci, C., Oliveri, S., Trovato, L., Dipineto, L., Rickerts, V., McCormick-Smith, I., Akcaglar, S., Tore, O., Mlinaric-Missoni, E., Bertout, S., Mallié, M., Martins, M.d.L., Vencà, A.C.F., Vieira, M.L., Sampaio, A.C., Pereira, C., Criseo, G., Romeo, O., Ranque, S., Al-Yasiri, M.H.Y., Kaya, M., Cerikcioglu, N., Marchese, A., Vezzulli, L., Ilkit, M., Desnos-Ollivier, M., Pasquale, V., Korem, M., Polacheck, I., Scopa, A., Meyer, W., Ferreira-Paim, K., Hagen, F., Theelen, B., Boekhout, T., Lockhart, S.R., Tintelnot, K., Tortorano, A.M., Dromer, F., Varma, A., Kwon-Chung, K.J., Inácio, J., Alonso, B. and Colom, M.F. (2016) 'Environmental distribution of *Cryptococcus neoformans* and *C. gattii* around the Mediterranean basin', *FEMS Yeast Research*, 16(4).

Cohen, L. and Eyal, Z. (1993) 'The histology of processes associated with the infection of resistant and susceptible wheat cultivars with *Septoria tritici*', *Plant Pathology*, 42(5), pp. 737-743.

Coleman, M., Henricot, B., Arnau, J. and Oliver, R.P. (1997) 'Starvation-induced genes of the tomato pathogen *Cladosporium fulvum* are also induced during growth in planta', *Mol Plant Microbe Interact*, 10(9), pp. 1106-9.

Collopy-Junior, I., Esteves, F.F., Nimrichter, L., Rodrigues, M.L., Alviano, C.S. and Meyer-Fernandes, J.R. (2006) 'An ectophosphatase activity in *Cryptococcus neoformans*', *FEMS Yeast Res*, 6(7), pp. 1010-7.

Coster, J., McCauley, R. and Hall, J. (2004) 'Glutamine: metabolism and application in nutrition support', *Asia Pac J Clin Nutr*, 13(1), pp. 25-31.

Courchesne, W.E. and Magasanik, B. (1988) 'Regulation of nitrogen assimilation in *Saccharomyces cerevisiae*: roles of the URE2 and GLN3 genes', *J Bacteriol*, 170(2), pp. 708-13.

Cousin, A., Mehrabi, R., Guilleroux, M., Dufresne, M., T, V.D.L., Waalwijk, C., Langin, T. and Kema, G.H. (2006) 'The MAP kinase-encoding gene MgFus3 of the non-appressorium phytopathogen *Mycosphaerella graminicola* is required for penetration and in vitro pycnidia formation', *Mol Plant Pathol*, 7(4), pp. 269-78.

Crabtree, J.N., Okagaki, L.H., Wiesner, D.L., Strain, A.K., Nielsen, J.N. and Nielsen, K. (2012) 'Titan Cell Production Enhances the Virulence of *Cryptococcus neoformans*', *Infection and Immunity*, 80(11), p. 3776.

Crespo, J.L., Helliwell, S.B., Wiederkehr, C., Demougin, P., Fowler, B., Primig, M. and Hall, M.N. (2004) 'NPR1 kinase and RSP5-BUL1/2 ubiquitin ligase control GLN3-dependent transcription in *Saccharomyces cerevisiae*', *J Biol Chem*, 279(36), pp. 37512-7.

Cross, C.E. and Bancroft, G.J. (1995) 'Ingestion of acapsular *Cryptococcus neoformans* occurs via mannose and beta-glucan receptors, resulting in cytokine production and increased phagocytosis of the encapsulated form', *Infect Immun*, 63(7), pp. 2604-11.

Cueto-Rojas, H.F., Milne, N., van Helmond, W., Pieterse, M.M., van Maris, A.J.A., Daran, J.-M. and Wahl, S.A. (2017) 'Membrane potential independent transport of NH(3) in the absence of ammonium permeases in *Saccharomyces cerevisiae*', *BMC systems biology*, 11(1), pp. 49-49.

Cullen, P.J. and Sprague, G.F., Jr. (2012) 'The regulation of filamentous growth in yeast', *Genetics*, 190(1), pp. 23-49.

Cunningham, T.S., Svetlov, V.V., Rai, R., Smart, W. and Cooper, T.G. (1996) 'G1n3p is capable of binding to UAS(NTR) elements and activating transcription in *Saccharomyces cerevisiae*', *J Bacteriol*, 178(12), pp. 3470-9.

Dabas, N. and Morschhauser, J. (2007) 'Control of ammonium permease expression and filamentous growth by the GATA transcription factors GLN3 and GAT1 in *Candida albicans*', *Eukaryot Cell*, 6(5), pp. 875-88.

Dambuza, I.M., Drake, T., Chapuis, A., Zhou, X., Correia, J., Taylor-Smith, L., LeGrave, N., Rasmussen, T., Fisher, M.C., Bicanic, T., Harrison, T.S., Jaspars, M., May, R.C., Brown, G.D., Yuecel, R., MacCallum, D.M. and Ballou, E.R. (2018) 'The *Cryptococcus neoformans* Titan cell is an inducible and regulated morphotype underlying pathogenesis', *PLoS Pathog*, 14(5), p. e1006978.

Day, P.R. and Anagnostakis, S.L. (1971) 'Corn Smut Dikaryon in Culture', *Nature New Biology*, 231(18), pp. 19-20.

De Craene, J.O., Soetens, O. and Andre, B. (2001) 'The Npr1 kinase controls biosynthetic and endocytic sorting of the yeast Gap1 permease', *J Biol Chem*, 276(47), pp. 43939-48.

Dean, R., Van Kan, J.A., Pretorius, Z.A., Hammond-Kosack, K.E., Di Pietro, A., Spanu, P.D., Rudd, J.J., Dickman, M., Kahmann, R., Ellis, J. and Foster, G.D. (2012) 'The Top 10 fungal pathogens in molecular plant pathology', *Mol Plant Pathol*, 13(4), pp. 414-30.

Dechant, R., Binda, M., Lee, S.S., Pelet, S., Winderickx, J. and Peter, M. (2010) 'Cytosolic pH is a second messenger for glucose and regulates the PKA pathway through V-ATPase', *Embo j*, 29(15), pp. 2515-26.

Decken, K., Kohler, G., Palmer-Lehmann, K., Wunderlin, A., Mattner, F., Magram, J., Gately, M.K. and Alber, G. (1998) 'Interleukin-12 is essential for a protective Th1 response in mice infected with *Cryptococcus neoformans*', *Infect Immun*, 66(10), pp. 4994-5000.

Deising, H.B., Werner, S. and Wernitz, M. (2000) 'The role of fungal appressoria in plant infection', *Microbes Infect*, 2(13), pp. 1631-41.

Deschuyteneer, A., Boeckstaens, M., De Mees, C., Van Vooren, P., Wintjens, R. and Marini, A.M. (2013) 'SNPs altering ammonium transport activity of human Rhesus factors characterized by a yeast-based functional assay', *PLoS One*, 8(8), p. e71092.

Dhillon, B., Gill, N., Hamelin, R.C. and Goodwin, S.B. (2014) 'The landscape of transposable elements in the finished genome of the fungal wheat pathogen *Mycosphaerella graminicola*', *BMC genomics*, 15(1), pp. 1132-1132.

Di Como, C.J. and Arndt, K.T. (1996) 'Nutrients, via the Tor proteins, stimulate the association of Tap42 with type 2A phosphatases', *Genes Dev*, 10(15), pp. 1904-16.

Didion, T., Regenberg, B., Jorgensen, M.U., Kielland-Brandt, M.C. and Andersen, H.A. (1998) 'The permease homologue Ssy1p controls the expression of amino acid and peptide transporter genes in *Saccharomyces cerevisiae*', *Mol Microbiol*, 27(3), pp. 643-50.

Divon, H.H., Ziv, C., Davydov, O., Yarden, O. and Fluhr, R. (2006) 'The global nitrogen regulator, FNR1, regulates fungal nutrition-genes and fitness during *Fusarium oxysporum* pathogenesis', *Mol Plant Pathol*, 7(6), pp. 485-97.

Donaton, M.C., Holsbeeks, I., Lagatie, O., Van Zeebroeck, G., Crauwels, M., Winderickx, J. and Thevelein, J.M. (2003) 'The Gap1 general amino acid permease acts as an amino acid sensor for activation of protein kinase A targets in the yeast *Saccharomyces cerevisiae*', *Mol Microbiol*, 50(3), pp. 911-29.

Duba, A., Goriewa-Duba, K. and Wachowska, U. (2018) 'A Review of the Interactions between Wheat and Wheat Pathogens: *Zymoseptoria tritici*, *Fusarium spp*. and *Parastagonospora nodorum*', *Int J Mol Sci*, 19(4).

Duncan, K.E. and Howard, R.J. (2000) 'Cytological analysis of wheat infection by the leaf blotch pathogen *Mycosphaerella graminicola*', *Mycological Research*, 104(9), pp. 1074-1082.

Elion, E.A., Grisafi, P.L. and Fink, G.R. (1990) 'FUS3 encodes a cdc2+/CDC28-related kinase required for the transition from mitosis into conjugation', *Cell*, 60(4), pp. 649-64.

Emerson, K., Russo, R.C., Lund, R.E. and Thurston, R.V. (1975) 'Aqueous Ammonia Equilibrium Calculations: Effect of pH and Temperature', *Journal of the Fisheries Research Board of Canada*, 32(12), pp. 2379-2383.

Eraso, P. and Gancedo, C. (1987) 'Activation of yeast plasma membrane ATPase by acid pH during growth', *FEBS Lett*, 224(1), pp. 187-92.

Fernandes, J.D.S., Martho, K., Tofik, V., Vallim, M.A. and Pascon, R.C. (2015) 'The Role of Amino Acid Permeases and Tryptophan Biosynthesis in *Cryptococcus neoformans* Survival', *PLOS ONE*, 10(7), p. e0132369.

Forsberg, H. and Ljungdahl, P.O. (2001) 'Sensors of extracellular nutrients in *Saccharomyces cerevisiae*', *Curr Genet*, 40(2), pp. 91-109.

Fu, J., Morris, I.R. and Wickes, B.L. (2013) 'The production of monokaryotic hyphae by Cryptococcus neoformans can be induced by high temperature arrest of the cell cycle and is independent of same-sex mating', *PLoS Pathog*, 9(5), p. e1003335.

Fu, M.S., Coelho, C., De Leon-Rodriguez, C.M., Rossi, D.C.P., Camacho, E., Jung, E.H., Kulkarni, M. and Casadevall, A. (2018) '*Cryptococcus neoformans* urease affects the outcome of intracellular pathogenesis by modulating phagolysosomal pH', *PLoS Pathog*, 14(6), p. e1007144.

Fu, Y.H. and Marzluf, G.A. (1990) 'nit-2, the major positive-acting nitrogen regulatory gene of *Neurospora crassa*, encodes a sequence-specific DNA-binding protein', *Proc Natl Acad Sci U S A*, 87(14), pp. 5331-5.

Gazzoni, A.F., Severo, C.B., Barra, M.B. and Severo, L.C. (2009) 'Atypical micromorphology and uncommon location of cryptococcosis: a histopathologic study using special histochemical techniques (one case report)', *Mycopathologia*, 167(4), pp. 197-202.

Georis, I., Tate, J.J., Cooper, T.G. and Dubois, E. (2011) 'Nitrogen-responsive regulation of GATA protein family activators Gln3 and Gat1 occurs by two distinct pathways, one inhibited by rapamycin and the other by methionine sulfoximine', *The Journal of biological chemistry*, 286(52), pp. 44897-44912.

Gerstein, A.C., Fu, M.S., Mukaremera, L., Li, Z., Ormerod, K.L., Fraser, J.A., Berman, J. and Nielsen, K. (2015) 'Polyploid Titan Cells Produce Haploid and Aneuploid Progeny To Promote Stress Adaptation', *mBio*, 6(5), pp. e01340-15.

Giles, S.S., Zaas, A.K., Reidy, M.F., Perfect, J.R. and Wright, J.R. (2007) '*Cryptococcus neoformans* is resistant to surfactant protein A mediated host defense mechanisms', *PLoS One*, 2(12), p. e1370.

Giots, F., Donaton, M.C. and Thevelein, J.M. (2003) 'Inorganic phosphate is sensed by specific phosphate carriers and acts in concert with glucose as a nutrient signal for activation of the protein kinase A pathway in the yeast *Saccharomyces cerevisiae'*, *Mol Microbiol*, 47(4), pp. 1163-81.

Girard, L. and Freeling, M. (1999) 'Regulatory changes as a consequence of transposon insertion', *Dev Genet*, 25(4), pp. 291-6.

Gisi, U., Sierotzki, H., Cook, A. and McCaffery, A. (2002) 'Mechanisms influencing the evolution of resistance to Qo inhibitor fungicides', *Pest Manag Sci*, 58(9), pp. 859-67.

Gold, S., Duncan, G., Barrett, K. and Kronstad, J. (1994) 'cAMP regulates morphogenesis in the fungal pathogen *Ustilago maydis*', *Genes Dev*, 8(23), pp. 2805-16.

Gonzalez, A. and Hall, M.N. (2017) 'Nutrient sensing and TOR signaling in yeast and mammals', *Embo j*, 36(4), pp. 397-408.

Goodwin, S.B., M'Barek S, B., Dhillon, B., Wittenberg, A.H., Crane, C.F., Hane, J.K., Foster, A.J., Van der Lee, T.A., Grimwood, J., Aerts, A., Antoniw, J., Bailey, A., Bluhm,

B., Bowler, J., Bristow, J., van der Burgt, A., Canto-Canche, B., Churchill, A.C., Conde-Ferraez, L., Cools, H.J., Coutinho, P.M., Csukai, M., Dehal, P., De Wit, P., Donzelli, B., van de Geest, H.C., van Ham, R.C., Hammond-Kosack, K.E., Henrissat, B., Kilian, A., Kobayashi, A.K., Koopmann, E., Kourmpetis, Y., Kuzniar, A., Lindquist, E., Lombard, V., Maliepaard, C., Martins, N., Mehrabi, R., Nap, J.P., Ponomarenko, A., Rudd, J.J., Salamov, A., Schmutz, J., Schouten, H.J., Shapiro, H., Stergiopoulos, I., Torriani, S.F., Tu, H., de Vries, R.P., Waalwijk, C., Ware, S.B., Wiebenga, A., Zwiers, L.H., Oliver, R.P., Grigoriev, I.V. and Kema, G.H. (2011) 'Finished genome of the fungal wheat pathogen *Mycosphaerella graminicola* reveals dispensome structure, chromosome plasticity, and stealth pathogenesis', *PLoS Genet*, 7(6), p. e1002070.

Goodwin, T.J. and Poulter, R.T. (2001) 'The diversity of retrotransposons in the yeast *Cryptococcus neoformans*', *Yeast*, 18(9), pp. 865-80.

Graff, L., Obrdlik, P., Yuan, L., Loqué, D., Frommer, W.B. and von Wirén, N. (2010) 'N-terminal cysteines affect oligomer stability of the allosterically regulated ammonium transporter LeAMT1;1', *Journal of Experimental Botany*, 62(4), pp. 1361-1373.

Granger, D.L., Perfect, J.R. and Durack, D.T. (1985) 'Virulence of *Cryptococcus neoformans*. Regulation of capsule synthesis by carbon dioxide', *J Clin Invest*, 76(2), pp. 508-16.

Grasso, V., Palermo, S., Sierotzki, H., Garibaldi, A. and Gisi, U. (2006) 'Cytochrome b gene structure and consequences for resistance to Qo inhibitor fungicides in plant pathogens', *Pest Manag Sci*, 62(6), pp. 465-72.

Gruswitz, F., Chaudhary, S., Ho, J.D., Schlessinger, A., Pezeshki, B., Ho, C.M., Sali, A., Westhoff, C.M. and Stroud, R.M. (2010) 'Function of human Rh based on structure of RhCG at 2.1 A', *Proc Natl Acad Sci U S A*, 107(21), pp. 9638-43.

Gugnani, H.C., Mitchell, T.G., Litvintseva, A.P., Lengeler, K.B., Heitman, J., Kumar, A., Basu, S. and Paliwal-Joshi, A. (2005) 'Isolation of *Cryptococcus gattii* and *Cryptococcus neoformans var. grubii* from the flowers and bark of Eucalyptus trees in India', *Med Mycol*, 43(6), pp. 565-9.

Hayes, L.E., Sackett, K.E., Anderson, N.P., Flowers, M.D. and Mundt, C.C. (2016) 'Evidence of Selection for Fungicide Resistance in *Zymoseptoria tritici* Populations on Wheat in Western Oregon', *Plant Dis*, 100(2), pp. 483-489.

Heitman, J., Movva, N.R. and Hall, M.N. (1991) 'Targets for cell cycle arrest by the immunosuppressant rapamycin in yeast', *Science*, 253(5022), pp. 905-9.

Hess, D.C., Lu, W., Rabinowitz, J.D. and Botstein, D. (2006) 'Ammonium toxicity and potassium limitation in yeast', *PLoS Biol*, 4(11), p. e351.

Hilu, H.M. and Bevee, W.M. (1957) 'Inoculation, oversummering, and susceptpathogen relationship of *Septoria tritici* on *Triticum species*', *Phytopathology*, 47(8), pp. 474-480 pp.

Hirimburegama, K., Durnez, P., Keleman, J., Oris, E., Vergauwen, R., Mergelsberg, H. and Thevelein, J.M. (1992) 'Nutrient-induced activation of trehalase in nutrient-starved cells of the yeast *Saccharomyces cerevisiae*: cAMP is not involved as second messenger', *J Gen Microbiol*, 138(10), pp. 2035-43.

Ho, M.N., Hill, K.J., Lindorfer, M.A. and Stevens, T.H. (1993) 'Isolation of vacuolar membrane H(+)-ATPase-deficient yeast mutants; the *VMA5* and *VMA4* genes are essential for assembly and activity of the vacuolar H(+)-ATPase', *J Biol Chem*, 268(1), pp. 221-7.

Hobbelen, P.H., Paveley, N.D. and van den Bosch, F. (2014) 'The emergence of resistance to fungicides', *PLoS One*, 9(3), p. e91910.

Holsbeeks, I., Lagatie, O., Van Nuland, A., Van de Velde, S. and Thevelein, J.M. (2004) 'The eukaryotic plasma membrane as a nutrient-sensing device', *Trends Biochem Sci*, 29(10), pp. 556-64.

Huergo, L.F. and Dixon, R. (2015) 'The Emergence of 2-Oxoglutarate as a Master Regulator Metabolite', *Microbiology and Molecular Biology Reviews*, 79(4), p. 419.

Jacinto, E., Guo, B., Arndt, K.T., Schmelzle, T. and Hall, M.N. (2001) 'TIP41 interacts with TAP42 and negatively regulates the TOR signaling pathway', *Mol Cell*, 8(5), pp. 1017-26.

Jauniaux, J.C., Vandenbol, M., Vissers, S., Broman, K. and Grenson, M. (1987) 'Nitrogen catabolite regulation of proline permease in *Saccharomyces cerevisiae*. Cloning of the *PUT4* gene and study of *PUT4* RNA levels in wild-type and mutant strains', *Eur J Biochem*, 164(3), pp. 601-6.

Javelle, A., Lupo, D., Zheng, L., Li, X.D., Winkler, F.K. and Merrick, M. (2006) 'An unusual twin-his arrangement in the pore of ammonia channels is essential for substrate conductance', *J Biol Chem*, 281(51), pp. 39492-8.

Javelle, A., Morel, M., Rodriguez-Pastrana, B.R., Botton, B., Andre, B., Marini, A.M., Brun, A. and Chalot, M. (2003) 'Molecular characterization, function and regulation of ammonium transporters (Amt) and ammonium-metabolizing enzymes (GS, NADP-GDH) in the ectomycorrhizal fungus *Hebeloma cylindrosporum*', *Mol Microbiol*, 47(2), pp. 411-30.

Javelle, A., Severi, E., Thornton, J. and Merrick, M. (2004) 'Ammonium sensing in *Escherichia coli*. Role of the ammonium transporter AmtB and AmtB-GlnK complex formation', *J Biol Chem*, 279(10), pp. 8530-8.

Jiang, P., Peliska, J.A. and Ninfa, A.J. (1998) 'Enzymological Characterization of the Signal-Transducing Uridylyltransferase/Uridylyl-Removing Enzyme (EC 2.7.7.59) of *Escherichia coli* and Its Interaction with the PII Protein', *Biochemistry*, 37(37), pp. 12782-12794.

Kane, P.M. (2016) 'Proton Transport and pH Control in Fungi', *Adv Exp Med Biol*, 892, pp. 33-68.

Kankipati, H.N., Rubio-Texeira, M., Castermans, D., Diallinas, G. and Thevelein, J.M. (2015) 'Sul1 and Sul2 sulfate transceptors signal to protein kinase A upon exit of sulfur starvation', *The Journal of biological chemistry*, 290(16), pp. 10430-10446.

Kawakami, K., Koguchi, Y., Qureshi, M.H., Miyazato, A., Yara, S., Kinjo, Y., Iwakura, Y., Takeda, K., Akira, S., Kurimoto, M. and Saito, A. (2000) 'IL-18 contributes to host resistance against infection with *Cryptococcus neoformans* in mice with defective IL-12 synthesis through induction of IFN-gamma production by NK cells', *J Immunol*, 165(2), pp. 941-7.

Kazazian, H.H., Jr. (2004) 'Mobile elements: drivers of genome evolution', *Science*, 303(5664), pp. 1626-32.

Kechichian, T.B., Shea, J. and Del Poeta, M. (2007) 'Depletion of alveolar macrophages decreases the dissemination of a glucosylceramide-deficient mutant of *Cryptococcus neoformans* in immunodeficient mice', *Infect Immun*, 75(10), pp. 4792-8.

Kema, G.H., van der Lee, T.A., Mendes, O., Verstappen, E.C., Lankhorst, R.K., Sandbrink, H., van der Burgt, A., Zwiers, L.H., Csukai, M. and Waalwijk, C. (2008) 'Large-scale gene discovery in the septoria tritici blotch fungus *Mycosphaerella graminicola* with a focus on in planta expression', *Mol Plant Microbe Interact*, 21(9), pp. 1249-60.

Kema, G.H., Verstappen, E.C., Todorova, M. and Waalwijk, C. (1996) 'Successful crosses and molecular tetrad and progeny analyses demonstrate heterothallism in *Mycosphaerella graminicola*', *Curr Genet*, 30(3), pp. 251-8.

Keon, J., Antoniw, J., Carzaniga, R., Deller, S., Ward, J.L., Baker, J.M., Beale, M.H., Hammond-Kosack, K. and Rudd, J.J. (2007) 'Transcriptional adaptation of *Mycosphaerella graminicola* to programmed cell death (PCD) of its susceptible wheat host', *Mol Plant Microbe Interact*, 20(2), pp. 178-93.

Keon, J.P., White, G.A. and Hargreaves, J.A. (1991) 'Isolation, characterization and sequence of a gene conferring resistance to the systemic fungicide carboxin from the maize smut pathogen, *Ustilago maydis'*, *Curr Genet*, 19(6), pp. 475-81.

Khademi, S., Connell, J., Remis, J., Robles-Colmenares, Y., Miercke, L.J.W. and Stroud, R.M. (2004) 'Mechanism of Ammonia Transport by Amt/MEP/Rh: Structure of AmtB at 1.35 Å', *Science*, 305(5690), p. 1587.

Khamzina, L., Veilleux, A., Bergeron, S. and Marette, A. (2005) 'Increased activation of the mammalian target of rapamycin pathway in liver and skeletal muscle of obese rats: possible involvement in obesity-linked insulin resistance', *Endocrinology*, 146(3), pp. 1473-81.

Khayhan, K., Hagen, F., Pan, W., Simwami, S., Fisher, M.C., Wahyuningsih, R., Chakrabarti, A., Chowdhary, A., Ikeda, R., Taj-Aldeen, S.J., Khan, Z., Ip, M., Imran, D., Sjam, R., Sriburee, P., Liao, W., Chaicumpar, K., Vuddhakul, V., Meyer, W., Trilles, L., van Iersel, L.J.J., Meis, J.F., Klaassen, C.H.W. and Boekhout, T. (2013) 'Geographically structured populations of *Cryptococcus neoformans* Variety *grubii* in Asia correlate with HIV status and show a clonal population structure', *PloS one*, 8(9), pp. e72222-e72222.

Kildea, S., Ransbotyn, V., Khan, M.R., Fagan, B., Leonard, G., Mullins, E. and Doohan, F.M. (2008) '*Bacillus megaterium* shows potential for the biocontrol of *septoria tritici* blotch of wheat', *Biological Control*, 47(1), pp. 37-45.

Kim, J., Kundu, M., Viollet, B. and Guan, K.L. (2011) 'AMPK and mTOR regulate autophagy through direct phosphorylation of Ulk1', *Nat Cell Biol*, 13(2), pp. 132-41.

Kingsbury, J.M. and McCusker, J.H. (2008) 'Threonine biosynthetic genes are essential in *Cryptococcus neoformans*', *Microbiology*, 154(Pt 9), pp. 2767-2775.

Kira, S., Kumano, Y., Ukai, H., Takeda, E., Matsuura, A. and Noda, T. (2016) 'Dynamic relocation of the TORC1-Gtr1/2-Ego1/2/3 complex is regulated by Gtr1 and Gtr2', *Molecular biology of the cell*, 27(2), pp. 382-396.

Ko, L.J. and Engel, J.D. (1993) 'DNA-binding specificities of the GATA transcription factor family', *Mol Cell Biol*, 13(7), pp. 4011-22.

Kozubowski, L. and Heitman, J. (2012) 'Profiling a killer, the development of *Cryptococcus neoformans'*, *FEMS microbiology reviews*, 36(1), pp. 78-94.

Krishnan, P., Meile, L., Plissonneau, C., Ma, X., Hartmann, F.E., Croll, D., McDonald, B.A. and Sánchez-Vallet, A. (2018) 'Transposable element insertions shape gene regulation and melanin production in a fungal pathogen of wheat', *BMC biology*, 16(1), pp. 78-78.

Krouk, G., Tillard, P. and Gojon, A. (2006) 'Regulation of the high-affinity NO3- uptake system by NRT1.1-mediated NO3- demand signaling in Arabidopsis', *Plant Physiol*, 142(3), pp. 1075-86.

Kwon-Chung, K.J. (1975) 'A New Genus, Filobasidiella, the Perfect State of *Cryptococcus neoformans'*, *Mycologia*, 67(6), pp. 1197-1200.

Kwon-Chung, K.J. and Bennett, J.E. (1978) 'Distribution of alpha and alpha mating types of *Cryptococcus neoformans* among natural and clinical isolates', *Am J Epidemiol*, 108(4), pp. 337-40.

Lanquar, V. and Frommer, W.B. (2010) 'Adjusting ammonium uptake via phosphorylation', *Plant Signal Behav*, 5(6), pp. 736-8.

Lee, I.R., Yang, L., Sebetso, G., Allen, R., Doan, T.H.N., Blundell, R., Lui, E.Y.L., Morrow, C.A. and Fraser, J.A. (2013) 'Characterization of the complete uric acid degradation pathway in the fungal pathogen *Cryptococcus neoformans'*, *PloS one*, 8(5), pp. e64292-e64292.

Lee, S.C., Phadke, S., Sun, S. and Heitman, J. (2012) 'Pseudohyphal growth of *Cryptococcus neoformans* is a reversible dimorphic transition in response to ammonium that requires Amt1 and Amt2 ammonium permeases', *Eukaryot Cell*, 11(11), pp. 1391-8.

Lengeler, K.B., Fox, D.S., Fraser, J.A., Allen, A., Forrester, K., Dietrich, F.S. and Heitman, J. (2002) 'Mating-type locus of *Cryptococcus neoformans:* a step in the evolution of sex chromosomes', *Eukaryotic cell*, 1(5), pp. 704-718.

Leroux, P., Albertini, C., Gautier, A., Gredt, M. and Walker, A.S. (2007) 'Mutations in the CYP51 gene correlated with changes in sensitivity to sterol 14 alpha-demethylation inhibitors in field isolates of *Mycosphaerella graminicola*', *Pest Manag Sci*, 63(7), pp. 688-98.

Lin, X., Chacko, N., Wang, L. and Pavuluri, Y. (2015) 'Generation of stable mutants and targeted gene deletion strains in *Cryptococcus neoformans* through electroporation', *Med Mycol*, 53(3), pp. 225-34.

Lin, X. and Heitman, J. (2005) 'Chlamydospore Formation during Hyphal Growth in *Cryptococcus neoformans*', *Eukaryotic Cell*, 4(10), p. 1746.

Lin, X. and Heitman, J. (2006) 'The biology of the *Cryptococcus neoformans* species complex', *Annu Rev Microbiol*, 60, pp. 69-105.

Lin, X., Huang, J.C., Mitchell, T.G. and Heitman, J. (2006) 'Virulence attributes and hyphal growth of *C. neoformans* are quantitative traits and the MATalpha allele enhances filamentation', *PLoS genetics*, 2(11), pp. e187-e187.

Lin, X., Hull, C.M. and Heitman, J. (2005) 'Sexual reproduction between partners of the same mating type in Cryptococcus neoformans', *Nature*, 434(7036), pp. 1017-21.

Liu, T.-B., Perlin, D.S. and Xue, C. (2012) 'Molecular mechanisms of cryptococcal meningitis', *Virulence*, 3(2), pp. 173-181.

Loewith, R. and Hall, M.N. (2011) 'Target of rapamycin (TOR) in nutrient signaling and growth control', *Genetics*, 189(4), pp. 1177-201.

Loewith, R., Jacinto, E., Wullschleger, S., Lorberg, A., Crespo, J.L., Bonenfant, D., Oppliger, W., Jenoe, P. and Hall, M.N. (2002) 'Two TOR complexes, only one of which is rapamycin sensitive, have distinct roles in cell growth control', *Mol Cell*, 10(3), pp. 457-68.

Loftus, B.J., Fung, E., Roncaglia, P., Rowley, D., Amedeo, P., Bruno, D., Vamathevan, J., Miranda, M., Anderson, I.J., Fraser, J.A., Allen, J.E., Bosdet, I.E., Brent, M.R., Chiu, R., Doering, T.L., Donlin, M.J., D'Souza, C.A., Fox, D.S., Grinberg, V., Fu, J., Fukushima, M., Haas, B.J., Huang, J.C., Janbon, G., Jones, S.J., Koo, H.L., Krzywinski, M.I., Kwon-Chung, J.K., Lengeler, K.B., Maiti, R., Marra, M.A., Marra, R.E., Mathewson, C.A., Mitchell, T.G., Pertea, M., Riggs, F.R., Salzberg, S.L., Schein, J.E., Shvartsbeyn, A., Shin, H., Shumway, M., Specht, C.A., Suh, B.B., Tenney, A., Utterback, T.R., Wickes, B.L., Wortman, J.R., Wye, N.H., Kronstad, J.W., Lodge, J.K., Heitman, J., Davis, R.W., Fraser, C.M. and Hyman, R.W. (2005) 'The genome of the basidiomycetous yeast and human pathogen *Cryptococcus neoformans*', *Science*, 307(5713), pp. 1321-4.

Lohmann-Matthes, M.L., Steinmuller, C. and Franke-Ullmann, G. (1994) 'Pulmonary macrophages', *Eur Respir J*, 7(9), pp. 1678-89.

López-Berges, M.S., Rispail, N., Prados-Rosales, R.C. and Di Pietro, A. (2010) 'A nitrogen response pathway regulates virulence functions in *Fusarium oxysporum* via

the protein kinase TOR and the bZIP protein MeaB', *The Plant cell*, 22(7), pp. 2459-2475.

Loque, D., Lalonde, S., Looger, L.L., von Wiren, N. and Frommer, W.B. (2007) 'A cytosolic trans-activation domain essential for ammonium uptake', *Nature*, 446(7132), pp. 195-8.

Lorenz, M.C. and Heitman, J. (1998) 'The MEP2 ammonium permease regulates pseudohyphal differentiation in *Saccharomyces cerevisiae'*, *Embo j*, 17(5), pp. 1236-47.

Ludewig, U., von Wirén, N., Rentsch, D. and Frommer, W.B. (2001) 'Rhesus factors and ammonium: a function in efflux?', *Genome biology*, 2(3), pp. REVIEWS1010-REVIEWS1010.

Ludewig, U., Wilken, S., Wu, B., Jost, W., Obrdlik, P., El Bakkoury, M., Marini, A.M., Andre, B., Hamacher, T., Boles, E., von Wiren, N. and Frommer, W.B. (2003) 'Homo- and hetero-oligomerization of ammonium transporter-1 NH4 uniporters', *J Biol Chem*, 278(46), pp. 45603-10.

Lui, G., Lee, N., Ip, M., Choi, K.W., Tso, Y.K., Lam, E., Chau, S., Lai, R. and Cockram, C.S. (2006) 'Cryptococcosis in apparently immunocompetent patients', *Qjm*, 99(3), pp. 143-51.

Macher, A.M., Bennett, J.E., Gadek, J.E. and Frank, M.M. (1978) 'Complement Depletion in *Cryptococcal* Sepsis', *The Journal of Immunology*, 120(5), p. 1686.

Magasanik, B. (2003) 'Ammonia assimilation by *Saccharomyces cerevisiae'*, *Eukaryotic cell*, 2(5), pp. 827-829.

Magasanik, B. and Kaiser, C.A. (2002) 'Nitrogen regulation in *Saccharomyces cerevisiae*', *Gene*, 290(1-2), pp. 1-18.

Mahmoud, S., Planes, M.D., Cabedo, M., Trujillo, C., Rienzo, A., Caballero-Molada, M., Sharma, S.C., Montesinos, C., Mulet, J.M. and Serrano, R. (2017) 'TOR complex 1 regulates the yeast plasma membrane proton pump and pH and potassium homeostasis', *FEBS Lett*, 591(13), pp. 1993-2002.

Marini, A.-M. and André, B. (2000) 'In vivo N-glycosylation of the Mep2 high-affinity ammonium transporter of *Saccharomyces cerevisiae* reveals an extracytosolic N-terminus', *Molecular Microbiology*, 38(3), pp. 552-564.

Marini, A.M., Soussi-Boudekou, S., Vissers, S. and Andre, B. (1997) 'A family of ammonium transporters in *Saccharomyces cerevisiae'*, *Mol Cell Biol*, 17(8), pp. 4282-93.

Martho, K.F.C., de Melo, A.T., Takahashi, J.P.F., Guerra, J.M., Santos, D.C.d.S., Purisco, S.U., Melhem, M.d.S.C., Fazioli, R.d.A., Phanord, C., Sartorelli, P., Vallim, M.A. and Pascon, R.C. (2016) 'Amino Acid Permeases and Virulence in *Cryptococcus neoformans*', *PLOS ONE*, 11(10), p. e0163919.

Marzluf, G.A. (1997) 'Genetic regulation of nitrogen metabolism in the fungi', *Microbiol Mol Biol Rev*, 61(1), pp. 17-32.

Mayer, M., Dynowski, M. and Ludewig, U. (2006) 'Ammonium ion transport by the AMT/Rh homologue LeAMT1;1', *The Biochemical journal*, 396(3), pp. 431-437.

McClelland, C.M., Chang, Y.C. and Kwon-Chung, K.J. (2005) 'High frequency transformation of *Cryptococcus neoformans* and *Cryptococcus gattii* by *Agrobacterium tumefaciens'*, *Fungal Genetics and Biology*, 42(11), pp. 904-913.

McClintock., B. (1950) 'The origin and behavior of mutable loci in maize', *Proc Natl Acad Sci U S A*, 36(6), pp. 344-55.

McDonald, B.A. and Mundt, C.C. (2016) 'How Knowledge of Pathogen Population Biology Informs Management of Septoria Tritici Blotch', *Phytopathology*, 106(9), pp. 948-955.

McQuiston, T.J. and Williamson, P.R. (2012) 'Paradoxical roles of alveolar macrophages in the host response to *Cryptococcus neoformans*', *J Infect Chemother*, 18(1), pp. 1-9.

Meara, T.R. and Alspaugh, J.A. (2012) 'The *Cryptococcus neoformans* Capsule: a Sword and a Shield', *Clinical Microbiology Reviews*, 25(3), p. 387.

Mehrabi, R. and Kema, G.H. (2006) 'Protein kinase A subunits of the ascomycete pathogen *Mycosphaerella graminicola* regulate asexual fructification, filamentation, melanization and osmosensing', *Mol Plant Pathol*, 7(6), pp. 565-77.

Mehrabi, R., Zwiers, L.H., de Waard, M.A. and Kema, G.H. (2006) 'MgHog1 regulates dimorphism and pathogenicity in the fungal wheat pathogen *Mycosphaerella graminicola*', *Mol Plant Microbe Interact*, 19(11), pp. 1262-9.

Mentlak, T.A., Kombrink, A., Shinya, T., Ryder, L.S., Otomo, I., Saitoh, H., Terauchi, R., Nishizawa, Y., Shibuya, N., Thomma, B.P. and Talbot, N.J. (2012) 'Effector-mediated suppression of chitin-triggered immunity by *Magnaporthe oryzae* is necessary for rice blast disease', *Plant Cell*, 24(1), pp. 322-35.

Minc, N. and Chang, F. (2010) 'Electrical control of cell polarization in the fission yeast *Schizosaccharomyces pombe*', *Current biology : CB*, 20(8), pp. 710-716.

Mitchell, A.P. and Magasanik, B. (1984) 'Biochemical and physiological aspects of glutamine synthetase inactivation in *Saccharomyces cerevisiae'*, *J Biol Chem*, 259(19), pp. 12054-62.

Morais do Amaral, A., Antoniw, J., Rudd, J.J. and Hammond-Kosack, K.E. (2012) 'Defining the predicted protein secretome of the fungal wheat leaf pathogen *Mycosphaerella graminicola*', *PloS one*, 7(12), pp. e49904-e49904.

Motteram, J., Kufner, I., Deller, S., Brunner, F., Hammond-Kosack, K.E., Nurnberger, T. and Rudd, J.J. (2009) 'Molecular characterization and functional analysis of MgNLP, the sole NPP1 domain-containing protein, from the fungal wheat leaf pathogen *Mycosphaerella graminicola*', *Mol Plant Microbe Interact*, 22(7), pp. 790-9.

Motteram, J., Lovegrove, A., Pirie, E., Marsh, J., Devonshire, J., van de Meene, A., Hammond-Kosack, K. and Rudd, J.J. (2011) 'Aberrant protein N-glycosylation impacts upon infection-related growth transitions of the haploid plant-pathogenic fungus *Mycosphaerella graminicola*', *Mol Microbiol*, 81(2), pp. 415-33.

Mylonakis, E., Moreno, R., El Khoury, J.B., Idnurm, A., Heitman, J., Calderwood, S.B., Ausubel, F.M. and Diener, A. (2005) 'Galleria mellonella as a model system to study *Cryptococcus neoformans* pathogenesis', *Infect Immun*, 73(7), pp. 3842-50.

Nagasu, T. and Hall, B.D. (1985) 'Nucleotide sequence of the GDH gene coding for the NADP-specific glutamate dehydrogenase of *Saccharomyces cerevisiae'*, *Gene*, 37(1), pp. 247-253.

Neuhauser, B., Dunkel, N., Satheesh, S.V. and Morschhauser, J. (2011) 'Role of the Npr1 kinase in ammonium transport and signaling by the ammonium permease Mep2 in *Candida albicans'*, *Eukaryot Cell*, 10(3), pp. 332-42.

Neuhauser, B., Dynowski, M., Mayer, M. and Ludewig, U. (2007) 'Regulation of NH4+ transport by essential cross talk between AMT monomers through the carboxyl tails', *Plant Physiol*, 143(4), pp. 1651-9.

Nielsen, K., Cox, G.M., Wang, P., Toffaletti, D.L., Perfect, J.R. and Heitman, J. (2003) 'Sexual cycle of *Cryptococcus neoformans var. grubii* and virulence of congenic a and alpha isolates', *Infect Immun*, 71(9), pp. 4831-41.

Nilsson, I., Johnson, A.E. and von Heijne, G. (2003) 'How hydrophobic is alanine?', *J Biol Chem*, 278(32), pp. 29389-93.

Noda, T. and Ohsumi, Y. (1998) 'Tor, a phosphatidylinositol kinase homologue, controls autophagy in yeast', *J Biol Chem*, 273(7), pp. 3963-6.

Nosanchuk, J.D., Rudolph, J., Rosas, A.L. and Casadevall, A. (1999) 'Evidence That *Cryptococcus neoformans* Is Melanized in Pigeon Excreta: Implications for Pathogenesis', *Infection and Immunity*, 67(10), p. 5477.

Obara, K., Yamamoto, H. and Kihara, A. (2012) 'Membrane protein Rim21 plays a central role in sensing ambient pH in *Saccharomyces cerevisiae*', *J Biol Chem*, 287(46), pp. 38473-81.

Okagaki, L.H. and Nielsen, K. (2012) 'Titan Cells Confer Protection from Phagocytosis in *Cryptococcus neoformans* Infections', *Eukaryotic Cell*, 11(6), p. 820.

Okagaki, L.H., Strain, A.K., Nielsen, J.N., Charlier, C., Baltes, N.J., Chretien, F., Heitman, J., Dromer, F. and Nielsen, K. (2010) '*Cryptococcal* cell morphology affects host cell interactions and pathogenicity', *PLoS Pathog*, 6(6), p. e1000953.

Omrane, S., Audeon, C., Ignace, A., Duplaix, C., Aouini, L., Kema, G., Walker, A.S. and Fillinger, S. (2017) 'Plasticity of the MFS1 Promoter Leads to Multidrug Resistance in the Wheat Pathogen *Zymoseptoria tritici*', *mSphere*, 2(5).

Ormerod, K.L., Morrow, C.A., Chow, E.W., Lee, I.R., Arras, S.D., Schirra, H.J., Cox, G.M., Fries, B.C. and Fraser, J.A. (2013) 'Comparative Genomics of Serial Isolates of *Cryptococcus neoformans* Reveals Gene Associated With Carbon Utilization and Virulence', *G3 (Bethesda)*, 3(4), pp. 675-686.

Orton, E.S., Rudd, J.J. and Brown, J.K.M. (2017) 'Early molecular signatures of responses of wheat to *Zymoseptoria tritici* in compatible and incompatible interactions', *Plant Pathology*, 66(3), pp. 450-459.

Ozcan, S., Dover, J. and Johnston, M. (1998) 'Glucose sensing and signaling by two glucose receptors in the yeast *Saccharomyces cerevisiae*', *Embo j*, 17(9), pp. 2566-73.

Ozcan, S., Dover, J., Rosenwald, A.G., Wölfl, S. and Johnston, M. (1996) 'Two glucose transporters in *Saccharomyces cerevisiae* are glucose sensors that generate a signal for induction of gene expression', *Proceedings of the National Academy of Sciences of the United States of America*, 93(22), pp. 12428-12432.

Panchaud, N., Peli-Gulli, M.P. and De Virgilio, C. (2013) 'Amino acid deprivation inhibits TORC1 through a GTPase-activating protein complex for the Rag family GTPase Gtr1', *Sci Signal*, 6(277), p. ra42.

Paul, J.A., Barati, M.T., Cooper, M. and Perlin, M.H. (2014) 'Physical and genetic interaction between ammonium transporters and the signaling protein Rho1 in the plant pathogen *Ustilago maydis'*, *Eukaryotic cell*, 13(10), pp. 1328-1336.

Pechmann, S. and Frydman, J. (2013) 'Evolutionary conservation of codon optimality reveals hidden signatures of cotranslational folding', *Nature structural & molecular biology*, 20(2), pp. 237-243.

Pellier, A.L., Lauge, R., Veneault-Fourrey, C. and Langin, T. (2003) 'CLNR1, the AREA/NIT2-like global nitrogen regulator of the plant fungal pathogen *Colletotrichum lindemuthianum* is required for the infection cycle', *Mol Microbiol*, 48(3), pp. 639-55.

Phadke, S.S., Feretzaki, M. and Heitman, J. (2013) 'Unisexual reproduction enhances fungal competitiveness by promoting habitat exploration via hyphal growth and sporulation', *Eukaryot Cell*, 12(8), pp. 1155-9.

Pham, C.D., Yu, Z., Sandrock, B., Bolker, M., Gold, S.E. and Perlin, M.H. (2009) '*Ustilago maydis* Rho1 and 14-3-3 homologues participate in pathways controlling cell separation and cell polarity', *Eukaryot Cell*, 8(7), pp. 977-89.

Poulsen, P., Gaber, R.F. and Kielland-Brandt, M.C. (2008) 'Hyper- and hyporesponsive mutant forms of the *Saccharomyces cerevisiae* Ssy1 amino acid sensor', *Mol Membr Biol*, 25(2), pp. 164-76.

Poulsen, P., Wu, B., Gaber, R.F., Ottow, K., Andersen, H.A. and Kielland-Brandt, M.C. (2005) 'Amino acid sensing by Ssy1', *Biochem Soc Trans*, 33(Pt 1), pp. 261-4.

Prentis, P.J., Wilson, J.R., Dormontt, E.E., Richardson, D.M. and Lowe, A.J. (2008) 'Adaptive evolution in invasive species', *Trends Plant Sci*, 13(6), pp. 288-94.

Randhawa, H.S., Mussa, A.Y. and Khan, Z.U. (2001) 'Decaying wood in tree trunk hollows as a natural substrate for *Cryptococcus neoformans* and other yeast-like fungi of clinical interest', *Mycopathologia*, 151(2), pp. 63-9.

Rane, H.S., Hayek, S.R., Frye, J.E., Abeyta, E.L., Bernardo, S.M., Parra, K.J. and Lee, S.A. (2019) '*Candida albicans* Pma1p Contributes to Growth, pH Homeostasis, and Hyphal Formation', *Frontiers in Microbiology*, 10(1012).

Rayhane, N., Lortholary, O., Fitting, C., Callebert, J., Huerre, M., Dromer, F. and Cavaillon, J.M. (1999) 'Enhanced sensitivity of tumor necrosis factor/lymphotoxin-alpha-deficient mice to *Cryptococcus neoformans* infection despite increased levels of nitrite/nitrate, interferon-gamma, and interleukin-12', *J Infect Dis*, 180(5), pp. 1637-47.

Regenberg, B., During-Olsen, L., Kielland-Brandt, M.C. and Holmberg, S. (1999) 'Substrate specificity and gene expression of the amino-acid permeases in *Saccharomyces cerevisiae*', *Curr Genet*, 36(6), pp. 317-28.

Retini, C., Vecchiarelli, A., Monari, C., Bistoni, F. and Kozel, T.R. (1998) 'Encapsulation of *Cryptococcus neoformans* with Glucuronoxylomannan Inhibits the Antigen-Presenting Capacity of Monocytes', *Infection and Immunity*, 66(2), p. 664.

Roberts, R.L. and Fink, G.R. (1994) 'Elements of a single MAP kinase cascade in *Saccharomyces cerevisiae* mediate two developmental programs in the same cell type: mating and invasive growth', *Genes Dev*, 8(24), pp. 2974-85.

Robzyk, K. and Kassir, Y. (1992) 'A simple and highly efficient procedure for rescuing autonomous plasmids from yeast', *Nucleic Acids Res*, 20(14), p. 3790.

Rohel, E.A., Payne, A.C., Fraaije, B.A. and Hollomon, D.W. (2001) 'Exploring infection of wheat and carbohydrate metabolism in *Mycosphaerella graminicola* transformants with differentially regulated green fluorescent protein expression', *Mol Plant Microbe Interact*, 14(2), pp. 156-63.

Rosas, A.L. and Casadevall, A. (1997) 'Melanization affects susceptibility of *Cryptococcus neoformans* to heat and cold', *FEMS Microbiol Lett*, 153(2), pp. 265-72.

Rudd, J.J., Kanyuka, K., Hassani-Pak, K., Derbyshire, M., Andongabo, A., Devonshire, J., Lysenko, A., Saqi, M., Desai, N.M., Powers, S.J., Hooper, J., Ambroso, L., Bharti, A., Farmer, A., Hammond-Kosack, K.E., Dietrich, R.A. and Courbot, M. (2015) 'Transcriptome and metabolite profiling of the infection cycle of *Zymoseptoria tritici* on wheat reveals a biphasic interaction with plant immunity involving differential pathogen chromosomal contributions and a variation on the hemibiotrophic lifestyle definition', *Plant Physiol*, 167(3), pp. 1158-85.

Rutherford, J.C., Chua, G., Hughes, T., Cardenas, M.E. and Heitman, J. (2008a) 'A Mep2-dependent transcriptional profile links permease function to gene expression during pseudohyphal growth in *Saccharomyces cerevisiae*', *Molecular biology of the cell*, 19(7), pp. 3028-3039.

Rutherford, J.C., Lin, X., Nielsen, K. and Heitman, J. (2008b) 'Amt2 permease is required to induce ammonium-responsive invasive growth and mating in *Cryptococcus neoformans*', *Eukaryot Cell*, 7(2), pp. 237-46.

Ryan, O., Shapiro, R.S., Kurat, C.F., Mayhew, D., Baryshnikova, A., Chin, B., Lin, Z.Y., Cox, M.J., Vizeacoumar, F., Cheung, D., Bahr, S., Tsui, K., Tebbji, F., Sellam, A., Istel, F., Schwarzmuller, T., Reynolds, T.B., Kuchler, K., Gifford, D.K., Whiteway, M., Giaever, G., Nislow, C., Costanzo, M., Gingras, A.C., Mitra, R.D., Andrews, B., Fink, G.R., Cowen, L.E. and Boone, C. (2012) 'Global gene deletion analysis exploring yeast filamentous growth', *Science*, 337(6100), pp. 1353-6.

Saintenac, C., Lee, W.-S., Cambon, F., Rudd, J.J., King, R.C., Marande, W., Powers, S.J., Bergès, H., Phillips, A.L., Uauy, C., Hammond-Kosack, K.E., Langin, T. and Kanyuka, K. (2018) 'Wheat receptor-kinase-like protein Stb6 controls gene-for-gene resistance to fungal pathogen *Zymoseptoria tritici*', *Nature Genetics*, 50(3), pp. 368-374.

Salas, S.D., Bennett, J.E., Kwon-Chung, K.J., Perfect, J.R. and Williamson, P.R. (1996) 'Effect of the laccase gene CNLAC1, on virulence of *Cryptococcus neoformans'*, *The Journal of Experimental Medicine*, 184(2), p. 377.

Saliba, E., Evangelinos, M., Gournas, C., Corrillon, F., Georis, I. and André, B. (2018) 'The yeast H(+)-ATPase Pma1 promotes Rag/Gtr-dependent TORC1 activation in response to H(+)-coupled nutrient uptake', *eLife*, 7, p. e31981.

Samyn, D.R., Ruiz-Pavon, L., Andersson, M.R., Popova, Y., Thevelein, J.M. and Persson, B.L. (2012) 'Mutational analysis of putative phosphate- and proton-binding sites in the *Saccharomyces cerevisiae* Pho84 phosphate:H(+) transceptor and its effect on signalling to the PKA and PHO pathways', *Biochem J*, 445(3), pp. 413-22.

Sancak, Y., Bar-Peled, L., Zoncu, R., Markhard, A.L., Nada, S. and Sabatini, D.M. (2010) 'Ragulator-Rag complex targets mTORC1 to the lysosomal surface and is necessary for its activation by amino acids', *Cell*, 141(2), pp. 290-303.

Sancak, Y., Peterson, T.R., Shaul, Y.D., Lindquist, R.A., Thoreen, C.C., Bar-Peled, L. and Sabatini, D.M. (2008) 'The Rag GTPases bind raptor and mediate amino acid signaling to mTORC1', *Science*, 320(5882), pp. 1496-501.

Sanchez-Vallet, A., Mesters, J.R. and Thomma, B.P. (2015) 'The battle for chitin recognition in plant-microbe interactions', *FEMS Microbiol Rev*, 39(2), pp. 171-83.

Sanderson, F.R., Scharen, A.L., Scott, P.R., (1985) 'Sources and importance of primary infection and identities of associated propagules,' *ARS U.S. Department of Agriculture, Agricultural Research Service*, 12.

Santangelo, R., Zoellner, H., Sorrell, T., Wilson, C., Donald, C., Djordjevic, J., Shounan, Y. and Wright, L. (2004) 'Role of Extracellular Phospholipases and Mononuclear Phagocytes in Dissemination of *Cryptococcosis* in a Murine Model', *Infection and Immunity*, 72(4), p. 2229.

Scherens, B., Feller, A., Vierendeels, F., Messenguy, F. and Dubois, E. (2006) 'Identification of direct and indirect targets of the Gln3 and Gat1 activators by transcriptional profiling in response to nitrogen availability in the short and long term', *FEMS Yeast Research*, 6(5), pp. 777-791.

Schiestl, R.H. and Gietz, R.D. (1989) 'High efficiency transformation of intact yeast cells using single stranded nucleic acids as a carrier', *Current Genetics*, 16(5-6), pp. 339-346.

Schmidt, A., Beck, T., Koller, A., Kunz, J. and Hall, M.N. (1998) 'The TOR nutrient signalling pathway phosphorylates NPR1 and inhibits turnover of the tryptophan permease', *Embo j*, 17(23), pp. 6924-31.

Schreve, J.L., Sin, J.K. and Garrett, J.M. (1998) 'The *Saccharomyces cerevisiae* YCC5 (YCL025c) gene encodes an amino acid permease, Agp1, which transports asparagine and glutamine', *J Bacteriol*, 180(9), pp. 2556-9.

Schuh, W. (1990) 'Influence of tillage systems on disease intensity and spatial pattern of *Septoria* leaf blotch', *Phytopathology*, 80(12), pp. 1337-1340.

Severi, E., Javelle, A. and Merrick, M. (2007) 'The conserved carboxy-terminal region of the ammonia channel AmtB plays a critical role in channel function', *Mol Membr Biol*, 24(2), pp. 161-71.

Shadomy, H.J. and Utz, J.P. (1966) 'Preliminary studies on a hyphaforming mutant of *Cryptococcus neoformans*', *Mycologia*, 58(3), pp. 383-90.

Sharp, P.M., Tuohy, T.M. and Mosurski, K.R. (1986) 'Codon usage in yeast: cluster analysis clearly differentiates highly and lowly expressed genes', *Nucleic Acids Res*, 14(13), pp. 5125-43.

Shearer, W.A.S.R.J.B.A.R.I. (1971) 'The common *Septoria* diseases of wheat', *The Botanical Review*, 37, pp. 231–262.

Shen, W.-C., Davidson, R.C., Cox, G.M. and Heitman, J. (2002) 'Pheromones stimulate mating and differentiation via paracrine and autocrine signaling in *Cryptococcus neoformans', Eukaryotic cell*, 1(3), pp. 366-377.

Shetty, N.P., Mehrabi, R., Lutken, H., Haldrup, A., Kema, G.H., Collinge, D.B. and Jorgensen, H.J. (2007) 'Role of hydrogen peroxide during the interaction between the hemibiotrophic fungal pathogen *Septoria tritici* and wheat', *New Phytol*, 174(3), pp. 637-47.

Siegel, M. (1981) 'Sterol-inhibiting fungicides: effects on sterol biosynthesis and sites of action', *Plant Diseases*.

Sierotzki, H., Frey, R., Wullschleger, J., Palermo, S., Karlin, S., Godwin, J. and Gisi, U. (2007) 'Cytochrome b gene sequence and structure of Pyrenophora teres and P. tritici-repentis and implications for QoI resistance', *Pest Manag Sci*, 63(3), pp. 225-33.

Sierotzki, H. and Scalliet, G. (2013) 'A review of current knowledge of resistance aspects for the next-generation succinate dehydrogenase inhibitor fungicides', *Phytopathology*, 103(9), pp. 880-7.

Sikorski, R.S. and Hieter, P. (1989) 'A system of shuttle vectors and yeast host strains designed for efficient manipulation of DNA in *Saccharomyces cerevisiae*', *Genetics*, 122(1), pp. 19-27.

Smith, D.G., Garcia-Pedrajas, M.D., Gold, S.E. and Perlin, M.H. (2003) 'Isolation and characterization from pathogenic fungi of genes encoding ammonium permeases and their roles in dimorphism', *Mol Microbiol*, 50(1), pp. 259-75.

Spina-Tensini, T., Muro, M.D., Queiroz-Telles, F., Strozzi, I., Moraes, S.T., Petterle, R.R., Vettorello, M., Staudacher, C., Miguez, L.A. and de Almeida, S.M. (2017) 'Geographic distribution of patients affected by *Cryptococcus neoformans/Cryptococcus gattii species* complexes meningitis, pigeon and tree populations in Southern Brazil', *Mycoses*, 60(1), pp. 51-58.

Steinberg, G. (2015) 'Cell biology of Zymoseptoria tritici: Pathogen cell organization and wheat infection', *Fungal Genet Biol*, 79, pp. 17-23.

Steyfkens, F., Zhang, Z., Van Zeebroeck, G. and Thevelein, J.M. (2018) 'Multiple Transceptors for Macro- and Micro-Nutrients Control Diverse Cellular Properties Through the PKA Pathway in Yeast: A Paradigm for the Rapidly Expanding World of Eukaryotic Nutrient Transceptors Up to Those in Human Cells', *Frontiers in Pharmacology*, 9(191).

Stracka, D., Jozefczuk, S., Rudroff, F., Sauer, U. and Hall, M.N. (2014) 'Nitrogen source activates TOR (target of rapamycin) complex 1 via glutamine and independently of Gtr/Rag proteins', *J Biol Chem*, 289(36), pp. 25010-20.

Syme, R.M., Spurrell, J.C., Ma, L.L., Green, F.H. and Mody, C.H. (2000) 'Phagocytosis and protein processing are required for presentation of *Cryptococcus neoformans* mitogen to T lymphocytes', *Infect Immun*, 68(11), pp. 6147-53.

Tate, J.J., Tolley, E.A. and Cooper, T.G. (2019) 'Sit4 and PP2A Dephosphorylate Nitrogen Catabolite Repression-Sensitive Gln3 When TorC1 Is Up- as Well as Downregulated', *Genetics*, 212(4), p. 1205.

Teichert, S., Rutherford, J.C., Wottawa, M., Heitman, J. and Tudzynski, B. (2008) 'Impact of Ammonium Permeases MepA, MepB, and MepC on Nitrogen-Regulated Secondary Metabolism in *Fusarium fujikuroi*', *Eukaryotic Cell*, 7(2), p. 187.

Thanki, N., Thornton, J.M. and Goodfellow, J.M. (1988) 'Distributions of water around amino acid residues in proteins', *J Mol Biol*, 202(3), pp. 637-57.

Thevelein, J.M. and de Winde, J.H. (1999) 'Novel sensing mechanisms and targets for the cAMP-protein kinase A pathway in the yeast *Saccharomyces cerevisiae*', *Mol Microbiol*, 33(5), pp. 904-18.

Thevelein, J.M. and Voordeckers, K. (2009) 'Functioning and evolutionary significance of nutrient transceptors', *Mol Biol Evol*, 26(11), pp. 2407-14.

Thomas, G., Coutts, G. and Merrick, M. (2000) 'The glnKamtB operon. A conserved gene pair in prokaryotes', *Trends Genet*, 16(1), pp. 11-4.

Torriani, S.F., Brunner, P.C., McDonald, B.A. and Sierotzki, H. (2009) 'QoI resistance emerged independently at least 4 times in European populations of *Mycosphaerella graminicola*', *Pest Manag Sci*, 65(2), pp. 155-62.

Torriani, S.F.F., Melichar, J.P.E., Mills, C., Pain, N., Sierotzki, H. and Courbot, M. (2015) '*Zymoseptoria tritici*: A major threat to wheat production, integrated approaches to control', *Fungal Genetics and Biology*, 79, pp. 8-12.

Tudzynski, B. (2014) 'Nitrogen regulation of fungal secondary metabolism in fungi', *Frontiers in microbiology*, 5, pp. 656-656.

Ukai, H., Araki, Y., Kira, S., Oikawa, Y., May, A.I. and Noda, T. (2018) 'Gtr/Ego-independent TORC1 activation is achieved through a glutamine-sensitive interaction with Pib2 on the vacuolar membrane', *PLoS Genet*, 14(4), p. e1007334.

Ulaszewski, S., Coddington, A. and Goffeau, A. (1986) 'A new mutation for multiple drug resistance and modified plasma membrane ATPase activity in *Schizosaccharomyces pombe*', *Curr Genet*, 10(5), pp. 359-64.

Ullmann, R.T., Andrade, S.L.A. and Ullmann, G.M. (2012) 'Thermodynamics of Transport Through the Ammonium Transporter Amt-1 Investigated with Free Energy Calculations', *The Journal of Physical Chemistry B*, 116(32), pp. 9690-9703.

Urban, J., Soulard, A., Huber, A., Lippman, S., Mukhopadhyay, D., Deloche, O., Wanke, V., Anrather, D., Ammerer, G., Riezman, H., Broach, J.R., De Virgilio, C., Hall, M.N. and Loewith, R. (2007) 'Sch9 Is a Major Target of TORC1 in *Saccharomyces cerevisiae*', *Molecular Cell*, 26(5), pp. 663-674.

van den Berg, B., Chembath, A., Jefferies, D., Basle, A., Khalid, S. and Rutherford, J.C. (2016) 'Structural basis for Mep2 ammonium transceptor activation by phosphorylation', *Nat Commun*, 7, p. 11337.

van Duin, D., Casadevall, A. and Nosanchuk, J.D. (2002) 'Melanization of *Cryptococcus neoformans* and Histoplasma capsulatum Reduces Their Susceptibilities to Amphotericin B and Caspofungin', *Antimicrobial Agents and Chemotherapy*, 46(11), p. 3394.

Van Nuland, A., Vandormael, P., Donaton, M., Alenquer, M., Lourenço, A., Quintino, E., Versele, M. and Thevelein, J.M. (2006) 'Ammonium permease-based sensing mechanism for rapid ammonium activation of the protein kinase A pathway in yeast', *Molecular Microbiology*, 59(5), pp. 1485-1505.

Van Zeebroeck, G., Bonini, B.M., Versele, M. and Thevelein, J.M. (2009) 'Transport and signaling via the amino acid binding site of the yeast Gap1 amino acid transceptor', *Nat Chem Biol*, 5(1), pp. 45-52.

Van Zeebroeck, G., Kimpe, M., Vandormael, P. and Thevelein, J.M. (2011) 'A split-ubiquitin two-hybrid screen for proteins physically interacting with the yeast amino acid transceptor Gap1 and ammonium transceptor Mep2', *PloS one*, 6(9), pp. e24275-e24275.

Van Zeebroeck, G., Rubio-Texeira, M., Schothorst, J. and Thevelein, J.M. (2014) 'Specific analogues uncouple transport, signalling, oligo-ubiquitination and endocytosis in the yeast Gap1 amino acid transceptor', *Mol Microbiol*, 93(2), pp. 213-33.

Varlakhanova, N.V., Tornabene, B.A. and Ford, M.G.J. (2018) 'Feedback regulation of TORC1 by its downstream effectors Npr1 and Par32', *Molecular biology of the cell*, 29(22), pp. 2751-2765.

Vartivarian, S.E., Anaissie, E.J., Cowart, R.E., Sprigg, H.A., Tingler, M.J. and Jacobson, E.S. (1993) 'Regulation of *cryptococcal* capsular polysaccharide by iron', *J Infect Dis*, 167(1), pp. 186-90.

Vecchiarelli, A., Retini, C., Pietrella, D., Monari, C., Tascini, C., Beccari, T. and Kozel, T.R. (1995) 'Downregulation by *cryptococcal* polysaccharide of tumor necrosis factor alpha and interleukin-1 beta secretion from human monocytes', *Infection and Immunity*, 63(8), p. 2919.

Velagapudi, R., Hsueh, Y.-P., Geunes-Boyer, S., Wright, J.R. and Heitman, J. (2009) 'Spores as Infectious Propagules of *Cryptococcus neoformans*', *Infection and Immunity*, 77(10), p. 4345.

Vieira, P.L., de Jong, E.C., Wierenga, E.A., Kapsenberg, M.L. and Kalinski, P. (2000) 'Development of Th1-inducing capacity in myeloid dendritic cells requires environmental instruction', *J Immunol*, 164(9), pp. 4507-12.

Wacker, T., Garcia-Celma, J.J., Lewe, P. and Andrade, S.L.A. (2014) 'Direct observation of electrogenic NH4(+) transport in ammonium transport (Amt) proteins', *Proceedings of the National Academy of Sciences*, 111(27), p. 9995.

Wagner, D., Wiemann, P., Huss, K., Brandt, U., Fleissner, A. and Tudzynski, B. (2013) 'A sensing role of the glutamine synthetase in the nitrogen regulation network in *Fusarium fujikuroi*', *PLoS One*, 8(11), p. e80740.

Wang, H., Wang, X. and Jiang, Y. (2003) 'Interaction with Tap42 is required for the essential function of Sit4 and type 2A phosphatases', *Mol Biol Cell*, 14(11), pp. 4342-51.

Wang, P., Perfect, J.R. and Heitman, J. (2000) 'The G-protein beta subunit GPB1 is required for mating and haploid fruiting in *Cryptococcus neoformans'*, *Molecular and cellular biology*, 20(1), pp. 352-362.

Wang, S., Orabi, E.A., Baday, S., Bernèche, S. and Lamoureux, G. (2012) 'Ammonium Transporters Achieve Charge Transfer by Fragmenting Their Substrate', *Journal of the American Chemical Society*, 134(25), pp. 10419-10427.

Wang, Y. and Casadevall, A. (1994) 'Susceptibility of melanized and nonmelanized *Cryptococcus neoformans* to nitrogen- and oxygen-derived oxidants', *Infection and Immunity*, 62(7), p. 3004.

Westhoff, C.M. and Wylie, D.E. (2006) 'Transport characteristics of mammalian Rh and Rh glycoproteins expressed in heterologous systems', *Transfus Clin Biol*, 13(1-2), pp. 132-8.

Wicker, T., Sabot, F., Hua-Van, A., Bennetzen, J.L., Capy, P., Chalhoub, B., Flavell, A., Leroy, P., Morgante, M., Panaud, O., Paux, E., SanMiguel, P. and Schulman, A.H.

(2007) 'A unified classification system for eukaryotic transposable elements', *Nat Rev Genet*, 8(12), pp. 973-82.

Wickes, B.L., Mayorga, M.E., Edman, U. and Edman, J.C. (1996) 'Dimorphism and haploid fruiting in *Cryptococcus neoformans*: association with the alpha-mating type', *Proceedings of the National Academy of Sciences*, 93(14), p. 7327.

Wiese R.A (1987) *Compendium of Wheat Diseases*. Minnesota, USA: The American Phytopathological Society.

Wittenberg, A.H., van der Lee, T.A., Ben M'barek, S., Ware, S.B., Goodwin, S.B., Kilian, A., Visser, R.G., Kema, G.H. and Schouten, H.J. (2009) 'Meiosis drives extraordinary genome plasticity in the haploid fungal plant pathogen *Mycosphaerella graminicola'*, *PLoS One*, 4(6), p. e5863.

Wong, K.H., Hynes, M.J. and Davis, M.A. (2008) 'Recent advances in nitrogen regulation: a comparison between *Saccharomyces cerevisiae* and filamentous fungi', *Eukaryot Cell*, 7(6), pp. 917-25.

Wu, B., Ottow, K., Poulsen, P., Gaber, R.F., Albers, E. and Kielland-Brandt, M.C. (2006) 'Competitive intra- and extracellular nutrient sensing by the transporter homologue Ssy1p', *The Journal of cell biology*, 173(3), pp. 327-331.

Xu, J.R. and Hamer, J.E. (1996) 'MAP kinase and cAMP signaling regulate infection structure formation and pathogenic growth in the rice blast fungus *Magnaporthe grisea'*, *Genes Dev*, 10(21), pp. 2696-706.

Xu, Y., Cheah, E., Carr, P.D., van Heeswijk, W.C., Westerhoff, H.V., Vasudevan, S.G. and Ollis, D.L. (1998) 'GlnK, a PII-homologue: structure reveals ATP binding site and indicates how the T-loops may be involved in molecular recognition11Edited by R. Huber', *Journal of Molecular Biology*, 282(1), pp. 149-165.

Xue, C., Tada, Y., Dong, X. and Heitman, J. (2007) 'The Human Fungal Pathogen *Cryptococcus* Can Complete Its Sexual Cycle during a Pathogenic Association with Plants', *Cell Host & Microbe*, 1(4), pp. 263-273.

Yan, G., Shen, X. and Jiang, Y. (2006) 'Rapamycin activates Tap42-associated phosphatases by abrogating their association with Tor complex 1', *The EMBO journal*, 25(15), pp. 3546-3555.

Yang, F., Li, W. and Jorgensen, H.J. (2013) 'Transcriptional reprogramming of wheat and the hemibiotrophic pathogen *Septoria tritici* during two phases of the compatible interaction', *PLoS One*, 8(11), p. e81606.

Yemelin, A., Brauchler, A., Jacob, S., Laufer, J., Heck, L., Foster, A.J., Antelo, L., Andresen, K. and Thines, E. (2017) 'Identification of factors involved in dimorphism and pathogenicity of *Zymoseptoria tritici'*, *PLoS One*, 12(8), p. e0183065.

Yu, C.-H., Dang, Y., Zhou, Z., Wu, C., Zhao, F., Sachs, M.S. and Liu, Y. (2015) 'Codon Usage Influences the Local Rate of Translation Elongation to Regulate Co-translational Protein Folding', *Molecular cell*, 59(5), pp. 744-754.

Zaragoza, O., Chrisman, C.J., Castelli, M.V., Frases, S., Cuenca-Estrella, M., Rodriguez-Tudela, J.L. and Casadevall, A. (2008) 'Capsule enlargement in *Cryptococcus neoformans* confers resistance to oxidative stress suggesting a mechanism for intracellular survival', *Cell Microbiol*, 10(10), pp. 2043-57.

Zaragoza, O., Garcia-Rodas, R., Nosanchuk, J.D., Cuenca-Estrella, M., Rodriguez-Tudela, J.L. and Casadevall, A. (2010) 'Fungal cell gigantism during mammalian infection', *PLoS Pathog*, 6(6), p. e1000945.

Zhan, F., Xie, Y., Zhu, W., Sun, D., McDonald, B.A. and Zhan, J. (2016) 'Linear Correlation Analysis of *Zymoseptoria tritici* Aggressiveness with In Vitro Growth Rate', *Phytopathology*, 106(11), pp. 1255-1261.

Zhang, T., Peli-Gulli, M.P., Yang, H., De Virgilio, C. and Ding, J. (2012) 'Ego3 functions as a homodimer to mediate the interaction between Gtr1-Gtr2 and Ego1 in the ego complex to activate TORC1', *Structure*, 20(12), pp. 2151-60.

Zhao, Y., Lin, J., Fan, Y. and Lin, X. (2019) 'Life Cycle of *Cryptococcus neoformans'*, *Annu Rev Microbiol*, 73, pp. 17-42.

Zheng, L., Kostrewa, D., Bernèche, S., Winkler, F.K. and Li, X.-D. (2004) 'The mechanism of ammonia transport based on the crystal structure of AmtB of *Escherichia coli*', *Proceedings of the National Academy of Sciences of the United States of America*, 101(49), p. 17090.

Zhu, X., Garrett, J., Schreve, J. and Michaeli, T. (1996) 'GNP1, the high-affinity glutamine permease of *S. cerevisiae*', *Curr Genet*, 30(2), pp. 107-14.

Zhu, X., Gibbons, J., Garcia-Rivera, J., Casadevall, A. and Williamson, P.R. (2001) 'Laccase of *Cryptococcus neoformans* is a cell wall-associated virulence factor', *Infection and immunity*, 69(9), pp. 5589-5596.